Cranfield UNIVERSITY

Raja Javed Razzaq

Nonlinear Static and Dynamic Analysis of Composite Layered Plates and Shells Using Finite Strip Methods

School of Engineering

PhD Thesis
2003

Cranfield UNIVERSITY

School of Engineering

Department of Automotive Mechanical & Structural Engineering

PhD Thesis
1999-2002

Raja Javed Razzaq

Nonlinear Static and Dynamic Analysis of Composite Layered Plates and Shells Using Finite Strip Methods

Supervisor: Dr. A El-Zafrany

October 2003

This thesis is submitted in fulfilment of the requirements for the degree of Doctor of Philosophy

This work is dedicated to the memory

of my younger brother

Raja Abid Razzaq

Abstract

In this thesis, a new concept of finite strip elements is introduced. Lagrangian, Hermitian and spline-type interpolations have been used independently along the two axes of the plate mid-plane. Different plate-bending theories; Mindlin, Reissner and Kirchhoff theories have been applied in the derivations of the new finite-strip elements, for isotropic and composite materials. The new elements have also been extended to work as faceted shell elements for the analysis of cylindrical shells, folded plates and stiffened plates.

An efficient modular programming package based on those elements was designed, and it is capable of performing linear and non-linear stress analysis, buckling analysis and natural frequency analysis. The modular package, which was coded in FORTRAN has different solvers and a built-in mesh generator for different types of plate structures.

A number of case studies have been employed for the validation of the package and testing its different capabilities. The package has proved to be an efficient tool for numerical modelling of plates, cylindrical shells, folded plates and stiffened plates made of isotropic and composite layered materials.

List of Contents

List of Tables

List of Figures

List of Notations and Abbreviations

a	Acceleration
$\boldsymbol{B}$	Strain-displacement matrix
B	Width of the plate in y-direction
$\boldsymbol{D}$	Material stiffness matrix
E	Young's modulus
$\boldsymbol{F}$	Equivalent nodal force vector
h	Plate thickness
$\boldsymbol{J}$	Jacobian matrix
$\boldsymbol{K}$	Stiffness matrix
L	Length of the plate in x-direction
l,m,n	Directional cosines
$\boldsymbol{M}$	Mass matrix
N	Total number of nodes
U	Strain energy
u,v,w	Displacement components in the x,y and z directions, respectively
x,y,z	Global Cartesian co-ordinates
$x`, y`, z`$	Material principal axes
$\underline{x},\underline{y},\underline{z}$	Local Cartesian co-ordinates
γ	Shear strain
$\boldsymbol{\delta}$	Nodal displacement vector
$\boldsymbol{\varepsilon}$	Strain vector
θ	Slope angle
μ	Shear modulus
ρ	Density
R	Residual vector
$\boldsymbol{\sigma}$	Stress vector
τ	Shear stress
υ	Poisson's ratio
ω	Natural frequency
$\mathfrak{R}$	Element rotation matrix
FEM	Finite Element Method
FSM	Finite Strip Method
KFSM	Kirchhoff Finite Strip Method
RFSM	Reissner Finite Strip Method
-lns	Linear stress analysis
-nls	Non-linear stress analysis
C/E	Carbon/Epoxy composite materials
E/G	Glass/Epoxy composite materials

Some other parameters are defined within the text.

Acknowledgements

The author would like to express his deep gratitude to his supervisor Dr. A. El-Zafrany for his stimulating supervision, support and encouragement throughout this research. The author wishes to thank him also for his limitless and unconditional hospitality and generosity. In fact the author feels it was impossible for him to complete this work without his help and guidance.

The author is deeply grateful to his father for his moral support and inspiration.

Finally but no means least the author would like to extend his sincere gratitude and thanks to rest of his family for the help, encouragement, and moral support that they have given during the course of this work.

Chapter 1

Introduction

1. Introduction

1.1 GENERAL INTRODUCTION

The finite strip method (FSM) is well known and established as a powerful and versatile tool of solution in structural analysis, and for many structures having regular geometric planes and simple boundary conditions a full finite element analysis is often both extravagant and unnecessary and sometimes even impossible. The cost of the solution is very high and sometimes it goes even more expensive when a more refined higher dimensional analysis is required.

The above observations are especially true for static analysis of three dimensional solids and for eigenvalue problems. In vibration and buckling analysis of plate and shell structures, an alternative method which can reduce the computational effort, but at the same time retaining to some extent the versatility of the finite element analysis is evidently desirable for these structures.

These requirements can be satisfied fully by the recently developed FSM. In this method, the structure is divided into two dimensional strips or three dimensional (prisms, layers) sub-domains, in which one opposite pair of sides (2D) or one or more opposite pairs of faces (3D) of such domains are in coincidence with the boundaries of the structures.

The geometry of the structure is usually uniform along one or two co-ordinate axes, so that the width of a strip or the cross-section of a prism or layer will not change from one end to the other. Therefore while box girder bridges and slabs are conveniently divided into strips or prisms, for thick isotropic or multi-layered plates and shells a division into layers would definitely be more suitable.

The finite strip method can be considered as a special form of finite element procedure using the displacement approach. Unlike the standard finite element method (FEM) which uses polynomial displacement functions in all direction, the finite strip method calls for use of simple polynomial in some directions and a continuously differentiable smooth series in other directions, which satisfies a priori the boundary conditions at the ends of the strips or prisms.

Composite materials are widely used in the current design practice of many of today's engineering disciplines. The use of composite materials in the automobile and marine engineering industries is to be noted in particular and it is envisaged that these materials will have still a wider role to play in the future as more is realised of their capabilities through continued applied research and development.

Composites have the advantage of fibre orientation is that a structural component can be tailored for a specific requirement simply by controlling the direction of the fibres and choosing a favourable ply stacking sequence.

The mechanical response of composite structural element is significantly different to that

of similar conventional metallic components and thus elaborate and detailed analytical solution procedures are necessary to account for the complexities associated with the anisotropic nature of typical glass and carbon fibre composite materials. Many of the design problems in fibre reinforced composite structures stem from the fact that the fibres are joined together by a matrix material which has a relatively low strength and stiffness through the thickness of a laminated component which can be of the order of a few percent of its in-plane longitudinal strength and this gives rise to unusual failure mechanisms unique to composite construction.

The classical implementation of the FSM was based on the use of trigonometric functions (harmonics) along the direction with uniform geometry, and from the orthogonality of those functions equations associated for each harmonic are decoupled and solved independently.

For the case of general composite layered plates, this decoupling is not possible except for linear analysis of symmetric composites. For non-linear stress analysis and buckling analysis the full equations for all harmonics have to be solved simultaneously. The main advantage of the FSM for such cases is the reduction of finite element modelling time. The coupling of harmonics has inspired researchers to use different types of interpolation instead of trigonometric series, and the concept of spline finite strip method has been created, and used for non-linear and buckling analysis of plates.

1.2 RESEARCH OBJECTIVES

The main objective of the PhD research is to derive new and efficient finite strip elements and procedures for the nonlinear static, dynamic and instability analysis of composite layered plates and box structures. The interpolation theorems employed along the length of the plate are piecewise one-dimensional Lagrangian or Hermitian interpolation. A new type of finite strip elements will be derived based on the use of different types of one-dimensional polynomial interpolation along the plate width, including a spline-type interpolation. This may involve the following tasks:

(i) Derivation of the finite strip equations for composite layered plates using Kirchhoff, Mindlin and Reissner plate bending theories.

(ii) Derivation of linear, nonlinear and dynamic equations using faceted shell finite strip elements based on the newly derived plate elements.

(iii) Investigation of efficient interpolation theories for elements and along strip width.

(iv) Developing a computer software based on those derivations for the static, buckling and natural frequency analysis of composite layered plates and box structures. Efficient built-in mesh generators should also be considered.

(v) Validation and justification of the developed work via case studies, involving comparison with finite element solutions.

1.3 THESIS LAYOUT

Chapter 1 gives the general introduction about the research and the finite strip method, which leads to the research objectives. It also contains a short summary of the layout of the thesis.

Chapter 2 reviews the latest status of the composite materials, the history of finite strip method and the application of the finite strip method to composite materials. It also reviews the recent modifications applied to finite strip methods such as the spline finite strip method.

Chapter 3 gives the summary of the constitutive stress-strain equations for a lamina or layer of a composite plate with respect to material and local axes. A review of the basic plate-bending theories for Kirchhoff-type, Reissner-type and the Mindlin-type elements (finite elements or finite strip elements) is presented for the case of transversely isotropic composite plates. It also contains a summary of the different one-dimensional interpolation theorems employed in this work, including the new spline-type interpolation. The chapter ends with a brief description of local and intrinsic coordinates used for trapezoidal strips together with the equations of a simple mesh generator as employed in this work.

Chapter 4 introduces a new type of finite strip elements based upon the Reissner plate bending theory. The interpolation theorems employed along the length of the plate are piecewise one-dimensional Lagrangian interpolation for in-plane components and Hermitian interpolation for the lateral deflection. This chapter also contains the derivations of stiffness and mass matrices, and equivalent nodal loading vector for practical cases of loading. A new method of derivation, based on strain energy variations, is presented where linear and non-linear terms are separated, making it easier to extract the equations for buckling analysis.

Chapter 5 reviews the derivations of Kirchhoff-type finite strip elements using the Kirchhoff plate bending theory, and the new approach of applying polynomial interpolations along the plate width. Most of the equations can be extracted from those of Reissner-type elements given in chapter 4, and only relevant equations for Kirchhoff-type elements are summarized in this chapter.

Chapter 6 introduces the derivations of new Mindlin-type finite strip elements based on the same concepts employed for Mindlin finite elements. One-dimensional Lagrangian interpolation is employed along x and y directions for all the parameters together with appropriate reduced integration schemes, but the method of derivation is similar to that employed for Reissner-type and Kirchhoff-type finite strip elements.

Chapter 7 discusses how the different finite strip elements derived in the previous chapters for composite plates can be employed for box structures, stiffened plates, and curved shells, and it also contains an algorithm to transform element matrices to the global axes for such structures. A non-linear static stress analysis algorithm, dynamic analysis (natural frequency analysis) and buckling analysis algorithm based on the equations given

in previous chapters are also explained.

Chapter 8 gives the detailed structure of the finite strip programming package, which has a fully modular structure with user-friendly data modules. The package was coded with FORTRAN 77 and has different linking options depending on the type of element and the type of analysis to be carried out. It has been tested successfully on PC's and Unix workstations.

Chapter 9 is dedicated to the description and discussion of the results by employing a number of case studies for the validation of the package. Several case studies made of different types of composite layered materials have been considered for linear and non-linear static analysis, natural frequency analysis, and buckling analysis. Finite strip results have mainly been compared with corresponding finite element results.

Chapter 10 summarises the final conclusions and some recommendations for future work.

Linking instructions of FORTRAN files to form the different programs of the package, and some samples of input data files are given in the Appendix.

Chapter 2

Literature Review

2. Literature Review

2.1 HISTORY OF FINITE STRIP METHOD

The finite strip method described in general terms in the text of Cheung (1976) has been used quite widely in the analysis of rectangular plates and plate structures, in the area of vibration and buckling analysis and with the classical plate theory (CPT) used as the model of plate bending behaviour. The early work dealing with single plates included that of Cheung & Cheung (1971) and Babu & Reddy (1971) within the context to the use of the CPT. The analysis of prismatic plate structures has been considered and also by many others, such as Cheung (1976), Cheung & Cheung (1971), Turvey & Wittrick (1973), Plank & Wittrick (1974), Dawe (1978) and Morris & Dawe (1980). Most of these analyses are of single term type either corresponding strictly to diaphragm end conditions or to the rather more general complex quantity approach that allows the presence of applied shear stress (Plank & Wittrick, 1974). However, a minority of researchers (Cheung & Cheung,1971) have used the multi term type which allows consideration of plates and plate structures of finite length which have other than diaphragm end conditions.

In the context of the use of shear deformation theory to represent out-of-plane behaviour, Dawe and his colleagues (1989,1993 and 1999) have examined the application of the approximate finite strip method to the solution of buckling and vibration problems.

For individual plates, this includes analysis of the single-term type for plates with simply supported ends (Dawe, 1978) and of the multi-type (Dawe & Wang, 1993) for plates with general end conditions and/or applied shear stress or anisotropic material behaviour: For prismatic plate assemblies, only the single term approach has been used (Dawe & Peshkam, 1989), though this has included adoption of the complex quantity philosophy to account for applied shear stress and anisotropic material when dealing with long structures (Craig & Dawe, 1987). The numerical applications in (Dawe & Peshkam, 1989) broadly demonstrate that depending upon relative thickness and precise material properties the effect of through thickness shear deformation can be significant for single plates and for plate structures when vibrating or buckling in a local mode, the effect is usually small for overall modes of plate structures.

A stress version of the finite strip method is established by Hu (1997) and is applied to orthotropic and isotropic rectangular plates. This work is based on the modified complementary energy principle and in this method stress in the strip and the displacements at the boundaries between the strips are assumed.

Michael & Averashi (1994) presented an approach to a solution based on combining the boundary element method and the finite strip method, taking the advantages of both. The finite strip method is installed into the boundary element method by expanding the unknown parameters terms of a trigonometric series and evaluating the unknown coefficients of this series. It is noted that the finite strip solution gives us a reduction of a semi-dimension in the mesh generation and the boundary element method reduces one dimension.

The finite strip method was extended to dynamic analysis of engine case and supporting system (Lu *et al.* 1994). The engine case was simplified into a revolutionary shell supported at a shaft and frame by means of several supporting plates and then was analysed by a finite strip method. The effect of the supporting plate on the revolutionary shell was considered by adding the transformed stiffness matrices of the plate to the shell stiffness matrix at the conditions of the displacement equality of contact points of the plates and the shell. The local stress near the plates and shell were obtained from substructure analysis using finite element of plate and shell.

Chan & Chung (1986) introduced a novel analytical method based on the finite strip method based on finite strip representation of a structure. By applying the U-transformation into the finite strip method, the equations of finite strip elements can be uncoupled so that the problem of the whole structure can be simplified into an equivalent problem of the single strip element.

In stress analysis, the energy principles are used in the Rayleigh Ritz method to obtain approximate solutions to elasticity problems (Khong, 1991a). In the Rayleigh Ritz method a continuum, infinite number of degrees of freedom system is approximated by a finite number of degrees of freedom system. The method thus reduces the problem to that of solving a set of simultaneous algebraic equations. This method is employed in the finite element method and the finite strip method which is concerned with replacing continuum problems with those pertaining to substitute discrete systems.

A finite strip method is used to model large deflections of plates (Cheung & Li, 1986). In this analysis the modified Newton-Raphson iteration method is used for non-linear analysis and the initial linear elastic stiffness matrix of the plate is kept unchanged during iteration to make the best use of the orthogonal property between different eigenfunctions and enhance the efficiency of the analysis but the bending stiffness matrix of the plate has to be multiplied by an amplification factor to ensure the convergence of iterations.

A hybrid finite strip method (Tarn & Sa, 1987) is developed for analysing the bending problem of multilayer laminated plates of rectangular shape. This method combines the basic ideas of hybrid stress model and the finite strip method.

2.2 APPLICATIONS OF FSM TO COMPOSITE MATERIALS

Composite materials are widely used in the current design practice of many of today's engineering disciplines. The use of composite materials in the automobile and marine engineering industries is to be noted in particular and it is envisaged that these materials will have still a wider role to play in the future as more is realised of their capabilities through continued applied research and development.

Composites have the advantage of fibre orientation is that a structural component can be tailored for a specific requirement simply by controlling the direction of the fibres and choosing a favourable ply stacking sequence.

The mechanical response of composite structural element is significantly different to that of similar conventional metallic components and thus elaborate and detailed analytical solution procedures are necessary to account for the complexities associated with the anisotropic nature of typical glass and carbon fibre composite materials. Many of the design problems in fibre reinforced composite structures stem from the fact that the fibres are joined together by a matrix material which has a relatively low strength and stiffness through the thickness of a laminated component which can be of the order of a few percent of its in-plane longitudinal strength and this gives rise to unusual failure mechanisms unique to composite construction.

A great many researchers have outlined the importance of anisotropy in composite materials. Nemeth (1986) and Grensestedt (1989) have studied the effect of the out-of-plane, bending and twisting properties pertaining to symmetrically laminated composite plates on compressive buckling capacity, The interactive in-plane and out-of-plane coupling properties associated with anti-symmetric laminated plates have been considered by Sharma *et al.* (1980), for the case of compressive loading and by Hui (1984) for the case of in-plane shear loading.

The nonlinear behaviour of rectangular laminated plates and sandwich panels was examined by Minguet *et al.* (1989), who employed the Rayleigh-Ritz method in conjunction with a direct energy minimisation technique to solve the buckling problem numerically.

The compressive behaviour of composite stiffened panels have been studied by Starns *et al.* (1985), Sheinmen *et al.* (1988) and by Snell & Greaves (1990) with regard to buckling and strength.

The effect of inter-laminar fracture toughness on the delamination buckling of composite laminates has been given some attention by Donaldson (1987), who determined the critical compressive load required to propagate delaminating cracks according to different failure criteria.

The finite strip method has been employed by Chai & Khong (1993) to study the buckling response of composite laminated plates. The reduced bending stiffness concept was utilised in the development of their finite strip formulation to account for the influence for the mechanical couplings. The results reported in these works are for the anti-symmetric cross and angle ply plates corresponding to linearly varying compressive loading and for different combinations of the support boundary conditions. The finite strip formulation of Chai & Khong (1993) uses only a single trigonometric term to represent the strip along its length and as such it is clearly limited in its application. Buckling solutions corresponding to the in-plane shear loading of composite laminates are, of course, unable to be accommodated using this formulation since the single term along the strip length is unable to represent the distorted nodal lines of the shear buckling mode and indeed gives a geometric stiffness matrix which is identically zero for the shear loading case. It is also noted that buckling response of simply supported cross-ply laminates as considered by Chai & Khong (1993) is linear.

The theoretical study of the shear buckling response of laminated composite plates has been undertaken by Hui (1984). In this work consideration is given to symmetric and anti-symmetric angle-ply laminates as well as to symmetric unbalanced laminates and configurations which are generally unsymmetric in nature. Load combinations of compression and shear are dealt with and in order to obtain buckling solution for all the lay-ups considered, clamped conditions were made to prevail at the plate boundaries. The influence of the applied shear direction on the buckling performance of anisotropic laminates is highlighted by Wang & Dawe (1997) in some detail and thus the possibility of enhancing the compressive buckling capability of some laminates through the introduction of in-plane shear loading is indicated.

The finite strip method of analysis has been used by Loughlan & Delaunoy (1993) and Loughlan (1993) to determine the buckling performance of composite stiffened panel structures. The finite strip method is able to predict the complex buckling modes associated with in-plane shear loading and the approach can allow for other loading configurations whose associated pre- buckling stresses are not so obviously realised. The non-uniform per-buckling stress associated with partial edge loading are accounted by Loughlan (1991) whilst pure shear loading and combined compression and shear loading are given consideration in (Loughlan,1993). It is also clear from (Loughlan,1991) that fibre orientation has an important role to play in composite materials construction in that a structural component can be tailored for a specific requirement by controlling the direction of the fibres to provide the best response to loading. For the case of plain flat outstands or blade stiffeners attached to one side of a thin composite skin it is shown (Loughlan & Delaunoy, 1993) that optimum stiffener depths are realised as the buckling mode changes from general to local in nature with increasing stiffener depth.

A load increment procedure is presented (Lam & Zou, 1999) for the buckling analysis of laminated plates when subjected to uniform end shortening using finite strip method. In his work the Newton-Raphson procedure is employed and the procedure is developed in the context of both classical and first- order shear deformable plate theories.

In Rayleigh-Ritz types of structural analysis, the choice of the trial displacement functions is at utmost importance. Tarn & Sa (1987) presented a finite strip method for the analysis of deep beams, shear walls and thin plates with abrupt changes of thickness.

The buckling stresses and natural frequencies of composite laminated plates and shells having arbitrary lay ups and boundary conditions were presented by Dawe & Tan (1999) by means of a general spline FSM capability developed in the framework of both the classical and the first shear deformation plate and shell theories.

Finite Strip method (Hu, 1997) is used to evaluate natural frequencies and modes of symmetrical, cylindrical honeycomb panels. In this the convergence of high-order natural frequencies versus strip division and the constraint conditions at the straight ends are considered in detail. It has been found from this work that some natural frequencies predicted are independent of the strip division and the finite strip analysis always gives one more natural frequency than the analytical solutions.

Cheung & Li (1986) have developed a finite strip method for the vibration and stability analyses of anisotropic laminated composite plates by using the higher-order shear deformation theory. This theory accounts for the parabolic distribution of the transverse shear strains through the thickness of the plate and for zero transverse shear stresses on the plate surfaces.

A finite strip method implemented on the buckling analysis of laminated composite panels is presented by Khong (1991b). In this analysis, the out of plane behaviour of the composite panel is described by thin plate theory and the deformation variations across the panel are presented by a fifth degree polynomial function. Elementary beam theory is used to account for the in-plane destabilising effects. The Rayleigh Ritz method is employed for the formulation of stiffness matrices through minimizing the total potential energy with respect to the displacement parameters.

The buckling analysis of laminated composite plates using the finite strip method was also presented by Chai & Khong (1993). In this work the plates are subjected to in-plane compression and their boundary conditions on the unloaded edges are simulated to vary from the free condition to clamp condition using a quintic polynomial function. Also along the loaded edges three different support conditions were simulated using single term trigonometric functions. The coupling influence in these laminated plates on the buckling behaviour was accounted for in the analysis through the use of the reduced stiffness bending concept.

A finite strip method was developed by Dawe *et al.* (1993) for predicting the geometrically non-linear response of rectangular composite laminates with simply supported ends when subjected to uniform end shortening in their plane. At the load ends lateral in-plane expansion may be allowed freely or may be prevented completely in different versions of the approach. The permitted laminate material properties are quite general in this case. The analysis is based on the use of the classical plate theory and the non-linearity is introduced in the strain-displacement equations.

A spline finite strip method (Sheikh, 1997) has been applied to determine the natural frequencies of plates and stiffened plates with edges elastically restrained against translation and rotation.

The problem of predicting the geometrically nonlinear response of rectangular laminated plates subjected to uniform end shortening is analysed in the context of a first-order shear deformation plate theory (Dawe *et al.* 1993). In this work finite strip method is used as the main numerical analysis procedure, with subsidiary use made of the finite element method.

Free vibration of prismatic plate structures of laminated composite material and having diaphragm end supports is considered using the finite strip method. In this method Criag & Dawe (1987) have developed stiffness and mass matrices for both out of plane and in-plane deformation of a family of strip models. Also the former deformation is based on first-order shear deformation plate theory, rather than the classical plate theory.

The dynamic stability of rectangular layered plates due to periodic in-plane load is presented by Srinivasan & Chellapandi (1986) using the finite strip method with the advantage that the problem is reduced to that of one with finite degrees of freedom, then following Bolton's procedure, the regions of parametric instability have been determined.

The prediction of buckling stresses and natural frequencies of prismatic plate structure made of composite laminated is considered (Peshkam & Dawe, 1989) using the finite strip method. In this work different analysis procedures are outlined, dependent upon whether the plate structure has finite length or is long and on whether shear deformation plate theory or classical plate theory is used. The spline finite strip method has been applied by Cheung *et al.* (1989) to the free vibration analysis of a singly curved shell panel.

2.3 SPLINE FINITE STRIP METHOD

Structures used in engineering applications have openings for functional purposes. The elastic analysis of floor slabs with rectangular opening or wide column supports by classical plate theory predicts singular moments and shear forces at the corners of such openings and supports. Although the FEM guarantees a solution, the rate of convergence may be significantly reduced, and to overcome this either the finite element mesh is refined locally or a special purpose finite element model based on hybrid stress formulation is used (Wang & Dawe 1997).

The first option leads to a large number of degrees of freedom, thereby increasing the computational time. The second option is more complicated and time consuming than the displacement based FEM and the FSM will face difficulty in modelling the problems with steep stress gradients, due to the higher order continuity of their displacement functions (Tham, 1990, Madasamy, 1993, and Cheung & Li, 1986).

In order to overcome these problems the spline finite strip method (SFSM) based on classical thin plates theory has been used. The spline finite strip method was developed by Cheung & Fan (1983) as an alternative of FSM. The unknowns in the SFSM are the displacement parameters at the intersection knots of the longitudinal nodal lines and transverse sections.

The SFSM adopts B3-splines as displacement function in the longitudinal direction and cubic Hermite shape functions in the transverse direction. The B3- splines are continuous over four sections and the overall displacement representation in the longitudinal direction is given by a linear combination of the local B3-splines. If the section knots are equally spaced the B3-spline function has C^2 continuity and this order of continuity can be lowered to C^1 or C^0 near the stress concentration regions by using uneven spacing of the section knots.

The rate of convergence of the deflections and stresses can be increased by using unequal section knots of B3-splines in plate bending analysis using SFSM and this has been demonstrated by Chen *et al.* (1991) for rectangular plates.

The SFSM results indicated monotonic convergence of stress instead of oscillatory convergence of stress (Gibb's phenomenon) encountered while using FSM. The SFSM results are more accurate with a fewer global degrees of freedom compared to FSM, as discussed by Cheung & Fan (1983).

The large amplitude free flexural vibration of stiffened plates has been investigated by Sheikh, Abdul Hamid (1997) using spline finite strip method. In this work the effect of large amplitude have been taken into account by adopting Von Karman's large deflection plate bending theory and the formulation has been done in the total Langrangian coordinate system. The stiffener has been elegantly modelled so that it can be placed anywhere within the plate strip and it need not to follow the nodal lines.

The stability of shear-deformable plates under constant initial stresses was studied by the spline finite strip method (Cheung & Kong, 1995) Third order plate theory was used as the basis for developing the strip element. The classical B3-spline function is modified in such a way that the resulting spline finite strip element incorporates the merits of spline interpolation and the versatility of the finite strip method.

Dawe & Tan (1997) have used the spline finite strip method to predict the natural frequencies and buckling stresses of rectangular plates which have one or more step changes in properties along their length. The main step changes of interest are those of thickness and such step changes can occur at arbitrary locations in many practical situations.

The spline finite strip method (Tham & Szeto, 1990) was applied to the buckling analysis of arbitrary shaped plates. The plate is first mapped into a rectangular domain in the natural coordinate planes by the sub-parametric transformation and the mapped plate was discretised into a number of strips. The displacements of each strip were described by interpolation functions which were given as products of piecewise polynomials and B-3 spline functions. The eigenvalue matrix equation for the buckling analysis was then formulated and solved by the same procedure as that of the standard finite element method.

The basic disadvantages of the SFSM are the difficulties of the derivation of spline functions, and in the associating physical meanings to the nodal values, making it difficult to cope with different types of boundary conditions along the strip width.

Chapter 3

Introductory Concepts

3. Introductory Concepts

3.1 INTRODUCTION

In this chapter, the constitutive stress-strain equations for a lamina or layer of a composite plate are summarised with respect to material and local axes. For plate analysis, the values of σ_z and ε_z are negligible or function of other components, and will be excluded from the equations. Transverse isotropy may be assumed to simplify the stress-strain equations.

A review of the basic plate-bending theories for Kirchhoff-type, Reissner-type and Mindlin-type elements (finite elements or finite strip elements) is presented for the case of transversely isotropic composite plate. A summary of the different one-dimensional interpolation theorems employed in this work, including the new spline-type interpolation, is given. The chapter ends with a brief description of local and intrinsic coordinates used for trapezoidal strips together with the equations of a simple mesh generator as employed in this work.

3.2 STRESS-STRAIN RELATIONSHIPS FOR LAYERED COMPOSITES

A composite layered plate or shell usually consists of a number of layers *(N_l)* bonded firmly with each other. Each layer is a lamina and it is flat for plates and curved for shells, and it represents an assemblage of reinforcing fibres in a supporting isotropic matrix. The material properties of the layer are defined with respect to the material principal axes $x`$, $y`$, $z`$ such that ; the $z`$ axis is normal to the midsurface of the layer and the $x`$, $y`$ axes are normal to the $z`$ axis, i.e. they are in the midplane of the layer for the case of plates and tangential to the midsurface of the layer for the case of curved shells.

The material properties which are required for an elastic analysis are:

$E_x^`$ , $E_y^`$, $E_z^`$ Young's moduli in the $x`$, $y`$, $z`$ directions respectively,

$\nu_{xy}^`$, $\nu_{yz}^`$, $\nu_{zx}^`$ Poisson's ratios, with respect to $x`$, $y`$, $z`$ axes, and

$\mu_{xy}^`$, $\mu_{yz}^`$, $\mu_{zx}^`$ Shear moduli, with respect to $x`$, $y`$, $z`$ axes.

In this work different layers will be assumed of the same original composite material, i.e. the above properties will be the same for every layer and the density ρ is also the same for all layers. Since the transverse shear stresses and strains are small or negligible, we consider the composite material to be transversely isotropic with respect to the $y` - z`$ plane, i.e. $E_y^` = E_z^`$, $\nu_{yz}^` = \nu_{zx}^`$, $\mu_{yz}^` = \mu_{zx}^`$.

The stress and strain states at any point inside a layer may be defined in terms of the following stress and strain vectors:

$$\sigma_{6\times1} = \{\sigma_x \quad \sigma_y \quad \sigma_z \quad \tau_{xy} \quad \tau_{yz} \quad \tau_{zx}\} \tag{3.1}$$

$$\varepsilon_{6\times1} = \{\varepsilon_x \quad \varepsilon_y \quad \varepsilon_z \quad \gamma_{xy} \quad \gamma_{yz} \quad \gamma_{zx}\} \tag{3.2}$$

and for an orthotropic layer, the elastic stress-strain equations may be expressed in the following matrix form:

$$\boldsymbol{\varepsilon}^{\backprime} = \boldsymbol{C}^{\backprime}\,\boldsymbol{\sigma}^{\backprime} \tag{3.3}$$

and $$\boldsymbol{\sigma}^{\backprime} = \boldsymbol{D}^{\backprime}\,\boldsymbol{\varepsilon}^{\backprime} \tag{3.4}$$

where $\boldsymbol{D}^{\backprime} = \boldsymbol{C}^{\backprime -1}$ (3.5)

and

$$\boldsymbol{C}^{\backprime} = \begin{bmatrix} \frac{1}{E_x^{\backprime}} & -\frac{\nu_{yx}^{\backprime}}{E_y^{\backprime}} & -\frac{\nu_{zx}^{\backprime}}{E_z^{\backprime}} & 0 & 0 & 0 \\ -\frac{\nu_{xy}^{\backprime}}{E_x^{\backprime}} & \frac{1}{E_y^{\backprime}} & -\frac{\nu_{zy}^{\backprime}}{E_z^{\backprime}} & 0 & 0 & 0 \\ -\frac{\nu_{xz}^{\backprime}}{E_x^{\backprime}} & -\frac{\nu_{yz}^{\backprime}}{E_y^{\backprime}} & \frac{1}{E_z^{\backprime}} & 0 & 0 & 0 \\ 0 & 0 & 0 & \frac{1}{\mu_{xy}^{\backprime}} & 0 & 0 \\ 0 & 0 & 0 & 0 & \frac{1}{\mu_{yz}^{\backprime}} & 0 \\ 0 & 0 & 0 & 0 & 0 & \frac{1}{\mu_{zx}^{\backprime}} \end{bmatrix} \tag{3.6}$$

where $(\,)^{\backprime}$ refers to properties measured with respect to $x^{\backprime}$, $y^{\backprime}$, $z^{\backprime}$ axes, and from the symmetry of the $\boldsymbol{C}^{\backprime}$ matrix it can be deduced that:

$$\frac{\nu_{yx}^{\backprime}}{E_y^{\backprime}} = \frac{\nu_{xy}^{\backprime}}{E_x^{\backprime}}, \quad \frac{\nu_{zx}^{\backprime}}{E_z^{\backprime}} = \frac{\nu_{xz}^{\backprime}}{E_x^{\backprime}}, \quad \frac{\nu_{zy}^{\backprime}}{E_z^{\backprime}} = \frac{\nu_{yz}^{\backprime}}{E_y^{\backprime}}$$

Using minors and cofactors the $\boldsymbol{C}^{\backprime}$ matrix can be inverted, resulting in the following $\boldsymbol{D}^{\backprime}$ matrix:

$$\boldsymbol{D}^{\backprime} = \left[\begin{array}{c|ccc} \boldsymbol{d}^{\backprime}{}_{3\times3} & \multicolumn{3}{c}{\mathbf{O}_{3\times3}} \\ \hline & \mu_{xy}^{\backprime} & 0 & 0 \\ \mathbf{O}_{3\times3} & 0 & \mu_{yz}^{\backprime} & 0 \\ & 0 & 0 & \mu_{zx}^{\backprime} \end{array}\right] \tag{3.7}$$

$$\text{where } d'_{3\times3} = \frac{1}{Q}\begin{bmatrix} E'_x(1-\nu'_{yz}\nu'_{zy}) & E'_x(\nu'_{yx}+\nu'_{zx}\nu'_{yz}) & E'_x(\nu'_{zx}+\nu'_{yx}\nu'_{zy}) \\ E'_y(\nu'_{xy}+\nu'_{zy}\nu'_{xz}) & E'_y(1-\nu'_{xz}\nu'_{zx}) & E'_y(\nu'_{zy}+\nu'_{xy}\nu'_{zx}) \\ E'_z(\nu'_{xz}+\nu'_{yz}\nu'_{xy}) & E'_z(\nu'_{yz}+\nu'_{xz}\nu'_{yx}) & E'_z(1-\nu'_{xy}\nu'_{yx}) \end{bmatrix} \tag{3.7a}$$

$$\text{and} \quad Q = 1 - \nu'_{xy}\nu'_{yx} - \nu'_{yz}\nu'_{zy} - \nu'_{zx}\nu'_{xz} - \nu'_{xy}\nu'_{yz}\nu'_{zx} - \nu'_{xz}\nu'_{zy}\nu'_{yx} \tag{3.7b}$$

Generally the layers of composite plates or shells are made of the same material, but each lamina (layer) has its fibres placed in a different angle, *i.e.* each layer l will have different x', y' axes, rotated by an angle θ_l from element local x, y, z axes. For the case of plates, the local z axis is always normal to the layer midplane and in the direction of the material z' axis, and it is useful to define the material axes with respect to element local axes in terms of the angle θ_l.

Using rotated equations for stress and strain matrices, the stress-strain equations with respect to the local axes of the element $\{x, y, z\}$, can be expressed as follows:

$$\boldsymbol{\sigma}_{6\times1} = \boldsymbol{D}_{6\times6}\ \boldsymbol{\varepsilon}_{6\times1} \tag{3.8}$$

where the rotated $\boldsymbol{D}$ matrix can be expanded and represented by the following terms:

$$d_{11} = m^4 d'_{11} + n^4 d'_{22} + 2m^2n^2(d'_{12}+2d'_{44})$$

$$d_{22} = n^4 d'_{11} + m^4 d'_{22} + 2m^2n^2(d'_{12}+2d'_{44})$$

$$d_{12} = m^2n^2(d'_{11}+d'_{22}) + (m^4+n^4)d'_{12} - 4m^2n^2 d'_{44}$$

$$d_{13} = m^2 d'_{13} + n^2 d'_{23}$$

$$d_{23} = n^2 d'_{13} + m^2 d'_{23}$$

$$d_{14} = -mn\left[n^2 d'_{22} - m^2 d'_{11} + (m^2-n^2)(d'_{12}+2d'_{44})\right]$$

$$d_{24} = -mn\left[m^2 d'_{22} - n^2 d'_{11} + (n^2-m^2)(d'_{12}+2d'_{44})\right]$$

$$d_{15} = d_{16} = d_{25} = d_{26} = 0$$

$$d_{33} = d'_{33}$$

$$
\begin{aligned}
d_{34} &= -mn(d_{23}^{\backprime} - d_{13}^{\backprime}) \\
d_{44} &= m^2 n^2 (d_{11}^{\backprime} + d_{22}^{\backprime} - 2d_{12}^{\backprime}) + (m^2 - n^2)^2 d_{44}^{\backprime} \\
d_{35} &= d_{36} = d_{45} = d_{46} = 0 \\
d_{55} &= m^2 d_{55}^{\backprime} + n^2 d_{66}^{\backprime} \\
d_{66} &= n^2 d_{55}^{\backprime} + m^2 d_{66}^{\backprime} \\
d_{56} &= -mn(d_{55}^{\backprime} - d_{66}^{\backprime}) \\
d_{ji} &= d_{ij}
\end{aligned}
$$

and $m = \cos\theta, \quad n = \sin\theta.$

For the lth layer, equation (3.8) can be partitioned as follows:

$$
\begin{bmatrix} \sigma_x \\ \sigma_y \\ \tau_{xy} \end{bmatrix} = \boldsymbol{D}^{(l)} \begin{bmatrix} \varepsilon_x \\ \varepsilon_y \\ \gamma_{xy} \end{bmatrix} \tag{3.9}
$$

$$
\text{and} \quad \begin{bmatrix} \tau_{xz} \\ \tau_{yz} \end{bmatrix} = \boldsymbol{\mu}^{(l)} \begin{bmatrix} \gamma_{xz} \\ \gamma_{yz} \end{bmatrix} \tag{3.10}
$$

$$
\text{where} \quad \boldsymbol{D}^{(l)} \equiv \begin{bmatrix} d_{11} & d_{12} & d_{14} \\ d_{21} & d_{22} & d_{24} \\ d_{41} & d_{42} & d_{44} \end{bmatrix} \tag{3.11}
$$

$$
\text{and} \quad \boldsymbol{\mu}^{(l)} \equiv \begin{bmatrix} d_{55} & d_{56} \\ d_{65} & d_{66} \end{bmatrix} \tag{3.12}
$$

with the d_{ij} as been defined previously. Notice also that for the case with $\mu_{31} = \mu_{32} = \mu$, the transverse shear modulus, then for every layer:

$$
\boldsymbol{\mu}^{(l)} \equiv \begin{bmatrix} \mu & 0 \\ 0 & \mu \end{bmatrix}.
$$

3.3 PLATE BENDING THEORIES

3.3.1 Basic assumptions

Consider a plate defined in terms of a midplane in the Cartesian x-y plane, and a thickness distribution $h(x, y)$ measured in the z-direction, as shown in figure 3.1. The upper surface of the plate $(z = h/2)$ is considered been subjected to a shear force per unit area $q_u(x, y)$ and the lower surface $(z = -h/2)$ is subjected to a shear force per unit area $q_l(x, y)$. Other types of loading may also be considered, as will be discussed within finite strip derivations.

Plate theories are based upon the following assumptions and approximations:

(i) The composite material of the plate is homogeneous, and linearly elastic. The stress-strain relationships are, therefore, governed by equation (3.8).

(ii) Displacement gradients are finite, such that Cauchy's strain-displacement relationships are no longer acceptable, and large deflection analysis will be considered. However, the transverse shear strains are assumed infinitesimal and continuous along the plate width.

(iii) The midplane remains unstrained after bending, i.e. it is a neutral plane in bending.

(iv) The lateral deflection w, the displacement component in the z-direction, is independent of z, i.e. $w \approx w(x, y)$.

For thin plates, the following additional assumptions are also considered.

(v) The transverse shear strains; γ_{xz}, γ_{yz} are negligible, leading to plane sections initially normal to the midsurface remain plane and normal to the midsurface after bending.

(vi) The transverse normal stress σ_z is small compared with other stress components and can be neglected.

3.3.2 Transverse stress modelling

Considering the equation of surface traction at the upper surface of the plate, it can be deduced that:

$$\tau_{xz} = \tau_{yz} = 0, \quad \sigma_z = q_u \tag{3.13}$$

Similarly, at the lower surface of the plate:

$$\tau_{xz} = \tau_{yz} = 0, \quad \sigma_z = -q_l \tag{3.14}$$

Hence, it can also be deduced that:

$$\gamma_{xz} = \gamma_{yz} = 0 \quad \text{at } z = \pm h/2 \tag{3.15}$$

Using a three-point Lagrangian interpolation (Hegaze, 2002), then parabolic distributions of γ_{xz} and γ_{yz} may be obtained in terms of their values at the three points; $z_1 = -h/2$, $z_2 = 0$,

$z_3 = +h/2$, as follows:

$$\gamma_{xz} = \gamma^{o}_{xz}(x,y)\left[1 - \frac{4z^2}{h^2}\right] \tag{3.16}$$

$$\gamma_{yz} = \gamma^{o}_{yz}(x,y)\left[1 - \frac{4z^2}{h^2}\right] \tag{3.17}$$

where γ^{o}_{xz}, γ^{o}_{yz} are the values of transverse shear strains at $z = 0$.

3.3.3 Displacement equations for thin plates

Using the previous assumptions, and strain-displacement relationships, it can be shown that:

$$\left.\begin{aligned} \frac{\partial u}{\partial z} &= \gamma_{xz} - \frac{\partial w}{\partial x} \approx -\frac{\partial w}{\partial x} \\ \frac{\partial v}{\partial z} &= \gamma_{yz} - \frac{\partial w}{\partial y} \approx -\frac{\partial w}{\partial y} \end{aligned}\right\} \tag{3.18}$$

where u, v are the displacement components in the x and y directions, respectively. Integrating the previous equations with respect to z, it can be shown that:

$$\left.\begin{aligned} u(x,y,z) &= u^{o}(x,y) - z\frac{\partial w}{\partial x} \\ v(x,y,z) &= v^{o}(x,y) - z\frac{\partial w}{\partial y} \end{aligned}\right\} \tag{3.19}$$

where u^{o}, v^{o} are displacement components at $z = 0$. These equations will be employed for Kirchhoff-type elements.

3.3.4 Displacement equations for thick plates

It can be deduced from equations (3.16), (3.17) that:

$$\gamma_{xz} = \gamma^{o}_{xz}\left[1 - \frac{4z^2}{h^2}\right] \equiv \frac{\partial u}{\partial z} + \frac{\partial w}{\partial x}$$

and $$\gamma_{yz} = \gamma^{o}_{yz}\left[1 - \frac{4z^2}{h^2}\right] \equiv \frac{\partial v}{\partial z} + \frac{\partial w}{\partial y}$$

i.e. $$\frac{\partial u}{\partial z} = -\frac{\partial w}{\partial x} + \gamma^{o}_{xz}\left[1 - \frac{4z^2}{h^2}\right]$$

and $$\frac{\partial v}{\partial z} = -\frac{\partial w}{\partial y} + \gamma_{yz}^{o}\left[1 - \frac{4z^2}{h^2}\right]$$

Integrating the previous equations with respect to z, it can be proved that:

$$u(x,y,z) = u^{o}(x,y) - z\frac{\partial w}{\partial x} + \gamma_{xz}^{o}\left[z - \frac{4z^3}{3h^2}\right] \tag{3.20}$$

$$v(x,y,z) = v^{o}(x,y) - z\frac{\partial w}{\partial y} + \gamma_{yz}^{o}\left[z - \frac{4z^3}{3h^2}\right] \tag{3.21}$$

To simplify the thick plate problem, transverse shear stresses and strains averaged over the thickness may be employed without violating equilibrium or strain energy contributions. Defining average transverse shear stresses $\bar{\tau}_{xz}$, $\bar{\tau}_{yz}$ so as to maintain internal equilibrium, then:

$$(Q_x, Q_y) = \int_{-h/2}^{h/2} (\bar{\tau}_{xz}, \bar{\tau}_{yz})\, dz \equiv \int_{-h/2}^{h/2} (\tau_{xz}, \tau_{yz})\, dz \tag{3.22}$$

i.e. $$\bar{\tau}_{xz} = \frac{Q_x}{h} \equiv \frac{2}{3}\mu\,\gamma_{xz}^{o}, \quad \bar{\tau}_{yz} = \frac{Q_y}{h} \equiv \frac{2}{3}\mu\,\gamma_{yz}^{o} \tag{3.23}$$

Defining average transverse shear strains $\bar{\gamma}_{xz}$, $\bar{\gamma}_{yz}$ so as to maintain strain energy contributions, then:

$$\int_{-h/2}^{h/2} \bar{\tau}_{xz}\bar{\gamma}_{xz}\, dz \equiv \int_{-h/2}^{h/2} \tau_{xz}\gamma_{xz}\, dz \tag{3.24}$$

and $$\int_{-h/2}^{h/2} \bar{\tau}_{yz}\bar{\gamma}_{yz}\, dz \equiv \int_{-h/2}^{h/2} \tau_{yz}\gamma_{yz}\, dz \tag{3.25}$$

Considering first equation (3.24), then it can be deduced that:

$$h\,\bar{\tau}_{xz}\bar{\gamma}_{xz} = \frac{9\,\bar{\tau}_{xz}^2}{4\mu}\int_{-h/2}^{h/2}\left(1 - \frac{4z^2}{h^2}\right)^2 dz$$

i.e. $$\bar{\gamma}_{xz} = \bar{\tau}_{xz} / \frac{5}{6}\mu \tag{3.26}$$

Similarly, it can be deduced from equation (3.25) that:

$$\bar{\gamma}_{yz} = \bar{\tau}_{yz} / \frac{5}{6}\mu \tag{3.27}$$

Comparing with equation (3.23), it can also be shown that:

$$\gamma^{o}_{xz} = \frac{5}{4}\bar{\gamma}_{xz}, \quad \gamma^{o}_{yz} = \frac{5}{4}\bar{\gamma}_{yz} \tag{3.28}$$

and equations (3.20), (3.21) can be rewritten as follows:

$$u(x,y,z) = u^{o}(x,y) - z\frac{\partial w}{\partial x} + \frac{5}{4}\bar{\gamma}_{xz}\left[z - \frac{4z^3}{3h^2}\right] \tag{3.29}$$

$$v(x,y,z) = v^{o}(x,y) - z\frac{\partial w}{\partial y} + \frac{5}{4}\bar{\gamma}_{yz}\left[z - \frac{4z^3}{3h^2}\right] \tag{3.30}$$

which will be employed for Reissner-type elements.

If averaged displacement components are defined according to strain-displacement equations of averaged strains, then:

$$\bar{\gamma}_{xz} = \frac{\partial \bar{u}}{\partial z} + \frac{\partial w}{\partial x} \tag{3.31}$$

$$\bar{\gamma}_{yz} = \frac{\partial \bar{v}}{\partial z} + \frac{\partial w}{\partial y} \tag{3.32}$$

and it can be deduced that:

$$\bar{u}(x,y,z) = u^{o}(x,y) - z\left(\frac{\partial w}{\partial x} - \bar{\gamma}_{xz}\right)$$

$$\equiv u^{o}(x,y) + z\theta_y \tag{3.33}$$

$$\bar{v}(x,y,z) = v^{o}(x,y) - z\left(\frac{\partial w}{\partial y} - \bar{\gamma}_{yz}\right)$$

$$\equiv v^{o}(x,y) - z\theta_x \tag{3.34}$$

where $\theta_x = \frac{\partial w}{\partial y} - \bar{\gamma}_{yz}$ (3.35)

and $\theta_y = -\left(\frac{\partial w}{\partial x} - \bar{\gamma}_{xz}\right)$ (3.36)

which are the corresponding average slope angles. Equations (3.33) and (3.34) will be employed for Mindlin-type elements.

3.4 INTERPOLATION THEOREMS

Three different one-dimensional interpolation theorems are employed in this work. They are summarized for the functions of an intrinsic coordinate ξ, where $0 \leq \xi \leq 1$, as follows:

3.4.1 Lagrangian interpolation theorem

Defining a function $f(\xi)$ in terms of $f_1, f_2, ..., f_n$ at $\xi_1, \xi_2, ..., \xi_n$ then according to Lagrange's interpolation theorem (Kopal, 1961):

$$f(\xi) = \sum_{i=1}^{n} \mathcal{L}_i^n(\xi) f_i \tag{3.37}$$

where Lagrange's multipliers are defined as follows:

$$\mathcal{L}_i^n(\xi) = \prod_{\substack{r=1, \\ r \neq i}}^{n} \frac{\xi - \xi_r}{\xi_i - \xi_r} \tag{3.38}$$

and for the special case of points at equal distances, or

$$\xi_r = \frac{r-1}{n-1} \tag{3.39}$$

it can be deduced that:

$$\mathcal{L}_i^n(\xi) = \prod_{\substack{r=1, \\ r \neq i}}^{n} \frac{(n-1)\xi - (r-1)}{i - r} \tag{3.40}$$

3.4.2 C^1-continuous Hermitian interpolation theorem

Consider a field function $f(\xi)$ defined in terms of its values, and the values of its first order derivative at $\xi_1, \xi_2, ..., \xi_n$ where

$$f_i \equiv f(\xi_i), \quad f_{i,\xi} \equiv \frac{df}{d\xi} \quad \text{at } \xi_i$$

Then using Hermitian interpolation theorem (Kopal, 1961):

$$f(\xi) = \sum_{i=1}^{n} [\, g_i(\xi) f_i + h_i(\xi) f_{i,\xi} \,] \tag{3.41}$$

where $g_i(\xi) = \left[1 - 2\alpha_i(\xi - \xi_i) \right] \left[\mathcal{L}_i^n(\xi) \right]^2$ (3.42)

$$h_i(\xi) = (\xi - \xi_i) \left[\mathcal{L}_i^n(\xi) \right]^2 \tag{3.43}$$

and $\alpha_i \equiv \sum_{\substack{r=1, \\ r \neq i}}^{n} \frac{1}{\xi_i - \xi_r}$ (3.44)

If $\xi_r = \dfrac{r-1}{n-1}$, then $\xi_i = \dfrac{i-1}{n-1}$, and it can be deduced that:

$$\alpha_i = \sum_{\substack{r=1,\\ r\neq i}}^{n} \frac{n-1}{i-r} \tag{3.45}$$

3.4.3 C^1-continuous spline-type interpolation

The conditions for this type of interpolation are:

at ξ_1: $f_1, f_{1,\xi}$ are given,

at ξ_n: $f_n, f_{n,\xi}$ are given,

at ξ_i, $1<i<n$: only f_i is given.

Using El-Zafrany & Cookson (1985), the interpolation equation can be expressed as follows:

$$f(\xi) = \sum_{i=1}^{n} [\, g_i^s(\xi) f_i + h_i^s(\xi) f_{i,\xi} \,] \tag{3.46}$$

where $g_1^s(\xi) = [\,1+(1-\alpha_1)\,\xi\,](1-\xi)\mathcal{L}_1^n(\xi)$ (3.47)

$$h_1^s(\xi) = \xi(1-\xi)\mathcal{L}_1^n(\xi) \tag{3.48}$$

$$g_n^s(\xi) = [\,1+(1+\alpha_n)(1-\xi)\,]\,\xi\,\mathcal{L}_n^n(\xi) \tag{3.49}$$

$$h_n^s(\xi) = -\xi(1-\xi)\mathcal{L}_n^n(\xi) \tag{3.50}$$

and for $1<i<n$:

$$g_i^s(\xi) = \frac{\xi(1-\xi)}{\xi_i(1-\xi_i)}\mathcal{L}_i^n(\xi), \quad h_i^s(\xi) = 0 \tag{3.51}$$

Notice that when $n = 2$, the previous interpolation is the same as the Hermitian interpolation.

3.5 STRIP GENERATION AND INTRINSIC COORDINATES

We shall consider a general trapezoidal panel, as shown in figure 3.2, where the mid-plane is defined geometrically in terms of:

L = Length of the panel in x-direction,

B_1 = First width in y- direction,

B_2 = Second width in y-direction,

and to define the axes precisely, x will start from the LHS edge and the two lower corners have y_1, y_2 as their given y coordinates.

3.5.1 Generation of strip

A number say m_s of n-node strips is assumed, each strip (e) will have the following length:

$$l = L/m_s = \text{constant} \quad \text{(for simplicity).}$$

The equation of the lower edge of the panel is:

$$\frac{y - y_1}{y_2 - y_1} = \frac{x - 0}{L - 0}$$

$$\text{or} \qquad y = y_1 + \frac{(y_2 - y_1)}{L} x \tag{3.52}$$

and for the strip abcd of number e:

$$x_a = x_d = (e - 1)\frac{L}{m_s} = (e - 1)l \tag{3.53}$$

$$x_b = x_c = e\frac{L}{m_s} = el \tag{3.54}$$

where $e = 1, 2, ..., m_s$

Notice also that:

$$y_a = y_1 + \frac{(e - 1)}{m_s}(y_2 - y_1) \tag{3.55}$$

$$y_b = y_1 + \frac{e}{m_s}(y_2 - y_1) \tag{3.56}$$

The equation of the upper edge is therefore:

$$\frac{y - (y_1 + B_1)}{(y_2 + B_2) - (y_1 + B_1)} = \frac{x}{L}$$

Hence

$$y = y_1 + B_1 + \left[(y_2 - y_1) + (B_2 - B_1)\right]\frac{x}{L} \tag{3.57}$$

and it can be deduced that:

$$y_d = y_1 + B_1 + \frac{(e - 1)}{m_s}\left[(y_2 - y_1) + (B_2 - B_1)\right] \tag{3.58}$$

$$\text{and} \qquad y_c = y_1 + B_1 + \left(\frac{e}{m_s}\right)\left[(y_2 - y_1) + (B_2 - B_1)\right] \tag{3.59}$$

then the widths of the opposite sides of strip abcd are:

$$b_1 = y_d - y_a = B_1 + \left(\frac{e - 1}{m_s}\right)(B_2 - B_1) \tag{3.60}$$

$$b_2 = y_c - y_b$$

$$= B_1 + \left(\frac{e}{m_s}\right)(B_2 - B_1) \tag{3.61}$$

3.5.2 Generation of nodes on *x*-line

Every new n-node strip will add only $n - 1$ nodes to the previous one, i.e.

Total number of nodes $N = n + (m_s - 1)(n - 1)$

or $$N = m_s(n - 1) + 1 \tag{3.62}$$

and for every ith node (as a global number)

$$x_i = \left(\frac{i - 1}{N - 1}\right)L \tag{3.63}$$

if all the nodes are equally spaced.

3.5.3 Topology array for each *e*th strip

The first node of each of eth strip is $(e - 1)(n - 1) + 1$,

and for jth local node in the eth strip , its global number is:

$$TA(e, j) = (e - 1)(n - 1) + j \tag{3.64}$$

3.5.4 Intrinsic coordinates for the *e*th strip

We shall use x local measured from LHS edge of the strip with

$$\xi = x/l \tag{3.65}$$

From figure 3.3, the equation of the lower edge ab can be obtained from:

$$\xi = \frac{x}{l} = \frac{y_l(x) - y_a}{y_b - y_a}$$

i.e. $$y_l(x) = y_a + \xi(y_b - y_a) \tag{3.66}$$

Similarly

$$b(x) = b_1 + \xi(b_2 - b_1) \tag{3.67}$$

An intrinsic coordinate η, is defined such that:

$$\eta(\xi) = \frac{y - y_l(\xi)}{b(\xi)}$$

Hence

$$y(\xi, \eta) = b(\xi)\eta + y_l(\xi) \tag{3.69}$$

3.5.5 Double integrals over the strip

Differentiating equation (3.69) at ξ = constant:

$$dy = b(\xi)\, d\eta \equiv J_y(\xi)\, d\eta \tag{3.70}$$

where $J_y(\xi) = b(\xi)$. (3.71)

Similarly, from equation (3.65):

$$dx = l\, d\xi \equiv J_x\, d\xi \tag{3.72}$$

where $J_x = l$. (3.73)

Hence, it can be deduced that:

$$\int\int_{strip} f(\xi, \eta)\, dy\, dx \equiv \int_0^1\int_0^1 f(\xi, \eta)\, J_y(\xi)\, J_x\, d\eta\, d\xi \tag{3.74}$$

which can be evaluated numerically using the modified Gaussian quadrature (El-Zafrany, 2000).

Chapter 4

Reissner-Type Finite Strip Elements

4. Reissner-Type Finite Strip Elements

4.1 INTRODUCTION

This chapter introduces a new type of finite strip element based upon the Reissner plate bending theory, in which parabolic distributions for transverse shear strains are assumed. The interpolation theorems employed along the length of the plate are piecewise one-dimensional Lagrangian interpolation for in-plane components and Hermitian interpolation for the lateral deflection. Along the plate width, different types of one-dimensional polynomial or harmonic interpolation can be applied. The use of polynomial interpolation will result in fully coupled equations, but this is always the case for non-linear and buckling analysis.

We started with Reissner-type elements as they represent the most general elements in this work, whilst the special cases of Kirchhoff-type and Mindlin-type elements will be summarised in chapters 5 and 6, respectively.

This chapter contains the derivations of stiffness and mass matrices, and equivalent nodal loading vector for practical cases of loading. A new method of derivation, based on strain energy variations, is presented where linear and non-linear terms are separated, making it easier to extract the equations for buckling analysis. Separate matrices associated with different terms (or harmonics) of interpolation along the width are formulated thus minimizing computer memory requirements, when programming those derivations.

4.2 STRESS AND STRAIN EQUATIONS

4.2.1 Displacement equations

Consider a composite layered plate at an instant of time t consisting of a number of orthotropic layers. Let the midplane of the plate be the Cartesian x-y plane, and the total thickness at any point (x,y) on the midplane is h, then based on the assumptions and approximations given in section 3.3.1, the displacement equations at any point (x,y,z) inside the plate can be expressed as follows:

$$u(x,y,z,t) = u^{o}(x,y,t) - z\frac{\partial w}{\partial x} - \psi_y\left[\frac{3}{2}z - \frac{2z^3}{h^2}\right] \tag{4.1}$$

$$v(x,y,z,t) = v^{o}(x,y,t) - z\frac{\partial w}{\partial y} + \psi_x\left[\frac{3}{2}z - \frac{2z^3}{h^2}\right] \tag{4.2}$$

where u^{o}, v^{o} represent the values of u, v at $z = o$, and

$$\psi_x = \frac{2}{3}\gamma^{o}_{yz} = \bar{\gamma}_{yz}, \quad \psi_y = -\frac{2}{3}\gamma^{o}_{xz} = -\bar{\gamma}_{xz}$$

The lateral deflection w will be approximated in this work such that it will be considered independent of z i.e.

$$w(x,y,z,t) \approx w(x,y,t) \tag{4.3}$$

The velocity components can be expressed by differentiating equations (4.1)-(4.3) with respect to time, i.e.

$$\dot{u}(x,y,z,t) = \dot{u}^{o}(x,y,t) - z\frac{\partial \dot{w}}{\partial x} - \dot{\psi}_y\left[\frac{3}{2}z - \frac{2z^3}{h^2}\right] \tag{4.4}$$

$$\dot{v}(x,y,z,t) = \dot{v}^{o}(x,y,t) - z\frac{\partial \dot{w}}{\partial y} + \dot{\psi}_x\left[\frac{3}{2}z - \frac{2z^3}{h^2}\right] \tag{4.5}$$

$$\dot{w}(x,y,z,t) \approx \dot{w}(x,y,t) \tag{4.6}$$

where $\dot{f} = \dfrac{\partial f}{\partial t}$.

Differentiating the above equations again with respect to time, the acceleration components can be obtained as follows:

$$\ddot{u}(x,y,z,t) = \ddot{u}^{o}(x,y,t) - z\frac{\partial \ddot{w}}{\partial x} - \ddot{\psi}_y\left[\frac{3}{2}z - \frac{2z^3}{h^2}\right] \tag{4.7a}$$

$$\ddot{v}(x,y,z,t) = \ddot{v}^{o}(x,y,t) - z\frac{\partial \ddot{w}}{\partial y} + \ddot{\psi}_x\left[\frac{3}{2}z - \frac{2z^3}{h^2}\right] \tag{4.7b}$$

$$\ddot{w}(x,y,z,t) \approx \ddot{w}(x,y,t) \tag{4.8}$$

where $\ddot{f} = \dfrac{\partial^2 f}{\partial t^2}$.

In the remaining parts of this chapter, except in section 4.7, we shall ignore the parameter t, with the understanding that for static analysis element equations are independent of time, which has only to be considered for dynamic analysis.

4.2.2 Strain components

4.2.2.1 Transverse shear strains

These are always assumed infinitesimal and are as defined by the following equations

$$\gamma_{xz} = -\frac{3}{2}\psi_y(x,y)\left[1 - \frac{4z^2}{h^2}\right] \tag{4.9}$$

$$\gamma_{yz} = \frac{3}{2}\psi_x(x,y)\left[1 - \frac{4z^2}{h^2}\right] \tag{4.10}$$

The previous equations can be written in a matrix form as follows:

$$\gamma = \begin{bmatrix}\gamma_{xz}\\ \gamma_{yz}\end{bmatrix} = f_\gamma(z) \quad \hat{\gamma}(x,y) \tag{4.11}$$

where $f_\gamma = \frac{3}{2}\left[1 - \frac{4z^2}{h^2}\right]$ (4.12)

and $\hat{\gamma}(x,y) = \begin{bmatrix} -\psi_y \\ +\psi_x \end{bmatrix}$ (4.13)

4.2.2.2 Infinitesimal x-y strains

These are defined by Cauchy strain-displacement equations:

$$\varepsilon_x^s = \frac{\partial u}{\partial x} \quad , \quad \varepsilon_y^s = \frac{\partial v}{\partial y} \quad , \quad \gamma_{xy}^s = \frac{\partial u}{\partial y} + \frac{\partial v}{\partial x} \tag{4.14}$$

Substituting from equations (4.1), (4.2) into the above equations, the components of infinitesimal strain can be expressed as follows:

$$\varepsilon_x^s = \frac{\partial u^o}{\partial x} - z\frac{\partial^2 w}{\partial x^2} - f_\psi(z)\frac{\partial \psi_y}{\partial x} \tag{4.15}$$

$$\varepsilon_y^s = \frac{\partial v^o}{\partial y} - z\frac{\partial^2 w}{\partial y^2} + f_\psi(z)\frac{\partial \psi_x}{\partial y} \tag{4.16}$$

$$\gamma_{xy}^s = \frac{\partial u^o}{\partial y} + \frac{\partial v^o}{\partial x} - 2z\frac{\partial^2 w}{\partial x \partial y} + f_\psi(z)\left[-\frac{\partial \psi_y}{\partial y} + \frac{\partial \psi_x}{\partial x}\right] \tag{4.17}$$

where $f_\psi(z) = \frac{3}{2}z - \frac{2z^3}{h^2}$ (4.18)

These previous equations can be written in the following matrix form:

$$\varepsilon_s(x,y,z) = \varepsilon_o(x,y) - z\,\hat{\varepsilon}_b(x,y) + f_\psi(z)\,\hat{\varepsilon}_\psi(x,y) \tag{4.19}$$

where

$$\varepsilon_o(x,y) = \begin{bmatrix} \frac{\partial u^o}{\partial x} \\ \frac{\partial v^o}{\partial y} \\ \frac{\partial u^o}{\partial y} + \frac{\partial v^o}{\partial x} \end{bmatrix} \tag{4.20}$$

$$\hat{\boldsymbol{\varepsilon}}_b(x,y) = \begin{bmatrix} \dfrac{\partial^2 w}{\partial x^2} \\ \dfrac{\partial^2 w}{\partial y^2} \\ 2\dfrac{\partial^2 w}{\partial x \partial y} \end{bmatrix} \tag{4.21}$$

$$\hat{\boldsymbol{\varepsilon}}_\psi(x,y) = \begin{bmatrix} -\dfrac{\partial \psi_y}{\partial x} \\ \dfrac{\partial \psi_x}{\partial y} \\ \dfrac{\partial \psi_x}{\partial x} - \dfrac{\partial \psi_y}{\partial y} \end{bmatrix} \tag{4.22}$$

and $$\boldsymbol{\varepsilon}_s \equiv \begin{Bmatrix} \varepsilon_x^s & \varepsilon_y^s & \gamma_{xy}^s \end{Bmatrix} \tag{4.23}$$

4.2.2.3 Finite strain components

For the case of finite strains, Green's strain-displacement equations are used such that:

$$\varepsilon_x = \varepsilon_x^s + \varepsilon_x^l \tag{4.24}$$

$$\varepsilon_y = \varepsilon_y^s + \varepsilon_y^l \tag{4.25}$$

$$\gamma_{xy} = \gamma_{xy}^s + \gamma_{xy}^l \tag{4.26}$$

where

$$\varepsilon_x^l = \frac{1}{2}\left[\left(\frac{\partial u}{\partial x}\right)^2 + \left(\frac{\partial v}{\partial x}\right)^2 + \left(\frac{\partial w}{\partial x}\right)^2\right] \tag{4.27}$$

$$\varepsilon_y^l = \frac{1}{2}\left[\left(\frac{\partial u}{\partial y}\right)^2 + \left(\frac{\partial v}{\partial y}\right)^2 + \left(\frac{\partial w}{\partial y}\right)^2\right] \tag{4.28}$$

$$\gamma_{xy}^l = \frac{\partial u}{\partial x}\frac{\partial u}{\partial y} + \frac{\partial v}{\partial x}\frac{\partial v}{\partial y} + \frac{\partial w}{\partial x}\frac{\partial w}{\partial y} \tag{4.29}$$

Hence, the additional (nonlinear) terms due to finite strains can be expressed in the following matrix form:

$$\boldsymbol{\varepsilon}_l = \boldsymbol{\varepsilon}_m(x,y) + \boldsymbol{\varepsilon}_w(x,y) - z\hat{\boldsymbol{\varepsilon}}_{m\theta}(x,y) + z^2\hat{\boldsymbol{\varepsilon}}_\theta(x,y) \tag{4.30}$$

where $\boldsymbol{\varepsilon}_l = \{ \varepsilon_x^l \quad \varepsilon_y^l \quad \gamma_{xy}^l \}$ (4.31)

and

$$\boldsymbol{\varepsilon}_m(x,y) = \frac{1}{2}\begin{bmatrix} \left(\frac{\partial u^o}{\partial x}\right)^2 + \left(\frac{\partial v^o}{\partial x}\right)^2 \\ \left(\frac{\partial u^o}{\partial y}\right)^2 + \left(\frac{\partial v^o}{\partial y}\right)^2 \\ 2\frac{\partial u^o}{\partial x}\frac{\partial u^o}{\partial y} + 2\frac{\partial v^o}{\partial x}\frac{\partial v^o}{\partial y} \end{bmatrix} \tag{4.32}$$

$$\boldsymbol{\varepsilon}_w(x,y) = \frac{1}{2}\begin{bmatrix} \left(\frac{\partial w}{\partial x}\right)^2 \\ \left(\frac{\partial w}{\partial y}\right)^2 \\ 2\frac{\partial w}{\partial x}\frac{\partial w}{\partial y} \end{bmatrix} \tag{4.33}$$

$$\hat{\boldsymbol{\varepsilon}}_\theta(x,y) = \frac{1}{2}\begin{bmatrix} \left(\frac{\partial^2 w}{\partial x^2}\right)^2 + \left(\frac{\partial^2 w}{\partial x \partial y}\right)^2 \\ \left(\frac{\partial^2 w}{\partial y \partial x}\right)^2 + \left(\frac{\partial^2 w}{\partial y^2}\right)^2 \\ 2\frac{\partial^2 w}{\partial x^2}\frac{\partial^2 w}{\partial x \partial y} + 2\frac{\partial^2 w}{\partial x \partial y}\frac{\partial^2 w}{\partial y^2} \end{bmatrix} \tag{4.34}$$

$$\hat{\boldsymbol{\varepsilon}}_{m\theta}(x,y) = \begin{bmatrix} \frac{\partial u^o}{\partial x}\frac{\partial^2 w}{\partial x^2} + \frac{\partial v^o}{\partial x}\frac{\partial^2 w}{\partial x \partial y} \\ \frac{\partial u^o}{\partial y}\frac{\partial^2 w}{\partial y \partial x} + \frac{\partial v^o}{\partial y}\frac{\partial^2 w}{\partial y^2} \\ \frac{\partial u^o}{\partial y}\frac{\partial^2 w}{\partial x^2} + \frac{\partial u^o}{\partial x}\frac{\partial^2 w}{\partial y \partial x} + \frac{\partial v^o}{\partial y}\frac{\partial^2 w}{\partial x \partial y} + \frac{\partial v^o}{\partial x}\frac{\partial^2 w}{\partial y^2} \end{bmatrix} \tag{4.35}$$

Finally the vector of total x-y strain components is:

$$\begin{aligned} \boldsymbol{\varepsilon}(x,y,z) &= \boldsymbol{\varepsilon}_s + \boldsymbol{\varepsilon}_l \\ &= (\boldsymbol{\varepsilon}_o + \boldsymbol{\varepsilon}_m + \boldsymbol{\varepsilon}_w) - z(\hat{\boldsymbol{\varepsilon}}_b + \hat{\boldsymbol{\varepsilon}}_{m\theta}) + z^2\hat{\boldsymbol{\varepsilon}}_\theta + f_\psi(z)\hat{\boldsymbol{\varepsilon}}_\psi(x,y) \end{aligned} \tag{4.36}$$

4.2.2.4 *Matrix representation of finite strains*

Defining the following vectors which are functions of x, y :

$$\boldsymbol{\theta}_m = \left\{ \frac{\partial u^o}{\partial x} \quad \frac{\partial v^o}{\partial x} \quad \frac{\partial u^o}{\partial y} \quad \frac{\partial v^o}{\partial y} \right\} \tag{4.37}$$

$$\boldsymbol{\theta}_w = \left\{ \frac{\partial w}{\partial x} \quad \frac{\partial w}{\partial y} \right\} \tag{4.38}$$

$$\boldsymbol{\theta}_\theta = \left\{ \frac{\partial^2 w}{\partial x^2} \quad \frac{\partial^2 w}{\partial x \partial y} \quad \frac{\partial^2 w}{\partial y \partial x} \quad \frac{\partial^2 w}{\partial y^2} \right\} \tag{4.39}$$

then it can be deduced that:

$$\boldsymbol{\varepsilon}_m = \frac{1}{2} \boldsymbol{A}_m(x,y) \quad \boldsymbol{\theta}_m(x,y) \tag{4.40}$$

$$\boldsymbol{\varepsilon}_w = \frac{1}{2} \boldsymbol{A}_w(x,y) \quad \boldsymbol{\theta}_w(x,y) \tag{4.41}$$

$$\hat{\boldsymbol{\varepsilon}}_{m\theta} = \boldsymbol{A}_m \, \boldsymbol{\theta}_\theta = \boldsymbol{A}_\theta \, \boldsymbol{\theta}_m \tag{4.42}$$

$$\hat{\boldsymbol{\varepsilon}}_\theta = \frac{1}{2} \boldsymbol{A}_\theta(x,y) \quad \boldsymbol{\theta}_\theta(x,y) \tag{4.43}$$

where the $\boldsymbol{A}$ matrices are defined as follows:

$$\boldsymbol{A}_m(x,y) = \begin{bmatrix} \frac{\partial u^o}{\partial x} & \frac{\partial v^o}{\partial x} & 0 & 0 \\ 0 & 0 & \frac{\partial u^o}{\partial y} & \frac{\partial u^o}{\partial y} \\ \frac{\partial u^o}{\partial y} & \frac{\partial v^o}{\partial y} & \frac{\partial u^o}{\partial x} & \frac{\partial v^o}{\partial x} \end{bmatrix} \tag{4.44}$$

$$\boldsymbol{A}_w(x,y) = \begin{bmatrix} \frac{\partial w}{\partial x} & 0 \\ 0 & \frac{\partial w}{\partial y} \\ \frac{\partial w}{\partial y} & \frac{\partial w}{\partial x} \end{bmatrix} \tag{4.45}$$

and

$$A_\theta(x,y) = \begin{bmatrix} \frac{\partial^2 w}{\partial x^2} & \frac{\partial^2 w}{\partial x \partial y} & 0 & 0 \\ 0 & 0 & \frac{\partial^2 w}{\partial y \partial x} & \frac{\partial^2 w}{\partial y^2} \\ \frac{\partial^2 w}{\partial y \partial x} & \frac{\partial^2 w}{\partial y^2} & \frac{\partial^2 w}{\partial x^2} & \frac{\partial^2 w}{\partial x \partial y} \end{bmatrix} \tag{4.46}$$

Notice also that the variation of strain terms can be obtained as follows:

$$d\boldsymbol{\varepsilon}_m = \boldsymbol{A}_m \; d\boldsymbol{\theta}_m \tag{4.47}$$

$$d\boldsymbol{\varepsilon}_w = \boldsymbol{A}_w \; d\boldsymbol{\theta}_w \tag{4.48}$$

$$d\hat{\boldsymbol{\varepsilon}}_{m\theta} = \boldsymbol{A}_\theta \; d\boldsymbol{\theta}_m + \boldsymbol{A}_m \; d\boldsymbol{\theta}_\theta \tag{4.49}$$

$$d\hat{\boldsymbol{\varepsilon}}_\theta = \boldsymbol{A}_\theta \; d\boldsymbol{\theta}_\theta \tag{4.50}$$

4.2.3 Strain energy variations

4.2.3.1 Introduction

Using equations (3.9) and (3.10) stress components at any point (x,y,z) inside the lth layer of a composite layered plate can be expressed in terms of strain components with the following matrix equations:

$$\boldsymbol{\sigma} = \begin{bmatrix} \sigma_x \\ \sigma_y \\ \tau_{xy} \end{bmatrix} = \boldsymbol{D}^{(l)} \boldsymbol{\varepsilon} \tag{4.51}$$

$$\text{and} \quad \boldsymbol{\tau} = \begin{bmatrix} \tau_{xy} \\ \tau_{yz} \end{bmatrix} = \boldsymbol{\mu}^{(l)} \boldsymbol{\gamma} \tag{4.52}$$

where $\boldsymbol{\sigma}$, $\boldsymbol{\varepsilon}$ are the x-y stress and strain vectors, and $\boldsymbol{\tau}$, $\boldsymbol{\gamma}$ are the vectors of transverse shear stress and strain, respectively.

The variation of strain energy density (strain energy per unit volume) at any point inside the plate due to a variation of the displacement field can be expressed as follows:

$$\delta \bar{U} = \delta \boldsymbol{\gamma}^t \boldsymbol{\tau} + \delta \boldsymbol{\varepsilon}^t \boldsymbol{\sigma} \equiv \delta \boldsymbol{\gamma}^t \boldsymbol{\tau} + (\delta \boldsymbol{\varepsilon}_s^t + \delta \boldsymbol{\varepsilon}_l^t) \boldsymbol{\sigma} \tag{4.53a}$$

which can also be rewritten as:

$$\delta\bar{U} = (\delta\gamma^t\tau + \delta\varepsilon_s^t\sigma_s) + \delta\varepsilon_l^t\sigma + \delta\varepsilon_s^t\sigma_l \quad (4.53b)$$

where $\sigma_s = D^{(l)}\varepsilon_s$ (4.54)

and $\sigma_l = D^{(l)}\varepsilon_l$ (4.55)

Hence, the variation of the strain energy density can be represented in terms of three parts as follow:

$$\delta\bar{U} = \delta\bar{U}_{small} + \delta\bar{U}_l + \delta\bar{U}_{sl} \quad (4.56)$$

where

$$\delta\bar{U}_{small} = \delta\gamma^t\tau + \delta\varepsilon_s^t\sigma_s \equiv \delta\bar{U}_\gamma + \delta\bar{U}_s \quad (4.57)$$

which represents the variation due to infinitesimal strains and corresponding stresses, with:

$$\delta\bar{U}_\gamma = \delta\gamma^t\tau = \delta\gamma^t\mu^{(l)}\gamma \quad (4.58)$$

and $\delta\bar{U}_s = \delta\varepsilon_s^t\sigma_s = \delta\varepsilon_s^t D^{(l)}\varepsilon_s$ (4.59)

The part: $\delta\bar{U}_l = \delta\varepsilon_l^t\sigma$ (4.60)

represents the variation due to a variation of the additional finite strain terms, whilst the part:

$$\delta\bar{U}_{sl} = \delta\varepsilon_s^t\sigma_l \quad (4.61)$$

represents a coupling term due to the variation of infinitesimal strains, and the additional stresses obtained from the additional finite strain terms.

Each part of the strain energy variation will be analysed and integrated with respect to z along the layers of the composite plate, where the following notation is used:

$$\delta U' = \int_{-h/2}^{h/2} \delta\bar{U}(x,y,z)\,dz \quad (4.62)$$

4.2.3.2 Analysis of the part $\delta\bar{U}_{small}$

From equations (4.11) and (4.58) it can be deduced that:

$$\delta\bar{U}_\gamma(x,y,z) = f_\gamma^2(z)\,d\hat{\gamma}^t(x,y)\,\mu^{(l)}\hat{\gamma}(x,y) \quad (4.63)$$

where $$f_\gamma(z) = \frac{3}{2}\left(1 - \frac{4z^2}{h^2}\right) \tag{4.64}$$

Defining the following matrix:

$$\boldsymbol{\mu}_{\gamma\gamma} = \int_{-h/2}^{h/2} f_\gamma^2(z)\,\boldsymbol{\mu}^{(l)}\,dz \tag{4.65}$$

and integrating equation (4.63) with respect to z, it can be deduced that:

$$\delta U'_\gamma(x,y) = \delta\hat{\boldsymbol{\gamma}}^t(x,y)\;\boldsymbol{\mu}_{\gamma\gamma}\,\hat{\boldsymbol{\gamma}}(x,y) \tag{4.66}$$

Substituting from equation (4.19) into equation (4.59) then:

$$\delta\bar{U}_s = \left(\delta\boldsymbol{\varepsilon}_o^t - z\delta\hat{\boldsymbol{\varepsilon}}_b^t + f_\psi(z)\,\delta\hat{\boldsymbol{\varepsilon}}_\psi^t\right)\boldsymbol{D}^{(l)}\left(\boldsymbol{\varepsilon}_o - z\hat{\boldsymbol{\varepsilon}}_b + f_\psi(z)\,\hat{\boldsymbol{\varepsilon}}_\psi\right) \tag{4.67}$$

where

$$f_\psi(z) = \frac{3}{2}z - 2\frac{z^3}{h^2} \tag{4.68}$$

Expanding equation (4.67), we can deduce that:

$$\delta\bar{U}_s = \delta\bar{U}_{oo} + \delta\bar{U}_{bb} + \delta\bar{U}_{\psi\psi} + (\delta\bar{U}_{ob} + \delta\bar{U}_{bo}) + (\delta\bar{U}_{o\psi} + \delta\bar{U}_{\psi o}) + (\delta\bar{U}_{b\psi} + \delta\bar{U}_{\psi b}) \tag{4.69}$$

where

$$\delta\bar{U}_{oo} = \delta\boldsymbol{\varepsilon}_o^t(x,y)\,\boldsymbol{D}^{(l)}\,\boldsymbol{\varepsilon}_o(x,y) \tag{4.70}$$

$$\delta\bar{U}_{bb} = z^2\,\delta\hat{\boldsymbol{\varepsilon}}_b^t(x,y)\,\boldsymbol{D}^{(l)}\,\hat{\boldsymbol{\varepsilon}}_b(x,y) \tag{4.71}$$

$$\delta\bar{U}_{\psi\psi} = [f_\psi(z)]^2\,\delta\hat{\boldsymbol{\varepsilon}}_\psi^t(x,y)\,\boldsymbol{D}^{(l)}\,\hat{\boldsymbol{\varepsilon}}_\psi(x,y) \tag{4.72}$$

$$\delta\bar{U}_{ob} = -z\,\delta\boldsymbol{\varepsilon}_o^t(x,y)\,\boldsymbol{D}^{(l)}\,\hat{\boldsymbol{\varepsilon}}_b(x,y) \tag{4.73}$$

$$\delta\bar{U}_{bo} = -z\,\delta\hat{\boldsymbol{\varepsilon}}_b^t(x,y)\,\boldsymbol{D}^{(l)}\,\boldsymbol{\varepsilon}_o(x,y) \tag{4.74}$$

$$\delta\bar{U}_{o\psi} = f_\psi(z)\,\delta\boldsymbol{\varepsilon}_o^t(x,y)\,\boldsymbol{D}^{(l)}\,\hat{\boldsymbol{\varepsilon}}_\psi(x,y) \tag{4.75}$$

$$\delta\bar{U}_{\psi o} = f_\psi(z)\,\delta\hat{\boldsymbol{\varepsilon}}_\psi^t(x,y)\,\boldsymbol{D}^{(l)}\,\boldsymbol{\varepsilon}_o(x,y) \tag{4.76}$$

$$\delta\bar{U}_{b\psi} = -zf_\psi(z)\,\delta\hat{\boldsymbol{\varepsilon}}_b^t(x,y)\,\boldsymbol{D}^{(l)}\,\hat{\boldsymbol{\varepsilon}}_\psi(x,y) \tag{4.77}$$

$$\delta\bar{U}_{\psi b} = -zf_\psi(z)\,\delta\hat{\boldsymbol{\varepsilon}}_\psi^t(x,y)\,\boldsymbol{D}^{(l)}\,\hat{\boldsymbol{\varepsilon}}_b(x,y) \tag{4.78}$$

Integrated $\boldsymbol{D}$ matrices are required for the integration of the above equations with respect to z and are defined as follows:

$$\boldsymbol{D}_{oo} = \int_{-h/2}^{h/2} \boldsymbol{D}^{(l)}\, dz \tag{4.79}$$

$$\boldsymbol{D}_{ob} = \boldsymbol{D}_{bo} = \int_{-h/2}^{h/2} z\, \boldsymbol{D}^{(l)}\, dz \tag{4.80}$$

$$\boldsymbol{D}_{bb} = \int_{-h/2}^{h/2} z^2\, \boldsymbol{D}^{(l)}\, dz \tag{4.81}$$

$$\boldsymbol{D}_{\psi\psi} = \int_{-h/2}^{h/2} f_\psi^{\,2}\, \boldsymbol{D}^{(l)}\, dz \tag{4.82}$$

$$\boldsymbol{D}_{o\psi} = \boldsymbol{D}_{\psi o} = \int_{-h/2}^{h/2} f_\psi(z)\, \boldsymbol{D}^{(l)}\, dz \tag{4.83}$$

$$\boldsymbol{D}_{b\psi} = \boldsymbol{D}_{\psi b} = \int_{-h/2}^{h/2} z\, f_\psi(z)\, \boldsymbol{D}^{(l)}\, dz \tag{4.84}$$

Integrating equations (4.70) - (4.78) with respect to z over the plate thickness, it can be deduced that:

$$\delta U'_{oo} = \delta\boldsymbol{\varepsilon}_o^t(x,y)\, \boldsymbol{D}_{oo}\, \boldsymbol{\varepsilon}_o(x,y) \tag{4.85}$$

$$\delta U'_{bb} = \delta\hat{\boldsymbol{\varepsilon}}_b^t(x,y)\, \boldsymbol{D}_{bb}\, \hat{\boldsymbol{\varepsilon}}_b(x,y) \tag{4.86}$$

$$\delta U'_{\psi\psi} = \delta\hat{\boldsymbol{\varepsilon}}_\psi^t(x,y)\, \boldsymbol{D}_{\psi\psi}\, \hat{\boldsymbol{\varepsilon}}_\psi(x,y) \tag{4.87}$$

$$\delta U'_{ob} = -\delta\boldsymbol{\varepsilon}_o^t(x,y)\, \boldsymbol{D}_{ob}\, \hat{\boldsymbol{\varepsilon}}_b(x,y) \tag{4.88}$$

$$\delta U'_{bo} = -\delta\hat{\boldsymbol{\varepsilon}}_b^t(x,y)\, \boldsymbol{D}_{bo}\, \boldsymbol{\varepsilon}_o(x,y) \tag{4.89}$$

$$\delta U'_{o\psi} = \delta\boldsymbol{\varepsilon}_o^t(x,y)\, \boldsymbol{D}_{o\psi}\, \hat{\boldsymbol{\varepsilon}}_\psi(x,y) \tag{4.90}$$

$$\delta U'_{\psi o} = \delta\hat{\boldsymbol{\varepsilon}}_b^t(x,y)\, \boldsymbol{D}_{\psi o}\, \boldsymbol{\varepsilon}_o(x,y) \tag{4.91}$$

$$\delta U'_{b\psi} = -\delta\hat{\boldsymbol{\varepsilon}}_b^t(x,y)\, \boldsymbol{D}_{b\psi}\, \hat{\boldsymbol{\varepsilon}}_\psi(x,y) \tag{4.92}$$

$$\delta U'_{\psi b} = -\delta\hat{\boldsymbol{\varepsilon}}_\psi^t(x,y)\, \boldsymbol{D}_{\psi b}\, \hat{\boldsymbol{\varepsilon}}_b(x,y) \tag{4.93}$$

4.2.3.3 Strain energy variation part $(\delta \bar{U}_l)$

It can be deduced that from equation (4.60) and equation (4.30) that:

$$\delta \bar{U}_l = \delta \boldsymbol{\varepsilon}_l^t \boldsymbol{\sigma} = (\delta \boldsymbol{\varepsilon}_m^t + \delta \boldsymbol{\varepsilon}_w^t - z \delta \hat{\boldsymbol{\varepsilon}}_{m\theta}^t + z^2 \delta \hat{\boldsymbol{\varepsilon}}_\theta^t) \boldsymbol{\sigma}$$

which can be rewritten as follows:

$$\delta \bar{U}_l = \delta \bar{U}_m + \delta \bar{U}_w + \delta \bar{U}_{m\theta} + \delta \bar{U}_\theta \tag{4.94}$$

where

$$\delta \bar{U}_m = \delta \boldsymbol{\varepsilon}_m^t \boldsymbol{\sigma} \tag{4.95}$$

$$\delta \bar{U}_w = \delta \boldsymbol{\varepsilon}_w^t \boldsymbol{\sigma} \tag{4.96}$$

$$\delta \bar{U}_{m\theta} = -z \, \delta \hat{\boldsymbol{\varepsilon}}_{m\theta}^t \boldsymbol{\sigma} \tag{4.97}$$

$$\delta \bar{U}_\theta = z^2 \delta \hat{\boldsymbol{\varepsilon}}_\theta^t \boldsymbol{\sigma} \tag{4.98}$$

and

$$\boldsymbol{\sigma} = \boldsymbol{D}^{(l)} (\boldsymbol{\varepsilon}_s + \boldsymbol{\varepsilon}_l)$$

$$= \boldsymbol{D}^{(l)} \{ (\boldsymbol{\varepsilon}_o + \boldsymbol{\varepsilon}_m + \boldsymbol{\varepsilon}_w) - z (\hat{\boldsymbol{\varepsilon}}_b + \hat{\boldsymbol{\varepsilon}}_{m\theta}) + z^2 \hat{\boldsymbol{\varepsilon}}_\theta + f_\psi(z) \hat{\boldsymbol{\varepsilon}}_\psi \} \tag{4.99}$$

Substituting from equation (4.47) into equation(4.95) then:

$$\delta \bar{U}_m = \delta \boldsymbol{\theta}_m^t \boldsymbol{A}_m^t \boldsymbol{\sigma} \equiv \delta \boldsymbol{\theta}_m^t(x,y) \, \boldsymbol{A}_m^t(x,y) \, \boldsymbol{\sigma}(x,y,z) \tag{4.100}$$

Hence

$$\delta U'_m = \int_{-h/2}^{h/2} \delta \bar{U}_m dz \equiv \delta \boldsymbol{\theta}_m^t \boldsymbol{A}_m^t \int_{-h/2}^{h/2} \boldsymbol{\sigma} dz$$

or $$\delta U'_m = \delta \boldsymbol{\theta}_m^t(x,y) \, \boldsymbol{A}_m^t(x,y) \, \boldsymbol{\sigma}_m(x,y) \tag{4.101}$$

where $$\boldsymbol{\sigma}_m(x,y) = \int_{-h/2}^{h/2} \boldsymbol{\sigma}(x,y,z) \, dz \tag{4.102}$$

and by using the integrated $\boldsymbol{D}$ matrices:

$$\boldsymbol{\sigma}_m = \boldsymbol{D}_{oo} (\boldsymbol{\varepsilon}_o + \boldsymbol{\varepsilon}_m + \boldsymbol{\varepsilon}_w) - \boldsymbol{D}_{ob} (\hat{\boldsymbol{\varepsilon}}_b + \hat{\boldsymbol{\varepsilon}}_{m\theta}) + \boldsymbol{D}_{bb} \hat{\boldsymbol{\varepsilon}}_\theta + \boldsymbol{D}_{o\psi} \hat{\boldsymbol{\varepsilon}}_\psi \tag{4.103}$$

Using matrix multiplication, equation (4.101) can be rewritten as follow:

$$\delta U'_m = \delta 0_m^t \, S_{mm} \, 0_m \tag{4.104}$$

where

$$S_{mm} = \begin{bmatrix} \sigma_x^m I_2 & \tau_{xy}^m I_2 \\ \tau_{xy}^m I_2 & \sigma_y^m I_2 \end{bmatrix}$$

and $$I_2 = \begin{bmatrix} 1 & 0 \\ 0 & 1 \end{bmatrix}, \qquad \sigma_m = \begin{bmatrix} \sigma_x^m \\ \sigma_y^m \\ \tau_{xy}^m \end{bmatrix} \tag{4.105}$$

Similarly, it can be shown that

$$\delta \bar{U}_w = \delta 0_w^t(x,y) \, A_w^t(x,y) \, \sigma(x,y,z) \tag{4.106}$$

and $$\delta U'_w = \delta \theta_w^t \, S_{ww} \, 0_w \tag{4.107}$$

where

$$S_{ww} = \begin{bmatrix} \sigma_x^m & \tau_{xy}^m \\ \tau_{xy}^m & \sigma_y^m \end{bmatrix} \tag{4.108}$$

Substituting from equation (4.49) into equation (4.97) then

$$\delta \bar{U}_{m\theta} = (\delta \theta_m^t \, A_\theta^t + \delta \theta_m^t \, A_\theta^t) \, (-z\sigma) \tag{4.109}$$

Defining

$$\sigma_{m\theta} = \sigma_{\theta m} = \int_{-h/2}^{h/2} (-z\sigma) dz \tag{4.110}$$

then

$$\sigma_{m\theta} = \sigma_{\theta m} = -D_{ob}(\varepsilon_o + \varepsilon_m + \varepsilon_w) + D_{bb}(\hat{\varepsilon}_b + \hat{\varepsilon}_{m\theta}) - D_{(3)}\hat{\varepsilon}_\theta - D_{b\psi}\hat{\varepsilon}_\psi \tag{4.111}$$

with $D_{(n)} = \int_{-h/2}^{h/2} z^n D^{(l)} dz$, and $D_{b\psi}$ is defined by equation (4.84).

Hence it can be shown that:

$$\delta U'_{m\theta} = \delta \theta_m^t \, S_{m\theta} 0_\theta + \delta 0_\theta^t \, S_{\theta m} 0_m \tag{4.112}$$

where

$$S_{m\theta} = S_{\theta m} = \begin{bmatrix} \sigma_x^{m\theta} I_2 & \tau_{xy}^{m\theta} I_2 \\ \tau_{xy}^{m\theta} I_2 & \sigma_y^{m\theta} I_2 \end{bmatrix} \quad (4.113)$$

Similarly, it can be shown that:

$$\delta \bar{U}_\theta = d\theta_\theta^t(x,y) A_\theta^t(x,y) \{z^2 \boldsymbol{\sigma}(x,y,z)\} \quad (4.114)$$

Defining

$$\boldsymbol{\sigma}_\theta = \int_{-h/2}^{h/2} (z^2 \boldsymbol{\sigma}) dz$$

then

$$\boldsymbol{\sigma}_\theta = D_{bb}(\boldsymbol{\varepsilon}_o + \boldsymbol{\varepsilon}_m + \boldsymbol{\varepsilon}_w) - D_{(3)}(\hat{\boldsymbol{\varepsilon}}_b + \hat{\boldsymbol{\varepsilon}}_{m\theta}) + D_{(4)}\hat{\boldsymbol{\varepsilon}}_\theta + D_{bb\psi}\hat{\boldsymbol{\varepsilon}}_\psi \quad (4.115)$$

where $$D_{bb\psi} = \int_{-h/2}^{h/2} z^2 f_\psi^2 D^{(l)} dz \quad (4.116)$$

Therefore, it can be deduced that

$$\delta U'_\theta = \delta\theta_\theta^t S_{\theta\theta} \theta_\theta \quad (4.117)$$

where

$$S_{\theta\theta} = \begin{bmatrix} \sigma_x^\theta I_2 & \tau_{xy}^\theta I_2 \\ \tau_{xy}^\theta I_2 & \sigma_y^\theta I_2 \end{bmatrix} \quad (4.118)$$

4.2.3.4 Strain energy variation part ($\delta \bar{U}_{sl}$)

This was defined as follows:

$$\delta \bar{U}_{sl} = \delta\varepsilon_s^t \boldsymbol{\sigma}_l \quad (4.119)$$

where $$\delta\varepsilon_s = \delta\varepsilon_o - z\,\delta\hat{\varepsilon}_b + f_\psi(z)\,\delta\hat{\varepsilon}_\psi \quad (4.120)$$

Substituting from equation (4.120) into equation (4.119) then

$$\delta \bar{U}_{sl} = (\delta\varepsilon_o^t - z\delta\hat{\varepsilon}_b^t + f_\psi(z)\,\delta\hat{\varepsilon}_\psi^t)\,\boldsymbol{\sigma}_l \quad (4.121)$$

which can be rewritten as follows:

$$\delta\bar{U}_{sl} = (\delta\bar{U}_o)_{sl} + (\delta\bar{U}_b)_{sl} + (\delta\bar{U}_\psi)_{sl} \tag{4.122}$$

where

$$(\delta\bar{U}_o)_{sl} = \delta\varepsilon_o^t \boldsymbol{\sigma}_l \tag{4.123}$$

$$(\delta\bar{U}_b)_{sl} = -z\,\delta\hat{\varepsilon}_b^t \boldsymbol{\sigma}_l \tag{4.124}$$

$$(\delta\bar{U}_\psi)_{sl} = f_\psi(z)\,\delta\hat{\varepsilon}_\psi^t \boldsymbol{\sigma}_l \tag{4.125}$$

Defining the following integrated stress vector:

$$\boldsymbol{\sigma}_o(x,y) = \int_{-h/2}^{h/2} \boldsymbol{\sigma}_l(x,y,z)\,dz \tag{4.126}$$

then, it can be shown that

$$\boldsymbol{\sigma}_o(x,y) = \boldsymbol{D}_{oo}(\boldsymbol{\varepsilon}_m + \boldsymbol{\varepsilon}_w) - \boldsymbol{D}_{ob}(\hat{\boldsymbol{\varepsilon}}_{m\theta}) + \boldsymbol{D}_{bb}(\hat{\boldsymbol{\varepsilon}}_\theta) \tag{4.127}$$

Hence

$$(\delta U'_o)_{sl} = \int_{-h/2}^{h/2} (\delta\bar{U}_o)_{sl}\,dz = \delta\varepsilon_o^t \boldsymbol{\sigma}_o \tag{4.128}$$

Similarly by defining the following integrated stress vector:

$$\boldsymbol{\sigma}_b(x,y) = -\int_{-h/2}^{h/2} z\boldsymbol{\sigma}_l(x,y,z)\,dz \tag{4.129}$$

then it can be proved that:

$$\boldsymbol{\sigma}_b(x,y) = -\boldsymbol{D}_{ob}(\boldsymbol{\varepsilon}_m + \boldsymbol{\varepsilon}_w) + \boldsymbol{D}_{bb}(\hat{\boldsymbol{\varepsilon}}_{m\theta}) - \boldsymbol{D}_{(3)}(\hat{\boldsymbol{\varepsilon}}_\theta) \tag{4.130}$$

and $$(\delta U'_b)_{sl} = \delta\hat{\varepsilon}_b^t \boldsymbol{\sigma}_b \tag{4.131}$$

Defining also:

$$\boldsymbol{\sigma}_\psi(x,y) = -\int_{-h/2}^{h/2} f_\psi(z)\boldsymbol{\sigma}_l(x,y,z)\,dz \tag{4.132}$$

Hence

$$\boldsymbol{\sigma}_\psi(x,y) = -\boldsymbol{D}_{o\psi}(\boldsymbol{\varepsilon}_m + \boldsymbol{\varepsilon}_w) + \boldsymbol{D}_{b\psi}(\hat{\boldsymbol{\varepsilon}}_{m\theta}) - \boldsymbol{D}_{bb\psi}(\hat{\boldsymbol{\varepsilon}}_\theta) \tag{4.133}$$

and $$(\delta U'_\psi)_{sl} = \delta\hat{\varepsilon}_\psi^t \boldsymbol{\sigma}_\psi \tag{4.134}$$

4.3 INTERPOLATED EQUATIONS

4.3.1 Interpolation in *x*-direction

(a) Interpolated parameters using Lagrangian interpolation

The in-plane displacement components and average shear strains, at the midplane z=0: $u^{o}(x,y)$, $v^{o}(x,y)$, $\psi_x(x,y)$ and $\psi_y(x,y)$ do not require more than C^{o} continuity and can be interpolated in x-direction via Lagrangian interpolation i.e. for an n-node strip:

$$u^{o}(x,y) = \sum_{i=1}^{n} N_i(\xi)\, u^{o}{}_i(y) \tag{4.135}$$

$$v^{o}(x,y) = \sum_{i=1}^{n} N_i(\xi)\, v^{o}{}_i(y) \tag{4.136}$$

$$\psi_x(x,y) = \sum_{i=1}^{n} N_i(\xi) \left(\psi_x(y)\right)_i \tag{4.137}$$

$$\psi_y(x,y) = \sum_{i=1}^{n} N_i(\xi) \left(\psi_y(y)\right)_i \tag{4.138}$$

where $$N_i(\xi) = \prod_{\substack{r=1 \\ r\neq i}}^{n} \frac{\xi - \xi_r}{\xi_i - \xi_r} \equiv \left[\mathcal{L}_i^{n}(\xi)\right] \tag{4.139}$$

which represents one-dimensional Lagrangian shape functions.

(b) Interpolation of lateral deflection *w*

Hermitian or spline-type interpolation can be used to maintain the C^1 continuity of w i.e.

$$w(x,y) = \sum_{i=1}^{n} \left[G_i(\xi) w_i(y) + H_i(\xi) w_{i,x}(y) \right] \tag{4.140}$$

- Hermitian interpolation:

$$G_i(\xi) = g_i(\xi), \qquad H_i(\xi) = J_x h_i(\xi) \tag{4.141}$$

where g_i, h_i are one-dimensional Hermitian shape functions, as defined by equations (3.42) and (3.44)

- Spline-type interpolation:

$$G_i(\xi) = g_i^{s}(\xi), \qquad H_i(\xi) = J_x h_i^{s}(\xi) \tag{4.142}$$

where g_i^{s}, h_i^{s} are as defined by equations (3.47)-(3.51).

4.3.2 Interpolation in *y*-direction

(a) General expressions

The nodal functions in the previous expressions are interpolated in *y*-direction as follows:

$$u_i^o(y) = \sum_{r=1}^{m} f_u^r(\eta)\, u_i^r \tag{4.143}$$

$$v_i^o(y) = \sum_{r=1}^{m} f_v^r(\eta)\, v_i^r \tag{4.144}$$

$$\left(\psi_x(y)\right)_i = \sum_{r=1}^{m} f_{\psi_x}^r(\eta)\, (\psi_x^r)_i \tag{4.145}$$

$$\left(\psi_y(y)\right)_i = \sum_{r=1}^{m} f_{\psi_y}^r(\eta)\, (\psi_y^r)_i \tag{4.146}$$

$$w_i(y) = \sum_{r=1}^{m} f_w^r(\eta)\, w_i^r \tag{4.147}$$

$$w_{i,x}(y) = \sum_{r=1}^{m} f_w^r(\eta)\, w_{i,x}^r \tag{4.148}$$

where $dy = J_y\, d\eta$ (4.149)

Hence the full *x*-*y* interpolated parameters can be expressed for an *n*-node strip as follows:

$$u^o(x,y) = \sum_{i=1}^{n}\sum_{r=1}^{m} N_i(\xi)\, f_u^r(\eta)\, u_i^r \tag{4.150}$$

$$v^o(x,y) = \sum_{i=1}^{n}\sum_{r=1}^{m} N_i(\xi)\, f_v^r(\eta)\, v_i^r \tag{4.151}$$

$$\psi_x(x,y) = \sum_{i=1}^{n}\sum_{r=1}^{m} N_i(\xi)\, f_{\psi_x}^r(\eta)\left(\psi_x^r\right)_i \tag{4.152}$$

$$\psi_y(x,y) = \sum_{i=1}^{n}\sum_{r=1}^{m} N_i(\xi)\, f_{\psi_y}^r(\eta)\left(\psi_y^r\right)_i \tag{4.153}$$

$$w(x,y) = \sum_{i=1}^{n}\sum_{r=1}^{m} f_w^r(\eta)\left[\, G_i(\xi) w_i^r + H_i(\xi) w_{i,x}^r \,\right] \tag{4.154}$$

(b) Trigonometric interpolation

This depends on the boundary conditions and for an example, where w, u are restrained on the edges $\eta = o$, $\eta = 1$:

$$f_u^r(\eta) = \sin(r\pi\eta) \tag{4.155}$$

$$f_v^r(\eta) = \cos(r\pi\eta) \tag{4.156}$$

$$f_w^r(\eta) = \sin(r\pi\eta) \tag{4.157}$$

$$f_{\psi_x}^r(\eta) = \frac{\partial f_w^r(\eta)}{\partial\eta} = (r\pi)\cos(r\pi\eta) \tag{4.158}$$

$$f_{\psi_y}^r(\eta) = f_w^r(\eta) = \sin(r\pi\eta) \tag{4.159}$$

(c) Lagrangian interpolation

This can be used for u, v, ψ_x, ψ_y, i.e.

$$f_u^r(\eta) = f_v^r(\eta) = f_{\psi_x}^r(\eta) = f_{\psi_y}^r(\eta) = \mathcal{L}_r^m(\eta) \tag{4.160}$$

where
$$\mathcal{L}_r^m(\eta) = \prod_{\substack{j=1 \\ j\neq r}}^{m} \frac{(m-1)\eta - (j-1)}{r-j} \tag{4.161}$$

Notice that we can set boundary conditions at y edges, since u_i^1 , v_i^1 etc. represent nodal values at edge$(\eta = 0)$ and u_i^m , v_i^m etc. represent nodal values at edge$(\eta = 1)$.

(d) Hermitian interpolation

This may be used for w if m is an even number, and in this case:

$$\begin{aligned} f_w^r &= G_{r'}(m',\eta) \quad \text{for} \quad r = 1,3,5,... \\ &= H_{r'}(m',\eta) \quad \text{for} \quad r = 2,4,6,... \end{aligned} \tag{4.162}$$

where

$$m' = \frac{m}{2} \quad , \qquad r' = \frac{r+1}{2}$$

and $G_{r'}$, $H_{r'}$ are based on Hermitian interpolation for m' points. The boundary conditions at y edges can also be set as follows:

(i) Edge $(\eta = 0)$*:*

The superscript $r = 1$, represents the values w_i^1 , $w_{i,x}^1$ at the edge η=0, and the superscript $r = 2$, represents dw/dy values at that edge, i.e.

$$w_i^2 \equiv \left(\frac{dw}{dy}\right) \quad \text{at node } i,\ \eta = 0,$$

$$w^{2}_{i,x} \equiv \frac{d}{dy}\left(\frac{dw}{dx}\right) \quad \text{at node } i,\ \eta = 0.$$

(ii) Edge ($\eta = 1$):

The values of the superscript r at that edge are: $r = m-1, m$. Hence,

$$w_i^{m-1} \equiv w_i \qquad \text{at node } i \text{ and } \eta = 1,$$

$$w_{i,x}{}^{m-1} \equiv \left(\frac{dw}{dx}\right)_i \qquad \text{at node } i \text{ and } \eta = 1,$$

$$w_i^{m} \equiv \left(\frac{dw}{dy}\right)_i \qquad \text{at node } i \text{ and } \eta = 1,$$

$$w^{m}{}_{i,x} \equiv \frac{d}{dy}\left(\frac{dw}{dx}\right)_i \qquad \text{at node } i \text{ and } \eta = 1.$$

(e) Spline-type interpolation

This type of interpolation is mainly used for lateral deflection w but it can also be employed for other parameters. Defining: $m' = m-2$, and $r' = r-1$, then the interpolation functions depend on the values of the superscript r, and for the example of w they can be listed as follows:

(i) Case of $r = 1, 2$

$$f_w^1(\eta) = g_1^s(\eta) = \left[1 + (1-\alpha'_1)\eta\right]\left[1-\eta\right]\left[\mathcal{L}_1^{m'}(\eta)\right]$$

$$f_w^2(\eta) = J_y h_1^s(\eta) = J_y \eta(1-\eta)\left[\mathcal{L}_1^{m'}(\eta)\right]$$

where $$\alpha'_j = \sum_{\substack{k=1 \\ k\neq j}}^{m'} \frac{m'-1}{j-k}$$

(ii) Case of $r = m-1, m$

$$f_w^{m-1}(\eta) = g^s_{m'}(\eta) = \left[1 + (1+\alpha'_{m'})(1-\eta)\right]\eta\left[\mathcal{L}^{m'}_{m'}(\eta)\right]$$

$$f_w^{m}(\eta) = J_y h^s_{m'}(\eta) = -J_y \eta(1-\eta)\left[\mathcal{L}^{m'}_{m'}(\eta)\right]$$

(iii) Case of $r = 3, 4, \ldots, m-2$

$$f_w^r(\eta) = g_{r'}^s(\eta) = \frac{\eta(1-\eta)}{\eta_{r'}(1-\eta_{r'})}\left[\mathcal{L}_{r'}^{m'}(\eta)\right]$$

with $\eta_{r'} = \dfrac{r'-1}{m'-1} \equiv \dfrac{r-2}{m-3}$ and m should be greater than 3.

Boundary conditions at y edges:

These are similar to the case with Hermitian interpolation, i.e.

w_i^1 = The value of w at $\eta = 0$, node i

$w_{i,x}^1$ = The value of $\dfrac{dw}{dx}$ at $\eta = 0$, node i,

w_i^2 = The value of $\dfrac{dw}{dy}$ at $\eta = 0$, node i,

$w_{i,x}^2$ = The value of $\dfrac{d^2w}{dxdy}$ at $\eta = 0$, node i,

w_i^{m-1} = The value of w at $\eta = 1$, node i,

$w_{i,x}^{m-1}$ = The value of $\dfrac{dw}{dx}$ at $\eta = 1$, node i,

w_i^m = The value of $\dfrac{dw}{dy}$ at $\eta = 1$, node i,

$w_{i,x}^m$ = The value of $\dfrac{d^2w}{dxdy}$ at $\eta = 1$, node i.

4.4 ELEMENT LINEAR STIFFNESS MATRIX

4.4.1 Infinitesimal strain components

The nodal displacement vector per rth harmonic or y term for an n node strip can be partitioned as follows:

$$\boldsymbol{\delta}^r = \begin{bmatrix} \boldsymbol{\delta}_o^r \\ \boldsymbol{\delta}_b^r \\ \boldsymbol{\delta}_\psi^r \end{bmatrix} \qquad (4.163)$$

where

$$\boldsymbol{\delta}_o^r = \left\{ u_1^r v_1^r \quad u_2^r v_2^r \quad \ldots \quad u_n^r v_n^r \right\} \tag{4.164}$$

$$\boldsymbol{\delta}_b^r = \left\{ w_1^r w_{1,x}^r \quad w_2^r w_{2,x}^r \quad \ldots \quad w_n^r w_{n,x}^r \right\} \tag{4.165}$$

$$\boldsymbol{\delta}_\psi^r = \left\{ (\psi_x^r)_1 \quad (\psi_y^r)_2 \quad \ldots \quad (\psi_x^r)_n \quad (\psi_y^r)_n \right\} \tag{4.166}$$

Using interpolation equations (4.150), (4.151) then equation (4.20) can be written in terms of nodal values as follows:

$$\boldsymbol{\varepsilon}_o = \sum_{r=1}^{m} \boldsymbol{B}_o^r(\xi,\eta)\, \boldsymbol{\delta}_o^r \tag{4.167}$$

where $\boldsymbol{B}_o^r(\xi,\eta) =$

$$\begin{bmatrix} \ldots & \dfrac{N'_i(\xi)}{J_x} f_u^r(\eta) & 0 & \ldots \\ \ldots & 0 & \dfrac{N_i(\xi)}{J_y} f_{v,\eta}^r(\eta) & \ldots \\ \ldots & \dfrac{N_i(\xi)}{J_y} f_{u,\eta}^r(\eta) & \dfrac{N'_i(\xi)}{J_x} f_v^r(\eta) & \ldots \end{bmatrix} \tag{4.168}$$

and $\quad N'_i = \dfrac{dN_i}{d\xi}, \quad f_{u,\eta}^r = \dfrac{df_u^r}{d\eta}$, etc.

Using interpolation equation (4.154), then equation (4.21) can be expressed in terms of nodal values as follows

$$\hat{\boldsymbol{\varepsilon}}_b = \sum_{r=1}^{m} \boldsymbol{B}_b^r(\xi,\eta)\, \boldsymbol{\delta}_b^r \tag{4.169}$$

where $\boldsymbol{B}_b^r =$

$$\begin{bmatrix} \ldots & \dfrac{G''_i(\xi)}{J_x^2} f_w^r(\eta) & \dfrac{H''_i(\xi)}{J_x^2} f_w^r(\eta) & \ldots \\ \ldots & \dfrac{G_i(\xi)}{J_y^2} f_{w,\eta\eta}^r(\eta) & \dfrac{H_i(\xi)}{J_y^2} f_{w,\eta\eta}^r(\eta) & \ldots \\ \ldots & 2\dfrac{G'_i(\xi)}{J_x J_y} f_{w,\eta}^r(\eta) & 2\dfrac{H'_i(\xi)}{J_x J_y} f_{w,\eta}^r(\eta) & \ldots \end{bmatrix} \tag{4.170}$$

and $\quad G'_i = \dfrac{dG_i}{d\xi}, \; G''_i = \dfrac{d^2 G_i}{d\xi^2}, \; f_{w,\eta\eta}^r = \dfrac{d^2 f_w^r}{d\eta^2}$, etc.

Substituting from equations (4.152), (4.153) into (4.22) then:

$$\hat{\varepsilon}_{\psi} = \sum_{r=1}^{m} \boldsymbol{B}_{\psi}^{r}(\xi,\eta)\,\boldsymbol{\delta}_{\psi}^{r} \tag{4.171}$$

$$\text{where } \boldsymbol{B}_{\psi}^{r}(\xi,\eta) = \begin{bmatrix} \cdots & 0 & -\dfrac{N'_i(\xi)}{J_x} f_{\psi_y}^{r}(\eta) & \cdots \\ \cdots & \dfrac{N_i(\xi)}{J_y} f_{\psi_{x,\eta}}^{r}(\eta) & 0 & \cdots \\ \cdots & \dfrac{N'_i(\xi)}{J_x} f_{\psi_x}^{r}(\eta) & -\dfrac{N_i(\xi)}{J_y} f_{\psi_{y,\eta}}^{r}(\eta) & \cdots \end{bmatrix} \tag{4.172}$$

Substituting from equations (4.152), (4.153) into (4.11) then:

$$\hat{\gamma}(x,y) = \begin{bmatrix} -\psi_y \\ +\psi_x \end{bmatrix} = \sum_{r=1}^{m} \boldsymbol{B}_{\gamma}^{r}(\xi,\eta)\,\boldsymbol{\delta}_{\psi}^{r} \tag{4.173}$$

$$\text{where } \boldsymbol{B}_{\gamma}^{r}(\xi,\eta) = \begin{bmatrix} \cdots & 0 & -N_i(\xi) f_{\psi_y}^{r} & \cdots \\ \cdots & N_i(\xi) f_{\psi_x}^{r} & 0 & \cdots \end{bmatrix} \tag{4.174}$$

4.4.2 Strain energy variation and element stiffness matrix

Using equation (4.66) and equations (4.85)-(4.93), the strain energy variation per unit area for the case of infinitesimal strains can be expressed as follows:

$$\delta U'_{small} = (\delta U'_{\gamma} + \delta U'_{oo} + \delta U'_{bb} + \delta U'_{\psi'\psi}) + (\delta U'_{ob} + \delta U'_{bo}) + (\delta U'_{o\psi} + \delta U'_{\psi o}) + (\delta U'_{b\psi} + \delta U'_{\psi b}) \tag{4.175}$$

Each term will be represented in terms of nodal displacement values and integrated with respect to the *x*-*y* plane of the strip, where:

$$\delta U_{\alpha\beta} = \iint_{strip} \delta U'_{\alpha\beta}\,dx\,dy \equiv \int_0^1 \int_0^1 \delta U'_{\alpha\beta}\,J_x J_y\,d\xi\,d\eta \tag{4.176}$$

4.4.2.1 Strain energy variation term dU_{γ}

Substituting from equation (4.173) into (4.66), it can be deduced that:

$$dU'_{\gamma} = \sum_{s=1}^{m}\sum_{r=1}^{m} (d\boldsymbol{\delta}_{\psi}^{s})^{t}\,(\boldsymbol{B}_{\gamma}^{s})^{t}\,\boldsymbol{\mu}_{\gamma\gamma}\,\boldsymbol{B}_{\gamma}^{r}\,\boldsymbol{\delta}_{\psi}^{r} \tag{4.177}$$

Therefore, by integrating equation (4.177) over the element x-y area, it can be proved that:

$$dU_{\gamma} = \int_0^1 \int_0^1 \delta U'_{\gamma} J_x J_y \, d\xi \, d\eta \equiv \sum_{s=1}^{m} \sum_{r=1}^{m} (d\delta_{\psi}^{s})^t \, \boldsymbol{K}_{\gamma\gamma}^{sr} \, \delta_{\psi}^{r} \tag{4.178}$$

where $\boldsymbol{K}_{\gamma\gamma}^{sr} = \int_0^1 \int_0^1 (\boldsymbol{B}_{\gamma}^{s})^t \, \boldsymbol{\mu}_{\gamma\gamma} \, \boldsymbol{B}_{\gamma}^{r} \, J_x J_y \, d\xi \, d\eta$ (4.179)

4.4.2.2 Strain energy variation term dU_{oo}

Substituting from equation (4.167) into equation (4.85) then

$$dU'_{oo} = \sum_{s=1}^{m} \sum_{r=1}^{m} (d\delta_{o}^{s})^t \, (\boldsymbol{B}_{o}^{s})^t \, \boldsymbol{D}_{oo} \, \boldsymbol{B}_{o}^{r} \, \delta_{o}^{r} \tag{4.180}$$

Hence similar to equation (4.178), it can be deduced that

$$dU_{oo} = \sum_{s=1}^{m} \sum_{r=1}^{m} (d\delta_{o}^{s})^t \, \boldsymbol{K}_{oo}^{sr} \, \delta_{o}^{r} \tag{4.181}$$

where $\boldsymbol{K}_{oo}^{sr} = \int_0^1 \int_0^1 (\boldsymbol{B}_{o}^{s})^t \, \boldsymbol{D}_{oo} \, \boldsymbol{B}_{o}^{r} \, J_x J_y \, d\xi \, d\eta$ (4.182)

4.4.2.3 Strain energy variation term dU_{bb}

Substituting from equation (4.169) into (4.86) then

$$dU'_{bb} = \sum_{s=1}^{m} \sum_{r=1}^{m} (d\delta_{b}^{s})^t \, (\boldsymbol{B}_{b}^{s})^t \, \boldsymbol{D}_{bb} \, \boldsymbol{B}_{b}^{r} \, \delta_{b}^{r} \tag{4.183}$$

and it can be shown that

$$dU_{bb} = \sum_{s=1}^{m} \sum_{r=1}^{m} (d\delta_{b}^{s})^t \, \boldsymbol{K}_{bb}^{sr} \, \delta_{b}^{r} \tag{4.184}$$

where $\boldsymbol{K}_{bb}^{sr} = \int_0^1 \int_0^1 (\boldsymbol{B}_{b}^{s})^t \, \boldsymbol{D}_{bb} \, \boldsymbol{B}_{b}^{r} \, J_x J_y \, d\xi \, d\eta$ (4.185)

4.4.2.4 Strain energy variation term $dU_{\psi\psi}$

Substituting from equation (4.171) into equation (4.87), then

$$dU'_{\psi\psi} = \sum_{s=1}^{m} \sum_{r=1}^{m} (d\delta_{\psi}^{s})^t \, (\boldsymbol{B}_{\psi}^{s})^t \, \boldsymbol{D}_{\psi\psi} \, \boldsymbol{B}_{\psi}^{r} \, \delta_{\psi}^{r} \tag{4.186}$$

and by integration over the strip area:

$$dU_{\psi\psi} = \sum_{s=1}^{m}\sum_{r=1}^{m} (d\delta_{\psi}^{s})^{t} K_{\psi\psi}^{sr} \delta_{\psi}^{r} \tag{4.187}$$

where $$K_{\psi\psi}^{sr} = \int_{0}^{1}\int_{0}^{1} (B_{\psi}^{s})^{t} D_{\psi\psi} B_{\psi}^{r} J_x J_y \, d\xi \, d\eta \tag{4.188}$$

4.4.2.5 Strain energy variation terms dU_{ob}, dU_{bo}

Substituting from equation (4.167), (4.169) into (4.88), then

$$dU'_{ob} = \sum_{s=1}^{m}\sum_{r=1}^{m} (d\delta_{o}^{s})^{t} (B_{o}^{s})^{t} D_{ob} B_{b}^{r} \delta_{b}^{r} \tag{4.189}$$

and $$dU_{ob} = \sum_{s=1}^{m}\sum_{r=1}^{m} (d\delta_{o}^{s})^{t} K_{ob}^{sr} \delta_{b}^{r} \tag{4.190}$$

where $$K_{ob}^{sr} = \int_{0}^{1}\int_{0}^{1} (B_{o}^{s})^{t} D_{ob} B_{b}^{r} J_x J_y \, d\xi \, d\eta \tag{4.191}$$

Similarly, it can be deduced that

$$dU_{bo} = \sum_{s=1}^{m}\sum_{r=1}^{m} (d\delta_{b}^{s})^{t} K_{bo}^{sr} \delta_{o}^{r} \tag{4.192}$$

where $$K_{bo}^{sr} = \int_{0}^{1}\int_{0}^{1} (B_{b}^{s})^{t} D_{bo} B_{o}^{r} J_x J_y \, d\xi \, d\eta \tag{4.193}$$

4.4.2.6 Strain energy variation terms $dU_{o\psi}$, $dU_{\psi o}$

Substituting from equation (4.167), (4.171) into (4.90), then

$$dU'_{o\psi} = \sum_{s=1}^{m}\sum_{r=1}^{m} (d\delta_{o}^{s})^{t} (B_{o}^{s})^{t} D_{o\psi} B_{\psi}^{r} \delta_{\psi}^{r} \tag{4.194}$$

and

$$dU_{o\psi} = \sum_{s=1}^{m}\sum_{r=1}^{m} (d\delta_{o}^{s})^{t} K_{o\psi}^{sr} \delta_{\psi}^{r} \tag{4.195}$$

where $$K_{o\psi}^{sr} = \int_{0}^{1}\int_{0}^{1} (B_{o}^{s})^{t} D_{o\psi} B_{\psi}^{r} J_x J_y \, d\xi \, d\eta \tag{4.196}$$

Similarly it can be deduced that

$$dU_{\psi o} = \sum_{s=1}^{m}\sum_{r=1}^{m} (d\delta_{\psi}^{s})^{t} K_{\psi o}^{sr} \delta_{o}^{r} \tag{4.197}$$

where $K_{\psi o}^{sr} = \int_0^1 \int_0^1 (B_\psi^s)^t D_{\psi o} B_o^r J_x J_y \, d\xi \, d\eta$ (4.198)

4.4.2.7 Strain energy variation terms $dU_{b\psi}$, $dU_{\psi b}$

Substituting from equation (4.169), (4.171) into (4.92), then

$$dU'_{b\psi} = - \sum_{s=1}^{m} \sum_{r=1}^{m} (d\delta_b^s)^t (B_b^s)^t D_{b\psi} B_\psi^r \delta_\psi^r \quad (4.199)$$

and $$dU_{b\psi} = - \sum_{s=1}^{m} \sum_{r=1}^{m} (d\delta_b^s)^t K_{b\psi}^{sr} \delta_\psi^r \quad (4.200)$$

where $K_{b\psi}^{sr} = \int_0^1 \int_0^1 (B_b^s)^t D_{b\psi} B_\psi^r J_x J_y \, d\xi \, d\eta$ (4.201)

Similarly it can be deduced that

$$dU_{\psi b} = - \sum_{s=1}^{m} \sum_{r=1}^{m} (d\delta_\psi^s)^t K_{\psi b}^{sr} \delta_b^r \quad (4.202)$$

where $K_{\psi b}^{sr} = \int_0^1 \int_0^1 (B_\psi^s)^t D_{\psi b} B_b^r J_x J_y \, d\xi \, d\eta$ (4.203)

4.4.3 Small deflection element stiffness matrix

Substituting from equations (4.178), (4.181), (4.184), (4.187), (4.190), (4.192), (4.195), (4.197), (4.200), (4.202) into the *x*-*y* integration of (4.175), then we obtain:

$$\begin{aligned} dU_{small} = \sum_{s=1}^{m} \sum_{r=1}^{m} \Big\{ & (d\delta_\psi^s)^t K_{\gamma\gamma}^{sr} \delta_\psi^r + (d\delta_o^s)^t K_{oo}^{sr} \delta_o^r + (d\delta_b^s)^t K_{bb}^{sr} \delta_b^r + (d\delta_\psi^s)^t K_{\psi\psi}^{sr} \delta_\psi^r \\ & - (d\delta_o^s)^t K_{ob}^{sr} \delta_b^r - (d\delta_b^s)^t K_{bo}^{sr} \delta_o^r + (d\delta_o^s)^t K_{o\psi}^{sr} \delta_\psi^r + (d\delta_\psi^s)^t K_{\psi o}^{sr} \delta_o^r \\ & - (d\delta_b^s)^t K_{b\psi}^{sr} \delta_\psi^r - (d\delta_\psi^s)^t K_{\psi b}^{sr} \delta_b^r \Big\} \end{aligned} \quad (4.204)$$

which can be rewritten as:

$$dU_{small} = \sum_{s=1}^{m} \sum_{r=1}^{m} (d\delta^s)^t K^{sr} \delta^r \quad (4.205)$$

where

$$d\delta^s = \begin{bmatrix} d\delta_o^s \\ d\delta_b^s \\ d\delta_\psi^s \end{bmatrix}, \qquad \delta^r = \begin{bmatrix} \delta_o^r \\ \delta_b^r \\ \delta_\psi^r \end{bmatrix} \quad (4.206)$$

and

$$K^{sr} = \begin{bmatrix} K^{sr}_{oo} & -K^{sr}_{ob} & K^{sr}_{o\psi} \\ -K^{sr}_{bo} & K^{sr}_{bb} & -K^{sr}_{b\psi} \\ K^{sr}_{\psi o} & -K^{sr}_{\psi b} & K^{sr}_{\psi\psi} + K^{sr}_{\gamma\gamma} \end{bmatrix} \tag{4.207}$$

which represents the *sr* part in the strip stiffness matrix with infinitesimal strains being assumed. Notice that for symmetric composites:

$$D_{ob} = \mathbf{O}, \quad D_{o\psi} = \mathbf{O}, \text{ i.e.} \quad K^{sr}_{ob} = K^{sr}_{bo} = K^{sr}_{o\psi} = K^{sr}_{\psi o} = \mathbf{O}. \tag{4.208}$$

4.5 EQUIVALENT NODAL LOADING AND STATIC LINEAR EQUATIONS

Equivalent nodal loading vector per the *r*th harmonic, or *y* term, is partitioned as follows:

$$F^r = \{ F^r_o \quad F^r_b \quad F^r_\psi \} \tag{4.209}$$

and the equivalent loading vector is defined such that it does the same work done by actual loads due to a variational displacement field, i.e.

$$dW = \sum_{r=1}^{m} (d\delta)^t F^r = \sum_{r=1}^{m} \left[(d\delta^r_o)^t F^r_o + (d\delta^r_b)^t F^r_b + (d\delta^r_\psi)^t F^r_\psi \right] \tag{4.210}$$

$\equiv$ the work done by the actual load.

4.5.1 Distributed lateral loading with intensity q

If the strip is subjected to distributed loading in the *z* direction, with intensity *q(x,y)* (load per unit area), then the actual work done by that load due to displacement variation is:

$$\delta W = \int_{strip}\int q\, \delta w\, dx\, dy = \int_0^1\int_0^1 \delta w\, q\, J_x J_y\, d\xi\, d\eta$$

$$\equiv \sum_{i=1}^{n}\sum_{r=1}^{m} \int_0^1\int_0^1 q f^r_w(\eta) \left[G_i(\xi) w_i + H_i(\xi) w_{i,x} \right] J_x J_y\, d\xi\, d\eta \tag{4.211}$$

Comparing equation (4.210) with (4.211), it can be deduced that:

$$F^r_o = \mathbf{O}, \quad F^r_\psi = \mathbf{O} \tag{4.212}$$

and

$$F^r_b \equiv \{ (F^r_z)_1 \quad M^r_1 \quad (F^r_z)_2 \quad M^r_2 \quad \ldots \quad (F^r_z)_n \quad M^r_n \} \tag{4.213}$$

where

$$(F_z^r) = \int_0^1\int_0^1 q\, G_i(\xi) f_w^r(\eta)\, J_x J_y\, d\xi\, d\eta,\; M_i^r = \int_0^1\int_0^1 q\, H_i(\xi) f_w^r(\eta)\, J_x J_y\, d\xi\, d\eta \qquad (4.214)$$

4.5.2 Concentrated forces and moments at node *i* and $\eta = \eta_j$

These are defined in terms of five components $\{F_x \;\; F_y \;\; F_z \;\; M_x \;\; M_y\}$,where F_x, F_y, F_z are forces at *x*, *y*, *z* directions and M_x, M_y are the bending moments in *x*, *y* directions, respectively. Notice that average slope angles can be defined from equations (3.35) and (3.36) as follows:

$$\theta_y = -\frac{\partial w}{\partial x} - \psi_y,\;\; \theta_x = \frac{\partial w}{\partial y} - \psi_x \qquad (4.215)$$

Equivalent nodal loading exists only for the loaded node *i*, and using the following interpolation equations at $\eta = \eta_j$:

$$\delta u^{\circ}(\xi_i, \eta_j) = \sum_{r=1}^{m} f_u^r(\eta_j)\, \delta u_i^r \qquad (4.216)$$

$$\delta v^{\circ}(\xi_i, \eta_j) = \sum_{r=1}^{m} f_v^r(\eta_j)\, \delta v_i^r \qquad (4.217)$$

$$\delta w(\xi_i, \eta_j) = \sum_{r=1}^{m} f_w^r(\eta_j)\, \delta w_i^r \qquad (4.218)$$

$$\delta\theta_x(\xi_i, \eta_j) = \sum_{r=1}^{m} \left\{ \frac{f_{w,\eta}^r(\eta_j)}{J_y}\, \delta w_i^r - f_{\psi_x}^r(\eta_j)(\delta\psi_x^r)_i \right\} \qquad (4.219)$$

$$\delta\theta_y(\xi_i, \eta_j) = \sum_{r=1}^{m} \left\{ - f_w^r(\eta_j)\, \delta w_{i,x}^r - f_{\psi_y}^r(\eta_j)(\delta\psi_y^r)_i \right\} \qquad (4.220)$$

then it can be deduced that:

$$\delta W = \sum_{r=1}^{m} \left\{ F_x f_u^r(\eta_j)\, \delta u_i^r + F_y f_v^r(\eta_j)\, \delta v_i^r + F_z f_w^r(\eta_j)\, \delta w_i^r \right.$$
$$\left. + M_x \left[\frac{f_{w,\eta}^r(\eta_j)}{J_y}\, \delta w_i^r - f_{\psi_x}^r(\eta_j)(\delta\psi_x^r)_i \right] + M_y \left[- f_w^r(\eta_j)\, \delta w_{i,x}^r - f_{\psi_y}^r(\eta_j)(\delta\psi_y^r)_i \right] \right\} \qquad (4.221)$$

Comparing equation (4.221) with (4.210), then equivalent nodal load components exist only at node *i* and are defined as follows:

$$F_o^r = \left\{ 0 \;\; 0 \;\ldots\; (F_x^r)_i \;\; (F_y^r)_i \;\ldots\; 0 \;\; 0 \right\} \qquad (4.222)$$

$$F_b^r = \left\{0 \quad 0 \ldots (F_z^r)_i \quad M_i^r \ldots 0 \quad 0\right\} \tag{4.223}$$

$$F_\psi^r = \left\{0 \quad 0 \ldots (M_x^r)_i \quad (M_y^r)_i \ldots 0 \quad 0\right\} \tag{4.224}$$

where

$$(F_x^r)_i = F_x f_u^r(\eta_j) \tag{4.225}$$

$$(F_y^r)_i = F_y f_v^r(\eta_j) \tag{4.226}$$

$$(F_z^r)_i = F_z f_w^r(\eta_j) + M_x \frac{f_{w,\eta}^r}{J_y} \tag{4.227}$$

$$M_i^r = - M_y f_w^r(\eta_j) \tag{4.228}$$

$$(M_x^r)_i = - M_x f_{\psi_x}^r(\eta_j) \tag{4.229}$$

$$(M_y^r)_i = - M_y f_{\psi_y}^r(\eta_j) \tag{4.230}$$

4.5.3 Line loading at $\xi = \xi_i$

This will be defined in terms of loads and moments per unit length in *y*-direction; $\{ F_x^y, F_y^y, F_z^y, M_x^y, M_y^y \}$ and due to a variation in the displacement field, the following interpolation equations are obtained:

$$\delta u^o(\xi_i, \eta) = \sum_{r=1}^{m} f_u^r(\eta)\, \delta u_i^r \tag{4.231}$$

$$\delta v^o(\xi_i, \eta) = \sum_{r=1}^{m} f_v^r(\eta)\, \delta v_i^r \tag{4.232}$$

$$\delta w(\xi_i, \eta) = \sum_{r=1}^{m} f_w^r(\eta)\, \delta w_i^r \tag{4.233}$$

$$\delta\theta_x(\xi_i, \eta) = \sum_{r=1}^{m} \left\{\frac{f_{w,\eta}^r(\eta)}{J_y} \delta w_i^r - f_{\psi_x}^r(\eta)(\delta\psi_x^r)_i\right\} \tag{4.234}$$

$$\delta\theta_y(\xi_i, \eta) = \sum_{r=1}^{m} \left\{- f_w^r(\eta)\, \delta w_{i,x}^r - f_{\psi_y}^r(\eta)(\delta\psi_y^r)_i\right\} \tag{4.235}$$

At an infinitesimal length Δy, the force and moment components are:

$$\Delta F_x = F_x^y \Delta y = J_y F_x^y \Delta\eta \tag{4.236}$$

$$\Delta F_y = F_y^y \Delta y = J_y F_y^y \Delta\eta \tag{4.237}$$

.....

$$\Delta M_y = M_y^y \Delta y = J_y M_y^y \Delta\eta \tag{4.238}$$

Hence, the work done by this line loading can be expressed as follows:

$$\delta W = \sum_{r=1}^{m} \int_0^1 \Big\{ F_x^y f_u^r(\eta)\,\delta u_i^r + F_y^y f_v^r(\eta)\,\delta v_i^r + F_z^y f_w^r(\eta)\,\delta w_i^r + M_x \Big[\frac{f_{w,\eta}^r(\eta)}{J_y}\,\delta w_i^r - f_{\psi_x}^r(\eta)(\delta\psi_x^r)_i \Big] + M_y \Big[- f_w^r(\eta)\,\delta w_{i,x}^r - f_{\psi_y}^r(\eta)(\delta\psi_y^r)_i \Big] \Big\} J_y\, d\eta \tag{4.239}$$

and the equivalent nodal loading components, which exist only at node i, can be expressed as follows:

$$(F_x^r)_i = \int_0^1 F_x^y f_u^r(\eta)\, J_y\, d\eta \tag{4.240}$$

$$(F_y^r)_i = \int_0^1 F_y^y f_v^r(\eta)\, J_y\, d\eta \tag{4.241}$$

$$(F_z^r)_i = \int_0^1 \big[F_z^y\, f_w^r(\eta)\, J_y + M_x^y f_{w,\eta}^r(\eta) \big] d\eta \tag{4.242}$$

$$M_i^r = - \int_0^1 M_y^y f_w^r(\eta)\, J_y\, d\eta \tag{4.243}$$

$$(M_x^r)_i = - \int_0^1 M_x^y f_{\psi_x}^r(\eta)\, J_y\, d\eta \tag{4.244}$$

$$(M_y^r)_i = - \int_0^1 M_y^y f_{\psi_y}^r(\eta)\, J_y\, d\eta \tag{4.245}$$

4.5.4 Linear static analysis equation

Using the principle of virtual work, then the variation of the total potential energy is zero,

i.e. $$d\chi = dU - dW = 0 \tag{4.246}$$

where dU is the variation of the strain energy and dW is the variation of the work done by external loads. For the case of infinitesimal strains it can be deduced from equation (4.204) that:

$$dU \simeq dU_{small} = \sum_{s=1}^{m} \sum_{r=1}^{m} (d\boldsymbol{\delta}^s)^t \boldsymbol{K}^{sr} \boldsymbol{\delta}^r \tag{4.247}$$

Substituting from equations (4.247) and (4.210) into (4.246) it can be shown that:

$$d\chi = \sum_{s=1}^{m} \left\{ (d\delta^s)^t \right\} \left\{ \sum_{r=1}^{m} K^{sr} \delta^r - F^s \right\} = 0 \tag{4.248}$$

Hence, it can be deduced that:

$$\sum_{r=1}^{m} K^{sr} \delta^r - F^s = \mathbf{O}, \; s = 1, 2, \ldots, m \tag{4.249}$$

which can be rewritten in the following matrix form:

$$K \delta = F \tag{4.250}$$

where $F = \{ F^1 \quad F^2 \quad \ldots \quad F^m \}$ (4.251)

and

$$K = \begin{bmatrix} K^{11} & \ldots & K^{1r} & \ldots & K^{1m} \\ \ldots & \ldots & \ldots & \ldots & \ldots \\ K^{s1} & \ldots & K^{sr} & \ldots & K^{sm} \\ \ldots & \ldots & \ldots & \ldots & \ldots \\ K^{m1} & \ldots & K^{mr} & \ldots & K^{mm} \end{bmatrix} \tag{4.252}$$

Equation (4.250) represents linear static equation which can be employed for linear static stress analysis.

4.6 NONLINEAR MATRICES AND VECTORS

4.6.1 Large strain components

(i) Interpolated **0** *vector*

Substituting from equations (4.150), (4.151) into (4.37), it can be deduced that

$$\mathbf{0}_m = \sum_{r=1}^{m} G_m^r(\xi, \eta) \, \delta_o^r \tag{4.253}$$

where

$$G_m^r = \begin{bmatrix} \ldots & N'_i(\xi) f_u^r(\eta) / J_x & 0 & \ldots \\ \ldots & 0 & N'_i(\xi) f_v^r(\eta) / J_x & \ldots \\ \ldots & N_i(\xi) f_{u,\eta}^r(\eta) / J_y & 0 & \ldots \\ \ldots & 0 & N_i(\xi) f_{v,\eta}^r(\eta) / J_y & \ldots \end{bmatrix} \tag{4.254}$$

Similarly, it can be shown that:

$$\mathbf{0}_w = \sum_{r=1}^{m} \boldsymbol{G}_w^r(\xi,\eta)\,\boldsymbol{\delta}_b^r \tag{4.255}$$

where

$$\boldsymbol{G}_w^r = \begin{bmatrix} \cdots & G'_i(\xi) f_w^r(\eta)/J_x & H'_i(\xi) f_w^r(\eta)/J_x & \cdots \\ \cdots & G_i(\xi) f_{w,\eta}^r(\eta)/J_y & H_i(\xi) f_{w,\eta}^r(\eta)/J_y & \cdots \end{bmatrix} \tag{4.256}$$

and also: $$\mathbf{0}_\theta = \sum_{r=1}^{m} \boldsymbol{G}_\theta^r(\xi,\eta)\,\boldsymbol{\delta}_b^r \tag{4.257}$$

where

$$\boldsymbol{G}_\theta^r = \begin{bmatrix} \cdots & G''_i(\xi) f_w^r(\eta)/J_x^2 & H''_i(\xi) f_w^r(\eta)/J_x^2 & \cdots \\ \cdots & G'_i(\xi) f_{w,\eta}^r(\eta)/J_x J_y & H'_i(\xi) f_{w,\eta}^r(\eta)/J_x J_y & \cdots \\ \cdots & G'_i(\xi) f_{w,\eta}^r(\eta)/J_x J_y & H'_i(\xi) f_{w,\eta}^r(\eta)/J_x J_y & \cdots \\ \cdots & G_i(\xi) f_{w,\eta\eta}^r(\eta)/J_y^2 & H_i(\xi) f_{w,\eta\eta}^r(\eta)/J_y^2 & \cdots \end{bmatrix} \tag{4.258}$$

(ii) Finite strain values and strain increments

Using the previous equations of $\mathbf{0}$ in equations (4.40) - (4.43), it can be shown that:

$$\boldsymbol{\varepsilon}_m = \tfrac{1}{2} A_m(x,y) \sum_{r=1}^{m} \boldsymbol{G}_m^r(x,y)\,\boldsymbol{\delta}_o^r \tag{4.259}$$

$$\boldsymbol{\varepsilon}_w = \tfrac{1}{2} A_w(x,y) \sum_{r=1}^{m} \boldsymbol{G}_w^r(x,y)\,\boldsymbol{\delta}_b^r \tag{4.260}$$

$$\hat{\boldsymbol{\varepsilon}}_{m\theta} = A_m(x,y) \sum_{r=1}^{m} \boldsymbol{G}_\theta^r(x,y)\,\boldsymbol{\delta}_b^r = A_\theta(x,y) \sum_{r=1}^{m} \boldsymbol{G}_m^r(x,y)\,\boldsymbol{\delta}_m^r \tag{4.261}$$

$$\hat{\boldsymbol{\varepsilon}}_\theta = \tfrac{1}{2} A_\theta(x,y) \sum_{r=1}^{m} \boldsymbol{G}_\theta^r(x,y)\,\boldsymbol{\delta}_b^r \tag{4.262}$$

with the following differential values at (x, y):

$$d\boldsymbol{\varepsilon}_m = A_m \sum_{r=1}^{m} \boldsymbol{G}_m^r(\xi,\eta)\,d\boldsymbol{\delta}_o^r \tag{4.263}$$

$$d\boldsymbol{\varepsilon}_w = A_w \sum_{r=1}^{m} \boldsymbol{G}_w^r(\xi,\eta)\,d\boldsymbol{\delta}_b^r \tag{4.264}$$

$$d\hat{\boldsymbol{\varepsilon}}_{m\theta} = A_m \sum_{r=1}^{m} \boldsymbol{G}_\theta^r(\xi,\eta)\,d\boldsymbol{\delta}_b^r + A_\theta \sum_{r=1}^{m} \boldsymbol{G}_m^r(\xi,\eta)\,d\boldsymbol{\delta}_o^r \tag{4.265}$$

$$d\hat{\varepsilon}_\theta = A_\theta \sum_{r=1}^{m} G_\theta^r(\xi,\eta)\, d\delta_b^r \tag{4.266}$$

4.6.2 Derivation of non-linear stiffness matrix K_σ

Integrating equation (4.94) over the plate thickness, then:

$$dU'_l = dU'_m + dU'_w + dU'_{m\theta} + dU'_\theta \tag{4.267}$$

The terms in the previous equation can be integrated over the area of the strip leading to the derivation of the different terms of K_σ as follows:

(a) $$dU_m = \int_0^1\int_0^1 dU'_m\, J_x J_y\, d\xi\, d\eta \equiv \sum_{s=1}^{m}\sum_{r=1}^{m} (d\delta_o^s)^t\, K_{mm}^{sr}\, \delta_o^r \tag{4.268}$$

where $$K_{mm}^{sr} = \int_0^1\int_0^1 \left(G_m^s(\xi,\eta)\right)^t S_{mm}\, G_m^r(\xi,\eta)\, J_x J_y\, d\xi\, d\eta \tag{4.269}$$

(b) $$dU_w = \sum_{s=1}^{m}\sum_{r=1}^{m} (d\delta_b^s)^t\, K_{ww}^{sr}\, \delta_b^r \tag{4.270}$$

where $$K_{ww}^{sr} = \int_0^1\int_0^1 \left(G_w^s(\xi,\eta)\right)^t S_{ww}\, G_w^r(\xi,\eta)\, J_x J_y\, d\xi\, d\eta \tag{4.271}$$

(c) $$dU_{m\theta} = \sum_{s=1}^{m}\sum_{r=1}^{m} \left[(d\delta_o^s)^t\, K_{m\theta}^{sr}\, \delta_b^r + (d\delta_b^s)^t\, K_{\theta m}^{sr}\, \delta_o^r \right] \tag{4.272}$$

where $$K_{m\theta}^{sr} = \int_0^1\int_0^1 \left(G_m^s(\xi,\eta)\right)^t S_{m\theta}\, G_\theta^r(\xi,\eta)\, J_x J_y\, d\xi\, d\eta \tag{4.273a}$$

and $$K_{\theta m}^{sr} = \int_0^1\int_0^1 \left(G_\theta^s(\xi,\eta)\right)^t S_{\theta m}\, G_m^r(\xi,\eta)\, J_x J_y\, d\xi\, d\eta \tag{4.273b}$$

(d) $$dU_\theta = \sum_{s=1}^{m}\sum_{r=1}^{m} (d\delta_b^s)^t\, K_{\theta\theta}^{sr}\, \delta_b^r \tag{4.274}$$

where $$K_{\theta\theta}^{sr} = \int_0^1\int_0^1 \left(G_\theta^s(\xi,\eta)\right)^t S_{\theta\theta}\, G_\theta^r(\xi,\eta)\, J_x J_y\, d\xi\, d\eta \tag{4.275}$$

The strain energy variation part dU_l can now be expressed as follows:

$$dU_l = \sum_{s=1}^{m}\sum_{r=1}^{m} (d\delta^s)\, K_\sigma^{sr}\, \delta^r \tag{4.276}$$

Using: $\delta^r = \{ \delta_o^r \quad \delta_b^r \quad \delta_\psi^r \}$ then, it can be shown that:

$$K_\sigma^{sr} = \begin{bmatrix} K_{mm}^{sr} & K_{m\theta}^{sr} & \mathbf{O} \\ K_{\theta m}^{sr} & K_{ww}^{sr} + K_{\theta\theta}^{sr} & \mathbf{O} \\ \mathbf{O} & \mathbf{O} & \mathbf{O} \end{bmatrix} \tag{4.277}$$

4.6.3 Derivation of coupling vector $\mathbf{F}_l$

Notice that by integrating equation (4.122) over the plate thickness then:

$$dU_{sl}' = (dU_o')_{sl} + (dU_b')_{sl} + (dU_\psi')_{sl} \tag{4.278}$$

Substituting from equations (4.167), (4.169), (4.171) into equations (4.128), (4.131), (4.134) and integrating over the x-y plane of the strip, then the integrated terms of equation (4.278) can be expressed as follows:

(a) $$(dU_o)_{sl} = \sum_{s=1}^{m} (d\delta_o^s)^t (F_o^s)_l \tag{4.279}$$

where $$(F_o^s)_l = \int_0^1 \int_0^1 \left(B_o^s(\xi,\eta)\right)^t \sigma_o J_x J_y \, d\xi \, d\eta \tag{4.280}$$

(b) $$(dU_b)_{sl} = \sum_{s=1}^{m} (d\delta_b^s)^t (F_b^s)_l \tag{4.281}$$

where $$(F_b^s)_l = \int_0^1 \int_0^1 \left(B_b^s(\xi,\eta)\right)^t \sigma_b J_x J_y \, d\xi \, d\eta \tag{4.282}$$

(c) $$(dU_\psi)_{sl} = \sum_{s=1}^{m} (d\delta_\psi^s)^t (F_\psi^s)_l \tag{4.283}$$

where $$(F_\psi^s)_l = \int_0^1 \int_0^1 \left(B_\psi^s(\xi,\eta)\right)^t \sigma_\psi J_x J_y \, d\xi \, d\eta \tag{4.284}$$

Finally, the strain energy part dU_{sl} can be expressed as follows:

$$dU_{sl} = \sum_{s=1}^{m} (d\delta^s)^t (F^s)_l \tag{4.285}$$

where $$(F^s)_l \equiv \{ (F_o^s)_l \quad (F_b^s)_l \quad (F_\psi^s)_l \} \tag{4.286}$$

Equation (4.285) can also be written in the following matrix form :

$$dU_{sl} = d\delta^t F_l \tag{4.287}$$

where $$F_l \equiv \{ F_l^1 \quad F_l^2 \quad \ldots \quad F_l^s \quad \ldots \quad F_l^m \} \tag{4.288}$$

4.6.4 Non-linear static equations

Notice that it can be deduced from equation (4.56) that:

$$dU = dU_{small} + dU_l + dU_{sl} \tag{4.289}$$

Substituting from equations (4.205) , (4.276), (4.287) into equation (4.289), the variation of the strain energy for the case with finite strains can be written in the following matrix form:

$$dU = d\delta^t (K + K_\sigma)\,\delta + d\delta^t F_l \tag{4.290}$$

From equation (4.290) , (4.210) and the principle of virtual work, it can be shown that:

$$d\chi = dU - dW = d\delta^t \left\{ (K + K_\sigma)\,\delta + F_l - F \right\} = 0 \tag{4.291}$$

Hence, it can be deduced that:

$$(K + K_\sigma)\delta + F_l = F \tag{4.292}$$

which represents the non-linear static equation.

4.7 ELEMENT MASS MATRICES

4.7.1 Interpolated displacement, velocity and acceleration components at an instant of time t

Using equations (4.150) -(4.154), at an instant of time *t*, then:

$$u^o(x,y,t) = \sum_{i=1}^{n} \sum_{r=1}^{m} N_i(\xi)\, f_u^r(\eta)\, u_i^r(t) \tag{4.293}$$

$$v^o(x,y,t) = \sum_{i=1}^{n} \sum_{r=1}^{m} N_i(\xi)\, f_v^r(\eta)\, v_i^r(t) \tag{4.294}$$

$$w(x,y,t) = \sum_{i=1}^{n} \sum_{r=1}^{m} f_w^r(\eta) [\, G_i(\xi)\, w_i^r(t) + H_i(\xi)\, w_{i,x}^r(t) \,] \tag{4.295}$$

$$\psi_x(x,y,t) = \sum_{i=1}^{n} \sum_{r=1}^{m} N_i(\xi)\, f_{\psi_x}^r(\eta)\, \psi_{x_i}^r(t) \tag{4.296}$$

$$\psi_y(x,y,t) = \sum_{i=1}^{n}\sum_{r=1}^{m} N_i(\xi)\, f_{\psi_y}^{r}(\eta)\, \psi_y{}^{r}{}_{i}(t) \tag{4.297}$$

Equations (4.1) , (4.2) can also be written in the following matrix form:

$$q_m = \begin{bmatrix} u \\ v \end{bmatrix} = q_o - z q_\theta - f_\psi(z) q_\psi \tag{4.298}$$

where

$$q_o = \begin{bmatrix} u^o \\ v^o \end{bmatrix}, \qquad q_\theta = \begin{bmatrix} \partial w/\partial x \\ \partial w/\partial y \end{bmatrix}, \qquad q_\psi = \begin{bmatrix} -\psi_y \\ \psi_x \end{bmatrix} \tag{4.299}$$

Similarly from equation (4.3): $q_w \equiv [w]$ (4.300)

Substituting from equations (4.293)-(4.297) into equations (4.299) and (4.300) then they can be written as follows:

$$q_o = \begin{bmatrix} u^o \\ v^o \end{bmatrix} = \sum_{r=1}^{m} N_o^r(\xi,\eta)\, \delta_o^r(t) \tag{4.301}$$

$$q_\theta = \begin{bmatrix} \dfrac{\partial w}{\partial x} \\ \dfrac{\partial w}{\partial y} \end{bmatrix} = \sum_{r=1}^{m} N_\theta^r(\xi,\eta)\, \delta_b^r(t) \tag{4.302}$$

$$q_\psi = \begin{bmatrix} -\psi_y \\ \psi_x \end{bmatrix} = \sum_{r=1}^{m} N_\psi^r(\xi,\eta)\, \delta_\psi^r(t) \tag{4.303}$$

$$q_w = [w] = \sum_{r=1}^{m} N_w^r(\xi,\eta)\, \delta_b^r(t) \tag{4.304}$$

where

$$N_o^r(\xi,\eta) = \begin{bmatrix} \cdots & N_i(\xi) f_u^r(\eta) & 0 & \cdots \\ \cdots & 0 & N_i(\xi) f_v^r(\eta) & \cdots \end{bmatrix} \tag{4.305}$$

$$N^r{}_\theta(\xi,\eta) = \begin{bmatrix} \cdots & G'_i(\xi) f_w^r(\eta)/J_x & H'_i(\xi) f_w^r(\eta)/J_x & \cdots \\ \cdots & G_i(\xi) f_{w,\eta}^r(\eta)/J_y & H_i(\xi) f_{w,\eta}^r(\eta)/J_y & \cdots \end{bmatrix} \tag{4.306}$$

$$N_{\psi}^{r}(\xi,\eta) = \begin{bmatrix} \cdots & 0 & N_i(\xi) f_{\psi_y}^{r}(\eta) & \cdots \\ \cdots & -N_i(\xi) f_{\psi_x}^{r}(\eta) & 0 & \cdots \end{bmatrix} \tag{4.307}$$

$$N_{w}^{r}(\xi,\eta) = \begin{bmatrix} \cdots & G_i(\xi) f_{w}^{r}(\eta) & H_i(\xi) f_{w}^{r}(\eta) & \cdots \end{bmatrix} \tag{4.308}$$

Velocity and acceleration equation are obtained by differentiating displacement equation with respect to. time, hence

$$\dot{q}_m = \begin{bmatrix} \dot{u} \\ \dot{v} \end{bmatrix} = \dot{q}_o - z\dot{q}_\theta - f_\psi(z)\,\dot{q}_\psi \tag{4.309}$$

$$\dot{q}_w \equiv [\dot{w}] \tag{4.310}$$

$$\ddot{q}_m = \begin{bmatrix} \ddot{u} \\ \ddot{v} \end{bmatrix} = \ddot{q}_o - z\ddot{q}_\theta - f_\psi(z)\ddot{q}_\psi \tag{4.311}$$

$$\ddot{q}_w \equiv [\ddot{w}] \tag{4.312}$$

where

$$\dot{q}_o = \begin{bmatrix} \dot{u}^o \\ \dot{v}^o \end{bmatrix} = \sum_{r=1}^{m} N_o^r(\xi,\eta)\,\dot{\delta}_o^r(t) \tag{4.313}$$

$$\dot{q}_\theta = \begin{bmatrix} \dfrac{\partial \dot{w}}{\partial x} \\ \dfrac{\partial \dot{w}}{\partial y} \end{bmatrix} = \sum_{r=1}^{m} N_\theta^r(\xi,\eta)\,\dot{\delta}_b^r(t) \tag{4.314}$$

$$\dot{q}_\psi = \begin{bmatrix} \dot{\psi}_y \\ -\dot{\psi}_x \end{bmatrix} = \sum_{r=1}^{m} N_\psi^r(\xi,\eta)\,\dot{\delta}_\psi^r(t) \tag{4.315}$$

$$\dot{q}_w = [\dot{w}] = \sum_{r=1}^{m} N_w^r(\xi,\eta)\,\dot{\delta}_b^r(t) \tag{4.316}$$

Similarly, it can be deduced that:

$$\ddot{q}_o = \begin{bmatrix} \ddot{u}^o \\ \ddot{v}^o \end{bmatrix} = \sum_{r=1}^{m} N_o^r(\xi,\eta)\,\ddot{\delta}_o^r(t) \tag{4.317}$$

$$\ddot{q}_\theta = \begin{bmatrix} \dfrac{\partial \ddot{w}}{\partial x} \\ \dfrac{\partial \ddot{w}}{\partial y} \end{bmatrix} = \sum_{r=1}^{m} N_\theta^r(\xi,\eta)\, \ddot{\delta}_b^r(t) \tag{4.318}$$

$$\ddot{q}_\psi = \begin{bmatrix} \ddot{\psi}_y \\ -\ddot{\psi}_x \end{bmatrix} = \sum_{r=1}^{m} N_\psi^r(\xi,\eta)\, \ddot{\delta}_\psi^r(t) \tag{4.319}$$

$$\ddot{q}_w = [\ddot{w}] = \sum_{r=1}^{m} N_w^r(\xi,\eta)\, \ddot{\delta}_b^r(t) \tag{4.320}$$

4.7.2 Element mass matrix

Using D'Alembert's principle, the force vector due to an acceleration $\ddot{q}(x,y,z,t)$ at an infinitesimal volume $\Delta x\, \Delta y\, \Delta z$ is:

$$\Delta F = -\ddot{q}\, \Delta x\, \Delta y\, \Delta z \tag{4.321}$$

and the work done by that force due to a virtual displacement field dq is

$$dW_D = -\int\int\int \rho\, (dq^t\, \ddot{q})\, dx\, dy\, dz \equiv \int\int\int (d\bar{W}_D)\, dx\, dy\, dz = \int\int (dW'_D)\; dx\, dy \tag{4.322}$$

where

$$d\bar{W}_D = -\rho\, dq^t\, \ddot{q} \tag{4.323}$$

and

$$dW'_D = \int_{-h/2}^{h/2} (d\bar{W}_D)\, dz \tag{4.324}$$

From previous equations of displacement and acceleration, it can be shown that:

$$\begin{aligned} d\bar{W}_D &= -\rho\, (dq_m^t\, \ddot{q}_m + dq_w^t\, \ddot{q}_w) \\ &= -\rho\, (dq_o^t - z\, dq_\theta^t - f_\psi\, dq_\psi^t)(\ddot{q}_o - z\, \ddot{q}_\theta - f_\psi\, \ddot{q}_\psi) - \rho\, dq_w^t\, \ddot{q}_w \end{aligned} \tag{4.325}$$

Integrating over z, assuming the density ρ to be the same at all layers, then it can be deduced that:

$$\int_{-h/2}^{h/2} \rho\, dz = \rho\, h \tag{4.326}$$

$$\int_{-h/2}^{h/2} z\,\rho\,dz = 0 \tag{4.327}$$

$$\int_{-h/2}^{h/2} f_\psi(z)\,\rho\,dz = 0 \tag{4.328}$$

$$\int_{-h/2}^{h/2} z^2\,\rho\,dz = \rho\frac{h^3}{12} \tag{4.329}$$

$$\int_{-h/2}^{h/2} z\,f_\psi(z)\,\rho\,dz = \rho\frac{h^3}{10} \tag{4.330}$$

$$\int_{-h/2}^{h/2} f_\psi(z)^2\,\rho\,dz = \frac{17}{140}\rho\,h^3 \tag{4.331}$$

Hence it can be deduced that

$$dW_D' = dW'_o + dW'_\theta + dW'_\psi + dW'_w + dW'_{\theta\psi} + dW'_{\psi\theta} \tag{4.332}$$

where

$$dW'_o = -\rho\,h\,dq_o^t\,\ddot{q}_o \tag{4.333}$$

$$dW'_\theta = -\frac{1}{12}\rho\,h^3\,dq_\theta^t\,\ddot{q}_\theta \tag{4.334}$$

$$dW'_\psi = -\frac{17}{140}\rho\,h^3\,dq_\psi^t\,\ddot{q}_\psi \tag{4.335}$$

$$dW'_w = -\rho\,h\,q_w^t\,d\ddot{q}_w \tag{4.336}$$

$$dW'_{\theta\psi} = -\frac{1}{10}\rho\,h^3\,dq_\theta^t\,\ddot{q}_\psi \tag{4.337}$$

$$dW'_{\psi\theta} = -\frac{1}{10}\rho\,h^3\,dq_\psi^t\,\ddot{q}_\theta \tag{4.338}$$

Substituting from equations (4.301) , (4.317) into equation (4.333) and integrating over the *x*-*y* area of the strip, then it can be deduced that :

$$dW_o = -\sum_{s=1}^{m}\sum_{r=1}^{m}(d\delta_o^s)^t\,M_o^{sr}\,\ddot{\delta}_o^r \tag{4.339}$$

where $M_o^{sr} = \int_0^1 \int_0^1 \left(N_o^s(\xi,\eta)\right)^t N_o^r(\xi,\eta)\ \rho\ h\ J_x\ J_y\ d\xi\ d\eta$ (4.340)

Similarly it can be shown that

$$dW_\theta = -\sum_{s=1}^{m}\sum_{r=1}^{m} (d\delta_b^s)^t M_\theta^{sr} \ddot{\delta}_b^r \quad (4.341)$$

where $M_\theta^{sr} = \int_0^1 \int_0^1 \left(N_\theta^s(\xi,\eta)\right)^t N_\theta^r(\xi,\eta)\ \frac{\rho h^3}{12}\ J_x\ J_y\ d\xi\ d\eta$ (4.342)

$$dW_w = -\sum_{s=1}^{m}\sum_{r=1}^{m} (d\delta_b^s)^t M_w^{sr} \ddot{\delta}_b^r \quad (4.343)$$

where $M_w^{sr} = \int_0^1 \int_0^1 \left(N_w^s(\xi,\eta)\right)^t N_w^r(\xi,\eta)\ \rho\ h\ J_x\ J_y\ d\xi\ d\eta$ (4.344)

$$dW_\psi = -\sum_{s=1}^{m}\sum_{r=1}^{m} (d\delta_\psi^s)^t M_\psi^{sr} \ddot{\delta}_\psi^r \quad (4.345)$$

where $M_\psi^{sr} = \int_0^1 \int_0^1 \left(N_\psi^s(\xi,\eta)\right)^t N_\psi^r(\xi,\eta)\ \frac{17\rho h^3}{140}\ J_x\ J_y\ d\xi\ d\eta$ (4.346)

$$dW_{\theta\psi} = -\sum_{s=1}^{m}\sum_{r=1}^{m} (d\delta_b^s)^t M_{\theta\psi}^{sr} \ddot{\delta}_\psi^r \quad (4.347)$$

where $M_{\theta\psi}^{sr} = \int_0^1 \int_0^1 \left(N_\theta^s(\xi,\eta)\right)^t N_\psi^r(\xi,\eta)\ \frac{\rho h^3}{10}\ J_x\ J_y\ d\xi\ d\eta$ (4.348)

$$dW_{\psi\theta} = -\sum_{s=1}^{m}\sum_{r=1}^{m} (d\delta_\psi^s)^t M_{\psi\theta}^{sr} \ddot{\delta}_b^r \quad (4.349)$$

where $M_{\psi\theta}^{sr} = \int_0^1 \int_0^1 \left(N_\psi^s(\xi,\eta)\right)^t N_\theta^r(\xi,\eta)\ \frac{\rho h^3}{10}\ J_x\ J_y\ d\xi\ d\eta$ (4.350)

Hence

$$dW_D = -\sum_{s=1}^{m}\sum_{r=1}^{m}\left\{(d\delta_o^s)^t M_o^{sr}\ddot{\delta}_o^r + (d\delta_b^s)^t M_\theta^{sr}\ddot{\delta}_b^r + (d\delta_b^s)^t M_w^{sr}\ddot{\delta}_b^r + (d\delta_\psi^s)^t M_\psi^{sr}\ddot{\delta}_\psi^r + (d\delta_b^s)^t M_{\theta\psi}^{sr}\ddot{\delta}_\psi^r + (d\delta_\psi^s)^t M_{\psi\theta}^{sr}\ddot{\delta}_b^r\right\} \quad (4.351)$$

which can be rewritten as follows:

$$dW_D = -\sum_{s=1}^{m}\sum_{r=1}^{m}(d\boldsymbol{\delta}^s)^t M^{sr}\ddot{\boldsymbol{\delta}}^r \quad (4.352)$$

where

$$M^{sr} = \begin{bmatrix} M_o^{sr} & \mathbf{O} & \mathbf{O} \\ \mathbf{O} & M_\theta^{sr} + M_w^{sr} & M_{\theta\psi}^{sr} \\ \mathbf{O} & M_{\psi\theta}^{sr} & M_\psi^{sr} \end{bmatrix} \quad (4.353)$$

Equation (4.352) can also be written as

$$dW_D = -d\boldsymbol{\delta}^t(t)\, M\, \ddot{\boldsymbol{\delta}}(t) \quad (4.354)$$

4.7.3 Non-linear dynamic equation

Applying the principle of virtual work at an instant of time *t*, then

$$d\chi(t) = dU(t) - \sum dW(t)$$

$$= dU_{small}(t) + dU_l(t) + dU_{sl}(t) - dW(t) - dW_D(t) = 0 \quad (4.355)$$

and from previous equations, it can be deduced that:

$$d\chi(t) = d\boldsymbol{\delta}^t(t)\left\{M\ddot{\boldsymbol{\delta}} + [K + K_\sigma(t)]\boldsymbol{\delta}(t) + F_l(t) - F(t)\right\} = 0 \quad (4.356)$$

Hence

$$M\boldsymbol{\delta}^{\cdot\cdot}(t) + [K + K_\sigma(t)]\boldsymbol{\delta}(t) + F_l(t) = F(t) \quad (4.357)$$

which represents the non-linear dynamic equation.

Chapter 5

Kirchhoff-Type Finite Strip Elements

5. Kirchhoff-Type Finite Strip Elements

5.1 INTRODUCTION

Kirchhoff-type elements are based on Kirchhoff plate-bending theory, which ignores transverse shear stresses and strains. This chapter introduces the derivations of Kirchhoff-type finite strip elements using the new approach of applying polynomial interpolations along the plate width. Composite-layered plates, based on stress-strain equations as given in section 3.2, will be considered with: $\boldsymbol{\gamma} = \mathbf{O}$, $\boldsymbol{\tau} = \mathbf{O}$.

Most of the equations of these elements can be extracted from those of Reissner-type elements given in chapter 4, and only relevant equations for Kirchhoff-type elements are summarized in this chapter, for completeness.

5.2 STRESS AND STRAIN EQUATIONS

5.2.1 Displacement equations

Considering a composite layered plate at an instant of time t consisting of a number of orthotropic layers, and defining the midplane of the plate as the Cartesian x-y plane, then based on the analysis given in section 3.3.3, the displacement equations at any point (x,y,z) inside the plate can be expressed as follows:

$$u(x,y,z,t) = u^{o}(x,y,t) - z\frac{\partial w}{\partial x} \tag{5.1}$$

$$v(x,y,z,t) = v^{o}(x,y,t) - z\frac{\partial w}{\partial y} \tag{5.2}$$

$$w(x,y,z,t) \approx w(x,y,t) \tag{5.3}$$

where u^{o}, v^{o} represent the values of u, v at $z = o$.

The velocity components can be expressed by differentiating equations (5.1)-(5.3) with respect to time, i.e.

$$\dot{u}(x,y,z,t) = \dot{u}^{o}(x,y,t) - z\frac{\partial \dot{w}}{\partial x} \tag{5.4}$$

$$\dot{v}(x,y,z,t) = \dot{v}^{o}(x,y,t) - z\frac{\partial \dot{w}}{\partial y} \tag{5.5}$$

$$\dot{w}(x,y,z,t) \approx \dot{w}(x,y,t) \tag{5.6}$$

Differentiating the above equations again with respect to time, the acceleration components can be obtained as follows:

$$\ddot{u}(x,y,z,t) = \ddot{u}^{o}(x,y,t) - z\frac{\partial \ddot{w}}{\partial x} \tag{5.7}$$

$$\ddot{v}(x,y,z,t) = \ddot{v}^{o}(x,y,t) - z\frac{\partial \ddot{w}}{\partial y} \tag{5.8}$$

$$\ddot{w}(x,y,z,t) \approx \ddot{w}(x,y,t) \tag{5.9}$$

In the remaining parts of this chapter, except in section 5.7, the parameter t is ignored, and it has only been considered for dynamic analysis.

5.2.2 Strain components

5.2.2.1 Infinitesimal strains

These are defined by Cauchy strain-displacement equations:

$$\varepsilon_x^s = \frac{\partial u}{\partial x} \quad , \quad \varepsilon_y^s = \frac{\partial v}{\partial y} \quad , \quad \gamma_{xy}^s = \frac{\partial u}{\partial y} + \frac{\partial v}{\partial x} \tag{5.10}$$

Substituting from equations (5.1)-(5.3) into the above equations, the components of the infinitesimal strain can be expressed at any point inside the plate as follows:

$$\varepsilon_x^s = \frac{\partial u^o}{\partial x} - z\frac{\partial^2 w}{\partial x^2} \tag{5.11}$$

$$\varepsilon_y^s = \frac{\partial v^o}{\partial y} - z\frac{\partial^2 w}{\partial y^2} \tag{5.12}$$

$$\gamma_{xy}^s = \frac{\partial u^o}{\partial y} + \frac{\partial v^o}{\partial x} - 2z\frac{\partial^2 w}{\partial x \partial y} \tag{5.13}$$

which can be written in the following matrix form:

$$\boldsymbol{\varepsilon}_s(x,y,z) = \boldsymbol{\varepsilon}_o(x,y) - z\,\hat{\boldsymbol{\varepsilon}}_b(x,y) \tag{5.14}$$

where

$$\boldsymbol{\varepsilon}_o(x,y) = \begin{bmatrix} \dfrac{\partial u^o}{\partial x} \\ \dfrac{\partial v^o}{\partial y} \\ \dfrac{\partial u^o}{\partial y} + \dfrac{\partial v^o}{\partial x} \end{bmatrix} \tag{5.15}$$

$$\hat{\boldsymbol{\varepsilon}}_b(x,y) = \begin{bmatrix} \dfrac{\partial^2 w}{\partial x^2} \\ \dfrac{\partial^2 w}{\partial y^2} \\ 2\dfrac{\partial^2 w}{\partial x \partial y} \end{bmatrix} \tag{5.16}$$

and $\boldsymbol{\varepsilon}_s \equiv \{\varepsilon_x^s \quad \varepsilon_y^s \quad \gamma_{xy}^s\}$ (5.17)

5.2.2.2 Finite strain components

For the case of finite strains, Green's strain-displacement equations are used such that:

$$\varepsilon_x = \varepsilon_x^s + \varepsilon_x^l \tag{5.18}$$

$$\varepsilon_y = \varepsilon_y^s + \varepsilon_y^l \tag{5.19}$$

$$\gamma_{xy} = \gamma_{xy}^s + \gamma_{xy}^l \tag{5.20}$$

where ε_x^l, ε_y^l, γ_{xy}^l are as given by equations (4.27)-(4.29). Hence the additional (nonlinear) terms due to finite strains can be expressed in the following matrix form:

$$\boldsymbol{\varepsilon}_l = \boldsymbol{\varepsilon}_m(x,y) + \boldsymbol{\varepsilon}_w(x,y) - z\hat{\boldsymbol{\varepsilon}}_{m\theta}(x,y) + z^2\hat{\boldsymbol{\varepsilon}}_\theta(x,y) \tag{5.21}$$

where $\boldsymbol{\varepsilon}_l = \{\varepsilon_x^l \quad \varepsilon_y^l \quad \gamma_{xy}^l\}$ (5.22)

and $\boldsymbol{\varepsilon}_m$, $\boldsymbol{\varepsilon}_w$, $\hat{\boldsymbol{\varepsilon}}_{m\theta}$, $\hat{\boldsymbol{\varepsilon}}_\theta$ are as given by equations (4.32)-(4.35), respectively.

Finally the vector of total strain components at any point (x,y,z) inside the plate is:

$$\boldsymbol{\varepsilon}(x,y,z) = \boldsymbol{\varepsilon}_s + \boldsymbol{\varepsilon}_l$$

$$= (\boldsymbol{\varepsilon}_o + \boldsymbol{\varepsilon}_m + \boldsymbol{\varepsilon}_w) - z(\hat{\boldsymbol{\varepsilon}}_b + \hat{\boldsymbol{\varepsilon}}_{m\theta}) + z^2\hat{\boldsymbol{\varepsilon}}_\theta \tag{5.23}$$

where the vectors $\boldsymbol{\varepsilon}_o$, $\boldsymbol{\varepsilon}_m$, ..., $\hat{\boldsymbol{\varepsilon}}_\theta$ are all functions of (x,y) only.

5.2.2.3 Matrix representation of finite strains

Defining the following vectors which are functions of x, y :

$$\mathbf{0}_m = \left\{\frac{\partial u^o}{\partial x} \quad \frac{\partial v^o}{\partial x} \quad \frac{\partial u^o}{\partial y} \quad \frac{\partial v^o}{\partial y}\right\} \tag{5.24}$$

$$\boldsymbol{\theta}_w = \left\{ \frac{\partial w}{\partial x} \quad \frac{\partial w}{\partial y} \right\} \tag{5.25}$$

$$\boldsymbol{\theta}_\theta = \left\{ \frac{\partial^2 w}{\partial x^2} \quad \frac{\partial^2 w}{\partial x \partial y} \quad \frac{\partial^2 w}{\partial y \partial x} \quad \frac{\partial^2 w}{\partial y^2} \right\} \tag{5.26}$$

then it can be deduced that:

$$\boldsymbol{\varepsilon}_m = \frac{1}{2} \boldsymbol{A}_m(x,y) \quad \boldsymbol{\theta}_m(x,y) \tag{5.27}$$

$$\boldsymbol{\varepsilon}_w = \frac{1}{2} \boldsymbol{A}_w(x,y) \quad \boldsymbol{\theta}_w(x,y) \tag{5.28}$$

$$\hat{\boldsymbol{\varepsilon}}_{m\theta} = \boldsymbol{A}_m \, \boldsymbol{\theta}_\theta = \boldsymbol{A}_\theta \, \boldsymbol{\theta}_m \tag{5.29}$$

$$\hat{\boldsymbol{\varepsilon}}_\theta = \frac{1}{2} \boldsymbol{A}_\theta(x,y) \quad \boldsymbol{\theta}_\theta(x,y) \tag{5.30}$$

where the $\boldsymbol{A}$ matrices are as given by equations (4.44)-(4.46). Notice also that the variation of strain terms can be obtained as follows:

$$d\boldsymbol{\varepsilon}_m = \boldsymbol{A}_m \quad d\boldsymbol{\theta}_m \tag{5.31}$$

$$d\boldsymbol{\varepsilon}_w = \boldsymbol{A}_w \quad d\boldsymbol{\theta}_w \tag{5.32}$$

$$d\hat{\boldsymbol{\varepsilon}}_{m\theta} = \boldsymbol{A}_\theta \quad d\boldsymbol{\theta}_m + \boldsymbol{A}_m \quad d\boldsymbol{\theta}_\theta \tag{5.33}$$

$$d\hat{\boldsymbol{\varepsilon}}_\theta = \boldsymbol{A}_\theta \quad d\boldsymbol{\theta}_\theta \tag{5.34}$$

5.2.3 Strain energy variations

5.2.3.1 Introduction

Using equation (3.9) stress components at any point (x,y,z) inside the lth layer of a composite layered plate can be expressed in terms of strain components with the following matrix equation:

$$\boldsymbol{\sigma} = \begin{bmatrix} \sigma_x \\ \sigma_y \\ \tau_{xy} \end{bmatrix} = \boldsymbol{D}^{(l)} \boldsymbol{\varepsilon} \tag{5.35}$$

where $\boldsymbol{\sigma}$, $\boldsymbol{\varepsilon}$ are the stress and strain vectors.

The variation of strain energy density (strain energy per unit volume) at any point inside the plate due to a variation of the displacement field can be expressed as follows:

$$\delta\bar{U} = \delta\boldsymbol{\varepsilon}^t\boldsymbol{\sigma} = (\delta\boldsymbol{\varepsilon}_s^t + \delta\boldsymbol{\varepsilon}_l^t)\boldsymbol{\sigma} \equiv \delta\boldsymbol{\varepsilon}_s^t\boldsymbol{\sigma}_s + \delta\boldsymbol{\varepsilon}_l^t\boldsymbol{\sigma} + \delta\boldsymbol{\varepsilon}_s^t\boldsymbol{\sigma}_l \tag{5.36}$$

where $\boldsymbol{\sigma}_s = \boldsymbol{D}^{(l)}\boldsymbol{\varepsilon}_s$ (5.37a)

and $\boldsymbol{\sigma}_l = \boldsymbol{D}^{(l)}\boldsymbol{\varepsilon}_l$ (5.37b)

Hence, the variation of the strain energy density can be represented in terms of three parts as follow:

$$\delta\bar{U} = \delta\bar{U}_{small} + \delta\bar{U}_l + \delta\bar{U}_{sl} \tag{5.38}$$

where $\delta\bar{U}_{small} = \delta\boldsymbol{\varepsilon}_s^t\boldsymbol{\sigma}_s \equiv \delta\boldsymbol{\varepsilon}_s^t\boldsymbol{D}^{(l)}\boldsymbol{\varepsilon}_s$ (5.39)

which represents the variation due to infinitesimal strains and corresponding stresses. The part: $\delta\bar{U}_l = \delta\boldsymbol{\varepsilon}_l^t\boldsymbol{\sigma}$ (5.40)

represents the variation due to a variation of the additional finite strain terms, whilst the part: $\delta\bar{U}_{sl} = \delta\boldsymbol{\varepsilon}_s^t\boldsymbol{\sigma}_l$ (5.41)

represents a coupling term due to the variation of infinitesimal strains, and the additional stresses obtained from the additional finite strain terms.

5.2.3.2 Analysis of the part $\delta\bar{U}_{small}$

Substituting from equation (5.14) into equation (5.39) then:

$$\delta\bar{U}_{small} = \left(\delta\boldsymbol{\varepsilon}_o^t - z\delta\hat{\boldsymbol{\varepsilon}}_b^t\right)\boldsymbol{D}^{(l)}\left(\boldsymbol{\varepsilon}_o - z\hat{\boldsymbol{\varepsilon}}_b\right) \tag{5.42}$$

Expanding equation (5.42), we can deduce that:

$$\delta\bar{U}_{small} = \delta\bar{U}_{oo} + \delta\bar{U}_{bb} + (\delta\bar{U}_{ob} + \delta\bar{U}_{bo}) \tag{5.43}$$

where

$$\delta\bar{U}_{oo} = \delta\boldsymbol{\varepsilon}_o^t(x,y)\,\boldsymbol{D}^{(l)}\,\boldsymbol{\varepsilon}_o(x,y) \tag{5.44}$$

$$\delta\bar{U}_{bb} = z^2\,\delta\hat{\boldsymbol{\varepsilon}}_b^t(x,y)\,\boldsymbol{D}^{(l)}\,\hat{\boldsymbol{\varepsilon}}_b(x,y) \tag{5.45}$$

$$\delta\bar{U}_{ob} = -z\,\delta\boldsymbol{\varepsilon}_o^t(x,y)\,\boldsymbol{D}^{(l)}\,\hat{\boldsymbol{\varepsilon}}_b(x,y) \tag{5.46}$$

$$\delta\bar{U}_{bo} = -z\,\delta\hat{\boldsymbol{\varepsilon}}_b^t(x,y)\,\boldsymbol{D}^{(l)}\,\boldsymbol{\varepsilon}_o(x,y) \tag{5.47}$$

Integrated $\boldsymbol{D}$ matrices are defined for the integration of the above equations with respect to z and are as given by equations (4.79)-(4.81). Integrating equations (5.44) - (5.47) with respect to z over the plate thickness, it can be deduced that:

$$\delta U'_{oo} = \delta\boldsymbol{\varepsilon}_o^t(x,y)\,\boldsymbol{D}_{oo}\,\boldsymbol{\varepsilon}_o(x,y) \tag{5.48}$$

$$\delta U'_{bb} = \delta\hat{\boldsymbol{\varepsilon}}_b^t(x,y)\,\boldsymbol{D}_{bb}\,\hat{\boldsymbol{\varepsilon}}_b(x,y) \tag{5.49}$$

$$\delta U'_{ob} = -\delta\boldsymbol{\varepsilon}_o^t(x,y)\,\boldsymbol{D}_{ob}\,\hat{\boldsymbol{\varepsilon}}_b(x,y) \tag{5.50}$$

$$\delta U'_{bo} = -\delta\hat{\boldsymbol{\varepsilon}}_b^t(x,y)\,\boldsymbol{D}_{bo}\,\boldsymbol{\varepsilon}_o(x,y) \tag{5.51}$$

5.2.3.3 *Strain energy variation part* $(\delta\bar{U}_l)$

It can be deduced that from equation (5.21) and equation (5.40) that:

$$\delta\bar{U}_l = \delta\boldsymbol{\varepsilon}_l^t\boldsymbol{\sigma} = (\delta\boldsymbol{\varepsilon}_m^t + \delta\boldsymbol{\varepsilon}_w^t - z\delta\hat{\boldsymbol{\varepsilon}}_{m\theta}^t + z^2\delta\hat{\boldsymbol{\varepsilon}}_\theta^t)\boldsymbol{\sigma}$$

which can be rewritten as follows:

$$\delta\bar{U}_l = \delta\bar{U}_m + \delta\bar{U}_w + \delta\bar{U}_{m\theta} + \delta\bar{U}_\theta \tag{5.52}$$

where $\delta\bar{U}_m$, $\delta\bar{U}_w$, $\delta\bar{U}_{m\theta}$, $\delta\bar{U}_\theta$ are as defined by equations (4.95)-(4.98), with

$$\boldsymbol{\sigma} = \boldsymbol{D}^{(l)}\{(\boldsymbol{\varepsilon}_o + \boldsymbol{\varepsilon}_m + \boldsymbol{\varepsilon}_w) - z(\hat{\boldsymbol{\varepsilon}}_b + \hat{\boldsymbol{\varepsilon}}_{m\theta}) + z^2\hat{\boldsymbol{\varepsilon}}_\theta\} \tag{5.53}$$

Substituting from equation (5.27) into equation(4.95) then:

$$\delta\bar{U}_m = \delta\boldsymbol{\theta}_m^t\boldsymbol{A}_m^t\boldsymbol{\sigma} \equiv \delta\boldsymbol{\theta}_m^t(x,y)\,\boldsymbol{A}_m^t(x,y)\,\boldsymbol{\sigma}(x,y,z) \tag{5.54}$$

Hence

$$\delta U'_m = \int_{-h/2}^{h/2}\delta\bar{U}_m dz \equiv \delta\boldsymbol{\theta}_m^t(x,y)\,\boldsymbol{A}_m^t(x,y)\,\boldsymbol{\sigma}_m(x,y) \tag{5.55}$$

where $\boldsymbol{\sigma}_m(x,y) = \int_{-h/2}^{h/2}\boldsymbol{\sigma}(x,y,z)\,dz$ (5.56)

and by using the integrated $\boldsymbol{D}$ matrices, then for Kirchhoff-type elements:

$$\boldsymbol{\sigma}_m = \boldsymbol{D}_{oo}(\boldsymbol{\varepsilon}_o + \boldsymbol{\varepsilon}_m + \boldsymbol{\varepsilon}_w) - \boldsymbol{D}_{ob}(\hat{\boldsymbol{\varepsilon}}_b + \hat{\boldsymbol{\varepsilon}}_{m\theta}) + \boldsymbol{D}_{bb}\hat{\boldsymbol{\varepsilon}}_\theta \tag{5.57}$$

Using matrix multiplication rules, equation (5.55) can be rewritten as follow:

$$\delta U'_m = \delta\mathbf{0}_m^t\,\boldsymbol{S}_{mm}\,\mathbf{0}_m \tag{5.58}$$

where $\boldsymbol{S}_{mm}$ is as given by equation (4.105). Similarly, it can be shown that:

$$\delta\bar{U}_w = \delta\mathbf{0}_w^t(x,y)\,\boldsymbol{A}_w^t(x,y)\,\boldsymbol{\sigma}(x,y,z) \tag{5.59}$$

and $\delta U'_w = \delta 0_w^t S_{ww} 0_w$ (5.60)

where S_{ww} is as given by equation (4.108).

Defining

$$\sigma_{m\theta} = \sigma_{\theta m} = \int_{-h/2}^{h/2} (-z\sigma)dz \equiv -D_{ob}(\varepsilon_o + \varepsilon_m + \varepsilon_w) + D_{bb}(\hat{\varepsilon}_b + \hat{\varepsilon}_{m\theta}) - D_{(3)}\hat{\varepsilon}_\theta \quad (5.61)$$

then it can be shown that:

$$\delta U'_{m\theta} = \delta 0_m^t S_{m\theta} 0_\theta + \delta 0_\theta^t S_{\theta m} 0_m \quad (5.62)$$

where $S_{m\theta} = S_{\theta m}$ and are defined from $\sigma_{m\theta}$ by equation (4.113).

Similarly, it can be shown that:

$$\delta U'_\theta = \delta 0_\theta^t S_{\theta\theta} 0_\theta \quad (5.63)$$

where $S_{\theta\theta}$ is defined from σ_θ by an equation similar to (4.118) and

$$\sigma_\theta = D_{bb}(\varepsilon_o + \varepsilon_m + \varepsilon_w) - D_{(3)}(\hat{\varepsilon}_b + \hat{\varepsilon}_{m\theta}) + D_{(4)}\hat{\varepsilon}_\theta \quad (5.64)$$

5.2.3.4 Strain energy variation part $(\delta\bar{U}_{sl})$

This was defined as follows:

$$\delta\bar{U}_{sl} = \delta\varepsilon_s^t \sigma_l \equiv (\delta\varepsilon_o - z\,\delta\hat{\varepsilon}_b)\sigma_l \quad (5.65)$$

which can be rewritten in terms of two parts:

$$\delta\bar{U}_{sl} = (\delta\bar{U}_o)_{sl} + (\delta\bar{U}_b)_{sl} \quad (5.66)$$

where

$$\left(\delta\bar{U}_o\right)_{sl} = \delta\varepsilon_o^t \sigma_l \quad (5.67)$$

$$\left(\delta\bar{U}_b\right)_{sl} = -z\,\delta\hat{\varepsilon}_b^t \sigma_l \quad (5.68)$$

Defining the following integrated stress vectors:

$$\sigma_o(x,y) = \int_{-h/2}^{h/2} \sigma_l(x,y,z)dz, \quad \sigma_b(x,y) = -\int_{-h/2}^{h/2} z\sigma_l(x,y,z)dz \quad (5.69)$$

then $\boldsymbol{\sigma}_o$, $\boldsymbol{\sigma}_b$ will have equations similar to (4.127) and (4.130), and the z integrated strain energy segments become:

$$(\delta U'_o) = \int_{-h/2}^{h/2} (\delta \bar{U}_o)_{sl}\, dz = \delta \boldsymbol{\varepsilon}_o^t \boldsymbol{\sigma}_o \tag{5.70}$$

$$(\delta U'_b)_{sl} = \int_{-h/2}^{h/2} (\delta \bar{U}_b)_{sl}\, dz = \delta \hat{\boldsymbol{\varepsilon}}_b^t \boldsymbol{\sigma}_b \tag{5.71}$$

5.3 INTERPOLATED EQUATIONS

5.3.1 Interpolation in x-direction

(a) Interpolated parameters using Lagrangian interpolation

The in-plane displacement components at the midplane z=0; $u^o(x,y)$, $v^o(x,y)$ do not require more than C^o continuity and can be interpolated in x-direction via Lagrangian interpolation and for an n-node strip:

$$u^o(x,y) = \sum_{i=1}^{n} N_i(\xi)\, u^o{}_i(y) \tag{5.72}$$

$$v^o(x,y) = \sum_{i=1}^{n} N_i(\xi)\, v^o{}_i(y) \tag{5.73}$$

where $N_i(\xi)$ represents one-dimensional Lagrangian shape functions as defined by equation (4.139).

(b) Interpolation of lateral deflection w

Hermitian or spline-type interpolation can be used to maintain the C^1 continuity of w and for an n-node strip:

$$w(x,y) = \sum_{i=1}^{n} \left[G_i(\xi) w_i(y) + H_i(\xi) w_{i,x}(y) \right] \tag{5.74}$$

where $G_i(\xi)$, $H_i(\xi)$ represent either Hermitian interpolation shape functions as defined by equation (4.141) or spline-type shape functions as defined by equation (4.142).

5.3.2 Interpolation in y-direction

(a) General expressions

The nodal functions in the previous expressions are interpolated in y-direction as follows:

$$u_i^o(y) = \sum_{r=1}^{m} f_u^r(\eta)\, u_i^r \tag{5.75}$$

$$v_i^o(y) = \sum_{r=1}^{m} f_v^r(\eta)\, v_i^r \tag{5.76}$$

$$w_i(y) = \sum_{r=1}^{m} f_w^r(\eta)\, w_i^r \tag{5.77}$$

$$w_{i,x}(y) = \sum_{r=1}^{m} f_w^r(\eta)\, w_{i,x}^r \tag{5.78}$$

Hence the full x-y interpolated parameters can be expressed for an n-node strip as follows:

$$u^o(x,y) = \sum_{i=1}^{n}\sum_{r=1}^{m} N_i(\xi)\, f_u^r(\eta)\, u_i^r \tag{5.79}$$

$$v^o(x,y) = \sum_{i=1}^{n}\sum_{r=1}^{m} N_i(\xi)\, f_v^r(\eta)\, u_i^r \tag{5.80}$$

$$w(x,y) = \sum_{i=1}^{n}\sum_{r=1}^{m} f_w^r(\eta)\left[G_i(\xi) w_i^{\,r} + H_i(\xi) w_{i,x}^{\,r} \right] \tag{5.81}$$

(b) Trigonometric interpolation

This depends on the boundary conditions and for an example, where w , u are restrained on the edges $\eta = o$, $\eta = 1$:

$$f_u^r(\eta) = \sin(r\pi\eta) \tag{5.82}$$

$$f_v^r(\eta) = \cos(r\pi\eta) \tag{5.83}$$

$$f_w^r(\eta) = \sin(r\pi\eta) \tag{5.84}$$

(c) Lagrangian interpolation

This is used for u,v with equations similar to (4.160) and (4.161) and boundary conditions at y edges can also be set similarly.

(d) Hermitian and spline-type interpolations

These may be used for w as explained for the Reissner-type elements in section 4.3.2.

5.4 ELEMENT LINEAR STIFFNESS MATRIX

5.4.1 Infinitesimal strain components

The nodal displacement vector per rth harmonic or y term for an n node strip can be

partitioned as follows:

$$\boldsymbol{\delta}^r = \begin{bmatrix} \boldsymbol{\delta}_o^r \\ \boldsymbol{\delta}_b^r \end{bmatrix} \tag{5.85}$$

where

$$\boldsymbol{\delta}_o^r = \left\{ u_1^r v_1^r \quad u_2^r v_2^r \quad \ldots \quad u_n^r v_n^r \right\} \tag{5.86}$$

$$\boldsymbol{\delta}_b^r = \left\{ w_1^r w_{1,x}^r \quad w_2^r w_{2,x}^r \quad \ldots \quad w_n^r w_{n,x}^r \right\} \tag{5.87}$$

Using interpolation equations (5.79), (5.80) then equation (5.15) can be written in terms of nodal values as follows:

$$\boldsymbol{\varepsilon}_o = \sum_{r=1}^{m} \boldsymbol{B}_o^r(\xi,\eta)\, \boldsymbol{\delta}_o^r \tag{5.88}$$

where $\boldsymbol{B}_o^r(\xi,\eta)$ is as defined by equation (4.168).

Using interpolation equation (5.81), then equation (5.16) can be expressed in terms of nodal values as follows

$$\hat{\boldsymbol{\varepsilon}}_b = \sum_{r=1}^{m} \boldsymbol{B}_b^r(\xi,\eta)\, \boldsymbol{\delta}_b^r \tag{5.89}$$

where $\boldsymbol{B}_b^r$ is as defined by equation (4.170).

5.4.2 Strain energy variation and element stiffness matrix

Using equations (5.48)-(5.51), the strain energy variation per unit area can be expressed for the case of infinitesimal strains as follows:

$$\delta U'_{small} = \delta U'_{oo} + \delta U'_{bb} + (\delta U'_{ob} + \delta U'_{bo}) \tag{5.90}$$

Each term will be represented in terms of nodal displacement values and integrated with respect to the *x*-*y* plane of the strip as described in section 4.4.2.

5.4.2.1 Strain energy variation term dU_{oo}

This term can be obtained similar to equation (4.181), i.e.

$$dU_{oo} = \sum_{s=1}^{m} \sum_{r=1}^{m} (d\boldsymbol{\delta}_o^s)^t\, \boldsymbol{K}_{oo}^{sr}\, \boldsymbol{\delta}_o^r \tag{5.91}$$

where $\boldsymbol{K}_{oo}^{sr} = \int_0^1 \int_0^1 (\boldsymbol{B}_o^s)^t\, \boldsymbol{D}_{oo}\, \boldsymbol{B}_o^r\, J_x J_y\, d\xi\, d\eta$ (5.92)

5.4.2.2 *Strain energy variation term* dU_{bb}

This can also be expressed similar to equation (4.184) as follows:

$$dU_{bb} = \sum_{s=1}^{m}\sum_{r=1}^{m} (d\boldsymbol{\delta}_b^s)^t \boldsymbol{K}_{bb}^{sr} \boldsymbol{\delta}_b^r \tag{5.93}$$

where $\boldsymbol{K}_{bb}^{sr} = \int_0^1 \int_0^1 (\boldsymbol{B}_b^s)^t \boldsymbol{D}_{bb} \boldsymbol{B}_b^r J_x J_y \, d\xi \, d\eta$ (5.94)

5.4.2.3 *Strain energy variation terms* dU_{ob}, dU_{bo}

These terms are similar to those given by equations (4.190) and (4.192), i.e.

$$dU_{ob} = \sum_{s=1}^{m}\sum_{r=1}^{m} (d\boldsymbol{\delta}_o^s)^t \boldsymbol{K}_{ob}^{sr} \boldsymbol{\delta}_b^r \tag{5.95}$$

$$dU_{bo} = \sum_{s=1}^{m}\sum_{r=1}^{m} (d\boldsymbol{\delta}_b^s)^t \boldsymbol{K}_{bo}^{sr} \boldsymbol{\delta}_o^r \tag{5.296}$$

where $\boldsymbol{K}_{ob}^{sr} = \int_0^1 \int_0^1 (\boldsymbol{B}_o^s)^t \boldsymbol{D}_{ob} \boldsymbol{B}_b^r J_x J_y \, d\xi \, d\eta$ (5.97)

and $\boldsymbol{K}_{bo}^{sr} = \int_0^1 \int_0^1 (\boldsymbol{B}_b^s)^t \boldsymbol{D}_{bo} \boldsymbol{B}_o^r J_x J_y \, d\xi \, d\eta$ (5.98)

5.4.3 Small deflection element stiffness matrix

Substituting from equations (5.91), (5.93), (5.95), (5.96) into the *x*-*y* integration of (5.90), it can be deduced that:

$$dU_{small} = \sum_{s=1}^{m}\sum_{r=1}^{m} \left\{ (d\boldsymbol{\delta}_o^s)^t \boldsymbol{K}_{oo}^{sr} \boldsymbol{\delta}_o^r + (d\boldsymbol{\delta}_b^s)^t \boldsymbol{K}_{bb}^{sr} \boldsymbol{\delta}_b^r - (d\boldsymbol{\delta}_o^s)^t \boldsymbol{K}_{ob}^{sr} \boldsymbol{\delta}_b^r - (d\boldsymbol{\delta}_b^s)^t \boldsymbol{K}_{bo}^{sr} \boldsymbol{\delta}_o^r \right\} \tag{5.99}$$

which can be rewritten as:

$$dU_{small} = \sum_{s=1}^{m}\sum_{r=1}^{m} (d\boldsymbol{\delta}^s)^t \boldsymbol{K}^{sr} \boldsymbol{\delta}^r \tag{5.100}$$

where $\boldsymbol{K}^{sr} = \begin{bmatrix} \boldsymbol{K}_{oo}^{sr} & -\boldsymbol{K}_{ob}^{sr} \\ -\boldsymbol{K}_{bo}^{sr} & \boldsymbol{K}_{bb}^{sr} \end{bmatrix}$ (5.101)

5.5 EQUIVALENT NODAL LOADING AND STATIC LINEAR EQUATIONS

Equivalent nodal loading vector per the rth harmonic, or y term, is partitioned as follows:

$$F^r = \{F_o^r \quad F_b^r\} \tag{5.102}$$

and the equivalent loading vector is defined such that it does the same work done by actual loads due to a variational displacement field, i.e.

$$dW = \sum_{r=1}^{m} (d\delta^r)^t F^r = \sum_{r=1}^{m} \left[(d\delta_o^r)^t F_o^r + (d\delta_b^r)^t F_b^r\right] \tag{5.103}$$

$\equiv$ the work done by the actual load.

5.5.1 Distributed lateral loading with intensity q

If the strip is subjected to distributed loading in the z direction, with intensity $q(x,y)$ (load per unit area), then the actual work done by that load due to displacement variation is:

$$\delta W = \int\int_{strip} q\,\delta w\,dx\,dy = \int_0^1\int_0^1 \delta w\, q\, J_x J_y\, d\xi\, d\eta$$

$$\equiv \sum_{i=1}^{n}\sum_{r=1}^{m} \int_0^1\int_0^1 q f_w^r(\eta)\,[G_i(\xi)\,w_i + H_i(\xi)\,w_{i,x}]\,J_x J_y\,d\xi\,d\eta \tag{5.104}$$

Comparing equation (5.103) with (5.104), it can be deduced that:

$$F_o^r = \mathbf{O} \tag{5.105}$$

and

$$F_b^r \equiv \{(F_z^r)_1 \quad M_1^r \quad (F_z)_2 \quad M_2^r \quad \ldots \quad (F_z^r)_n \quad M_n^r\} \tag{5.106}$$

where

$$(F_z^r) = \int_0^1\int_0^1 q\,G_i(\xi) f_w^r(\eta)\,J_x J_y\,d\xi\,d\eta \tag{5.107}$$

$$M_i^r = \int_0^1\int_0^1 q\,H_i(\xi) f_w^r(\eta)\,J_x J_y\,d\xi\,d\eta \tag{5.108}$$

5.5.2 Concentrated forces and moments at node i and $\eta = \eta_j$

These are defined in terms of five components $\{F_x \quad F_y \quad F_z \quad M_x \quad M_y\}$,where F_x, F_y, F_z are forces at x, y, z directions and M_x, M_y are the bending moments in x, y directions, respectively. Notice that slope angles can be defined for the Kirchhoff-type elements from equation (3.19) as follows:

$$\theta_y = -\frac{\partial w}{\partial x},\quad \theta_x = \frac{\partial w}{\partial y} \tag{5.109}$$

Using the following interpolation equations at $\eta = \eta_j$:

$$\delta u^{o}(\xi_i, \eta_j) = \sum_{r=1}^{m} f_u^r(\eta_j)\, \delta u_i^r \tag{5.110}$$

$$\delta v^{o}(\xi_i, \eta_j) = \sum_{r=1}^{m} f_v^r(\eta_j)\, \delta v_i^r \tag{5.111}$$

$$\delta \theta_x(\xi_i, \eta_j) = \sum_{r=1}^{m} f_{w,\eta}^r(\eta_j)\, \delta w_i^r / J_y \tag{5.112}$$

$$\delta \theta_y(\xi_i, \eta_j) = -\sum_{r=1}^{m} f_w^r(\eta_j)\, \delta w_{i,x}^r \tag{5.113}$$

then it can be deduced that:

$$\delta W = \sum_{r=1}^{m} \Big\{ F_x f_u^r(\eta_j)\, \delta u_i^r + F_y f_v^r(\eta_j)\, \delta v_i^r + F_z f_w^r(\eta_j)\, \delta w_i^r + M_x f_{w,\eta}^r(\eta_j)\, \delta w_i^r / J_y - M_y f_w^r(\eta_j)\, \delta w_{i,x}^r \Big\} \tag{5.114}$$

Comparing equation (5.114) with (5.103), then equivalent nodal load components exist only at node *i* and are defined as follows:

$$F_o^r = \left\{ 0 \quad 0 \ \ldots \ (F_x^r)_i \quad (F_y^r)_i \ \ldots \ 0 \quad 0 \right\} \tag{5.115}$$

$$F_b^r = \left\{ 0 \quad 0 \ \ldots \ (F_z^r)_i \quad M_i^r \ \ldots \ 0 \quad 0 \right\} \tag{5.116}$$

where

$$(F_x^r)_i = F_x f_u^r(\eta_j) \tag{5.117}$$

$$(F_y^r)_i = F_y f_v^r(\eta_j) \tag{5.118}$$

$$(F_z^r)_i = F_z f_w^r(\eta_j) + M_x \frac{f_{w,\eta}^r}{J_y} \tag{5.119}$$

$$M_i^r = -M_y f_w^r(\eta_j) \tag{5.120}$$

5.5.3 Line loading at $\xi = \xi_i$

This will be defined in terms of loads and moments per unit length in *y*-direction; $\{ F_x^y, F_y^y, F_z^y, M_x^y, M_y^y \}$ and due to a variation in the displacement field, the following interpolation equations are obtained:

$$\delta u^{o}(\xi_i, \eta) = \sum_{r=1}^{m} f_u^r(\eta)\, \delta u_i^r \tag{5.121}$$

$$\delta v^{o}(\xi_i, \eta) = \sum_{r=1}^{m} f_v^r(\eta)\, \delta v_i^r \tag{5.122}$$

$$\delta w(\xi_i,\eta) = \sum_{r=1}^{m} f_w^r(\eta)\,\delta w_i^r \tag{5.123}$$

$$\delta\theta_x(\xi_i,\eta) = \sum_{r=1}^{m} f_{w,\eta}^r(\eta)\,\delta w_i^r / J_y \tag{5.124}$$

$$\delta\theta_y(\xi_i,\eta) = -\sum_{r=1}^{m} f_w^r(\eta)\,\delta w_{i,x}^r \tag{5.125}$$

At an infinitesimal length Δy, the force and moment components are:

$$\Delta F_x = F_x^y \Delta y = J_y F_x^y \Delta\eta \tag{5.126}$$

$$\Delta F_y = F_y^y \Delta y = J_y F_y^y \Delta\eta \tag{5.127}$$

.....

$$\Delta M_y = M_y^y \Delta y = J_y M_y^y \Delta\eta \tag{5.128}$$

Hence, the work done by this line loading can be expressed as follows:

$$\delta W = \sum_{r=1}^{m} \int_0^1 \Big\{ F_x^y f_u^r(\eta)\,\delta u_i^r + F_y^y f_v^r(\eta)\,\delta v_i^r + F_z^y f_w^r(\eta)\,\delta w_i^r + M_x f_{w,\eta}^r(\eta)\,\delta w_i^r / J_y - M_y f_w^r(\eta)\,\delta w_{i,x}^r \Big\} J_y\, d\eta \tag{5.129}$$

and the equivalent nodal loading components, which exist only at node i, can be expressed as follows:

$$(F_x^r)_i = \int_0^1 F_x^y f_u^r(\eta)\, J_y\, d\eta \tag{5.130}$$

$$(F_y^r)_i = \int_0^1 F_y^y f_v^r(\eta)\, J_y\, d\eta \tag{5.131}$$

$$(F_z^r)_i = \int_0^1 \left[F_z^y\, f_w^r(\eta)\, J_y + M_x^y f_{w,\eta}^r(\eta) \right] d\eta \tag{5.132}$$

$$M_i^r = -\int_0^1 M_y^y\, f_w^r(\eta)\, J_y\, d\eta \tag{5.133}$$

5.5.4 Linear static analysis equation

For the case of infinitesimal strains it can be deduced from equation (5.100) that:

$$dU \propto dU_{small} = \sum_{s=1}^{m}\sum_{r=1}^{m} (d\boldsymbol{\delta}^s)^t \boldsymbol{K}^{sr} \boldsymbol{\delta}^r \tag{5.134}$$

Using the principle of virtual work and substituting from equation (5.103) and (5.134) into (4.246) it can be shown that:

$$d\chi = \sum_{s=1}^{m} \left\{(d\boldsymbol{\delta}^s)^t\right\} \left\{\sum_{r=1}^{m} \boldsymbol{K}^{sr} \boldsymbol{\delta}^r - \boldsymbol{F}^s\right\} = 0 \tag{5.135}$$

Hence, it can be deduced that:

$$\sum_{r=1}^{m} \boldsymbol{K}^{sr} \boldsymbol{\delta}^r - \boldsymbol{F}^s = \mathbf{O}, \; s = 1, 2, \ldots, m \tag{5.136}$$

which can be rewritten in the following matrix form:

$$\boldsymbol{K}\,\boldsymbol{\delta} = \boldsymbol{F} \tag{5.137}$$

where $\boldsymbol{F} = \{ \boldsymbol{F}^1 \quad \boldsymbol{F}^2 \quad \ldots \quad \boldsymbol{F}^m \}$ (5.138)

and $$\boldsymbol{K} = \begin{bmatrix} \boldsymbol{K}^{11} & \ldots & \boldsymbol{K}^{1r} & \ldots & \boldsymbol{K}^{1m} \\ \ldots & \ldots & \ldots & \ldots & \ldots \\ \boldsymbol{K}^{s1} & \ldots & \boldsymbol{K}^{sr} & \ldots & \boldsymbol{K}^{sm} \\ \ldots & \ldots & \ldots & \ldots & \ldots \\ \boldsymbol{K}^{m1} & \ldots & \boldsymbol{K}^{mr} & \ldots & \boldsymbol{K}^{mm} \end{bmatrix} \tag{5.139}$$

5.6 NONLINEAR MATRICES AND VECTORS

5.6.1 Large strain components

Using an analysis similar to that given in section 4.6.1 the **0** vectors can be expressed in terms of nodal displacements as follows:

$$\mathbf{0}_m = \sum_{r=1}^{m} \boldsymbol{G}_m^r(\xi,\eta)\,\boldsymbol{\delta}_o^r \tag{5.140}$$

$$\mathbf{0}_w = \sum_{r=1}^{m} \boldsymbol{G}_w^r(\xi,\eta)\,\boldsymbol{\delta}_b^r \tag{5.141}$$

$$\mathbf{0}_\theta = \sum_{r=1}^{m} \boldsymbol{G}_\theta^r(\xi,\eta)\,\boldsymbol{\delta}_b^r \tag{5.142}$$

where $\boldsymbol{G}_m^r$, $\boldsymbol{G}_w^r$, $\boldsymbol{G}_\theta^r$ are as given by equations (4.254), (4.256), and (4.258), respectively. Hence, the strain vectors defined by equations (5.27)-(5.30) can be expressed in terms of nodal displacements as follows:

$$\varepsilon_m = \frac{1}{2} A_m(x,y) \sum_{r=1}^{m} G_m^r(x,y)\, \delta_o^r \tag{5.143}$$

$$\varepsilon_w = \frac{1}{2} A_w(x,y) \sum_{r=1}^{m} G_w^r(x,y)\, \delta_b^r \tag{5.144}$$

$$\hat{\varepsilon}_{m\theta} = A_m(x,y) \sum_{r=1}^{m} G_\theta^r(x,y)\, \delta_b^r = A_\theta(x,y) \sum_{r=1}^{m} G_m^r(x,y)\, \delta_m^r \tag{5.145}$$

$$\hat{\varepsilon}_\theta = \frac{1}{2} A_\theta(x,y) \sum_{r=1}^{m} G_\theta^r(x,y)\, \delta_b^r \tag{5.146}$$

with differential values similar to those given by equations (4.263)-(4.266).

5.6.2 Derivation of non-linear stiffness matrix K_σ

Using an analysis similar to that given in section 4.6.2, the strain energy variation part dU_l can be expressed as follows:

$$dU_l = \sum_{s=1}^{m} \sum_{r=1}^{m} (d\delta^t)\, K_\sigma^{sr}\, \delta^r \tag{5.147}$$

where

$$K_\sigma^{sr} = \begin{bmatrix} K_{mm}^{sr} & K_{m\theta}^{sr} \\ K_{\theta m}^{sr} & K_{ww}^{sr} + K_{\theta\theta}^{sr} \end{bmatrix} \tag{5.148}$$

where the sub-matrices K_{mm}^{sr}, K_{ww}^{sr}, $K_{m\theta}^{sr}$, $K_{\theta m}^{sr}$, $K_{\theta\theta}^{sr}$ are as given by equations (4.269), (4.271), (4.273), and (4.275), respectively.

5.6.3 Derivation of coupling vector F_l

The strain energy part dU_{sl} can be expressed as follows:

$$dU_{sl} = \sum_{s=1}^{m} (d\delta^s)^t\, (F^s)_l \tag{5.149}$$

where $(F^s)_l \equiv \{ (F_o^s)_l \quad (F_b^s)_l \}$ (5.150)

and $(F_o^s)_l$, $(F_b^s)_l$ are as given by equations (4.280) and (4.282).

Equation (5.149) can also be written in the following matrix form :

$$dU_{sl} = d\delta^t\, F_l \tag{5.151}$$

where $F_l \equiv \{ F_l^1 \quad F_l^2 \quad \ldots \quad F_l^s \quad \ldots \quad F_l^m \}$ (5.152)

5.6.4 Non-linear static equations

Integrating equation (5.38) over the volume of the strip, and substituting into the result from equations (5.100) , (5.147), and (5.149), the variation of the strain energy for the case with finite strains can be written in the following matrix form:

$$dU = d\delta^t (K + K_\sigma)\,\delta + d\delta^t F_l \tag{5.153}$$

Hence, it can be deduced from the principle of virtual work that:

$$(K + K_\sigma)\delta + F_l = F \tag{5.154}$$

which represents the non-linear static equation.

5.7 ELEMENT MASS MATRICES

5.7.1 Interpolated displacement, velocity and acceleration components at an instant of time t

Using equations (5.79) and (5.80), at an instant of time *t,* then:

$$u^o(x,y,t) = \sum_{i=1}^{n}\sum_{r=1}^{m} N_i(\xi)\, f_u^r(\eta)\, u_i^r(t) \tag{5.155}$$

$$v^o(x,y,t) = \sum_{i=1}^{n}\sum_{r=1}^{m} N_i(\xi)\, f_v^r(\eta)\, v_i^r(t) \tag{5.156}$$

$$w(x,y,t) = \sum_{i=1}^{n}\sum_{r=1}^{m} f_w^r(\eta)\,[\, G_i(\xi)\, w_i^r(t) + H_i(\xi)\, w_{i,x}^r(t)\,] \tag{5.157}$$

Equations (5.1) , (5.2) can also be written in the following matrix form:

$$q_m = \begin{bmatrix} u \\ v \end{bmatrix} = q_o - z q_\theta \tag{5.158}$$

where

$$q_o = \begin{bmatrix} u^o \\ v^o \end{bmatrix}, \qquad q_\theta = \begin{bmatrix} \partial w/\partial x \\ \partial w/\partial y \end{bmatrix} \tag{5.159}$$

Similarly from equation (5.3):

$$q_w \equiv [w] \tag{5.160}$$

Substituting from equations (5.155)-(5.157) into equations (5.159) and (5.160) then they can be written as follows:

$$q_o = \begin{bmatrix} u^o \\ v^o \end{bmatrix} = \sum_{r=1}^{m} N_o^r(\xi,\eta)\,\delta_o^r(t) \tag{5.161}$$

$$q_\theta = \begin{bmatrix} \dfrac{\partial w}{\partial x} \\ \dfrac{\partial w}{\partial y} \end{bmatrix} = \sum_{r=1}^{m} N_\theta^r(\xi,\eta)\,\delta_b^r(t) \tag{5.162}$$

$$q_w = [w] = \sum_{r=1}^{m} N_w^r(\xi,\eta)\,\delta_b^r(t) \tag{5.163}$$

where N_o^r, N_θ^r, N_w^r are as given by equations (4.305), (4.306), and (4.308).

Velocity and acceleration equation are obtained by differentiating displacement equation with respect to. time, hence

$$\dot{q}_m = \begin{bmatrix} \dot{u} \\ \dot{v} \end{bmatrix} = \dot{q}_o - z\dot{q}_\theta \tag{5.164}$$

$$\dot{q}_w \equiv [\dot{w}] \tag{5.165}$$

$$\ddot{q}_m = \begin{bmatrix} \ddot{u} \\ \ddot{v} \end{bmatrix} = \ddot{q}_o - z\ddot{q}_\theta \tag{5.166}$$

$$\ddot{q}_w \equiv [\ddot{w}] \tag{5.167}$$

where expressions for $\dot{q}_m$, $\dot{q}_\theta$, $\dot{q}_w$, $\ddot{q}_m$, $\ddot{q}_\theta$, $\ddot{q}_w$ in terms of nodal values and shape functions are as given by equations (4.313), (4.314), (4.316), (4.317), (4.318), and (4.320).

5.7.2 Element mass matrix

Using D'Alembert's principle, the force vector due to an acceleration $\ddot{q}(x,y,z,t)$ at an infinitesimal volume $\Delta x\,\Delta y\,\Delta z$ is:

$$\Delta F = -\ddot{q}\,\Delta x\,\Delta y\,\Delta z \tag{5.168}$$

and the work done by D'Alembert's force due to a virtual displacement field dq will be:

$$dW_D = -\int\int\int \rho\,(dq^t\,\ddot{q})\,dx\,dy\,dz = \int\int (dW_D')\,dx\,dy \tag{5.169}$$

Using an analysis similar to that given in section 4.7.2, then it can be deduced that:

$$dW_D' = dW'_o + dW'_\theta + dW'_w \tag{5.170}$$

where

$$dW'_{o} = - \rho\, h\, dq_{o}^{t}\, \ddot{q}_{o} \tag{5.171}$$

$$dW'_{\theta} = - \frac{1}{12} \rho\, h^{3}\, dq_{\theta}^{t}\, \ddot{q}_{\theta} \tag{5.172}$$

$$dW'_{w} = - \rho\, h\, q_{w}^{t}\, d\ddot{q}_{w} \tag{5.173}$$

Substituting from equations (5.171) - (5.173) into equation (5.170) and integrating over the x-y area of the strip, then it can be deduced that :

$$dW_{D} = - \sum_{s=1}^{m} \sum_{r=1}^{m} \left\{ (d\delta_{o}^{s})^{t}\, M_{o}^{sr}\, \ddot{\delta}_{o}^{r} + (d\delta_{b}^{s})^{t}\, M_{\theta}^{sr}\, \ddot{\delta}_{b}^{r} + (d\delta_{b}^{s})^{t}\, M_{w}^{sr}\, \ddot{\delta}_{b}^{r} \right\} \tag{5.174}$$

which can be rewritten as follows:

$$dW_{D} = - \sum_{s=1}^{m} \sum_{r=1}^{m} (d\delta^{s})^{t}\, M^{sr}\, \ddot{\delta}^{r} \tag{5.175}$$

where

$$M^{sr} = \begin{bmatrix} M_{o}^{sr} & \mathbf{O} \\ \mathbf{O} & M_{\theta}^{sr} + M_{w}^{sr} \end{bmatrix} \tag{5.176}$$

and M_{o}^{sr}, M_{θ}^{sr}, M_{w}^{sr} as given by equations (4.340), (4.342), and (4.344), respectively.

Equation (5.175) can also be written as

$$dW_{D} = - d\delta^{t}(t)\, M\, \ddot{\delta}(t) \tag{5.177}$$

5.7.3 Non-linear dynamic equation

Applying the principle of virtual work at an instant of time t, then

$$\begin{aligned} d\chi(t) &= dU(t) - \sum dW(t) \\ &= dU_{small}(t) + dU_{l}(t) + dU_{sl}(t) - dW(t) - dW_{D}(t) = 0 \end{aligned} \tag{5.178}$$

and from previous equations, it can be deduced that:

$$d\chi(t) = d\delta^{t}(t) \left\{ M\, \ddot{\delta} + [K + K_{\sigma}(t)]\delta(t) + F_{l}(t) - F(t) \right\} = 0 \tag{5.179}$$

Hence

$$M\, \ddot{\delta}(t) + [K + K_{\sigma}(t)]\delta(t) + F_{l}(t) = F(t) \tag{5.180}$$

which represents the non-linear dynamic equation.

Chapter 6

Mindlin-Type Finite Strip Elements

6. Mindlin-Type Finite Strip Elements

6.1 INTRODUCTION

Mindlin-type elements represent a simplified version of Reissner-type elements. They consider transverse shear stresses and strains but the averaged values over the thickness of transverse shear strains are employed so as to obtain in-plane displacement components linear in z. For the case of transversely isotropic composite plate, the transverse shear moduli for each layer are equal, or:

$$\mu_{13} = \mu_{23} = \mu . \tag{6.1}$$

This will allow us to represent average shear stresses in terms of average shear strains by equations similar to (3.26) and (3.27), i.e.

$$\bar{\tau}_{xz} = \frac{5}{6}\mu\,\bar{\gamma}_{xz}, \; \bar{\tau}_{yz} = \frac{5}{6}\mu\,\bar{\gamma}_{yz} \tag{6.2}$$

Average shear strains lead to the definitions of average slope angles, which are given by equations (3.35) and (3.36) as:

$$\theta_x = \frac{\partial w}{\partial y} - \bar{\gamma}_{yz} \tag{6.3}$$

$$\theta_y = -\left(\frac{\partial w}{\partial x} - \bar{\gamma}_{xz}\right) \tag{6.4}$$

From which the in-plane displacement components at any point (x,y,z) inside the plate can be approximated as follows:

$$u(x,y,z) \approx u^{o}(x,y) + z\,\theta_y \tag{6.5}$$

$$v(x,y,z) \approx v^{o}(x,y) - z\,\theta_x \tag{6.6}$$

and the lateral deflection w can also be approximated as:

$$w(x,y,z) \approx w(x,y) \tag{6.7}$$

where $u^{o}(x,y)$, $v^{o}(x,y)$, $w(x,y)$ are displacement components along the x, y, z directions, respectively, in the midplane of the plate, defined by $z = 0$.

Equations (6.3) and (6.4) have led finite element researchers to use the C^{o}-continuous Lagrangian interpolation for the parameters w, θ_x and θ_y, thus maintaining the C^{o} continuity of u and v without using the more sophisticated Hermitian interpolation. When the thickness of the plate is small, then the parameters w, θ_x and θ_y cannot be interpolated independently leading to wrong answers. This phenomenon is called shear locking, and has been tackled for Mindlin finite elements by using reduced integration (Zienkiewicz & Taylor, 2000).

This chapter introduces the derivations of new Mindlin-type finite strip elements based on the same concepts employed for Mindlin finite elements. One-dimensional Lagrangian interpolation will be employed along x and y directions for the parameters u, v, w, θ_x, θ_y together with appropriate reduced integration schemes. The method of derivation is similar to that employed for Reissner-type and Kirchhoff-type finite strip elements.

6.2 STRESS AND STRAIN EQUATIONS

6.2.1 Strain components

6.2.1.1 Transverse shear strains

These are always assumed infinitesimal and are as defined for Reissner-type elements by equations (4.9) and (4.10), which can be rewritten as follows:

$$\gamma_{xz} = \frac{3}{2}\left(1 - \frac{4z^2}{h^2}\right)\bar{\gamma}_{xz}\,, \quad \gamma_{yz} = \frac{3}{2}\left(1 - \frac{4z^2}{h^2}\right)\bar{\gamma}_{yz} \tag{6.8}$$

The previous equations can also be written in a matrix form as follows:

$$\gamma = \begin{bmatrix}\gamma_{xz}\\ \gamma_{yz}\end{bmatrix} = f_\gamma(z) \quad \hat{\gamma}(x,y) \tag{6.9}$$

$$\text{where } f_\gamma = \frac{3}{2}\left(1 - \frac{4z^2}{h^2}\right) \tag{6.10}$$

$$\text{and} \quad \hat{\gamma}(x,y) = \begin{bmatrix}\bar{\gamma}_{xy}\\ \\ \bar{\gamma}_{yz}\end{bmatrix} \equiv \begin{bmatrix}\dfrac{\partial w}{\partial x} + \theta_y\\ \\ \dfrac{\partial w}{\partial y} - \theta_x\end{bmatrix} \tag{6.11}$$

6.2.1.2 Infinitesimal x-y strains

These are defined by Cauchy strain-displacement equations:

$$\varepsilon_x^s = \frac{\partial u}{\partial x}\,, \quad \varepsilon_y^s = \frac{\partial v}{\partial y}\,, \quad \gamma_{xy}^s = \frac{\partial u}{\partial y} + \frac{\partial v}{\partial x} \tag{6.12}$$

Substituting from equations (6.5), (6.6) into the above equations, the components of infinitesimal strain can be expressed as follows:

$$\varepsilon_x^s = \frac{\partial u^o}{\partial x} + z\frac{\partial \theta_y}{\partial x} \tag{6.13}$$

$$\varepsilon_y^s = \frac{\partial v^o}{\partial y} - z\frac{\partial \theta_x}{\partial y} \tag{6.14}$$

$$\gamma_{xy}^{s} = \frac{\partial u^{o}}{\partial y} + \frac{\partial v^{o}}{\partial x} - z\left(-\frac{\partial \theta_{y}}{\partial y} + \frac{\partial \theta_{x}}{\partial x}\right) \tag{6.15}$$

These previous equations can be written in the following matrix form:

$$\varepsilon_{s}(x,y,z) = \varepsilon_{o}(x,y) - z\,\hat{\varepsilon}_{b}(x,y) \tag{6.16}$$

where

$$\varepsilon_{o}(x,y) = \begin{bmatrix} \dfrac{\partial u^{o}}{\partial x} \\ \dfrac{\partial v^{o}}{\partial y} \\ \dfrac{\partial u^{o}}{\partial y} + \dfrac{\partial v^{o}}{\partial x} \end{bmatrix} \tag{6.17}$$

$$\hat{\varepsilon}_{b}(x,y) = \begin{bmatrix} -\dfrac{\partial \theta_{y}}{\partial x} \\ \dfrac{\partial \theta_{x}}{\partial y} \\ \dfrac{\partial \theta_{x}}{\partial x} - \dfrac{\partial \theta_{y}}{\partial y} \end{bmatrix} \tag{6.18}$$

and $\varepsilon_{s} \equiv \left\{ \varepsilon_{x}^{s} \quad \varepsilon_{y}^{s} \quad \gamma_{xy}^{s} \right\}$ (6.19)

6.2.1.3 Finite strain components

For the case of finite strains, Green's strain-displacement equations are used such that:

$$\varepsilon_{x} = \varepsilon_{x}^{s} + \varepsilon_{x}^{l} \tag{6.20}$$

$$\varepsilon_{y} = \varepsilon_{y}^{s} + \varepsilon_{y}^{l} \tag{6.21}$$

$$\gamma_{xy} = \gamma_{xy}^{s} + \gamma_{xy}^{l} \tag{6.22}$$

where ε_{x}^{l}, ε_{y}^{l}, γ_{xy}^{l} are as defined by equations (4.27)-(4.29), respectively. Hence the additional (nonlinear) terms due to finite strains can be expressed in the matrix form:

$$\varepsilon_{l}(x,y,z) = \varepsilon_{m}(x,y) + \varepsilon_{w}(x,y) - z\hat{\varepsilon}_{m\theta}(x,y) + z^{2}\hat{\varepsilon}_{\theta}(x,y) \tag{6.23}$$

where $\varepsilon_{l} = \{ \varepsilon_{x}^{l} \quad \varepsilon_{y}^{l} \quad \gamma_{xy}^{l} \}$ (6.24)

$$\varepsilon_m(x,y) = \frac{1}{2}\begin{bmatrix} \left(\frac{\partial u^o}{\partial x}\right)^2 + \left(\frac{\partial v^o}{\partial x}\right)^2 \\ \left(\frac{\partial u^o}{\partial y}\right)^2 + \left(\frac{\partial v^o}{\partial y}\right)^2 \\ 2\frac{\partial u^o}{\partial x}\frac{\partial u^o}{\partial y} + 2\frac{\partial v^o}{\partial x}\frac{\partial v^o}{\partial y} \end{bmatrix} \tag{6.25}$$

$$\varepsilon_w(x,y) = \frac{1}{2}\begin{bmatrix} \left(\frac{\partial w}{\partial x}\right)^2 \\ \left(\frac{\partial w}{\partial y}\right)^2 \\ 2\frac{\partial w}{\partial x}\frac{\partial w}{\partial y} \end{bmatrix} \tag{6.26}$$

$$\hat{\varepsilon}_\theta(x,y) = \frac{1}{2}\begin{bmatrix} \left(\frac{\partial \theta_x}{\partial x}\right)^2 + \left(\frac{\partial \theta_y}{\partial x}\right)^2 \\ \left(\frac{\partial \theta_x}{\partial y}\right)^2 + \left(\frac{\partial \theta_y}{\partial y}\right)^2 \\ 2\frac{\partial \theta_x}{\partial x}\frac{\partial \theta_x}{\partial y} + 2\frac{\partial \theta_y}{\partial x}\frac{\partial \theta_y}{\partial y} \end{bmatrix} \tag{6.27}$$

$$\hat{\varepsilon}_{m\theta}(x,y) = \begin{bmatrix} -\frac{\partial u^o}{\partial x}\frac{\partial \theta_y}{\partial x} + \frac{\partial v^o}{\partial x}\frac{\partial \theta_x}{\partial x} \\ -\frac{\partial u^o}{\partial y}\frac{\partial \theta_y}{\partial y} + \frac{\partial v^o}{\partial y}\frac{\partial \theta_x}{\partial y} \\ -\frac{\partial u^o}{\partial y}\frac{\partial \theta_y}{\partial x} - \frac{\partial u^o}{\partial x}\frac{\partial \theta_y}{\partial y} + \frac{\partial v^o}{\partial y}\frac{\partial \theta_x}{\partial x} + \frac{\partial v^o}{\partial x}\frac{\partial \theta_x}{\partial y} \end{bmatrix} \tag{6.28}$$

Finally the vector of total x-y strain components is:

$$\varepsilon(x,y,z) = \varepsilon_s + \varepsilon_l = (\varepsilon_o + \varepsilon_m + \varepsilon_w) - z(\hat{\varepsilon}_b + \hat{\varepsilon}_{m\theta}) + z^2\hat{\varepsilon}_\theta \tag{6.29}$$

6.2.1.4 Matrix representation of finite strains

Defining the following vectors which are functions of x, y :

$$\mathbf{0}_m = \left\{\frac{\partial u^o}{\partial x} \quad \frac{\partial v^o}{\partial x} \quad \frac{\partial u^o}{\partial y} \quad \frac{\partial v^o}{\partial y}\right\} \tag{6.30}$$

$$\mathbf{0}_w = \left\{ \frac{\partial w}{\partial x} \quad \frac{\partial w}{\partial y} \right\} \tag{6.31}$$

$$\mathbf{0}_\theta = \left\{ -\frac{\partial \theta_y}{\partial x} \quad \frac{\partial \theta_x}{\partial x} \quad -\frac{\partial \theta_y}{\partial y} \quad \frac{\partial \theta_x}{\partial y} \right\} \tag{6.32}$$

then it can be deduced that:

$$\boldsymbol{\varepsilon}_m = \frac{1}{2} A_m(x,y) \quad \mathbf{0}_m(x,y) \tag{6.33}$$

$$\boldsymbol{\varepsilon}_w = \frac{1}{2} A_w(x,y) \quad \mathbf{0}_w(x,y) \tag{6.34}$$

$$\hat{\boldsymbol{\varepsilon}}_{m\theta} = A_m \, \mathbf{0}_\theta = A_\theta \, \mathbf{0}_m \tag{6.35}$$

$$\hat{\boldsymbol{\varepsilon}}_\theta = \frac{1}{2} A_\theta(x,y) \quad \mathbf{0}_\theta(x,y) \tag{6.36}$$

where the A matrices are defined as follows:

$$A_m(x,y) = \begin{bmatrix} \frac{\partial u^o}{\partial x} & \frac{\partial v^o}{\partial x} & 0 & 0 \\ 0 & 0 & \frac{\partial u^o}{\partial y} & \frac{\partial u^o}{\partial y} \\ \frac{\partial u^o}{\partial y} & \frac{\partial v^o}{\partial y} & \frac{\partial u^o}{\partial x} & \frac{\partial v^o}{\partial x} \end{bmatrix} \tag{6.37}$$

$$A_w(x,y) = \begin{bmatrix} \frac{\partial w}{\partial x} & 0 \\ 0 & \frac{\partial w}{\partial y} \\ \frac{\partial w}{\partial y} & \frac{\partial w}{\partial x} \end{bmatrix} \tag{6.38}$$

$$A_\theta(x,y) = \begin{bmatrix} -\frac{\partial \theta_y}{\partial x} & \frac{\partial \theta_x}{\partial x} & 0 & 0 \\ 0 & 0 & -\frac{\partial \theta_y}{\partial y} & \frac{\partial \theta_x}{\partial y} \\ -\frac{\partial \theta_y}{\partial y} & \frac{\partial \theta_x}{\partial y} & -\frac{\partial \theta_y}{\partial x} & \frac{\partial \theta_x}{\partial x} \end{bmatrix} \tag{6.39}$$

Notice also that the variation of strain terms can be obtained as follows:

$$d\boldsymbol{\varepsilon}_m = \boldsymbol{A}_m \; d\boldsymbol{0}_m \tag{6.40}$$

$$d\boldsymbol{\varepsilon}_w = \boldsymbol{A}_w \; d\boldsymbol{0}_w \tag{6.41}$$

$$d\hat{\boldsymbol{\varepsilon}}_{m\theta} = \boldsymbol{A}_\theta \; d\boldsymbol{0}_m + \boldsymbol{A}_m \; d\boldsymbol{0}_\theta \tag{6.42}$$

$$d\hat{\boldsymbol{\varepsilon}}_\theta = \boldsymbol{A}_\theta \; d\boldsymbol{0}_\theta \tag{6.43}$$

6.2.2 Strain energy variations

6.2.2.1 Introduction

Notice that stress components at any point (x,y,z) inside the lth layer of a composite layered plate can be expressed in terms of strain components as given by equations (4.51) and (4.52). The variation of strain energy density (strain energy per unit volume) at any point inside the plate due to a variation of the displacement field can be expressed as follows:

$$\delta\bar{U} = \delta\boldsymbol{\gamma}^t\boldsymbol{\tau} + \delta\boldsymbol{\varepsilon}^t\boldsymbol{\sigma} \equiv \delta\boldsymbol{\gamma}^t\boldsymbol{\tau} + (\delta\boldsymbol{\varepsilon}_s^t + \delta\boldsymbol{\varepsilon}_s^t)\,\boldsymbol{\sigma} \tag{6.44}$$

which can also be rewritten as:

$$\delta\bar{U} = (\delta\boldsymbol{\gamma}^t\boldsymbol{\tau} + \delta\boldsymbol{\varepsilon}_s^t\boldsymbol{\sigma}_s) + \delta\boldsymbol{\varepsilon}_l^t\boldsymbol{\sigma} + \delta\boldsymbol{\varepsilon}_s^t\boldsymbol{\sigma}_l \tag{6.45}$$

where $\boldsymbol{\sigma}_s = \boldsymbol{D}^{(l)}\boldsymbol{\varepsilon}_s$ (6.46)

and $\boldsymbol{\sigma}_l = \boldsymbol{D}^{(l)}\boldsymbol{\varepsilon}_l$ (6.47)

Hence, the variation of the strain energy density can be represented in terms of three parts as follow:

$$\delta\bar{U} = \delta\bar{U}_{small} + \delta\bar{U}_l + \delta\bar{U}_{sl} \tag{6.48}$$

where

$$\delta\bar{U}_{small} = \delta\boldsymbol{\gamma}^t\boldsymbol{\tau} + \delta\boldsymbol{\varepsilon}_s^t\boldsymbol{\sigma}_s \equiv \delta\bar{U}_\gamma + \delta\bar{U}_s \tag{6.49}$$

which represents the variation due to infinitesimal strains and corresponding stresses, with:

$$\delta\bar{U}_\gamma = \delta\boldsymbol{\gamma}^t\boldsymbol{\tau} = \delta\boldsymbol{\gamma}^t\boldsymbol{\mu}^{(l)}\boldsymbol{\gamma} \tag{6.50}$$

and $\delta\bar{U}_s = \delta\boldsymbol{\varepsilon}_s^t\boldsymbol{\sigma}_s = \delta\boldsymbol{\varepsilon}_s^t\boldsymbol{D}^{(l)}\boldsymbol{\varepsilon}_s$ (6.51)

The term: $\delta\bar{U}_l = \delta\boldsymbol{\varepsilon}_l^t\boldsymbol{\sigma}$ (6.52)

represents the variation due to a variation of the additional finite strain terms, and the third term: $\delta\bar{U}_{sl} = \delta\boldsymbol{\varepsilon}_s^t\boldsymbol{\sigma}_l$ (6.53)

represents a coupling term due to the variation of infinitesimal strains, and the additional stresses obtained from the additional finite strain terms.

6.2.2.2 Analysis of the term $\delta\bar{U}_{small}$

From equations (6.9) and (6.50) it can be deduced that:

$$\delta\bar{U}_{\gamma}(x,y,z) = f_{\gamma}^{2}(z)\, d\hat{\gamma}^{t}(x,y)\, \boldsymbol{\mu}^{(l)}\, \hat{\gamma}(x,y) \tag{6.54}$$

Integrating the previous equation with respect to z across the layers of the plate, it can be deduced that:

$$\delta U'_{\gamma}(x,y) \equiv \int_{-h/2}^{h/2} \delta\bar{U}_{\gamma}(x,y,z)\, dz = \delta\hat{\gamma}^{t}(x,y)\ \boldsymbol{\mu}_{\gamma\gamma}\, \hat{\gamma}(x,y) \tag{6.55}$$

where $\boldsymbol{\mu}_{\gamma\gamma}$ is as defined by equation (4.65).

Substituting from equation (6.16) into equation (6.51) then:

$$\delta\bar{U}_{s} = \left(\delta\boldsymbol{\varepsilon}_{o}^{t} - z\delta\hat{\boldsymbol{\varepsilon}}_{b}^{t}\right)\boldsymbol{D}^{(l)}\left(\boldsymbol{\varepsilon}_{o} - z\hat{\boldsymbol{\varepsilon}}_{b}\right) \tag{6.56}$$

Expanding equation (6.56), we can deduce that:

$$\delta\bar{U}_{s} = \delta\bar{U}_{oo} + \delta\bar{U}_{bb} + (\delta\bar{U}_{ob} + \delta\bar{U}_{bo}) \tag{6.57}$$

where $\delta\bar{U}_{oo} = \delta\boldsymbol{\varepsilon}_{o}^{t}(x,y)\, \boldsymbol{D}^{(l)}\, \boldsymbol{\varepsilon}_{o}(x,y)$ (6.58)

$$\delta\bar{U}_{bb} = z^{2}\, \delta\hat{\boldsymbol{\varepsilon}}_{b}^{t}(x,y)\, \boldsymbol{D}^{(l)}\, \hat{\boldsymbol{\varepsilon}}_{b}(x,y) \tag{6.59}$$

$$\delta\bar{U}_{ob} = -z\, \delta\boldsymbol{\varepsilon}_{o}^{t}(x,y)\, \boldsymbol{D}^{(l)}\, \hat{\boldsymbol{\varepsilon}}_{b}(x,y) \tag{6.60}$$

$$\delta\bar{U}_{bo} = -z\, \delta\hat{\boldsymbol{\varepsilon}}_{b}^{t}(x,y)\, \boldsymbol{D}^{(l)}\, \boldsymbol{\varepsilon}_{o}(x,y) \tag{6.61}$$

Integrating equations (6.58) - (6.61) with respect to z over the plate thickness, it can be deduced that:

$$\delta U'_{oo}(x,y) \equiv \int_{-h/2}^{h/2} \delta\bar{U}_{oo}(x,y,z)\, dz = \delta\boldsymbol{\varepsilon}_{o}^{t}(x,y)\, \boldsymbol{D}_{oo}\, \boldsymbol{\varepsilon}_{o}(x,y) \tag{6.62}$$

$$\delta U'_{bb}(x,y) \equiv \int_{-h/2}^{h/2} \delta\bar{U}_{bb}(x,y,z)\, dz = \delta\hat{\boldsymbol{\varepsilon}}_{b}^{t}(x,y)\, \boldsymbol{D}_{bb}\, \hat{\boldsymbol{\varepsilon}}_{b}(x,y) \tag{6.63}$$

$$\delta U'_{ob}(x,y) \equiv \int_{-h/2}^{h/2} \delta\bar{U}_{ob}(x,y,z)\, dz = -\delta\boldsymbol{\varepsilon}_{o}^{t}(x,y)\, \boldsymbol{D}_{ob}\, \hat{\boldsymbol{\varepsilon}}_{b}(x,y) \tag{6.64}$$

$$\delta U'_{bo}(x,y) \equiv \int_{-h/2}^{h/2} \delta \bar{U}_{bo}(x,y,z)\,dz = -\delta \hat{\varepsilon}_b^t(x,y)\,\boldsymbol{D}_{bo}\,\boldsymbol{\varepsilon}_o(x,y) \tag{6.65}$$

where $\boldsymbol{D}_{oo}$, $\boldsymbol{D}_{bb}$, $\boldsymbol{D}_{ob}$, $\boldsymbol{D}_{bo}$ are as defined by equations (4.79)-(4.81).

6.2.2.3 Strain energy variation term $(\delta \bar{U}_l)$

It can be deduced that from equation (6.52) and equation (6.29) that:

$$\delta \bar{U}_l = \delta \boldsymbol{\varepsilon}_l^t \boldsymbol{\sigma} = (\delta \boldsymbol{\varepsilon}_m^t + \delta \boldsymbol{\varepsilon}_w^t - z\delta \hat{\boldsymbol{\varepsilon}}_{m\theta}^t + z^2 \delta \hat{\boldsymbol{\varepsilon}}_\theta^t)\boldsymbol{\sigma} \tag{6.66}$$

which can be rewritten as follows:

$$\delta \bar{U}_l = \delta \bar{U}_m + \delta \bar{U}_w + \delta \bar{U}_{m\theta} + \delta \bar{U}_\theta \tag{6.67}$$

where $\delta \bar{U}_m$, $\delta \bar{U}_w$, $\delta \bar{U}_{m\theta}$, $\delta \bar{U}_\theta$ are as defined by equations (4.100), (4.106), (4.109), and (4.111), respectively. These terms can also be integrated with respect to z across the layers of the plate, and represented in matrix forms as follows:

$$\delta U'_m(x,y) = \int_{-h/2}^{h/2} \delta \bar{U}_m(x,y,z)\,dz \equiv \delta \mathbf{0}_m^t\, \boldsymbol{S}_{mm}\, \mathbf{0}_m \tag{6.68}$$

$$\delta U'_w(x,y) = \int_{-h/2}^{h/2} \delta \bar{U}_w(x,y,z)\,dz = \delta \mathbf{0}_w^t\, \boldsymbol{S}_{ww}\, \mathbf{0}_w \tag{6.69}$$

$$\delta U'_{m\theta}(x,y) = \int_{-h/2}^{h/2} \delta \bar{U}_{m\theta}(x,y,z)\,dz = \delta \mathbf{0}_m^t\, \boldsymbol{S}_{m\theta} \mathbf{0}_\theta + \delta \mathbf{0}_\theta^t\, \boldsymbol{S}_{\theta m} \mathbf{0}_m \tag{6.70}$$

$$\delta U'_\theta(x,y) = \int_{-h/2}^{h/2} \delta \bar{U}_\theta(x,y,z)\,dz = \delta \mathbf{0}_\theta^t \boldsymbol{S}_{\theta\theta}\, \mathbf{0}_\theta \tag{6.71}$$

where $\boldsymbol{S}_{mm}$, $\boldsymbol{S}_{ww}$, $\boldsymbol{S}_{m\theta}$, $\boldsymbol{S}_{\theta m}$, $\boldsymbol{S}_{\theta\theta}$ are as defined from $\boldsymbol{\sigma}_m$, $\boldsymbol{\sigma}_{m\theta}$, $\boldsymbol{\sigma}_\theta$ by equations similar to (4.105), (4.108), (4.113), (4.118), and the integrated stress vectors $\boldsymbol{\sigma}_m$, $\boldsymbol{\sigma}_{m\theta}$, $\boldsymbol{\sigma}_\theta$ are defined for Mindlin-type elements as follows:

$$\boldsymbol{\sigma}_m = \int_{-h/2}^{h/2} \boldsymbol{\sigma}\,dz = \boldsymbol{D}_{oo}(\boldsymbol{\varepsilon}_o + \boldsymbol{\varepsilon}_m + \boldsymbol{\varepsilon}_w) - \boldsymbol{D}_{ob}(\hat{\boldsymbol{\varepsilon}}_b + \hat{\boldsymbol{\varepsilon}}_{m\theta}) + \boldsymbol{D}_{bb}\,\hat{\boldsymbol{\varepsilon}}_\theta \tag{6.72}$$

$$\boldsymbol{\sigma}_{m\theta} = \int_{-h/2}^{h/2} (-z\,\boldsymbol{\sigma})\,dz = -\boldsymbol{D}_{ob}(\boldsymbol{\varepsilon}_o + \boldsymbol{\varepsilon}_m + \boldsymbol{\varepsilon}_w) + \boldsymbol{D}_{bb}(\hat{\boldsymbol{\varepsilon}}_b + \hat{\boldsymbol{\varepsilon}}_{m\theta}) - \boldsymbol{D}_{(3)}\hat{\boldsymbol{\varepsilon}}_\theta \tag{6.73}$$

$$\boldsymbol{\sigma}_\theta = \int_{-h/2}^{h/2} (z^2 \boldsymbol{\sigma})\, dz = \boldsymbol{D}_{bb}(\boldsymbol{\varepsilon}_o + \boldsymbol{\varepsilon}_m + \boldsymbol{\varepsilon}_w) - \boldsymbol{D}_{(3)}(\hat{\boldsymbol{\varepsilon}}_b + \hat{\boldsymbol{\varepsilon}}_{m\theta}) + \boldsymbol{D}_{(4)}\hat{\boldsymbol{\varepsilon}}_\theta \tag{6.74}$$

where $\boldsymbol{D}_{(n)} = \int_{-h/2}^{h/2} z^n \boldsymbol{D}^{(l)}\, dz.$

6.2.2.4 Strain energy variation term $(\delta \bar{U}_{sl})$

This term can be expressed as follows:

$$\delta \bar{U}_{sl} = \delta \boldsymbol{\varepsilon}_s^t \boldsymbol{\sigma}_l = (\delta \boldsymbol{\varepsilon}_o^t - z\delta \hat{\boldsymbol{\varepsilon}}_b^t)\boldsymbol{\sigma}_l \equiv (\delta \bar{U}_o)_{sl} + (\delta \bar{U}_b)_{sl} \tag{6.75}$$

where $(\delta \bar{U}_o)_{sl}$, $(\delta \bar{U}_b)_{sl}$ are as defined by equations (4.123) and (4.124). These two parts can also be integrated with respect to z over the plate thickness and expressed as follows:

$$(\delta U'_o)_{sl} = \int_{-h/2}^{h/2} (\delta \bar{U}_o)_{sl}\, dz = \delta \boldsymbol{\varepsilon}_o^t \boldsymbol{\sigma}_o \tag{6.76}$$

$$(\delta U'_b)_{sl} = \int_{-h/2}^{h/2} (\delta \bar{U}_b)_{sl}\, dz = \delta \hat{\boldsymbol{\varepsilon}}_b^t \boldsymbol{\sigma}_b \tag{6.77}$$

where $\boldsymbol{\sigma}_o$, $\boldsymbol{\sigma}_b$ are as defined by equations (4.127) and (4.130).

6.3 INTERPOLATED EQUATIONS

Mindlin-type finite strip elements are based on using piecewise one-dimensional Lagrangian interpolation along the length of the plate (x direction). Along the plate width (y direction) different types of interpolation, including the use of trigonometric functions could be used. Nevertheless, Lagrangian interpolation is preferred so as to keep the equations of those elements as simple as possible. The full x-y interpolated parameters can be expressed for an n-node Mindlin-type strip, with m y-terms (or harmonics) as follows:

$$u^o(x,y) = \sum_{i=1}^{n}\sum_{r=1}^{m} N_i(\xi) f_u^r(\eta) u_i^r \tag{6.78}$$

$$v^o(x,y) = \sum_{i=1}^{n}\sum_{r=1}^{m} N_i(\xi) f_v^r(\eta) u_i^r \tag{6.79}$$

$$w(x,y) = \sum_{i=1}^{n}\sum_{r=1}^{m} N_i(\xi) f_w^r(\eta) w_i^r \tag{6.80}$$

$$\theta_x(x,y) = \sum_{i=1}^{n}\sum_{r=1}^{m} N_i(\xi)\, f_{\theta_x}^{r}(\eta)\left(\theta_x^r\right)_i \tag{6.81}$$

$$\theta_y(x,y) = \sum_{i=1}^{n}\sum_{r=1}^{m} N_i(\xi)\, f_{\theta_y}^{r}(\eta)\left(\theta_y^r\right)_i \tag{6.82}$$

where $N_i(\xi)$ represents Lagrangian shape functions as given by equation (3.38), and if Lagrangian interpolation is employed in y direction then:

$$f_u^{r}(\eta) = f_v^{r}(\eta) = f_w^{r}(\eta) = f_{\theta_y}^{r}(\eta) = \mathcal{L}_r^{m}(\eta), \quad f_{\theta_x}^{r}(\eta) = \frac{df_w^r}{d\eta} \tag{6.83}$$

where $$\mathcal{L}_r^{m}(\eta) = \prod_{\substack{j=1 \\ j\neq r}}^{m} \frac{(m-1)\eta - (j-1)}{r-j} \tag{6.84}$$

Notice that we can set boundary conditions at y edges, since u_i^1 , v_i^1 etc. represent nodal values at edge$(\eta = 0)$ and u_i^m , v_i^m etc. represent nodal values at edge$(\eta = 1)$.

6.4 ELEMENT LINEAR STIFFNESS MATRIX

6.4.1 Infinitesimal strain components

The nodal displacement vector per rth harmonic or y term for an n node strip can be partitioned as follows:

$$\boldsymbol{\delta}^r = \begin{bmatrix} \boldsymbol{\delta}_o^r \\ \boldsymbol{\delta}_b^r \end{bmatrix} \tag{6.85}$$

where $\boldsymbol{\delta}_o^r = \left\{u_1^r\ v_1^r\ \ u_2^r\ v_2^r\ \ \ldots\ \ u_n^r\ v_n^r\right\}$ (6.86)

and $\boldsymbol{\delta}_b^r = \left\{w_1^r\ (\theta_x^r)_1\ (\theta_y^r)_1\ \ \ldots\ \ w_n^r\ (\theta_x^r)_n\ (\theta_y^r)_n\right\}$ (6.87)

Using interpolation equations (6.78), (6.79) then equation (6.17) can be written in terms of nodal values as follows:

$$\boldsymbol{\varepsilon}_o = \sum_{r=1}^{m} \boldsymbol{B}_o^r(\xi,\eta)\,\boldsymbol{\delta}_o^r \tag{6.88}$$

where $\boldsymbol{B}_o^r(\xi,\eta)$ is as given by equation (4.168).

Similarly by using interpolation equations (6.80)-(6.82), then equation (6.18) can be rewritten in terms of nodal values as follows

$$\hat{\boldsymbol{\varepsilon}}_b = \sum_{r=1}^{m} \boldsymbol{B}_b^r(\xi,\eta)\,\boldsymbol{\delta}_b^r \tag{6.89}$$

where

$$B_b^r(\xi,\eta) = \begin{bmatrix} \cdots & 0 & 0 & -\dfrac{N_i'(\xi)}{J_x} f_w^r(\eta) & \cdots \\ \cdots & 0 & \dfrac{N_i(\xi)}{J_y} f_{w,\eta\eta}^r(\eta) & 0 & \cdots \\ \cdots & 0 & \dfrac{N_i'(\xi)}{J_x} f_{w,\eta}^r(\eta) & -\dfrac{N_i(\xi)}{J_y} f_{w,\eta}^r(\eta) & \cdots \end{bmatrix} \tag{6.90}$$

and $N_i' = \dfrac{dN_i}{d\xi}$, $f_{w,\eta}^r = \dfrac{df_w^r}{d\eta}$, $f_{w,\eta\eta}^r = \dfrac{d^2 f_w^r}{d\eta^2}$.

Substituting from equations (6.80)-(6.82) into (6.11) then:

$$\hat{\gamma}(x,y) = \sum_{r=1}^{m} B_\gamma^r(\xi,\eta)\, \delta_b^r \tag{6.91}$$

where

$$B_\gamma^r(\xi,\eta) = \begin{bmatrix} \cdots & N_i'(\xi) f_w^r(\eta)/J_x & 0 & N_i(\xi) f_w^r(\eta) & \cdots \\ \cdots & N_i(\xi) f_{w,\eta}^r(\eta)/J_y & -N_i(\xi) f_{w,\eta}^r(\eta) & 0 & \cdots \end{bmatrix} \tag{6.92}$$

6.4.2 Strain energy variation and element stiffness matrix

Using equation (6.55) and equations (6.62)-(6.65), the strain energy variation per unit area for the case of infinitesimal strains can be expressed as follows:

$$\delta U'_{small} = (\delta U'_{\gamma} + \delta U'_{oo} + \delta U'_{bb}) + (\delta U'_{ob} + \delta U'_{bo}) \tag{6.93}$$

Each term can be represented in terms of nodal displacement values and integrated with respect to the *x*-*y* plane of the strip, as shown for Reissner-type elements in section 4.4.2. Hence:

$$dU_\gamma = \int_0^1 \int_0^1 \delta U'_\gamma J_x J_y \, d\xi \, d\eta \equiv \sum_{s=1}^{m} \sum_{r=1}^{m} (d\delta_b^s)^t K_{\gamma\gamma}^{sr} \delta_b^r \tag{6.94}$$

$$dU_{oo} = \int_0^1 \int_0^1 \delta U'_{oo} J_x J_y \, d\xi \, d\eta = \sum_{s=1}^{m} \sum_{r=1}^{m} (d\delta_o^s)^t K_{oo}^{sr} \delta_o^r \tag{6.95}$$

$$dU_{bb} = \int_0^1 \int_0^1 \delta U'_{bb} J_x J_y \, d\xi \, d\eta = \sum_{s=1}^{m} \sum_{r=1}^{m} (d\boldsymbol{\delta}_b^s)^t \boldsymbol{K}_{bb}^{sr} \boldsymbol{\delta}_b^r \tag{6.96}$$

$$dU_{ob} = \int_0^1 \int_0^1 \delta U'_{ob} J_x J_y \, d\xi \, d\eta = \sum_{s=1}^{m} \sum_{r=1}^{m} (d\boldsymbol{\delta}_o^s)^t \boldsymbol{K}_{ob}^{sr} \boldsymbol{\delta}_b^r \tag{6.97}$$

$$dU_{bo} = \int_0^1 \int_0^1 \delta U'_{bo} J_x J_y \, d\xi \, d\eta = \sum_{s=1}^{m} \sum_{r=1}^{m} (d\boldsymbol{\delta}_b^s)^t \boldsymbol{K}_{bo}^{sr} \boldsymbol{\delta}_o^r \tag{6.98}$$

where $\boldsymbol{K}_{\gamma\gamma}^{sr}$, $\boldsymbol{K}_{oo}^{sr}$, $\boldsymbol{K}_{bb}^{sr}$, $\boldsymbol{K}_{ob}^{sr}$, $\boldsymbol{K}_{bo}^{sr}$ can be defined by equations similar to those given by equations (4.179), (4.182), (4.185), (4.191), and (4.193), respectively.

6.4.3 Small deflection element stiffness matrix

Substituting from equations (6.94)-(6.98) into the *x*-*y* integration of (6.93), then the variation of the strain energy of the strip due to infinitesimal state of strains can be expressed as follows:

$$\begin{aligned} dU_{small} = \sum_{s=1}^{m} \sum_{r=1}^{m} \Big\{ & (d\boldsymbol{\delta}_b^s)^t \boldsymbol{K}_{\gamma\gamma}^{sr} \boldsymbol{\delta}_b^r + (d\boldsymbol{\delta}_o^s)^t \boldsymbol{K}_{oo}^{sr} \boldsymbol{\delta}_o^r + (d\boldsymbol{\delta}_b^s)^t \boldsymbol{K}_{bb}^{sr} \boldsymbol{\delta}_b^r \\ & + (d\boldsymbol{\delta}_o^s)^t \boldsymbol{K}_{ob}^{sr} \boldsymbol{\delta}_b^r + (d\boldsymbol{\delta}_b^s)^t \boldsymbol{K}_{bo}^{sr} \boldsymbol{\delta}_o^r \Big\} \end{aligned} \tag{6.99}$$

which can be rewritten as:

$$dU_{small} = \sum_{s=1}^{m} \sum_{r=1}^{m} (d\boldsymbol{\delta}^s)^t \boldsymbol{K}^{sr} \boldsymbol{\delta}^r \tag{6.100}$$

where

$$d\boldsymbol{\delta}^s = \begin{bmatrix} d\boldsymbol{\delta}_o^s \\ d\boldsymbol{\delta}_b^s \end{bmatrix}, \qquad \boldsymbol{\delta}^r = \begin{bmatrix} \boldsymbol{\delta}_o^r \\ \boldsymbol{\delta}_b^r \end{bmatrix} \tag{6.101}$$

and

$$\boldsymbol{K}^{sr} = \begin{bmatrix} \boldsymbol{K}_{oo}^{sr} & -\boldsymbol{K}_{ob}^{sr} \\ -\boldsymbol{K}_{bo}^{sr} & \boldsymbol{K}_{bb}^{sr} + \boldsymbol{K}_{\gamma\gamma}^{sr} \end{bmatrix} \tag{6.102}$$

which represents the *sr* part in the strip stiffness matrix (see equation 6.139) with infinitesimal strains being assumed. Notice that for symmetric composites:

$$\boldsymbol{D}_{ob} = \mathbf{O}, \text{i.e.} \quad \boldsymbol{K}_{ob}^{sr} = \boldsymbol{K}_{bo}^{sr} = \mathbf{O}. \tag{6.103}$$

6.5 EQUIVALENT NODAL LOADING AND STATIC LINEAR EQUATIONS

Equivalent nodal loading vector per the *r*th harmonic, or *y* term, is partitioned as follows:

$$F^r = \left\{ F_o^r \quad F_b^r \right\} \tag{6.104}$$

and the equivalent loading vector is defined such that it does the same work done by actual loads due to a variational displacement field, i.e.

$$dW = \sum_{r=1}^{m} (d\delta)^t F^r = \sum_{r=1}^{m} \left[(d\delta_o^r)^t F_o^r + (d\delta_b^r)^t F_b^r \right] \tag{6.105}$$

$\equiv$ the work done by the actual load.

6.5.1 Distributed lateral loading with intensity q

If the strip is subjected to distributed loading in the *z* direction, with intensity *q(x,y)* (load per unit area), then the actual work done by that load due to displacement variation is:

$$\delta W = \int_{strip}\int q\, \delta w\, dx\, dy = \int_0^1\int_0^1 \delta w\, q\, J_x J_y\, d\xi\, d\eta$$

$$\equiv \sum_{i=1}^{n}\sum_{r=1}^{m} \int_0^1\int_0^1 q\, N_i(\xi) f_w^r(\eta)\, w_i\, J_x J_y\, d\xi\, d\eta \tag{6.106}$$

Comparing equation (6.106) with (6.105), it can be deduced that:

$$F_o^r = \mathbf{O} \tag{6.107}$$

and

$$F_b^r \equiv \left\{ (F_z^r)_1 \quad 0 \quad 0 \quad (F_z^r)_2 \quad 0 \quad 0 \quad \ldots \quad (F_z^r)_n \quad 0 \quad 0 \right\} \tag{6.108}$$

where

$$(F_z^r) = \int_0^1\int_0^1 q\, N_i(\xi) f_w^r(\eta)\, J_x J_y\, d\xi\, d\eta \tag{6.109}$$

6.5.2 Concentrated forces and moments at node *i* and $\eta = \eta_j$

These are defined in terms of five components $\{ F_x \;\; F_y \;\; F_z \;\; M_x \;\; M_y \}$,where F_x, F_y, F_z are forces at *x*, *y*, *z* directions and M_x, M_y are the bending moments in *x*, *y* directions, respectively. Equivalent nodal loading exists only for the loaded node *i*, and using the following interpolation equations at $\eta = \eta_j$:

$$\delta u^o(\xi_i, \eta_j) = \sum_{r=1}^{m} f_u^r(\eta_j)\, \delta u_i^r \tag{6.110}$$

$$\delta v^{o}(\xi_i, \eta_j) = \sum_{r=1}^{m} f_v^r(\eta_j)\, \delta v_i^r \tag{6.111}$$

$$\delta w(\xi_i, \eta_j) = \sum_{r=1}^{m} f_w^r(\eta_j)\, \delta w_i^r \tag{6.112}$$

$$\delta \theta_x(\xi_i, \eta_j) = \sum_{r=1}^{m} f_{\theta_x}^r(\eta_j)(\delta \theta_x^r)_i \tag{6.113}$$

$$\delta \theta_y(\xi_i, \eta_j) = \sum_{r=1}^{m} f_{\theta_y}^r(\eta_j)(\delta \theta_y^r)_i \tag{6.114}$$

then it can be deduced that:

$$\delta W = \sum_{r=1}^{m} \Big\{ F_x f_u^r(\eta_j)\, \delta u_i^r + F_y f_v^r(\eta_j)\, \delta v_i^r + F_z f_w^r(\eta_j)\, \delta w_i^r + M_x f_{\theta_x}^r(\eta_j)(\delta \theta_x^r)_i + M_y f_{\theta_y}^r(\eta_j)(\delta \theta_y^r)_i \Big\} \tag{6.115}$$

Comparing equation (6.115) with (6.105), then equivalent nodal load components exist only at node *i* and are defined as follows:

$$F_o^r = \left\{ 0 \quad 0 \ \ldots \ (F_x^r)_i \quad (F_y^r)_i \ \ldots \ 0 \quad 0 \right\} \tag{6.116}$$

$$F_b^r = \left\{ 0 \quad 0 \quad 0 \ \ldots \ (F_z^r)_i \quad (M_x^r)_i \quad (M_y^r)_i \ \ldots \ 0 \quad 0 \quad 0 \right\} \tag{6.117}$$

where

$$(F_x^r)_i = F_x f_u^r(\eta_j) \tag{6.118}$$

$$(F_y^r)_i = F_y f_v^r(\eta_j) \tag{6.119}$$

$$(F_z^r)_i = F_z f_w^r(\eta_j) \tag{6.120}$$

$$(M_x^r)_i = M_x f_{\theta_x}^r(\eta_j) \tag{6.121}$$

$$(M_y^r)_i = M_y f_{\theta_y}^r(\eta_j) \tag{6.122}$$

6.5.3 Line loading at $\xi = \xi_i$

This will be defined in terms of loads and moments per unit length in *y*-direction; $\{ F_x^y, F_y^y, F_z^y, M_x^y, M_y^y \}$ and due to a variation in the displacement field, the following interpolation equations are obtained:

$$\delta u^{o}(\xi_i, \eta) = \sum_{r=1}^{m} f_u^r(\eta)\, \delta u_i^r \tag{6.123}$$

$$\delta v^{o}(\xi_i, \eta) = \sum_{r=1}^{m} f_v^r(\eta)\, \delta v_i^r \tag{6.124}$$

$$\delta w(\xi_i,\eta) = \sum_{r=1}^{m} f_w^r(\eta)\,\delta w_i^r \tag{6.125}$$

$$\delta\theta_x(\xi_i,\eta) = \sum_{r=1}^{m} f_{\theta_x}^r(\eta)(\delta\theta_x^r)_i \tag{6.126}$$

$$\delta\theta_y(\xi_i,\eta) = \sum_{r=1}^{m} f_{\theta_y}^r(\eta)(\delta\theta_y^r)_i \tag{6.127}$$

Hence, the work done by this line loading can be expressed as follows:

$$\delta W = \sum_{r=1}^{m}\int_0^1 \Big\{ F_x^y f_u^r(\eta)\,\delta u_i^r + F_y^y f_v^r(\eta)\,\delta v_i^r + F_z^y f_w^r(\eta)\,\delta w_i^r + M_x f_{\theta_x}^r(\eta)(\delta\theta_x^r)_i + M_y f_{\theta_y}^r(\eta)(\delta\theta_y^r)_i \Big\} J_y\,d\eta \tag{6.128}$$

and the equivalent nodal loading components, which exist only at node *i*, can be expressed as follows:

$$(F_x^r)_i = \int_0^1 F_x^y f_u^r(\eta)\,J_y\,d\eta \tag{6.129}$$

$$(F_y^r)_i = \int_0^1 F_y^y f_v^r(\eta)\,J_y\,d\eta \tag{6.130}$$

$$(F_z^r)_i = \int_0^1 F_z^y f_w^r(\eta)\,J_y\,d\eta \tag{6.131}$$

$$(M_x^r)_i = \int_0^1 M_x^y f_{\theta_x}^r(\eta)\,J_y\,d\eta \tag{6.132}$$

$$(M_y^r)_i = \int_0^1 M_y^y f_{\theta_y}^r(\eta)\,J_y\,d\eta \tag{6.133}$$

6.5.4 Linear static analysis equation

For the case of infinitesimal strains it can be deduced from equation (6.99) that:

$$dU \propto dU_{small} = \sum_{s=1}^{m}\sum_{r=1}^{m} (d\boldsymbol{\delta}^s)^t\,\boldsymbol{K}^{sr}\,\boldsymbol{\delta}^r \tag{6.134}$$

and from the principle of virtual work (equation 4.246), it can be shown that:

$$d\chi = \sum_{s=1}^{m} \left\{ (d\delta^s)^t \right\} \left\{ \sum_{r=1}^{m} K^{sr} \delta^r - F^s \right\} = 0 \tag{6.135}$$

Hence, it can be deduced that:

$$\sum_{r=1}^{m} K^{sr} \delta^r - F^s = \mathbf{O}, \; s = 1, 2, \ldots, m \tag{6.136}$$

which can be rewritten in the following matrix form:

$$K\delta = F \tag{6.137}$$

where $F = \{ F^1 \quad F^2 \quad \ldots \quad F^m \}$ (6.138)

and

$$K = \begin{bmatrix} K^{11} & \ldots & K^{1r} & \ldots & K^{1m} \\ \ldots & \ldots & \ldots & \ldots & \ldots \\ K^{s1} & \ldots & K^{sr} & \ldots & K^{sm} \\ \ldots & \ldots & \ldots & \ldots & \ldots \\ K^{m1} & \ldots & K^{mr} & \ldots & K^{mm} \end{bmatrix} \tag{6.139}$$

Equation (6.137) represents linear static equation which can be employed for linear static stress analysis.

6.6 NONLINEAR MATRICES AND VECTORS

6.6.1 Large strain components

(i) Interpolated $\mathbf{0}$ *vector*

Substituting from equations (6.78), (6.79) into equation (6.30), it can be deduced that

$$\mathbf{0}_m = \sum_{r=1}^{m} G_m^r(\xi, \eta)\, \delta_o^r \tag{6.140}$$

where G_m^r is as given by equation (4.254). Similarly, it can be shown that:

$$\mathbf{0}_w = \sum_{r=1}^{m} G_w^r(\xi, \eta)\, \delta_b^r \tag{6.141}$$

where

$$G_w^r = \begin{bmatrix} \ldots & N_i'(\xi) f_w^r(\eta)/J_x & 0 & 0 & \ldots \\ \ldots & N_i(\xi) f_{w,\eta}^r(\eta)/J_y & 0 & 0 & \ldots \end{bmatrix} \tag{6.142}$$

and also: $$\mathbf{0}_\theta = \sum_{r=1}^{m} G_\theta^r(\xi, \eta)\, \delta_b^r \tag{6.143}$$

where

$$G_\theta^r = \begin{bmatrix} \dots & 0 & 0 & -N_i'(\xi) f_w^r(\eta)/J_x & \dots \\ \dots & 0 & N_i'(\xi) f_{w,\eta}^r(\eta)/J_x & 0 & \dots \\ \dots & 0 & 0 & -N_i(\xi) f_{w,\eta}^r(\eta)/J_y & \dots \\ \dots & 0 & N_i(\xi) f_{w,\eta\eta}^r(\eta)/J_y & 0 & \dots \end{bmatrix} \tag{6.144}$$

(ii) Finite strain values and strain increments

Using the previous equations of **0** in equations (6.33) - (6.36), it can be shown that:

$$\varepsilon_m = \frac{1}{2} A_m(x,y) \sum_{r=1}^{m} G_m^r(x,y)\, \delta_o^r \tag{6.145}$$

$$\varepsilon_w = \frac{1}{2} A_w(x,y) \sum_{r=1}^{m} G_w^r(x,y)\, \delta_b^r \tag{6.146}$$

$$\hat{\varepsilon}_{m\theta} = A_m(x,y) \sum_{r=1}^{m} G_\theta^r(x,y)\, \delta_b^r = A_\theta(x,y) \sum_{r=1}^{m} G_m^r(x,y)\, \delta_m^r \tag{6.147}$$

$$\hat{\varepsilon}_\theta = \frac{1}{2} A_\theta(x,y) \sum_{r=1}^{m} G_\theta^r(x,y)\, \delta_b^r \tag{6.148}$$

which have differential expressions similar to those given by equations (4.263)-(4.266).

6.6.2 Derivation of non-linear stiffness matrix K_σ

Integrating equation (6.67) over the plate thickness, then:

$$dU'_l = dU'_m + dU'_w + dU'_{m\theta} + dU'_\theta \tag{6.149}$$

The terms in the previous equation can be integrated over the area of the strip leading to the derivation of the different terms of K_σ as follows:

$$dU_m = \int_0^1 \int_0^1 dU'_m\, J_x J_y\, d\xi\, d\eta \equiv \sum_{s=1}^{m} \sum_{r=1}^{m} (d\delta_o^s)^t\, K_{mm}^{sr}\, \delta_o^r \tag{6.150}$$

$$dU_w = \int_0^1 \int_0^1 dU'_w\, J_x J_y\, d\xi\, d\eta = \sum_{s=1}^{m} \sum_{r=1}^{m} (d\delta_b^s)^t\, K_{ww}^{sr}\, \delta_b^r \tag{6.151}$$

$$dU_{m\theta} = \int_0^1\int_0^1 dU'_{m\theta}\, J_x\, J_y\, d\xi\, d\eta = \sum_{s=1}^{m}\sum_{r=1}^{m}\left[(d\delta_o^s)^t\, K_{m\theta}^{sr}\, \delta_b^r + (d\delta_b^s)^t\, K_{\theta m}^{sr}\, \delta_o^r\right] \quad (6.152)$$

$$dU_{\theta} = \int_0^1\int_0^1 dU'_{\theta}\, J_x\, J_y\, d\xi\, d\eta = \sum_{s=1}^{m}\sum_{r=1}^{m}(d\delta_b^s)^t\, K_{\theta\theta}^{sr}\, \delta_b^r \quad (6.153)$$

where K_{mm}^{sr}, K_{ww}^{sr}, $K_{m\theta}^{sr}$, $K_{\theta m}^{sr}$, $K_{\theta\theta}^{sr}$ will have equations similar to those of Reissner-type elements as given by equations (4.269), (4.271), (4.273a), (4.273b), and (4.275), respectively. The strain energy variation part dU_l can now be expressed as follows:

$$dU_l = \sum_{s=1}^{m}\sum_{r=1}^{m}(d\delta^t)\, K_{\sigma}^{sr}\, \delta^r \quad (6.154)$$

where

$$K_{\sigma}^{sr} = \begin{bmatrix} K_{mm}^{sr} & K_{m\theta}^{sr} \\ K_{\theta m}^{sr} & K_{ww}^{sr} + K_{\theta\theta}^{sr} \end{bmatrix} \quad (6.155)$$

6.6.3 Derivation of coupling vector F_l

Using an analysis similar to that given in section 4.6.3, it can be shown that:

$$dU_{sl} = (dU_o)_{sl} + (dU_b)_{sl} \quad (6.156)$$

where

$$(dU_o)_{sl} = \int_0^1\int_0^1 (dU'_o)_{sl}\, J_x\, J_y\, d\xi\, d\eta = \sum_{s=1}^{m}(d\delta_o^s)^t\,(F_o^s)_l \quad (6.157)$$

$$(dU_b)_{sl} = \int_0^1\int_0^1 (dU'_b)_{sl}\, J_x\, J_y\, d\xi\, d\eta = \sum_{s=1}^{m}(d\delta_b^s)^t\,(F_b^s)_l \quad (6.158)$$

where $(F_o^s)_l$, $(F_b^s)_l$ are as given by equations (4.280) and (4.282), respectively.

Finally, the strain energy part dU_{sl} can be expressed as follows:

$$dU_{sl} = \sum_{s=1}^{m}(d\delta^s)^t\,(F^s)_l \quad (6.159)$$

where $$(F^s)_l \equiv \left\{(F_o^s)_l \quad (F_b^s)_l\right\} \quad (6.160)$$

6.6.4 Non-linear static equations

Using equations (6.100) , (6.154), (6.156) then the variation of the strain energy for the

case with finite strains can be written in the following matrix form:

$$dU = d\delta^t (K + K_\sigma)\,\delta + d\delta^t F_l \tag{6.161}$$

Hence, it can be deduced from the principle of virtual work that:

$$(K + K_\sigma)\delta + F_l = F \tag{6.162}$$

which represents the non-linear static equation.

6.7 ELEMENT MASS MATRICES

6.7.1 Interpolated displacement, velocity and acceleration components at an instant of time t

Using equations (6.78)-(6.82), at an instant of time *t*, then:

$$u^o(x,y,t) = \sum_{i=1}^{n}\sum_{r=1}^{m} N_i(\xi)\, f_u^r(\eta)\, u_i^r(t) \tag{6.163}$$

$$v^o(x,y,t) = \sum_{i=1}^{n}\sum_{r=1}^{m} N_i(\xi)\, f_v^r(\eta)\, v_i^r(t) \tag{6.164}$$

$$w(x,y,t) = \sum_{i=1}^{n}\sum_{r=1}^{m} N_i(\xi)\, f_w^r(\eta)\, w_i^r(t) \tag{6.165}$$

$$\theta_x(x,y,t) = \sum_{i=1}^{n}\sum_{r=1}^{m} N_i(\xi)\, f_{\theta_x}^r(\eta)\left(\theta_x^r(t)\right)_i \tag{6.166}$$

$$\theta_y(x,y,t) = \sum_{i=1}^{n}\sum_{r=1}^{m} N_i(\xi)\, f_{\theta_y}^r(\eta)\left(\theta_y^r(t)\right)_i \tag{6.167}$$

Equations (6.163)-(6.166) can also be written in the following matrix form:

$$q_m = \begin{bmatrix} u \\ v \end{bmatrix} = q_o - z q_\theta, \quad q_w \equiv [w] \tag{6.168}$$

where $q_o = \begin{bmatrix} u^o \\ v^o \end{bmatrix}$, $q_\theta = \begin{bmatrix} -\theta_y \\ \theta_x \end{bmatrix}$ (6.169)

Substituting from equations (6.163)-(6.167) into equations (6.168) and (6.169) then the displacement vectors can be expressed in terms of nodal values at an instant of time *t* as follows:

$$q_o = \begin{bmatrix} u^o \\ v^o \end{bmatrix} = \sum_{r=1}^{m} N_o^r(\xi,\eta)\,\delta_o^r(t) \tag{6.170}$$

$$q_\theta = \begin{bmatrix} -\theta_y \\ \theta_x \end{bmatrix} = \sum_{r=1}^{m} N_\theta^r(\xi,\eta)\,\delta_b^r(t) \tag{6.171}$$

$$q_w = [w] = \sum_{r=1}^{m} N_w^r(\xi,\eta)\,\delta_b^r(t) \tag{6.172}$$

where

$$N_o^r(\xi,\eta) = \begin{bmatrix} \ldots & N_i(\xi)f_u^r(\eta) & 0 & \ldots \\ \ldots & 0 & N_i(\xi)f_v^r(\eta) & \ldots \end{bmatrix} \tag{6.173}$$

$$N_\theta^r(\xi,\eta) = \begin{bmatrix} \ldots & 0 & 0 & -N_i(\xi)f_{\theta_y}^r(\eta) & \ldots \\ \ldots & 0 & N_i(\xi)f_{\theta_x}^r(\eta) & 0 & \ldots \end{bmatrix} \tag{6.174}$$

$$N_w^r(\xi,\eta) = \begin{bmatrix} \ldots & N_i(\xi)f_w^r(\eta) & 0 & 0 & \ldots \end{bmatrix} \tag{6.175}$$

Velocity and acceleration equation are obtained by differentiating displacement equation with respect to. time, hence

$$\dot{q}_m = \begin{bmatrix} \dot{u} \\ \dot{v} \end{bmatrix} = \dot{q}_o - z\dot{q}_\theta, \quad \dot{q}_w \equiv [\dot{w}] \tag{6.176}$$

$$\ddot{q}_m = \begin{bmatrix} \ddot{u} \\ \ddot{v} \end{bmatrix} = \ddot{q}_o - z\ddot{q}_\theta, \quad \ddot{q}_w \equiv [\ddot{w}] \tag{6.177}$$

where different velocity and acceleration vectors can be expressed in terms of corresponding nodal values at an instant of time t by equations similar to (4.170)-(4.172).

6.7.2 Element mass matrix

Using D'Alembert's principle, the force vector due to an acceleration $\ddot{q}(x,y,z,t)$ at an infinitesimal volume $\Delta x\,\Delta y\,\Delta z$ is:

$$\Delta F = -\ddot{q}\,\Delta x\,\Delta y\,\Delta z \tag{6.178}$$

and the work done by that force due to a virtual displacement field dq is

$$dW_D = -\int\int\int \rho\,(dq^t\,\ddot{q})\,dx\,dy\,dz \equiv dW_o + dW_\theta + dW_w \tag{6.179}$$

Using an analysis similar to that of Reissner-type elements as given in section 4.7.2, it can be shown that:

$$dW_o = -\int_0^1\int_0^1 (dq_o^t\,\ddot{q}_o)\,\rho\,h\,J_x\,J_y\,d\xi\,d\eta = -\sum_{s=1}^{m}\sum_{r=1}^{m} (d\delta_o^s)^t\,M_o^{sr}\,\ddot{\delta}_o^r \tag{6.180}$$

$$dW_\theta = -\int_0^1\int_0^1 (dq_\theta^t\,\ddot{q}_\theta)\,\rho\left(\frac{h^3}{12}\right)J_x\,J_y\,d\xi\,d\eta = -\sum_{s=1}^{m}\sum_{r=1}^{m} (d\delta_b^s)^t\,M_\theta^{sr}\,\ddot{\delta}_b^r \tag{6.181}$$

$$dW_w = -\int_0^1\int_0^1 (dq_w^t\,\ddot{q}_w)\,\rho\,h\,J_x\,J_y\,d\xi\,d\eta = -\sum_{s=1}^{m}\sum_{r=1}^{m} (d\delta_b^s)^t\,M_w^{sr}\,\ddot{\delta}_b^r \tag{6.182}$$

where M_o^{sr}, M_w^{sr}, M_θ^{sr} are as given by equations (4.340), (4.342), and (4.344).

Hence

$$dW_D = -\sum_{s=1}^{m}\sum_{r=1}^{m}\left\{(d\delta_o^s)^t\,M_o^{sr}\,\ddot{\delta}_o^r + (d\delta_b^s)^t\,M_\theta^{sr}\,\ddot{\delta}_b^r + (d\delta_b^s)^t\,M_w^{sr}\,\ddot{\delta}_b^r\right\} \tag{6.183}$$

which can be rewritten as follows:

$$dW_D = -\sum_{s=1}^{m}\sum_{r=1}^{m} (d\delta^s)^t\,M^{sr}\,\ddot{\delta}^r \tag{6.184}$$

where

$$M^{sr} = \begin{bmatrix} M_o^{sr} & \mathbf{O} \\ \mathbf{O} & M_\theta^{sr} + M_w^{sr} \end{bmatrix} \tag{6.185}$$

Equation (6.184) can also be written as

$$dW_D = -d\delta^t(t)\,M\,\ddot{\delta}(t) \tag{6.186}$$

6.7.3 Non-linear dynamic equation

Applying the principle of virtual work at an instant of time t, then

$$d\chi(t) = dU(t) - \sum dW(t)$$

$$= dU_{small}(t) + dU_{l}(t) + dU_{sl}(t) - dW(t) - dW_{D}(t) = 0 \qquad (6.187)$$

and from previous equations, it can be deduced that:

$$d\chi(t) = d\boldsymbol{\delta}^{t}(t)\left\{\boldsymbol{M}\,\ddot{\boldsymbol{\delta}} + [\boldsymbol{K} + \boldsymbol{K}_{\sigma}(t)]\boldsymbol{\delta}(t) + \boldsymbol{F}_{l}(t) - \boldsymbol{F}(t)\right\} = 0 \qquad (6.188)$$

Hence

$$\boldsymbol{M}\,\ddot{\boldsymbol{\delta}}(t) + [\boldsymbol{K} + \boldsymbol{K}_{\sigma}(t)]\boldsymbol{\delta}(t) + \boldsymbol{F}_{l}(t) = \boldsymbol{F}(t) \qquad (6.189)$$

which represents the non-linear dynamic equation.

Chapter 7

Static and Dynamic Analysis of Plates and Shells

7. Static and Dynamic Analysis of Plates and Shells

7.1 INTRODUCTION

In this chapter, we discuss first how the different finite strip elements derived in chapters 4,5, and 6 for composite plates can be employed for box structures, stiffened plates, and curved shells. The element matrices are transformed to the global axes of such structures, forming what is usually called the faceted shell element. The degrees of freedom for faceted shell elements may be greater or equal to the degrees of freedom for corresponding plate elements as will be explained in this chapter. A non-linear static stress analysis algorithm, based on the equations given in previous chapters will be explained. Dynamic analysis in this work is limited to natural frequency analysis, but the effect of pre-stressing on natural frequencies will be shown. A buckling algorithm based on the derivations given in previous chapters will also be demonstrated.

7.2 FACETED SHELL FINITE STRIP ELEMENTS

7.2.1 Local and global axes

7.2.1.1 Axes rotation matrices

All the derivations given in previous chapters are with respect to plate local axes (defined here as x, y, z axes), where the $x-y$ plane is the midplane at $z=0$ and the layer angles are measured with respect to the local x-axis shown in the figure 7.1. For box structures and stiffened plates there may be different systems of local axes for the different plate parts forming the structure, whilst it is advantageous to use just one unique global system of axes for the whole structure. For finite strip analysis, the y-axis will remain the same for all axes systems, i.e. the local y-axis is assumed parallel to the global y-axis for all the plate parts of the structure. The type of folded or stiffened plate will have uniform width (constant or linear) in the y-direction, but its x-z section may be as shown in the example of figure 7.2.

Local axes for a finite strip element are defined in terms of the two end points of the strip, such that:

- The local x-axis is from the first end to the second end in the midplane of the strip, and normal to the y-axis.
- The local z-axis is normal to the $x-y$ plane (the midplane $z=0$), across the thickness.

If $(x_1, y_1, z_1), (x_2, y_2, z_2)$ are the global coordinates of the two end points of the strip on the $x-z$ plane , i.e. with $y_1 = y_2 = 0$, then the angle α between the local x-axis and the global x-axis can be defined, as shown in figure 7.1, hence

$$\cos\alpha = \frac{x_2 - x_1}{L}, \quad \sin\alpha = \frac{z_2 - z_1}{L} \tag{7.1}$$

where $L = \sqrt{(x_2 - x_1)^2 + (z_2 - z_1)^2}$ (7.2)

which is the length of the finite strip element in the $\underline{x}$-direction. Hence the directional cosines (l_1, m_1, n_1) of the local x-axis can be defined with respect to the global axes as follows:

$$l_1 = \cos\alpha, \; m_1 = 0, \; n_1 = \sin\alpha \tag{7.3}$$

and from geometry, it is clear that the directional cosines, (l_3, m_3, n_3) of the local z-axis are:

$$l_3 = -\sin\alpha, \; m_3 = 0, \; n_3 = \cos\alpha \tag{7.4}$$

With the local y-axis being parallel to the global y-axis, the directional cosines (l_2, m_2, n_2) of the local y-axis will be:

$$l_2 = 0, \; m_2 = 1, \; n_2 = 0 \tag{7.5}$$

Hence the rotation matrix $\boldsymbol{R}$ of the local axes $(\underline{x}, \underline{y}, \underline{z})$ can be defined as follow:

$$\boldsymbol{R} = \begin{bmatrix} l_1 & m_1 & n_1 \\ l_2 & m_2 & n_2 \\ l_3 & m_3 & n_3 \end{bmatrix} = \begin{bmatrix} \cos\alpha & 0 & \sin\alpha \\ 0 & 1 & 0 \\ -\sin\alpha & 0 & \cos\alpha \end{bmatrix} \tag{7.6}$$

7.2.1.2 Rotation of a vector

Notice that if $\hat{i}, \hat{j}, \hat{k}$ are unit vectors in the global x, y, z directions, and $\hat{\underline{i}}, \hat{\underline{j}}, \hat{\underline{k}}$ are unit vectors in the local $\underline{x}$, $\underline{y}$, $\underline{z}$ directions then from the definitions of directional cosines it can be deduced that:

$$\left.\begin{aligned} \hat{\underline{i}} &= l_1\hat{i} + m_1\hat{j} + n_1\hat{k} \\ \hat{\underline{j}} &= l_2\hat{i} + m_2\hat{j} + n_2\hat{k} \equiv \hat{j} \\ \hat{\underline{k}} &= l_3\hat{i} + m_3\hat{j} + n_3\hat{k} \end{aligned}\right\} \tag{7.7}$$

which can be written in a matrix form as follows:

$$\begin{bmatrix} \hat{\underline{i}} \\ \hat{\underline{j}} \\ \hat{\underline{k}} \end{bmatrix} = \boldsymbol{R} \begin{bmatrix} \hat{i} \\ \hat{j} \\ \hat{k} \end{bmatrix} \tag{7.8}$$

Similarly it can be deduced that:

$$\begin{bmatrix} \hat{i} \\ \hat{j} \\ \hat{k} \end{bmatrix} = \boldsymbol{R}^t \begin{bmatrix} \hat{\imath} \\ \hat{\jmath} \\ \hat{k} \end{bmatrix} \tag{7.9}$$

$$\text{i.e.} \quad \boldsymbol{R}^{-1} = \boldsymbol{R}^t \tag{7.10}$$

A Cartesian vector $\vec{V}$ can be represented by its local components $(\underline{v}_x, \underline{v}_y, \underline{v}_z)$ or global components (v_x, v_y, v_z), i.e.

$$\vec{V} = \underline{v}_x\hat{\imath} + \underline{v}_y\hat{\jmath} + \underline{v}_z\hat{k} \equiv v_x\hat{i} + v_y\hat{j} + v_z\hat{k} \tag{7.11}$$

which can also be written in a matrix form as follow:

$$\boldsymbol{V} = \begin{bmatrix} \underline{v}_x & \underline{v}_y & \underline{v}_z \end{bmatrix} \begin{bmatrix} \hat{\imath} \\ \hat{\jmath} \\ \hat{k} \end{bmatrix} = \begin{bmatrix} v_x & v_y & v_z \end{bmatrix} \begin{bmatrix} \hat{i} \\ \hat{j} \\ \hat{k} \end{bmatrix} \equiv \begin{bmatrix} \underline{v}_x & \underline{v}_y & \underline{v}_z \end{bmatrix} \boldsymbol{R} \begin{bmatrix} \hat{i} \\ \hat{j} \\ \hat{k} \end{bmatrix} \tag{7.12}$$

Hence it can be deduced that:

$$\begin{bmatrix} v_x \\ v_y \\ v_z \end{bmatrix} = \boldsymbol{R}^t \begin{bmatrix} \underline{v}_x \\ \underline{v}_y \\ \underline{v}_z \end{bmatrix} \tag{7.13}$$

Similarly it can be proved that:

$$\begin{bmatrix} \underline{v}_x \\ \underline{v}_y \\ \underline{v}_z \end{bmatrix} = \boldsymbol{R} \begin{bmatrix} v_x \\ v_y \\ v_z \end{bmatrix} \tag{7.14}$$

7.2.2 Degrees of freedom and rotation matrix for Kirchhoff-type elements

It is clear from chapter 5 that the interpolation equations of this element are based upon four degrees of freedom per node and per *y*-term or harmonic, i.e. for the *i*th node and the *r*th *y*-term, the nodal displacement values are: u_i^r, v_i^r, w_i^r, $w_{i,x}^r$, where *u*, *v*, and *w* are by definition the displacement components in the x, y, z directions, respectively and $\partial w/\partial x$

represents a slope angle in y direction, as shown in figure 7.3. Hence it can deduced that:

$$\begin{bmatrix} u_i^r \\ v_i^r \\ w_i^r \\ w_{i,x}^r \end{bmatrix}_{local} = \begin{bmatrix} & \boldsymbol{R} & & 0 \\ & & & 0 \\ & & & 0 \\ 0 & 0 & 0 & 1 \end{bmatrix} \begin{bmatrix} u_i^r \\ v_i^r \\ w_i^r \\ w_{i,x}^r \end{bmatrix}_{Global} \equiv \boldsymbol{R}_k \begin{bmatrix} u_i^r \\ v_i^r \\ w_i^r \\ w_{i,x}^r \end{bmatrix}_{Global} \tag{7.15}$$

where $$\boldsymbol{R}_k = \begin{bmatrix} l_1 & m_1 & n_1 & 0 \\ l_2 & m_2 & n_2 & 0 \\ l_3 & m_3 & n_3 & 0 \\ 0 & 0 & 0 & 1 \end{bmatrix} \tag{7.16}$$

Equation (7.16) is based on the following assumptions:

- The local axes for each finite element strip are consistent, i.e. the axes rotation matrix $\boldsymbol{R}$ is the same at any node within the strip.
- The matrix $\boldsymbol{R}$ is also the same at any y-term.
- At the nodes on the intersection of different local planes, consistent interpolation in the y direction must be used for all displacement components, i.e. same trigonometric functions or polynomial interpolations are employed.

The element rotation matrix can be defined per one y term or harmonic, since it is the same for all y terms or harmonics, and hence for an n-node finite strip element:

$$\underset{4n\times 1}{\delta^r_{Local}} = \underset{4n\times 4n}{\mathfrak{R}} \; \underset{4n\times 1}{\delta^r_{Global}} \tag{7.17}$$

where $\mathfrak{R}$ is the element rotation matrix defined as follows:

$$\mathfrak{R} = \lceil \boldsymbol{R}_k \;\; \boldsymbol{R}_k \;\; \ldots \;\; \boldsymbol{R}_k \rfloor \tag{7.18}$$

7.2.3 Degrees of freedom and rotation matrix for Mindlin-type elements

The interpolation equations of this element are based upon five degrees of freedom u, v, w, θ_x, θ_y, as shown in figure 7.4. Hence for the ith node and the rth y term or harmonic, the nodal local displacement components can be written in terms of corresponding global components as follow:

$$\begin{bmatrix} u_i^r \\ v_i^r \\ w_i^r \end{bmatrix}_{Local} = \boldsymbol{R} \begin{bmatrix} u_i^r \\ v_i^r \\ w_i^r \end{bmatrix}_{Global} \tag{7.19}$$

For the faceted version of this element, an additional degree of freedom θ_z is required. To avoid singular stiffness and mass matrices, we have to distinguish between co-planar nodes (such as j_1, j_2 or j_3, j_4 for the example shown in figure 7.5) and nodes on the intersection of plates such as node i shown in figure 7.5.

(a) For co-planar nodes:

We assume that $\theta_z = 0$ and θ_x, θ_y will always be considered in the directions of the local x, y axes. i.e. no rotation is required for co-planar nodes, i.e. for a co-planar node j :

$$\begin{bmatrix} (\theta_x^r)_j \\ (\theta_y^r)_j \\ (\theta_z^r)_j \end{bmatrix}_{Local} = \boldsymbol{I}_{3\times 3} \begin{bmatrix} (\theta_x^r)_j \\ (\theta_y^r)_j \\ (\theta_z^r)_j \end{bmatrix}_{Global}, \quad (\theta_z^r)_j = 0 \tag{7.20}$$

(b) For a node i on the intersection of two plates:

The global θ_z may not be equal to zero and we use:

$$\begin{bmatrix} (\theta_x^r)_i \\ (\theta_y^r)_i \\ (\theta_z^r)_i \end{bmatrix}_{Local} = \boldsymbol{R} \begin{bmatrix} (\theta_x^r)_i \\ (\theta_y^r)_i \\ (\theta_z^r)_i \end{bmatrix}_{Global} \tag{7.21}$$

Hence the rotation matrix of the element at any node i and y value r can be defined such that:

$$\begin{bmatrix} u_i^r \\ v_i^r \\ w_i^r \\ (\theta_x^r)_i \\ (\theta_y^r)_i \\ (\theta_z^r)_i \end{bmatrix}_{Local} = \boldsymbol{R}_i^M \begin{bmatrix} u_i^r \\ v_i^r \\ w_i^r \\ (\theta_x^r)_i \\ (\theta_y^r)_i \\ (\theta_z^r)_i \end{bmatrix}_{Global} \tag{7.22}$$

where:

♦ For co-planar node *j*:

$$R_j^M = \begin{bmatrix} R_{3\times3} & \mathbf{O} \\ \mathbf{O} & I_{3\times3} \end{bmatrix} \tag{7.23}$$

♦ For node *i* at the intersection of two plates

$$R_i^M = \begin{bmatrix} R_{3\times3} & \mathbf{O} \\ \mathbf{O} & R_{3\times3} \end{bmatrix} \tag{7.24}$$

Finally for all the components of an *n*-node finite strip element at the *r*th *y* term or harmonic, we can deduce that:

$$\underset{6n\times1}{\delta^r_{Local}} = \underset{6n\times6n}{\Re}\ \underset{6n\times1}{\delta^r_{Global}} \tag{7.25}$$

where $\Re$ is the element rotation matrix defined as follows:

$$\Re = \left[R_1^M \;\; R_2^M \;\ldots\; R_i^M \;\ldots\; R_n^M \right] \tag{7.26}$$

Notice that an additional boundary condition should be implemented for every co-planar node *j*:

$$(\theta_z^r)_j = 0, \text{ for } r = 1, 2, \ldots, m \tag{7.27}$$

7.2.4 Degrees of freedom and rotation matrix for Reissner-type elements

The interpolation equations of this element are based upon six degrees of freedom per node *i* and per *y* term or harmonic *r*; u_i^r, v_i^r, w_i^r, $w_{i,x}^r$ $(\psi_x^r)_i$, $(\psi_y^r)_i$, with their directions as shown in figure 7.5. Because of rotation an additional degree of freedom $(\psi_z^r)_i$ is required with the following considerations:

(a) For co-planar nodes:

We consider $\psi_z = 0$ at all the *y* terms or harmonics, whilst ψ_x, ψ_y are always considered in the local directions, i.e. for a co-planar node *j*:

$$\begin{bmatrix} (\psi_x^r)_j \\ (\psi_y^r)_j \\ (\psi_z^r)_j \end{bmatrix}_{Local} = I_{3\times3} \begin{bmatrix} (\psi_x^r)_j \\ (\psi_y^r)_j \\ (\psi_z^r)_j \end{bmatrix}_{Global}, \quad (\psi_z^r)_j = 0 \tag{7.28}$$

(b) For a node i on the intersection of two plates:

This case implies that $(\psi_z^r)_i$ may not equal zero, and we use the following equation:

$$\begin{bmatrix} (\psi_x^r)_i \\ (\psi_y^r)_i \\ (\psi_z^r)_i \end{bmatrix}_{Local} = \boldsymbol{R} \begin{bmatrix} (\psi_x^r)_i \\ (\psi_y^r)_i \\ (\psi_z^r)_i \end{bmatrix}_{Global} \tag{7.29}$$

Hence the rotation matrix of the element at any node i and rth y value can be defined such that:

$$\begin{bmatrix} u_i^r \\ v_i^r \\ w_i^r \\ w_{i,x}^r \\ (\psi_x^r)_i \\ (\psi_y^r)_i \\ (\psi_z^r)_i \end{bmatrix}_{Local} = \underset{7\times7}{\boldsymbol{R}_i^H} \begin{bmatrix} u_i^r \\ v_i^r \\ w_i^r \\ w_{i,x}^r \\ (\psi_x^r)_i \\ (\psi_y^r)_i \\ (\psi_z^r)_i \end{bmatrix}_{Global} \tag{7.30}$$

where for a co-planar node j:

$$\boldsymbol{R}_j^H = \begin{bmatrix} \boldsymbol{R}_{3\times3} & \mathbf{O}_{3\times4} \\ \mathbf{O}_{4\times3} & \boldsymbol{I}_{4\times4} \end{bmatrix} \tag{7.31}$$

and for node i at the intersection of two plates:

$$\boldsymbol{R}_i^M = \begin{bmatrix} \boldsymbol{R}_{3\times3} & \mathbf{O}_{3\times1} & \mathbf{O}_{3\times3} \\ \mathbf{O}_{1\times3} & 1 & \mathbf{O}_{1\times3} \\ \mathbf{O}_{3\times3} & \mathbf{O}_{3\times1} & \boldsymbol{R}_{3\times3} \end{bmatrix} \tag{7.32}$$

and the null matrices are defined as follows:

$$\mathbf{O}_{3\times3} = \begin{bmatrix} 0 & 0 & 0 \\ 0 & 0 & 0 \\ 0 & 0 & 0 \end{bmatrix}, \quad \mathbf{O}_{3\times1} = \begin{bmatrix} 0 \\ 0 \\ 0 \end{bmatrix}, \quad \mathbf{O}_{1\times3} = \begin{bmatrix} 0 & 0 & 0 \end{bmatrix}, \quad \text{etc.} \tag{7.33}$$

Finally for all the components of an n-node finite strip element at rth y term or harmonic, we can deduce that:

$$\underset{7n\times 1}{\delta^{r}_{Local}} = \underset{7n\times 7n}{\Re}\ \underset{7n\times 1}{\delta^{r}_{Global}} \tag{7.34}$$

where $\Re$ is the element rotation matrix defined as follows:

$$\Re = \left[R_1^H \quad R_2^H \ \ldots\ R_i^H \ \ldots\ R_n^H \right] \tag{7.35}$$

Notice also that an additional boundary condition should be implemented for every co-planar node j:

$$(\psi_z^r)_j = 0 \quad \text{with } r = 1, 2, \ldots, m \tag{7.36}$$

7.2.5 Element vectors and matrices in terms of global axes

7.2.5.1 Nodal displacement and force vectors

From previous sections, local nodal displacement and force vectors at the rth value or harmonic can be expressed in terms of corresponding global vectors, as follows:

$$\delta^{r}_{Local} = \Re\, \delta^{r}_{Global} \tag{7.37}$$

$$F^{r}_{Local} = \Re\, F^{r}_{Global} \tag{7.38}$$

$$F^{r}_{l\,Local} = \Re\, F^{r}_{l\,Global} \tag{7.39}$$

where $\Re$ is the corresponding rotation matrix for the finite strip element. Notice also that:

$$\Re^{-1} = \Re^{t} \tag{7.40}$$

7.2.5.2 Element stiffness matrix

From all the derivations of the different finite strip elements discussed in previous chapters, the increment of strain energy part due to infinitesimal strains caused by a virtual displacement field can be expressed (for any element) as follows:

$$dU_{small} = \sum_{s=1}^{m}\sum_{r=1}^{m} (d\delta^{s})^{t}_{Local} K^{sr}_{Local} \delta^{r}_{Local} \tag{7.41}$$

Substituting from equation (7.37) into (7.41) then

$$dU_{small} = \sum_{s=1}^{m}\sum_{r=1}^{m} (d\delta^s)^t_{Global}\, \mathfrak{R}^t\, K^{sr}_{Local}\, \mathfrak{R}\, \delta^r_{Global}$$

$$\equiv \sum_{s=1}^{m}\sum_{r=1}^{m} (d\delta^s)^t_{Global}\, K^{sr}_{Global}\, \delta^r_{Global} \qquad (7.42)$$

Hence, it can be deduced that:

$$K^{sr}_{Global} = \mathfrak{R}^t\, K^{sr}_{Local}\, \mathfrak{R} \qquad (7.43)$$

7.2.5.3 Element K_σ

The increment of U_l due to a virtual displacement field, for any element has been defined as follows:

$$dU_l = \sum_{s=1}^{m}\sum_{r=1}^{m} (d\delta^s)^t_{Local}\, K^{sr}_{\sigma_{Local}}\, \delta^r_{Local} \qquad (7.44)$$

Substituting from equation (7.37) into (7.44), it can be deduced that:

$$dU_l = \sum_{s=1}^{m}\sum_{r=1}^{m} (d\delta^s)^t_{Global}\, K^{sr}_{\sigma_{Global}}\, \delta^r_{Global} \qquad (7.45)$$

where

$$K^{sr}_{\sigma_{Global}} = \mathfrak{R}^t\, K^{sr}_{\sigma_{Local}}\, \mathfrak{R}$$

7.2.5.4 Element mass matrix

The increment of kinetic energy (KE) due to a virtual displacement field (at an instant of time t) can be defined for any of the finite strip elements as:

$$dKE = \sum_{s=1}^{m}\sum_{r=1}^{m} (d\dot{\delta}^s)^t_{Local}\, M^{sr}_{Local}\, \dot{\delta}^r_{Local} \qquad (7.46)$$

Hence it can also be shown that:

$$dKE = \sum_{s=1}^{m}\sum_{r=1}^{m} (d\dot{\delta}^s)^t_{Global}\, M^{sr}_{Global}\, \dot{\delta}^r_{Global} \qquad (7.47)$$

where

$$M^{sr}_{Global} = \mathfrak{R}^t\, M^{sr}_{Local}\, \mathfrak{R} \qquad (7.48)$$

Notice that the matrices and vectors are rotated per y term or harmonic, to make the $\mathfrak{R}$ matrix of a small order. This rotation should be carried out before assembling element matrices. The resulting equations will be with respect to global axes, i.e. boundary conditions should also be defined with respect to global axes (except for those parameters defined always with respect to local axes). For stress and strain results, we have to use local displacement vectors, to make it easier to represent them with respect to material axes.

7.3 STATIC STRESS ANALYSIS

7.3.1 Linear static analysis

The vectors and matrices in the generalized equation of equilibrium (see equation 4.292, 5.154, or 6.162) will be evaluated for every finite strip of the component, and except for plates they will be rotated to the structural global axes, as shown in section 7.2.5. Then, they are assembled to form the structural matrix equation for static analysis, using standard FEM assembly rules, which can be written (after applying boundary conditions) as:

$$\left(K_{structure} + K_{\sigma_{structure}}\right)\delta_{structure} = F_{l_{structure}} + F_{structure} \tag{7.49}$$

For simplicity, the subscript *structure* will be dropped from the remaining equations given in this chapter, i.e. we use for the whole structure the following simplified equation:

$$\left(K + K_{\sigma}\right)\delta = F_{l} + F \tag{7.50}$$

If the resulting strains are infinitesimal, then large deflection matrices K_{σ} and F_{l} are negligible, and equation (7.50) is reduced to:

$$K\,\delta_{o} = F \tag{7.51}$$

which can be solved using any standard solver for simultaneous equations. Three different methods of assembly and solution were adopted in this work; ordinary solver, banded solver, and frontal solver, and all based on the Gauss-elimination procedure. Having obtained the nodal displacements, elemental nodal displacement vectors are found and rotated with respect to strip local axes, and hence the infinitesimal strain components are obtained at any point inside the strip by equations similar to those given in sections 4.4, 5.4, and 6.4. We select to calculate those components for every node and y value at three different z-points per each layer of the composite plate; the lower, the middle, and the upper points. Corresponding stress vectors will be obtained for each of those points by using stress-strain equations similar to equations (4.51) and (4.52).

7.3.2 Static analysis with geometrical non-linearity

Having solved linear equations, then strain values can be checked, and if the assumption of infinitesimal strains is no longer valid, then equation (7.49) should be considered for the stress analysis. In this equation the matrix K_{σ} and the vector F_{l} are functions of stresses. They can now be approximated in terms of the stresses obtained from the linear solution, and this may lead to violation of the generalized equation of equilibrium, resulting in the following residual vector:

$$\begin{aligned} R_{o} &= F - \left[K\,\delta_{o} + K_{\sigma}(\sigma_{o})\,\delta_{o} + F_{l}(\sigma_{o})\right] \\ &\equiv -\left[K_{\sigma}(\sigma_{o})\,\delta_{o} + F_{L}(\sigma_{o})\right] \end{aligned} \tag{7.52}$$

where $\boldsymbol{\sigma}_o = \boldsymbol{\sigma}(\boldsymbol{\delta}_o)$ which represent the stress field resulting from the linear solution. Hence, we can rewrite (7.52) as:

$$\boldsymbol{R}_o = \boldsymbol{F} - \left[\left(\boldsymbol{K} + \boldsymbol{K}_\sigma(\boldsymbol{\delta}_o)\right)\boldsymbol{\delta}_o + \boldsymbol{F}_l(\boldsymbol{\delta}_o)\right] \tag{7.53}$$

If $\boldsymbol{R}_o$ has significant values, it confirms that a non-linear analysis should be carried out. Therefore defining; $\boldsymbol{\delta}_1 = \boldsymbol{\delta}_o + \Delta\boldsymbol{\delta}_1$, such that equation (7.49) is satisfied, then

$$\left[\boldsymbol{K} + \boldsymbol{K}_\sigma(\boldsymbol{\delta}_o + \Delta\boldsymbol{\delta}_1)\right]\left[\boldsymbol{\delta}_o + \Delta\boldsymbol{\delta}_1\right] + \boldsymbol{F}_l(\boldsymbol{\delta}_o + \Delta\boldsymbol{\delta}_1) = \boldsymbol{F} \tag{7.54}$$

which can be approximated to

$$\left[\boldsymbol{K} + \boldsymbol{K}_\sigma(\boldsymbol{\delta}_o)\right]\left[\boldsymbol{\delta}_o + \Delta\boldsymbol{\delta}_1\right] + \boldsymbol{F}_l(\boldsymbol{\delta}_o) \approx \boldsymbol{F} \tag{7.55}$$

or
$$\left[\boldsymbol{K} + \boldsymbol{K}_\sigma(\boldsymbol{\delta}_o)\right]\Delta\boldsymbol{\delta}_1 = \boldsymbol{R}_o \tag{7.56}$$

which can be solved in $\Delta\boldsymbol{\delta}_1$ and a new residual vector is obtained.

After t iterations, we have obtained $\boldsymbol{\delta}_{t-1}$ and can calculate corresponding stresses and strains, the vector $\boldsymbol{F}_l(\boldsymbol{\delta}_{t-1})$, and the matrix $\boldsymbol{K}_\sigma(\boldsymbol{\delta}_{t-1})$, then the residual vector can be updated as follows:

$$\boldsymbol{R}_{t-1} = \boldsymbol{F} - \left[\boldsymbol{K}\,\boldsymbol{\delta}_{t-1} + \boldsymbol{K}_\sigma(\boldsymbol{\delta}_{t-1})\,\boldsymbol{\delta}_{t-1} + \boldsymbol{F}_l(\boldsymbol{\delta}_{t-1})\right] \tag{7.57}$$

If it has significant values, we assume

$$\boldsymbol{\delta}_t = \boldsymbol{\delta}_{t-1} + \Delta\boldsymbol{\delta}_t \tag{7.58}$$

such that

$$\left[\boldsymbol{K} + \boldsymbol{K}_\sigma(\boldsymbol{\delta}_t)\right]\boldsymbol{\delta}_t + \boldsymbol{F}_l(\boldsymbol{\delta}_t) = \boldsymbol{F}$$

i.e.
$$\left[\boldsymbol{K} + \boldsymbol{K}_\sigma(\boldsymbol{\delta}_{t-1})\right]\Delta\boldsymbol{\delta}_t \approx \boldsymbol{R}_{t-1} \tag{7.59}$$

which can be solved in $\Delta\boldsymbol{\delta}_t$ and a new residual vector is defined, an so on.

Iterations are carried out until convergence is achieved, i.e.:

$$\frac{\Delta\boldsymbol{\delta}_t^t\,\Delta\boldsymbol{\delta}_t}{\boldsymbol{\delta}_t^t\,\boldsymbol{\delta}_t} \leq \text{a permissible error}$$

7.4 NATURAL FREQUENCY ANALYSIS

7.4.1 Case without pre-stressing

Ignoring the effect of damping on natural frequencies and considering infinitesimal strains,

the dynamic equation of the structure, at an instant of time t, modelled via finite strip elements will be:

$$\boldsymbol{M}\,\ddot{\boldsymbol{\delta}}(t) + \boldsymbol{K}\,\boldsymbol{\delta}(t) = \boldsymbol{F}(t) \tag{7.60}$$

At a natural frequency ω, all the particles of the structure are vibrating with the same frequency, i.e. we can assume that the nodal displacement vector of the structure at an instant of time t will be:

$$\boldsymbol{\delta}(t) = \hat{\boldsymbol{\delta}}\cos(\omega t) \tag{7.61}$$

where $\hat{\boldsymbol{\delta}}$ represents the nodal amplitudes, hence

$$\ddot{\boldsymbol{\delta}}(t) = \left[\hat{\boldsymbol{\delta}}\cos(\omega t)\right](-\omega^2) \tag{7.62}$$

Substituting from equations (7.61) and (7.62) into (7.60) and assuming no load is applied, then it can be deduced that

$$(\boldsymbol{K} - \omega^2\boldsymbol{M})\hat{\boldsymbol{\delta}} = \mathbf{O} \tag{7.63}$$

or
$$\boldsymbol{K}\,\hat{\boldsymbol{\delta}} = \lambda\boldsymbol{M}\hat{\boldsymbol{\delta}} \tag{7.64}$$

where $\lambda \equiv \omega^2$, and the natural frequencies will be obtained from the condition of non-trivial solution to (7.63), or

$$|\boldsymbol{K} - \lambda\boldsymbol{M}| = 0 \tag{7.65}$$

We can use an eigenvalue solver, to find the natural frequencies, from the roots of equation (7.65). Since the matrix equation (7.64) usually has $\boldsymbol{K}$ and $\boldsymbol{M}$ with very large orders and only relatively few eigenvalues are required, subspace, or simultaneous iteration algorithm, which provides a very economical eigenvalue solver (see for e.g. Clint & Jennings, 1970, Corr & Jennings, 1976, and Bathe & Wilson, 1976) is employed in this work. The method is based on reducing $\boldsymbol{K}$ and $\boldsymbol{M}$ whilst retaining the lowest eigenvalues. The subspace iteration algorithm consists of the following steps.

(i) Assume a set of *load* vectors:

$$\boldsymbol{Y}_{m\times p} = \begin{bmatrix} y_1 & y_2 & \cdots & y_p \end{bmatrix} \tag{7.66}$$

where y_r is a vector of order m, $r = 1, 2, ..., p$
m is the total number of unknowns, or the order of the stiffness and mass matrices of the component,
p is the number of the required lowest eigenvalues.
A reasonable guess is to take $Y_{rs} = \delta_{rs}$.

(ii) Solve the following p sets of equations, using a static analysis solver:

$$K_{m\times m}\ \tilde{\boldsymbol{\delta}}_r = y_r \tag{7.67}$$

for $r = 1, 2, ..., p,$

For efficiency, the Choleski-factorization solver is employed, where matrix K is factorized into upper and lower triangular matrices with the first set, and then forward and backward substitutions are used with all sets of equations.

(iii) Form the following rectangular matrix of eigenvectors:

$$X_{m\times p} = \left[\tilde{\boldsymbol{\delta}}_1 \quad \tilde{\boldsymbol{\delta}}_2 \quad \ldots \quad \tilde{\boldsymbol{\delta}}_p\right] \tag{7.68}$$

(iv) Obtain the reduced or subspace stiffness and mass matrices as follows:

$$K^*_{p\times p} = \left(X^t\right)_{p\times m}\ K_{m\times m}\ X_{m\times p} \tag{7.69}$$

$$M^*_{p\times p} = \left(X^t\right)_{p\times m}\ M_{m\times m}\ X_{m\times p} \tag{7.70}$$

(v) Solve the subspace, or reduced, eigenvalue problem:

$$K^*_{p\times p}\ \tilde{\boldsymbol{\delta}}^*_{p\times 1} = \lambda\ M^*_{p\times p}\ \tilde{\boldsymbol{\delta}}^*_{p\times 1} \tag{7.71}$$

using any standard eigenvalue solver, as described in section 7.4.2.

(vi) Form the following square matrix of the reduced eigenvectors:

$$X^*_{p\times p} = \left[\tilde{\boldsymbol{\delta}}^*_1 \quad \tilde{\boldsymbol{\delta}}^*_2 \quad \ldots \quad \tilde{\boldsymbol{\delta}}^*_p\right] \tag{7.72}$$

(vii) Transform back to the original space, i.e.

$$\left(X_{m\times p}\right)_{new} = \left(X_{m\times p}\right)_{old}\ X^*_{p\times p} \tag{7.73}$$

(viii) Update the load vectors matrix, using:

$$\left(Y_{m\times p}\right)_{new} = M_{m\times m}\ \left(X_{m\times p}\right)_{new} \tag{7.74}$$

(ix) Iteration decision:

- Calculate the maximum error in the eigenvalues, i.e.

$$e_{max} = \text{Max}\left(\left|\lambda_{i_{new}} - \lambda_{i_{old}}\right|, \quad i = 1, 2, \ldots, p\right)$$

- If the maximum error is greater than a given permissible error then go to step (ii).

7.4.2 Eigenvalue solver

For natural frequency analysis, usually more than two eigenvalues are required, and we can use the simple iteration algorithm (El-Zafrany, 2000) for solving equation 7.71, or finding the roots of the following equation:

$$\left| K^*_{p\times p} - \lambda\, M^*_{p\times p} \right| = 0 \tag{7.75}$$

This algorithm converges to the lowest eigenvalues, but can diverge if the matrix K^* is not positive definite. For the case where no more than two eigenvalues are required a direct analytical solution, which is similar to that given by Attia (1996), can be employed as summarized next.

Using the subspace iteration algorithm with two eigenvalues required, equation (7.71) can then be rewritten as follows:

$$K^*_{2\times 2}\ \boldsymbol{\delta}^*_{2\times 1} = \lambda\, M^*_{2\times 2}\ \boldsymbol{\delta}^*_{2\times 1} \tag{7.76}$$

or explicitly:

$$\begin{bmatrix} K^*_{11} - \lambda M^*_{11} & K^*_{12} - \lambda M^*_{12} \\ K^*_{21} - \lambda M^*_{21} & K^*_{22} - \lambda M^*_{22} \end{bmatrix} \begin{bmatrix} \delta^*_1 \\ \delta^*_2 \end{bmatrix} = \mathbf{O} \tag{7.77}$$

For non-trivial solution, the determinant of the matrix of coefficients should equal to zero, i.e.

$$\begin{vmatrix} K^*_{11} - \lambda M^*_{11} & K^*_{12} - \lambda M^*_{12} \\ K^*_{21} - \lambda M^*_{21} & K^*_{22} - \lambda M^*_{22} \end{vmatrix} = 0 \tag{7.78}$$

which can be expanded to a second degree equation in λ as follows:

$$a_o \lambda^2 - a_1 \lambda + a_2 = 0 \tag{7.79}$$

where $a_o = M^*_{11} M^*_{22} - M^*_{12} M^*_{21} \equiv |M^*|$

$$a_1 = K^*_{11} M^*_{22} + M^*_{11} K^*_{22} - K^*_{12} M^*_{21} - K^*_{21} M^*_{12}$$

$$a_2 = K^*_{11} K^*_{22} - K^*_{12} K^*_{21} \equiv |K^*|$$

Hence, equation (7.79) has the following two roots:

$$\begin{matrix}\lambda_1 \\ \lambda_2\end{matrix} = \frac{a_1 \pm \sqrt{a_1^2 - 4\,a_o\,a_2}}{2a_o} \tag{7.80}$$

7.4.3 Case with pre-stressing

This is the case when the structure is already loaded and stressed at static equilibrium conditions, such as due to centrifugal loading which may cause centrifugal stiffening. The state of strain can still be considered infinitesimal and we solve the linear static equations under the given load, otherwise we solve the non-linear equations of stress analysis. From the stress distribution obtained we can calculate the matrix $\boldsymbol{K}_\sigma$. Hence, natural vibrations from static equilibrium position will have the following dynamic equation:

$$\boldsymbol{M}\,\ddot{\boldsymbol{\delta}}(t) + \left[\boldsymbol{K} + \boldsymbol{K}_\sigma\right]\boldsymbol{\delta}(t) = \mathbf{O} \tag{7.81}$$

Substituting from equations (7.61) and (7.62) into (7.81) then it can be deduced that:

$$(\boldsymbol{K} + \boldsymbol{K}_\sigma - \omega^2\boldsymbol{M})\hat{\boldsymbol{\delta}} = \mathbf{O}$$

or $$(\boldsymbol{K} + \boldsymbol{K}_\sigma)\hat{\boldsymbol{\delta}} = \lambda\boldsymbol{M}\hat{\boldsymbol{\delta}} \tag{7.82}$$

which is similar to equation (7.64), but with $\boldsymbol{K}_\sigma$ been added to $\boldsymbol{K}$.

7.5 BUCKLING ANALYSIS

We assume an initial loading distribution for the buckling mode required and calculate the corresponding equivalent nodal loading vector $\boldsymbol{F}_o$. Buckling is instability occurring whilst the strains are still infinitesimal, i.e. we solve the following linear static equation first:

$$\boldsymbol{K}\,\boldsymbol{\delta}_o = \boldsymbol{F}_o \tag{7.83}$$

If the actual load at the onset of buckling is proportional to the initial load by a factor λ, i.e. the equivalent nodal loading is:

$$\boldsymbol{F} = \lambda\,\boldsymbol{F}_o \tag{7.84}$$

then the resulting stress vector at any point ($\boldsymbol{\sigma}$) will be similarly proportional to the corresponding stress vector at the same point due to the initial load ($\boldsymbol{\sigma}_o$), i.e.

$$\boldsymbol{\sigma}(x, y, z) = \lambda\,\boldsymbol{\sigma}_o(x, yz) \tag{7.85}$$

Hence it can be deduced that at the application of the load which causes instability:

$$\boldsymbol{K}_\sigma(\boldsymbol{\sigma}) = \lambda\,\boldsymbol{K}_\sigma(\boldsymbol{\sigma}_o) \tag{7.86}$$

and the generalized equation of equilibrium just before the occurrence of buckling will be:

$$\left[\boldsymbol{K} + \lambda \boldsymbol{K}_{\sigma}(\boldsymbol{\sigma}_{o})\right]\boldsymbol{\delta} = \boldsymbol{F} \tag{7.87}$$

Instability means that the displacements assume infinite values, which is the case when the value of the determinant of the matrix of coefficients in equation (7.87) goes to zero, or

$$\left|\boldsymbol{K} + \lambda \boldsymbol{K}_{\sigma}(\boldsymbol{\sigma}_{o})\right| = 0 \tag{7.88}$$

Equation (7.88) will also result as the condition for non-trivial solution of the following matrix equation:

$$\left[\boldsymbol{K} + \lambda \boldsymbol{K}_{\sigma}(\boldsymbol{\sigma}_{o})\right]\hat{\boldsymbol{\delta}} = \mathbf{O} \tag{7.89}$$

where $\hat{\boldsymbol{\delta}}$ represents a vector of buckling mode shape. Rewriting equation (7.89) as:

$$\boldsymbol{K}\hat{\boldsymbol{\delta}} = -\lambda \boldsymbol{K}_{\sigma}(\boldsymbol{\sigma}_{o})\boldsymbol{\delta} \equiv \lambda\left[-\boldsymbol{K}_{\sigma}(\boldsymbol{\sigma}_{o})\right]\hat{\boldsymbol{\delta}} \tag{7.90}$$

thus we can define a *hypothetical* mass matrix as follows:

$$\boldsymbol{M} \equiv -\boldsymbol{K}_{\sigma}(\boldsymbol{\sigma}_{o}) \tag{7.91}$$

and equation(7.90) can be rewritten as:

$$\boldsymbol{K}\hat{\boldsymbol{\delta}} = \lambda \boldsymbol{M}\hat{\boldsymbol{\delta}} \tag{7.92}$$

which is similar to equation (7.64). Hence, dynamic eigenvalue solvers can be employed to find the eigenvalues λ and buckling mode shapes. For most practical applications, the minimum value of λ will define the buckling load. If this equation:

$$\left|\boldsymbol{K} + \lambda \boldsymbol{K}_{\sigma}(\boldsymbol{\sigma}_{o})\right| = 0 \tag{7.93}$$

has no real root, then the loading mode assumed will not cause instability such as the loads which produce tensile stresses.

Chapter 8

Programming Package

8. Programming Package

8.1 INTRODUCTION

In this work several types of new finite strip elements have been derived, as explained in previous chapters. An efficient modular programming package based on those elements, was established, and it is capable of performing linear and non-linear static stress analysis, buckling analysis, and natural frequency analysis. The modular package, which was coded in FORTRAN 77, has been built in a way that it is possible to use the same solver module for different elements or different solvers with the same element, using a linked executable program which contains only the relevant modules. The package has two main versions; the plate version and the faceted shell version, for finite strip analysis of plates and shells made of composite layered materials.

An attempt has been made in this chapter to describe the different modules used in this package, where each module is represented by a different programming file and contains a group of subroutines. The modular package has been divided into five main divisions according to the different types of elements been considered, which are as follows:

(i) Mindlin finite strip element division.

(ii) Kirchhoff finite strip element division.

(iii) Reissner finite strip element division.

(iv) Spline-type Kirchhoff finite strip element division.

(v) Spline-type Reissner finite strip element division.

Every division can perform static analysis (linear, non-linear, and buckling analysis) and dynamic analysis (natural frequency analysis) using ordinary, banded, or frontal solver as illustrated in figure 8.1.

All the divisions use the same data module, solver modules, and shape function modules, but the difference is in the subroutines based on a particular element theory, as will be explained in this chapter. Then each division has the following groups of modules:

(i) Data module, which is nearly the same for different types of elements and with plate and faceted shell versions. Each version has its own built in mesh generator. Element effect is mainly on data associated with degrees of freedom, such as loading and boundary conditions, but other data subroutines are the same for all elements.

(ii) Load module, which depends on the element type, and it contains subroutines for the evaluation of equivalent nodal loading for a number of practical types of loads.

(iii) Solver modules, which are independent of elements, and there are three different types of solvers; ordinary solver, banded solver, and frontal solver. For every type of solver we have four different modules; for linear stress analysis, non-linear stress analysis, natural frequency analysis, and buckling analysis.

(iv) Element modules, which are mainly for element stiffness matrix and element mass matrix generation, and all based on infinitesimal strains.

(v) Modules for linear stress analysis, which are element dependent, and contain subroutines for calculating infinitesimal strains averaged at nodes. They also have subroutines for generating output files for displacements, reactions, and nodal stresses and strains at different layers.

(vi) Modules for non-linear stress analysis, which are element dependent and contain subroutines for the evaluation of nodal finite strains averaged at nodes, and infinitesimal and finite strains at Gauss quadrature points. They also contain the subroutines for the generation of K_σ and F_l matrices required for non-linear stress analysis.

(vii) Eigenvalue solver modules, which are the same for all elements and contain the subroutines for the solution of a standard eigenvalue problem. There are two modules; one is based on simple iteration algorithm, and the second has an analytical solution for the small eigenvalue problem of buckling, where we are only interested in one or two eigenvalues.

(viii) Shape functions modules, which contain different types of one-dimensional shape functions, their derivatives, and their integrations.

In this chapter the main subroutines of each module will be highlighted, and for those associated with an element we usually start with those for Mindlin-type elements, and summarise the difference for the other types of elements.

8.2 DATA AND LOAD MODULES

8.2.1 Data module

This module like most of the other modules has a plate version and a faceted shell version, and it reads all required data for the analysis, and generates the finite strip mesh. The main difference between the two versions is in the mesh generation, where the plate version generates a one-dimensional mesh, whilst the faceted shell version generates the mesh of one-dimensional elements in two dimensions.

The main data subroutine calls a group of subroutines for reading the input file, which contains all the parameters needed to define the number of degrees of freedom, the number of harmonics, the geometry of the structure, the material properties for the composite material used in the analysis, the loading, the boundary conditions, the output required and the Gauss quadrature data, and all in a user-friendly format. Most of those subroutines contain simple error diagnostics, which perform basic checks on the data provided. Examples of input data files are given in Appendix B.

The data module has many subroutines which provide information to the subroutines of other modules through common blocks. The basic subroutines used in the Data module are summarised as follows:

(i) Subroutine SET FILE

This is the first subroutine to be called by any of the linked package programs, and it requires the case name interactively to define input and output files. All files for the same case will have the same case name, given by the user, and different three-letter extensions are used for different input and output files and are assigned by this subroutine.

(ii) Subroutine HARMONIC

This subroutine reads the data which defines the number of harmonics (or *y* terms), and the type of interpolation in *y* direction such as trigonometric, Lagrangian, Hermitian or the spline type, which may depend on the type of element been used in the analysis.

(iii) Subroutine STRIP

The plate version of this subroutine reads the data which defines the dimensions of the plate i.e. the plate length, and the widths at the two ends of the plate, to facilitate the analysis of trapezoidal plates. It also reads the number of strips to be generated and the number of nodes per strip. Then the subroutine generates the finite strip mesh in terms of nodal co-ordinates and topology arrays of the strips. The faceted shell version, which is suitable for box structures and stiffened plates, reads the geometrical data of each plate part of the structure with respect to a consistent system of global axes (*x*-*z* axes). This may involve defining the axis of every plate part in terms of the *x*-*z* coordinates of its two end points. It then performs the generation of one-dimensional finite strip elements in the two-dimensional *x*-*z* space, as required and calculates the rotation matrix for every plate part, i.e. the rotation matrix for every generated strip will be defined.

(iv) Subroutine COMPOSITE

In this subroutine the data for the composite material properties are defined, in terms of seven material properties, E_{11}, E_{22}, ν_{12}, μ_{12}, μ_{13}, μ_{23}, ρ, measured with respect to material principal axes. This subroutine reads also the number of layers, the thickness and the fibre angle of every layer. The faceted shell version also considers the case of a structure with different plate parts made of different composite materials, with different thicknesses and fibre orientations.

(v) Subroutine ISO

This subroutine reads the material data for the special case of an isotropic material, allowing the package to consider also the analysis of plates and shells made of isotropic materials.

(vi) Subroutine BOUNDARY

In this subroutine the data for the boundary conditions are defined for original block nodes, i.e. for the nodes defined before generating the mesh. This means that the user does not have to examine mesh generation results to define the boundary conditions. Boundary conditions along the length as well as the width of the plate are possible.

(vii) Subroutine LOAD

This subroutine reads the data which defines the type and magnitude of loads applied on particular nodes of the blocks. For non-linear analysis, it also defines the number of load increments and the load ratio for each increment. Different types of loading have been considered such as distributed loading, point loading, and line loading along lines parallel to x or y axis. Each type of loading requires a subroutine from the LOAD file to calculate the corresponding equivalent nodal loading vector.

(viii) Subroutine STATIC

This subroutine defines the type of static analysis; linear, or nonlinear analysis. For non-linear analysis, it also reads the maximum number of iterations, the maximum permissible error, and a convergence relaxation parameter.

(ix) Subroutine DYNAMIC

This subroutine defines the type of natural frequency analysis, i.e. whether or not pre-stressing will be considered. It also reads the number of eigenvalues, the maximum number of iterations, the maximum permissible error, and an eigenvalue shift parameter. For economical considerations, this module is also used for buckling analysis.

(x) Subroutine GAUSSDATA

It reads the number of original and reduced Gauss quadrature points in x and y directions, and calls subroutine GET GAUSS to read the corresponding Gauss quadrature data from a given data file (GAUSS.DAT). We have also tried to deduce internally the proper numbers of Gauss points for every type of element.

(xi) Subroutine SOUT

Based on user request, this subroutine defines two sets of nodes and y positions for displacement and stress/strain output results. This facilitates plotting of results for different types of elements, as we only need to collect the output files of a particular displacement or stress component in a spread sheet for plotting.

8.2.2 Load modules

These represent two modules (files) for every type of elements; one for the plate version and the other for the faceted shell version. Each module consists of a number of subroutines to calculate the equivalent nodal loading vector for a type of loading, and in the case of faceted shell version the load vector is also rotated in terms of the structure global axes. The main subroutines of a Load Module, for any type of elements, are as follows:

(i) **Subroutine DLOAD**, for distributed loading. This will involve a double integral over each finite strip.

(ii) **Subroutine NLOAD**, for concentrated load acting at a given node and a given y position.

(iii) **Subroutine XLOAD**, for line loading defined in terms of load components per unit length, along a line x = constant. This will involve integration with respect to y along that line.

(iv) **Subroutine YLOAD**, for line loading defined in terms of load components per unit length, along a line y = constant. This will involve integration with respect to x along that line.

8.3 SOLVER MODULES

These modules are divided according to the four types of analysis used in this work. For each type we can select an ordinary solver, a banded solver, or a frontal solver. A brief review of each module, based on the ordinary solver is given. Banded solvers have similar subroutines but structural matrices (stiffness and mass matrices) are assembled as rectangular matrices with the semi-band width being their number of columns. Frontal solvers are based on the same strategy set by Irons (Irons, 1970), and is similar to that used for finite element analysis.

8.3.1 Linear static solver module

This module contains the master program for linear static analysis and have a structure as that given in Figure 8.2, with the following subroutines:

(i) Subroutine ASSEMBLER

This subroutine calls the element stiffness matrix generator for the case of infinitesimal strains as described in section 8.4. Each element matrix is rotated with respect to the global axes of the structure (in the faceted shell version) and assembled into one global stiffness matrix for the whole structure.

(ii) Subroutine REDUCER

In this subroutine the boundary conditions are applied to the assembled equations, and a reduced stiffness matrix, and loading vector are obtained.

(iii) Subroutine SOLVER

The reduced equations are solved in this subroutine by using the Gauss elimination method.

(iv) Subroutine EXPANDER

This subroutine is used to expand the reduced solution to the global nodal displacement vector.

(v) Subroutine DECOUPLE

This subroutine decouples the global nodal displacement vector into sub-vectors for every *y* term or harmonic.

8.3.2 Non-linear static solver module

This module contains the master program for non-linear static analysis and have a structure as that given in Figure 8.3. It considers each load increment, and applies an iterative algorithm as shown in section 7.3.2. The FORTRAN file of the module has all the subroutines described in section 8.3.1, but the element stiffness matrix generator, called by the ASSEMBLER subroutine, calls also the non-linear stiffness matrix K_σ generator and add it to K. Other subroutines are called by the module, as shown in Figure 8.3, but these are given in other files.

8.3.3 Natural frequency solver module

This module contains the master program for natural frequency analysis based on the subspace iteration algorithm given in section 7.4.1. The program calls the following subroutines as shown in Figure 8.4:

(i) **DATA**, which defines problem parameters as discussed in section 8.2.

(ii) **DASSEMBLER**, which assembles the structure stiffness matrix by calling the element stiffness matrix generator, and it also assembles the structure mass matrix by calling the element mass matrix generator.

(iii) **DREDUCER**, which applies boundary conditions so as to obtain the reduced stiffness and mass matrices for the structure.

(iv) **INITIATE**, which assumes initial loading vectors, to form the rectangular matrix Y (see section 7.4.1).

(v) **DSOLVER**, which solves sets of equations $\boldsymbol{K}\boldsymbol{x}=\boldsymbol{y}$, to form the rectangular matrix of eigenvectors X. This is based on Choleski factorization solver.

(vi) **TPRODUCT**, which is called twice to form the subspace stiffness and mass matrices defined as follows:

$$K^* = X^t K X, \quad M^* = X^t M X$$

(vii) **EIGENV**. This subroutine is in the EIGEN module (file), and it uses a standard eigenvalue solver to find the eigenvalues and the subspace eigenvectors, for the reduced problem:

$$K^* x^* = \lambda M^* x^*$$

(viii) **TRANSF**, which calculates a new Y matrix for the next iteration.

(ix) **DOUTPUT**, which outputs the natural frequencies and corresponding mode shapes.

8.3.4 Buckling analysis solver module

This module contains the master program for buckling analysis, as shown in figure 8.5. After calling subroutine DATA, the master program calls a new subroutine LINEARAN, which performs linear stress analysis, as described in section 8.3.1. This will also allows the strain vectors to be calculated at all Gaussian quadrature points. Then subroutine SUBSPACE is called to find buckling eigenvalues using the subspace iteration algorithm as described in section 8.3.3. The so called MASS subroutine here is to calculate the hypothetical mass matrix $\boldsymbol{M} = -\boldsymbol{K}_{\sigma}$, as described in section 7.5.

8.4 ELEMENT STIFFNESS MATRIX MODULES

These are two modules for each type of elements; a plate version, and a faceted shell version. Each module is a combination of the main subroutines which lead to the derivation of element stiffness matrix. The module starts with subroutine STIF, which is the same for all types of elements and is called by the ASSEMBLER subroutine to prepare the data for one finite strip element. It then calls subroutine ESMGS to get the element stiffness matrix $\boldsymbol{K}$. For the case of non-linear analysis it also calls subroutine ESMGL, which is in the non-linear module, to get the matrix $\boldsymbol{K}_{\sigma}$ and then it adds it to $\boldsymbol{K}$.

For computational efficiency the element stiffness matrix is partitioned into sub-matrices, each evaluated by a separate subroutine at the y values (or harmonics) r,s such as $\boldsymbol{K}_{oo}^{rs}$, $\boldsymbol{K}_{bb}^{rs}$, etc., as discussed in previous chapters. Then all parts are assembled for all the y values to form the complete stiffness matrix of the element. For shell version, the element matrix is assembled first for one r-s part according to element local axes, then it is rotated with respect to global axes, before being assembled into the full element matrix. This makes the rotation process based on a small size rotation matrix for only one y value (or harmonic).

8.4.1 Mindlin-type element module

Different subroutines used in this file for both the plate version and the faceted shell version are as shown in figure 8.6. The stiffness matrix generator subroutines use Lagrangian interpolation subroutines from the Lagrangian shape functions module as will be discussed in section 8.9.1. The main subroutines for Mindlin-type element module are summarized as follows:

(i) Subroutine ESMGS

This subroutine calls the subroutines which calculate the different parts of the element stiffness matrix at r,s ($\boldsymbol{K}^{rs}$) as shown in equation (6.102). For faceted shell version, it also rotates it with respect to global axes as shown by equation (7.43). Then it assembles the full $\boldsymbol{K}$ matrix for the element as shown by equation (6.139).

(ii) Subroutine ESMGOO

This subroutine calculates the part $\boldsymbol{K}_{oo}^{rs}$ which is defined by an equation similar to

equation (4.182), using two subroutines; BMATRIXO and LANGRANGE subroutines. The first one is for the calculation of the matrix $\boldsymbol{B}_o^r$ which is defined by equation(4.168) and the second one, which is from the shape functions file, is to define Lagrangian shape functions and their derivatives. The double integrals in equation (4.182) are evaluated numerically using double summations of one-dimensional Gauss quadrature, along x and y directions. The number of quadrature points in the integration with respect to ξ is usually equal to the number of nodes, whilst the number of quadrature points in the integration with respect to η is usually equal to the number of y terms.

(iii) Subroutine ESMGBB

This subroutine calculates the sub-matrix $\boldsymbol{K}_{bb}^{rs}$ which is defined by an equation similar to equation (4.185), using the same LANGRANGE subroutine mentioned above. It also calls subroutine BMATRIXB to calculate the matrix $\boldsymbol{B}_b^r$ as defined by equation (6.90). The double integrals in equation (4.185) are also evaluated numerically by Gaussian quadrature schemes similar to that used for $\boldsymbol{K}_{oo}^{rs}$.

(iv) Subroutine ESMGGG

This subroutine calculates the sub-matrix $\boldsymbol{K}_{\gamma\gamma}^{rs}$ which is defined by an equation similar to equation (4.179), using the same LANGRANGE subroutine for shape functions. The matrix $\boldsymbol{B}_\gamma^r$ as defined by equation (6.92) is calculated by calling subroutine BMATRIXG. To avoid shear locking, the double integrals used for the evaluation of $\boldsymbol{K}_{\gamma\gamma}^{rs}$ are based on reduced Gaussian quadrature schemes which are of order less by one than those employed for $\boldsymbol{K}_{oo}^{rs}$ and $\boldsymbol{K}_{bb}^{rs}$.

(v) Subroutine ESMGOB

The sub-matrix $\boldsymbol{K}_{ob}^{rs}$ as defined by equation (4.191) is evaluated in this subroutine, using the same LANGRANGE subroutine mentioned above together with BMATRIXO subroutine for calculating the matrix $\boldsymbol{B}_o^r$ and BMATRIXB for calculating the matrix $\boldsymbol{B}_b^r$. The Gauss quadrature schemes employed here are non-reduced.

(vi) Subroutine ESMGBO

This subroutine calculates $\boldsymbol{K}_{bo}^{rs}$ which is as defined by equation (4.193), using the same subroutines employed for the previous subroutine.

(vii) Subroutine SMALLD

This subroutine is called once to calculate the integrated D matrices; $\boldsymbol{D}_{oo}$, $\boldsymbol{D}_{ob}$, $\boldsymbol{D}_{bb}$ as defined by equations (4.79)-(4.81).

8.4.2 Kirchhoff-type element module (Hermitian interpolation version)

This module has the main subroutines as in the Mindlin-type module, which have been discussed briefly in the previous section, except that there are some modifications done according to Kirchhoff plate-bending theory. The main differences in these subroutines are

the number of degrees of freedom which are different as compared to Mindlin finite strip element, and in the shape function file where Hermitian shape functions are also added. Hence, three new shape function subroutines (HERMITE, DHERMITE, and D2HERMINTE) have been used for the evaluation of Hermitian shape functions, and their first and second derivatives. The main subroutines used for the calculation of element stiffness matrix are illustrated in the following table:

Subroutine name	Matrix calculated	Defining equation Number
ESMGOO	K_{oo}^{rs}	5.92
ESMGBB	K_{bb}^{rs}	5.94
ESMGOB	K_{ob}^{rs}	5.97
ESMGBO	K_{bo}^{rs}	5.98

Notice that there is no reduced integration needed for that element.

8.4.3 Kirchhoff-type element module (spline-type interpolation version)

This module is the special case of Kirchhoff-type element as discussed in section 8.4.2, where the subroutines (SPLINE, DSPLINE, and D2SPLINE) have been called instead of the subroutines (HERMITE, DHERMITE, and D2HERMINTE) to provide spline-type shape functions. Those subroutines are found in spline-type shape functions modules as discussed in sections 8.9.3 and 8.9.4.

8.4.4 Reissner-type element module (Hermitian interpolation version)

This module has different subroutines for the different parts of the element stiffness matrix in a way similar to that employed for the Mindlin-type and Kirchhoff-type finite strip elements, which have been discussed in the previous sections, except that there are some modifications in terms of degrees of freedom and the shape function files. The subroutines BMATRIXO, BMATRIXB, BMATRIXT and BMATRIXG are also used to calculate the matrices B_o^r, B_b^r, B_ψ^r, B_γ^r as given by equations (4.168), (4.170), (4.172) and (4.174) respectively. Notice also that there is no reduced integration needed for that element. The module has also subroutine SMALLD, which is called once to calculate the integrated D matrices: D_{oo}, D_{ob}, D_{bb}, $D_{\psi\psi}$, $D_{o\psi}$, $D_{b\psi}$ as defined by equations (4.79)-(4.84).

The main subroutines used for the element stiffness matrix generation are listed in the following table:

Subroutine name	Matrix calculated	Defining equation Number
ESMGOO	$\boldsymbol{K}_{oo}^{rs}$	4.182
ESMGBB	$\boldsymbol{K}_{bb}^{rs}$	4.185
ESMGGG	$\boldsymbol{K}_{\gamma\gamma}^{rs}$	4.179
ESMGPP	$\boldsymbol{K}_{\psi\psi}^{rs}$	4.188
ESMGOB	$\boldsymbol{K}_{ob}^{rs}$	4.191
ESMGBO	$\boldsymbol{K}_{bo}^{rs}$	4.193
ESMGOP	$\boldsymbol{K}_{o\psi}^{rs}$	4.196
ESMGPO	$\boldsymbol{K}_{\psi o}^{rs}$	4.198
ESMGBP	$\boldsymbol{K}_{b\psi}^{rs}$	4.201
ESMGPB	$\boldsymbol{K}_{\psi b}^{rs}$	4.203

8.4.5 Reissner-type element module (spline-type interpolation version)

This module is the special case of Reissner-type element as discussed in section 8.4.4 where the subroutines (SPLINE, DSPLINE, and D2SPLINE) have been called instead of the subroutines (HERMITE, DHERMITE, and D2HERMINTE) to provide spline-type shape functions.

8.5 ELEMENT MASS MATRIX MODULES

These are also two modules for each type of elements for plates and faceted shells. Each module contains the main subroutines for the derivation of element mass matrix. The module starts also with subroutine MASS, which is the same for all types of elements and is called by DASSEMBLER subroutine to prepare the data for one finite strip element and calls EMMG to get the element mass matrix $\boldsymbol{M}$. The element mass matrix is also partitioned into sub-matrices, each evaluated by a separate subroutine at the y values (or harmonics) r,s. Then all parts are assembled for all the y values to form the complete mass matrix of the element. For shell version, the element matrix is evaluated first for one r-s part according to element local axes, then it is rotated with respect to global axes, before being assembled into the full element mass matrix.

8.5.1 Mindlin-type element module

The main subroutines of this module are as shown in figure 8.7 and they are summarized as follows:

(i) Subroutine EMMG

This subroutine calls the subroutines which calculate the different parts of the element mass matrix at *r,s* as shown in equation (6.185). For faceted shell version, it also rotates it with respect to global axes as shown by equation (7.48). Then it assembles the full M matrix for the element, in a way similar to that used for the assembly of element stiffness matrix as shown by equation (6.139).

(ii) Subroutine EMMGOO

This subroutine calculates the sub-matrix M_o^{sr} which is defined by equation (4.340). This subroutine calls first the subroutine SHAPEF from the shape function file, to define element shape functions and then it calls subroutine NMATRIXO twice to calculate N_o^r and $(N_o^s)^t$ which are defined by equation (6.173). Hence, by performing double Gaussian quadrature the sub-matrix M_o^{sr} is obtained.

(iii) Subroutine EMMGWW

This subroutine calculates the sub-matrix M_w^{sr} which is defined by equation (4.342). The same procedure is applied as in the above subroutine by calling subroutine SHAPEF, then calling subroutine NMATRIXW, which calculates N_w^r as defined by equation (6.175).

(iv) Subroutine EMMGTT

This subroutine calculates the sub-matrix M_θ^{sr} which is defined by equation (4.344) using the same procedure adopted in the above two subroutines, but it calls subroutine NMATRIXT, which calculates N_θ^r as defined by equation (6.174).

8.5.2 Kirchhoff-type element module (Hermitian interpolation version)

In this element mass matrix file the same procedure has been adopted as it had been used in Mindlin finite strip modules. The different subroutines with their relative equation numbers are illustrated in the following table:

Subroutine name	Matrix calculated	Defining equation Number
EMMGOO	M_{oo}^{rs}	4.340
EMMGWW	M_{ww}^{rs}	4.344
EMMGTT	$M_{\theta\theta}^{rs}$	4.342

These subroutines call LAGRANGE subroutine for the calculation of Lagrangian shape functions, and HERMITE and DHERMITE subroutines are also called for the calculation of Hermitian shape functions and their derivatives. They use subroutines NMATRIXO, NMATRIXW, and NMATRIXT to calculate the matrices N_o^r, N_w^r, N_θ^r which are defined by equations (4.305), (4.306), and (4.308) respectively.

8.5.3 Kirchhoff-type element module (spline-type interpolation version)

This module is the special case of Kirchhoff-type element as discussed in section 8.5.2 but it uses subroutines SPLINE and DSPLINE instead of HERMITE and DHERMITE in all the subroutines which call them, to provide spline-type shape functions.

8.5.4 Reissner-type element module (Hermitian interpolation version)

In this element mass matrix file, different subroutines with their relative equation numbers are illustrated in the following table:

Subroutine name	Matrix calculated	Defining equation No.
EMMGOO	M_{oo}^{rs}	4.340
EMMGWW	M_{ww}^{rs}	4.344
EMMGTT	$M_{\theta\theta}^{rs}$	4.342
EMMGTP	$M_{\theta\psi}^{rs}$	4.348
EMMGPT	$M_{\psi\theta}^{rs}$	4.350
EMMGPP	$M_{\psi\psi}^{rs}$	4.346

These subroutines call LAGRANGE subroutine for the calculation of Lagrangian shape functions, and call HERMITE and DHERMITE subroutines for the calculation of Hermitian shape functions and their derivatives. They also call subroutines NMATRIXO, NMATRIXW, NMATRIXT, NMATRIXP to calculate N_o^r, N_θ^r, N_ψ^r, N_w^r which are defined by equations (4.305), (4.306), (4.307) and (4.308) respectively.

8.5.5 Reissner-type element module (spline-type interpolation version)

This module is the special case of Reissner-type element as discussed in section 8.5.4 where the subroutines SPLINE and DSPLINE are called instead of HERMITE and DHERMITE to provide spline-type shape functions.

8.6 LINEAR STRESS ANALYSIS MODULES (-LNS FILES)

The -LNS file contains all additional subroutines for linear stress analysis and results output. There are two modules per each type of element for plate and faceted shell versions. Every module has the same subroutines, and the difference between them is due to element degrees of freedom, shape functions, and number of stress-strain components. The main subroutines in each -LNS file are summarized as follows:

(i) Subroutine DISP

In this subroutine the full nodal displacement vector is defined from the reduced and prescribed vectors. Also the displacement components are listed in the output file at every selected node, for the selected y values.

(ii) Subroutine REACT

This subroutine calculates the nodal reactions and residual vector R, which is defined as:

$$R = K\delta - F$$

and lists the results in the output file.

(iii) Subroutine LNSTRAINN

This subroutine calculates the x-y parts of the strain vector, averaged at nodes and y values. These parts are $\boldsymbol{\varepsilon}_o$, $\hat{\boldsymbol{\varepsilon}}_b$ for all elements, $\hat{\boldsymbol{\gamma}}$ for Mindlin and Reissner elements, in addition to $\hat{\boldsymbol{\varepsilon}}_\psi$ for Reissner elements. Every part is calculated by calling the appropriate B matrix subroutine (from the ESMG file).

(iv) Subroutine STRAIN

This subroutine calculates the actual strain vector for every given node and y value at three z-points per every layer; at its lower, middle, and upper surfaces. It then rotates the vector with respect to material axes before writing it in the output file.

(v) Subroutine STRESS

This subroutine calculates first the actual strain vector for every given node and y value at the three z-points per every layer; as before. It then calculates the corresponding stress vector by multiplying the layer D matrix by the strain vector. The stress vector is also rotated with respect to material axes before writing it in the output file.

8.7 NON-LINEAR STRESS ANALYSIS MODULES (-NLS FILES)

This file contains all the additional subroutines required for non-linear stress analysis and buckling analysis including K_σ and F_l generators for each type of finite strip elements, as will be explained in this section.

8.7.1 K_σ generators

These are groups of subroutines which calculate the element K_σ matrix. The main subroutines for each type of elements are summarized next.

8.7.1.1 Mindlin-type element subroutines

Different parts of K_σ for Mindlin elements are calculated by different subroutines and assembled in one matrix for the element in a way similar to that mentioned in section 8.4.1. The main subroutines are summarized as follows:

(i) Subroutine ESMGL

This subroutine calls the subroutines which calculate the different parts of the element non-linear stiffness matrix at *r,s* as shown in equation (6.155). For faceted shell version, it also rotates it with respect to global axes as shown by equation (7.43). Then it assembles the full K_σ matrix for the element in a way similar to that shown by equation (6.139).

(ii) Subroutine ESMGMM

This subroutine calculates the sub-matrix K^{sr}_{mm} using equation (4.269). The matrices G^r_m and S_{mm} needed for that equation are evaluated by the subroutines GMATM and SMATMM, which are also in the same file. These two matrices are as defined by equations (4.254) and (4.105). The numerical integrations are carried out using double Gaussian quadrature.

(iii) Subroutine ESMGWW

This subroutine calculates the sub-matrix K^{sr}_{ww} using equation (4.271). The terms G^r_w and S_{ww} are defined by equations (6.142) and (4.108) and calculated by the subroutines GMATW and SMATWW.

(iv) Subroutine ESMGTT

The sub-matrix K^{sr}_{00}, as defined by equation (4.275) is calculated by this subroutine, using GMATM and SMATTT subroutines for the evaluation of the terms G^r_0 and $S_{\theta\theta}$ as defined by equations (6.144) and (4.118).

(v) Subroutine ESMGMT

This subroutine calculates the sub-matrix $K^{\sigma}_{m\theta}$ using equation (4.273a), and this case requires three terms G^r_m, G^r_θ and $S_{m\theta}$ as defined by equations (4.254), (6.144) and (4.113), and evaluated by subroutines GMATM, GMATT and SMATMM, respectively.

(vi) Subroutine ESMGTM

This subroutine calculates the sub-matrix $K^{\sigma}_{\theta m}$ using equation (4.273b), in a way similar to that used for the previous sub-matrix.

8.7.1.2 Kirchhoff- and Reissner-type element subroutines

All different types of those elements use similar subroutines for the generation of the different sub-matrices defining the matrix $\boldsymbol{K}_{\sigma}^{sr}$ as listed in the following table:

Subroutine name	Matrix calculated	Defining equation Number
ESMGMM	$\boldsymbol{K}_{mm}^{rs}$	4.269
ESMGWW	$\boldsymbol{K}_{ww}^{rs}$	4.271
ESMGTT	$\boldsymbol{K}_{\theta\theta}^{rs}$	4.275
ESMGMT	$\boldsymbol{K}_{m\theta}^{rs}$	4.273a
ESMGTM	$\boldsymbol{K}_{\theta m}^{rs}$	4.273b

Subroutines GMATM, GMATW, GMATT are called to calculate the matrices $\boldsymbol{G}_{m}^{r}$, $\boldsymbol{G}_{w}^{r}$, $\boldsymbol{G}_{\theta}^{r}$ defined by equations (4.254), (4.256), and (4.258), where Hermitian shape functions are used with the Hermitian-interpolation version, and spline-type shape functions are used with the spline-interpolation version. Subroutines SMATMM, SMATWW, SMATTT are also employed for the calculation of matrices $\boldsymbol{S}_{mm}$, $\boldsymbol{S}_{ww}$, $\boldsymbol{S}_{\theta\theta}$ and $\boldsymbol{S}_{m\theta}$.

8.7.2 F_L generators

These are groups of subroutines which calculate the element $\boldsymbol{F}_l$ matrix. They depend on the type of elements as explained next.

8.7.2.1 Mindlin-type element subroutines

These subroutines calculate the element $\boldsymbol{F}_l$ vector in terms of two sub-vectors, and the main subroutines are summarized as follows:

(i) Subroutine FLVECTOR

This subroutine assembles first the vector $\boldsymbol{F}_l^s$ as defined by equation (6.160), and for the faceted shell version it rotates that vector with respect to global axes, before assembling the element $\boldsymbol{F}_l$ vector.

(ii) Subroutine FOVECTOR

In this subroutine the sub-vector $(\boldsymbol{F}_o^s)_l$ is calculated according to equation (4.280). Subroutines BMATRIXO and SVECO are also called to calculate $\boldsymbol{B}_o^r$, $\boldsymbol{\sigma}_o$ as given by equations (4.168) and (4.127).

(iii) Subroutine FBVECTOR

This subroutine calculates the sub-vector $(F_b^s)_l$ as defined by equation (4.282), using subroutines BMATRIXB, and SVECB, which estimate B_b^r, σ_b as defined by equations (6.90), and (4.130).

8.7.2.2 Kirchhoff- and Reissner-type element subroutines

These subroutines are similar to those discussed for the Mindlin-type element, but they use Hermitian or spline-type interpolation depending on the element type. For Reissner-type elements, there is also an additional subroutine FTVETOR which calculates the sub-vector $(F_\psi^s)_l$ as defined by equation (4.284).

8.7.3 Additional subroutines

(i) Subroutine CONVERGENCE

This subroutine calculates an error measure after every iteration, which is defined as:

$$\text{Error} = \frac{\Delta\delta^t \Delta\delta}{\delta^t \delta}$$

where $\Delta\delta$ represents the increment of nodal displacement vector due to residual forces, and δ is the total nodal displacement vector at the end of the iteration, as explained in section 7.3.2. That error measure will be compared with a given permissible error to decide whether or not convergence has been achieved.

(ii) Subroutine LNSTRAING

This subroutine calculates the *x-y* parts of the infinitesimal strain vector at Gauss quadrature points. These parts are ε_o, $\hat{\varepsilon}_b$ for all elements, $\hat{\gamma}$ for Mindlin and Reissner elements, in addition to $\hat{\varepsilon}_\psi$ for Reissner elements. These are required for the evaluation of K_σ for non-linear and buckling analysis, and F_l for non-linear analysis.

(iii) Subroutine NLSTRAINN

This subroutine calculates the *x-y* parts of the finite strain vector averaged at nodes using non-linear stress analysis. These are ε_m, ε_w, $\hat{\varepsilon}_{m\theta}$, $\hat{\varepsilon}_\theta$ for different types of elements.

(iv) Subroutine NLSTRAING

In this subroutine the *x-y* parts of the finite strain vector; ε_m, ε_w, $\hat{\varepsilon}_{m0}$, $\hat{\varepsilon}_0$ are calculated at Gaussian quadrature points for different types of elements.

8.8 EIGENVALUE SOLVER MODULE

This module or file has all the subroutines required to solve a standard eigenvalue problem, and is used for natural frequency and buckling analysis. If more than two eigenvalues are required, we have a module EIGENV1 based on the simple iteration algorithm (El-Zafrany,

2000). This algorithm converges to the lowest eigenvalues, but can diverge if the matrix (K^* in this case) is not positive definite. This may cause problems in some cases of buckling, if the assumed load does not cause buckling, and it is difficult to tell whether or not the divergence of the algorithm is due to that. Since the critical buckling load may occur within the first two eigenvalues, another module (EIGENV2), which is based on the direct analytical solution described in section 8.4.2, can be employed.

8.9 SHAPE FUNCTION MODULES

The shape functions module provides all one-dimensional shape functions required for interpolation along x and y directions. For efficient programming four different modules have been coded for different types of interpolation methods employed, as will be explained in this section. Every module is divided into two parts. The first part provides one-dimensional interpolation along the x direction for an n-node strip, according to the interpolation methods employed for the finite strip element. The second part contains interpolation functions along the y direction, and for historical reasons we kept the trigonometric functions as an option. Four different types of polynomial interpolation along the y direction are available, and each in a separate file, as explained in this section.

8.9.1 Lagrangian interpolation shape functions module

This module provides Lagrangian shape functions and their derivatives for use in the interpolation along the x direction, which is suitable for Mindlin-type finite strip elements. Along the width of the strip (the y direction), two options are provided; trigonometric functions and polynomial shape functions based also on Lagrangian interpolation. This means that with this module the available polynomial interpolation along the y direction for all displacement parameters is the Lagrangian interpolation. Numerical integrations of shape functions is also provided for use with the LOAD module subroutines.

8.9.2 Hermitian interpolation shape functions module

This module has all the subroutines of the Lagrangian shape functions file with an addition of some more subroutines which define the Hermitian shape functions, their first and second order derivatives, and their numerical integrations. It is mainly used with Reissner-type and Kirchhoff-type elements (Hermitian interpolation version) to provide Hermitian interpolation for the lateral deflection w along the x direction. The available polynomial interpolation along the y direction is Hermitian interpolation for w and Lagrangian interpolation for all other displacement parameters.

8.9.3 Spline-w interpolation shape functions module

This module contains all the subroutines in the Hermitian shape functions file, except we have some additional subroutines which defines the spline-type shape functions, their derivatives and their numerical integrations. It can be used with Reissner-type and Kirchhoff-type elements to provide spline-type interpolation for the lateral deflection w along the x direction.

The available polynomial interpolation along the *y* direction is spline-type interpolation for *w* and Lagrangian interpolation for all other displacement parameters. This file is designed to be used for Kirchhoff and Reissner elements with spline-type interpolation, but it can also be used with the Hermitian version of Reissner-type and Kirchhoff-type elements.

8.9.4 Spline-all interpolation shape functions module

This module is similar to the previous one and provides spline-type interpolation for the lateral deflection *w* along both *x* and *y* directions. It also provides spline-type interpolation for all other displacement components along *y* direction. This can also be used for all types of Kirchhoff and Reissner elements.

8.10 LINKING AND RUNNING THE PACKAGE

The programming package has been built of different modules, as discussed in the previous sections, which gives the flexibility to link only the relevant modules for the required types of analysis. This makes the executable program as small as possible and makes it suitable to be run on ordinary PC's. There are four different types of analysis available, and their linking structures are summarized in this section. The detailed linking instructions, with the file names as used in the package, are listed in Appendix A.

8.10.1 Linear static analysis

Figure 8.8 illustrates the modules required to form the executable file for linear static analysis. Every module has a plate version and a faceted shell version, to be selected according to the type of structure required. The linear solver module is a selection of one module from ordinary, banded, and frontal solver modules. The data module is almost the same for different types of elements. The other modules; LOAD, ESMG, -LNS and shape functions modules depend on the type of element used (Mindlin-type, Hermitian Kirchhoff-type, Hermitian Reissner-type, Spline-type Kirchhoff and Spline-type Reissner). For linear static analysis using Mindlin-type elements, for example, we have to start the linking with one of the three linear static solvers modules and after compilation we link this with the data module, LOAD module, ESMG module, -LNS module, for the Mindlin-type element and the Lagrangian shape function module. For the analysis with any other type of elements, we use the relevant modules of that element.

8.10.2 Non-linear static analysis

Figure 8.9 describes the modules required to form the executable file for non-linear static analysis. This is similar to the previous case but with the -NLS module added to provide additional subroutines required for non-linear stress analysis.

8.10.3 Natural frequency analysis

The relevant modules required for natural frequency are as shown in figure 8.10. We start

with a dynamic solver module; ordinary, banded or frontal solver module, which contains the subroutines for the subspace iteration procedure. This is to be linked with Data module, which is the same file for all types of analysis. Then the element dependent modules; LOAD, ESMG, and EMMG are added together with an eigenvalue solver module, and the appropriate shape functions module. The Lagrangian shape functions module is mainly used with Mindlin type elements, the Hermitian shape functions module is used with Kirchhoff and Reissner Hermitian elements, and the two spline-type shape functions files; SPLINE-W, SPLINE-ALL are used with Kirchhoff and Reissner spline-type elements.

8.10.4 Buckling analysis

Figure 8.11 demonstrates the modules required to form the executable file for Buckling analysis. We start with a buckling solver module; ordinary, banded or frontal module, which has two groups of subroutines; linear stress analysis subroutines and subspace iteration subroutines. This is to be linked with Data module, and the element dependent modules; *LOAD, ESMG, -LNS* and *-NLS* are modules together with an eigenvalue solver module, and the appropriate shape functions module, as described in the previous section.

Chapter 9

Results and Discussion

9. Results and Discussion

9.1 INTRODUCTION

Several types of finite strip elements have been derived in this work, using the new concept of polynomial and spline-type interpolation along the width of the plate or shell. This can lead to a very large number of options by changing the combinations of x and y interpolation theorems. It was decided to select a practical number of combinations, leading to the following definitions of elements:

(i) Mindlin-type elements, which are based on Lagrangian interpolation for all displacement parameters in x and y directions. It is possible to link the programs with Hermitian or spline-type shape functions to change the interpolation type along the y direction, but early tests have proven that such elements were best with Lagrangian interpolation in both x and y directions.

(ii) Kirchhoff-type and Reissner-type elements, which are based on Hermitian interpolation for the lateral deflection w in both x and y directions, and Lagrangian interpolation for other displacement parameters.

(iii) Spline-type Kirchhoff and Reissner elements, which are similar to the previous ones but with the default cases having the lateral deflection w interpolated in x and y directions with spline-type interpolation. For some cases, it was decided to test the elements with spline-type interpolations applied at y direction for all displacement parameters.

It was essential to validate those basic elements for different types of plates and shells and with different types of loading and boundary conditions. Due to time limitations, a reasonable number of cases have been selected and different types of analysis have been tested. Figures of results in this chapter have been generated using a built-in plotter, which takes the results files of different elements directly without any interference from the user. The package has also its own built-in mesh generator, which facilitates data preparation. We have focussed mainly on the p-type convergence of elements, where we use the same number of nodes for the same case with different types of elements. Nevertheless in one case, which has an analytical solution, we also investigated the h-type convergence.

9.2 STRESS ANALYSIS OF CANTILEVER PLATE

9.2.1 Case description

Several examples based on a rectangular cantilever plate, as shown in figure 9.1, have been considered, with

Length L in x direction = 2m,

Width B in y direction = 1m,

and each case consists of 12 layers of a composite material. Two different materials were selected, Carbon/Epoxy (C/E) and Glass/Epoxy (E/G), with properties as shown in table 9.1. Different data files were run with plate and facet versions of the package, to validate different types of analysis and to check also that the two versions of the package will give identical results for the same case.

Stress analysis was carried out with three cases of loading:

(a) Case under tensile load in terms of a uniform line tensile force of intensity: $f_1 = 1 \times 10^7$ N/m

(b) Case under in-plane bending, induced by a uniform in-plane line shear force of intensity: $f_2 = 1 \times 10^6$ N/m

(c) Case under out-of-plane bending, induced by a uniform out-of-plane line shear force of intensity: $f_3 = 1 \times 10^2$ N/m

Several finite strip meshes were employed, each has 13 nodes for plotting purposes:

(a) Two-node element meshes which consists of 12 elements.

(b) Three-node element meshes which consists of 6 elements.

(c) Four-node element meshes which consists of 4 elements.

We also compare the finite strip results with those obtained from an in-house FEM package, using 9-node Mindlin element, and a mesh with 6×3 square elements, which have 13 nodes along y = constant lines. All the results compared were plotted for the nodes on $y = 0$ line.

Different plots of deflection have been divided into two groups to avoid too many plots in the same figure:

(a) The first group is with polynomial finite strip elements, these are Mindlin-type elements, and Hermitian Kirchhoff-type, and Hermitian Reissner-type elements.

(b) The second group is with spline-type elements which have Kirchhoff and Reissner-type elements, based on spline-type interpolation.

FEM results have been plotted with the two groups to facilitate comparisons. The Carbon/Epoxy plate results will be referred to as the C/E results, whilst the Glass/Epoxy results will be referred to as the E/G results.

9.2.2 Linear stress analysis results

9.2.2.1 Plate under tensile loading

Distributions of the axial deflection u have been plotted against x value along $y = 0$ line. The results are divided into two groups as previously mentioned. The C/E results are shown in figures 9.2 and 9.3 whilst the E/G results are displayed in figures 9.4 and 9.5. It

is clear from those figures that the results obtained from all different types of finite strip elements agree very well with each other, and with the FEM results. All the curves are straight lines, as expected for such a case, with a small discrepancy near the fixed end. This is due to the complete fixation assumed there, and plotting the results at the edge ($y = 0$), where the Poisson's effect is maximum.

9.2.2.2 Plate under in-plane bending

Distribution of the transverse deflection v have been plotted against x for the nodes on the x-axis, as shown in figures 9.6 and 9.7 for the C/E plate, and figures 9.8 and 9.9 for the E/G plate. It can be noticed from those figures that all the results obtained from different finite strip elements have excellent agreement with each other and with the corresponding FEM results.

9.2.2.3 Plate under out-of-plane bending

For the plates under the out-of-plane bending, distributions of the lateral deflection w have been plotted against x for the nodes on the x-axis, as demonstrated for the C/E plate in figures 9.10 and 9.11, and for the E/G plate in figures 9.12 and 9.13. Examining those figures, we can notice that the Mindlin-type elements, which are based on Lagrangian interpolation agree with the FEM results which are based on a similar theory. Kirchhoff-type and Reissner-type elements have results close to each other but slightly lower than those of the Mindlin-type elements. This is mainly because Kirchhoff-type and Reissner-type elements use Hermitian or Spline-type interpolations for the lateral deflection w, which are based on a more accurate plate-bending theory.

9.2.3 Non-linear stress analysis results

The previous cases of loading were run using non-linear static analysis option. Each load was divided into 10 equal increments, and we realised that the full loads considered were too high for the E/G plate. This helped us to test the divergence measures in the package, including the termination of the program if divergence starts to occur, and using a relaxation factor to decelerate divergence. Displacement distributions for the first load increment of each loading case are presented, and load/ deflection curves are plotted for the cases which took the full load without divergence.

9.2.3.1 Plate under tensile loading

The axial deflection u obtained from the first load increment has been plotted against x for the two groups of finite elements together with the corresponding FEM results, as shown in figures 9.14 and 9.15 for the C/E plate, and figures 9.18 and 9.19 for the E/G plate. These figures prove the good agreement between the results of all the elements and the FEM results. The C/E plate case has convergence for all load increments, and the maximum value of u (at $x = L$) has been plotted against load ratio as shown in figures 9.16 and 9.17. These figures show also a good agreement at all load increments, between the results of different elements.

9.2.3.2 Plate under in-plane bending

For this case of loading, the significant displacement component is the transverse displacement v, which has been plotted against x for the two groups of elements. Figures 9.20 and 9.21 demonstrate the plots for the C/E results at the first load increment. At this small load the results obtained from all element agree very well with each other and with FEM results. The maximum value of v (at $x = L$), has also been plotted against load ratio, as shown in figures 9.22 and 9.23. At full load, the higher-order finite strip elements have given results slightly higher than Mindlin elements, as they use more accurate interpolation theorems. Figures 9.24 and 9.25 show the transverse displacement distributions for the E/G plate, which show also a good agreement between the results obtained from different elements.

9.2.3.3 Plate under out-of-plane bending

The lateral deflection w has been plotted against axial distance x for the first load increment, where figures 9.26 and 9.27 show the results for the C/E plate, and figures 9.28 and 9.29 display the results for the E/G plate. The curves are similar to those obtained with linear stress analysis (figures 9.10-9.13), with Mindlin-type elements having results slightly higher than those obtained by other elements due to different interpolation theorems employed.

9.3 STRESS ANALYSIS OF SQUARE PLATE

9.3.1 Case description

This case represents a square plate made of 8 layers of a composite material with properties as shown in table 9.2. The axes and geometry of the plate are as shown in figure 9.30, where a side length $L = 10$m was considered with a range of thickness values. The plate was subjected to a uniformly distributed loading in the z-direction, with intensity $q = 100\text{N/m}^2$.

A full symmetry has been assumed with respect to the plate central axes, allowing one quarter *(abcd)* of the plate to be modelled for finite element and finite strip analyses, with the following boundary conditions:

(a) For all elements:

$u = 0$ along edge *bc*,

$v = 0$ along edge *ab*,

$w = 0$ along edges *ad, dc.*

(b) For Mindlin elements, the following additional boundary conditions are also considered:

$\theta_x = 0$ along edge *ab*,

$\theta_y = 0$ along edge *bc.*

(c) For Kirchhoff-type and Reissner-type elements, they also have the following boundary condition:

$w_{i,x} = 0$ along edge *bc*.

(d) For Reissner-type elements, they also have the following boundary conditions:

$\psi_x = 0$ along edge *ab*,

$\psi_y = 0$ along edge *bc*.

Several meshes were selected with convenient nodes for plotting, where only the p-type convergence was tested. Finite element analysis was carried out using an in-house FEM package with 6×6 9-node Mindlin elements. The finite strip meshes had 12 two-node elements and 6 three-node elements.

This case helps to demonstrate the ability of the newly derived finite strip elements to deal with such different types of boundary conditions. Different values of length of the quarter of the plate over thickness ($L/2h$) ratios have been selected to test element accuracy in a wide range of thickness. Linear stress analysis was carried out for all the cases, to facilitate comparisons.

9.3.2 Thin plate results

This case has $L/2h = 25$, which represents a very thin plate. The lateral deflection w was plotted against distance on the x-axis, as shown in figures 9.31 and 9.32, for polynomial-type and spline-type elements respectively. All the results are close with each other, with slightly higher values for cases with more sophisticated interpolation theorems. Distributions of the axial stress (σ_x) through the thickness at the central node is also shown in figure 9.33, which shows the agreement of Reissner-type element with Mindlin element. Kirchhoff-type elements suppose to provide the most accurate answers for the thin range.

9.3.3 Thick plate results

This case has $L/2h = 5$, which represents a thick plate. The lateral deflection distributions over the x- axis are shown in figures 9.34 and 9.35. It is clear that the effect of transverse shear has made the results of Mindlin and Reissner-type much higher than those of Kirchhoff-type elements. We can also notice that the Reissner theory provides results slightly higher than those obtained by the Mindlin theory. The stress distribution (σ_x) through the thickness at the central node is shown in figure 9.36, which reflects also more or less similar observations.

9.3.4 Different thickness cases

Plates with ($L/2h$) ratios of 25,12.5,10, 6.25, 5, 4 and 2.5 were tested and the values of a non-dimensional lateral deflection $\bar{w}$ at the plate centre was tabulated, for different elements, as shown in table 9.3, where

$$\bar{w} = \frac{w_c E_{22} h^3}{q L^4} \times 100$$

and w_c is the lateral deflection at the plate centre. The following findings can be noticed from the table:

(a) Kirchhoff-type element non-dimensional results are independent of thickness, confirming that they only show bending deformation which is proportional to h^3.

(b) Mindlin-type elements work accurately for a wide range of thicknesses and provide the simplest type.

(c) Reissner-type element results are slightly higher than Mindlin-type results with the difference increasing with thickness.

(d) Two-node elements and three-node elements have led to almost identical results for each type of elements.

9.4 CURVED SHELL CASE

9.4.1 Case description

The main objective of this case is to test the ability of finite strip elements to model cylindrical shells. It was decided to test the *h*-convergence of one type of elements, the Mindlin-type. This type of element is based on Lagrangian interpolation, and more elements are required for a typical case than the elements of higher interpolation orders.

A curved cylindrical shell, as shown in figure 9.37 was selected with:

Mean radius $R = 100\text{mm}$,

Width $B = 10\text{mm}$

Thickness $h = 1\text{mm}$.

The shell is made of an isotropic material with

Young's modulus $E = 10^6\ \text{N/mm}^2$,

Poisson's ratio $\nu = 0.3$.

The choice of an isotropic material will allow the comparisons with an analytical solution, but the input data were presented in the form of a composite material with four layers each of thickness 0.25mm, with fibre angles (45, -45, 45, -45), and $E_{11} = E_{22} = E$, $\nu_{12} = \nu$, $\mu_{12} = \mu_{23} = \mu_{31} = E/2(1+\nu)$. This idea will enable testing the equations of all the rotated $\boldsymbol{D}$ matrices of the composite. Two cases of loading have also been considered:

(a) Horizontal unit loading in *x*-direction distributed uniformly at the free edge.

(b) Vertical unit loading in *z*-direction, distributed uniformly at the free edge.

The meshes used for the analysis are:

(i) Finite element mesh with 10 four-node Mindlin elements.

(ii) Coarse finite strip mesh with 10 two-node Mindlin elements.

(iii) Coarse finite strip mesh with 10 three-node Mindlin elements.

(iv) A similar mesh to the previous one, but with two *y*-terms (3/2 mesh)

(v) Fine mesh with 20 two-node Mindlin-type finite strip elements.

(vi) Fine mesh with 20 three-node Mindlin-type finite strip elements.

9.4.2 Case with horizontal loading

The horizontal and vertical deflections (*u,w*) have been plotted against *x*-values for all meshes together with the corresponding analytical solutions, as shown in figure 9.38 and 9.39, respectively. The convergence of finite strip solutions to analytical solution is clear from the figures, with the best results obtained from the two-node fine mesh. FEM results are higher than the corresponding two-node coarse mesh results.

The stress σ_x distribution over the thickness, at the fixed end, was also plotted as shown in figure 9.40, which demonstrates a good convergence to the analytical solution with the best results obtained from the fine mesh.

9.4.3 Case with vertical loading

The distributions of displacement components *u* and *w*, along the *x*-axis are shown in figures 9.41 and 9.42. A convergence, with the fine mesh results being very close to the analytical solution results, has been achieved. The stress σ_x distribution over the thickness is shown at the fixed end in figure 9.43 which confirms good convergence to the analytical solution.

9.5 STIFFENED PLATE CASE

9.5.1 Case description

This case represents an example to demonstrate the ability of the developed elements to deal with folded and stiffened plates. A simple stiffened plate with geometry as shown in figure 9.44 has been considered, where

Length in *x* direction $L = 2$ m,

Width in *y* direction $B = 1$ m,

Length of the stiffener in *z* direction $l = 0.5$m.

The plate consists of 12 layers of the C/E composite material with properties as shown in table 9.1. However, two cases of thickness have been considered:

(a) Thin plate with layer thickness 2.5 mm, and total thickness $h = 0.03$m,

(b) Thick plate with layer thickness12.5mm, and total thickness h =0.15m.

The upper opposite ends of the plate are fixed, and the plate was subjected to two different cases of loading:

(i) A line loading, as shown in figure 9.5, with load intensity = 1.0×10^5N/m,

(ii) A uniform distributed loading on the upper surface, along z direction, with intensity = 0.5×10^5N/m^2.

Each load has a total force = 1.0×10^5N, and causes the plate to bend symmetrically in the x-z plane. Two finite element meshes of the same number of nodes with four-node and nine-node elements, as shown in figures 9.45 and 9.46 were employed to obtain reliable FEM results for checking different finite strip results. Several types of finite strip elements were tested using meshes with the same node numbers and compatible with finite element meshes, i.e. with 25 nodes along the x-axis for the upper plate and 13 nodes along the z-axis for the stiffener.

9.5.2 Thin plate results

The distribution of the lateral deflection w along the x-axis (and $y=0$) for the upper surface of the plate has been plotted against x values, using results of different finite strip elements, together with FEM results. To make it easy to recognise different plots, the results of the two-node finite strip elements and those of the three-node finite strip elements were plotted in two different figures with the same scale values. In the captions of the plots, just Kirchhoff-type and Reissner-type elements mean that w was interpolated with Hermitian interpolation in x and y directions. Spline-w indicates that w was interpolated using spline-type interpolation in x and y directions, and spline-A is the same except we use spline-type interpolation in y direction for all displacement parameters.

(a) Case with line loading

The results of two-node and three-node finite strip elements are shown in figures 9.47 and 9.48 respectively, together with the results of the two finite element meshes in every figure. The FEM results have convergence proving that the finite element meshes are adequate. Figure 9.47 proves that most of the two-node finite strip elements have results very close to FEM results, except the two-node Mindlin-type element which seems to give less accurate results than other elements for the same number of elements. Figure 9.48 confirms that the three-node Mindlin-type element leads to very accurate results. Notice also that the three-node elements have better symmetric results than the two-node elements.

(b) Case with uniformly distributed loading

The two-node and three-node elements results are shown in figures 9.49 and 9.50 respectively. Observations similar to that for the previous case of loading can be noticed, with slightly bigger deviation for some cases. The three-node finite strip results have shown better symmetric results than FEM results.

9.5.3 Thick plate results

The distributions of the lateral deflection w for the upper plate have been plotted in two figures for each case of loading, in a way similar to the previous case.

(a) Case with line loading

Figure 9.51 demonstrates the results of some two-node finite strip elements, which show that the two-node Reissner-type element leads to results close to FEM results. Figure 9.52 displays the results of three-node finite strip elements, and it is clear that Mindlin-type and Reissner-type elements gave results very close to FEM results. It is clear in both figures that Kirchhoff-type elements have given lower results than others due to the transverse shear effect, as seen previously in section 9.3.

(b) Case with distributed loading

The results of two-node strip elements are shown in figure 9.53, whilst the results of three- node elements are displayed in figure 9.54. The Kirchhoff-type element results are lower than those of other elements as expected, due to the neglection of transverse shear effect. The three-node Mindlin-type elements lead to accurate and symmetric results.

9.6 NATURAL FREQUENCY AND BUCKLING ANALYSIS OF RECTANGULAR PLATE

9.6.1 Case description

This case represents a rectangular cantilever plate, similar to that shown in figure 9.1, but with following geometric properties:

Length in x direction $L = 180$ mm,

Width in y direction $B = 40$ mm.

Two types of materials were selected, C/E and E/G with properties as shown in table 9.4. these plates have been actually manufactured at Cranfield University (see Hagaze, 2002). Finite strip meshes with 13 nodes along the x direction have been used.

9.6.2 Natural frequency analysis

Natural frequency analysis has been carried out using the subspace iteration algorithm. Several mixed modes of vibration were obtained from different finite strip elements which have no FEM match. To facilitate comparison with FEM results, only the natural frequencies of the first three bending modes are listed as shown in tables 9.5 and 9.6 for C/E and E/G cases, respectively. It is clear from the two tables that all the finite strip elements tested lead to very close natural frequencies for the first bending mode. For the

second bending mode, the two-node Mindlin-type element lead to less accurate results, with better results for the third bending mode.

9.6.3 Buckling analysis

For buckling analysis, each plate was subjected initially to a compressive line loading along $x = L$ edge, with intensity f_o =-10N/mm or a total force F_o =-40N. After carrying out linear stress analysis, buckling analysis was employed to find the critical load ratio (or buckling eigenvalue) λ at which a force $F = \lambda F_o$ will cause instability or buckling. Two eigenvalues were calculated to check the programs, knowing that buckling will occur at the lower one. The buckling eigenvalues for different finite strip elements together with FEM results are listed in tables 9.7 and 9.8 for the C/E and E/G plates, respectively. It is clear that all the elements tested have led to very close values for the first and second buckling modes.

9.7 TRAPEZOIDAL PANEL CASE

9.7.1 Case description

One of the interesting features of our newly-derived elements is their ability to model plates with variable width in y direction. The built-in mesh generator can generate elements for a trapezoidal panel, as shown in figure 9.55, with the specification of B_1 and B_2, which is much simpler than finite element mesh generator. Most of the higher-order finite elements for plate bending work only for rectangular or parallelogramical shapes (see Attia,1996, and Hagaze, 2002). This is not the case for finite strip elements.

To test this claim a trapezoidal cantilever panel as shown in figure 9.55 was selected, where:

The length along x-axis: L = 180mm,

The width along y-axis, at x=0: B_1 = 50mm,

The width along y-axis, at x=L: B_2 = 30mm.

To facilitate the comparison with the previous case of rectangular plate, we use the same two materials of properties as shown in table 9.4. We also have the same area of the mid-plane which is 0.0072m^2.

9.7.2 Natural frequency analysis

The natural frequencies of the first three bending modes are listed in tables 9.9 and 9.10 for the C/E and E/G panels, respectively. Most elements lead to close values for the natural frequency of the first bending mode, except Kirchhoff-type element which have higher values. Kirchhoff-type and Reissner-type elements with spline-type interpolation give accurate results. Comparing with rectangular plate results in tables 9.5 and 9.6, the natural frequencies of bending modes for the trapezoidal panel are slightly higher than the corresponding natural frequencies for the rectangular plate of the same mass, as expected.

9.7.3 Stress analysis under compressive loading

A compressive load of initial value F_o = -40N, was applied uniformly at the free end. Due to the geometrical shape, the in-plane displacement distribution will not be linear, as in the tension case of section 9.2. The results for the two cases of materials are summarized next.

(a) Carbon/Epoxy Panel

The distribution of the axial displacement component u, along the x-axis (and $y = 0$), as obtained from different finite strip elements, have been demonstrated in figures 9.56 and 9.57, for polynomial and spline-type finite strip elements, respectively. It is clear from those figures that all elements tested have led to identical results. The stress (σ_x) distributions at $x = 0$, $y = 0$, have been plotted through the thickness, as shown in figures 9.58 and 9.59, for the two groups of elements. All the results of different elements are close, especially the spline-type elements.

(b) Glass/Epoxy Panel

The axial displacement distributions along the x-axis , at $y = 0$, have also been plotted for the two groups of elements, as shown in figures 9.60 and 9.61, which prove that all the finite strip elements lead to identical results. The stress distributions through the panel thickness are also plotted at node ($x = 0$, $y = 0$), in figures 9.62 and 9.63. A very good agreement between the results of the spline-type elements has been achieved.

9.7.4 Buckling analysis

A compressive load of value $F = \lambda F_o$ was assumed after carrying out the previous analysis, and the resulting buckling eigenvalues λ for the first two buckling modes are listed in tables 9.11 and 9.12, for the C/E and E/G panels, respectively. The best results agree with the observations of stress distributions discussed previously, i.e. the spline-type elements lead to results close to the FEM results. The Mindlin-type finite strip elements have also led to good results.

Chapter 10

Conclusions

10. Conclusions

It can be concluded from previous chapters that the Author has managed to achieve successfully most of the research objectives. The main original contribution can be summarized as follows:

(a) A new concept of polynomial and spline-type finite strip elements has been introduced for the first time. Although it does not lead to decoupling of harmonics as does the use of trigonometric series, but for buckling and non-linear analyses this decoupling is not always possible.

(b) Different plate-bending theories have been employed for the derivation of the new elements, allowing them to be used efficiently for thin and thick plates of isotropic and composite layered materials.

(c) The new elements have also been extended to work as faceted shell elements, for the analysis of cylindrical shells and folded and stiffened plates.

(d) The building of a sophisticated programming package, capable of linear and non-linear stress analysis, natural frequency analysis and buckling analysis with a built-in automatic mesh generator, which facilitates the use of the package for different geometrical configurations.

(e) The newly derived elements allow the use of different boundary conditions along any edge of the plate or shell.

(f) Several practical types of loading have been introduced, with their equivalent nodal loading been calculated.

The developed package has been successfully validated mainly against finite element results. Several observations have been noticed in the course of package validation, summarized as follows:

(i) While running the case studies, one can notice the big saving in modelling time and size, thus saving Human being time and computer resources.

(ii) Mindlin-type elements, with reduced integration and Lagrangian interpolation in the x and y directions, prove to be simple and accurate for a wide range of plate thicknesses, for curved shells and stiffened plates, with its best element for different cases being the three-node element.

(iii) The derived finite strip elements are capable of dealing with stiffened plates, with three-node elements behaving better than the two-node elements.

(iv) The new finite strip elements are much more efficient in modelling trapezoidal

plates than finite elements, in terms of modelling time and accuracy.

(v) The developed package has proved to be an efficient tool for stress, buckling and natural frequency analyses of plates and cylindrical shells made of isotropic and composite layered materials.

Recommendations for future work

There are some recommendations for future work which will make this work more useful for industrial applications:

(i) Investigation of damage assessment including progressive damage analysis and delamination.

(ii) Non-linear dynamic analysis, using the non-linear dynamic equations developed in this work.

(iii) Experimental validation, which may decide the practical limits of accuracy for different elements.

References

REFERENCES

1. Atkinson, K. E. *An introduction to numerical analysis.* John Wiley & sons, New York, 1978.

2. Attia, O. *Finite element static, dynamic, and flutter analysis of rotating composite layyered plates and shells.* PhD Thesis, Cranfield university, 1996.

3. Babu, P. V. T. & Reddy, D. V. Frequency analysis of skew orthotropic plates by the finite strip method. *J. Sound Vibration*, 18, 325-337, 1971.

4. Bathe, K. J. & Wilson, E. L. *Numerical methods in finite element analysis.* Prentice Hall Englewood Cliffs, New Jersey, 1976.

5. Borse, G. J. *FORTRAN 77 & numerical methods for engineers.* 2nd edition, PWS Engineering, Boston, 1991.

6. Chai, G.B. & Khong, P.W. The effect of varying the support conditions on the buckling of laminated composite plates. *Composite Structures*, 24, 99-106, 1993.

7. Chan,Y. & Chung,Y.K. Buckling of irregular plates by splined finite strips. *Structural dynamics and materials conference, 26th Orlando, AIAA J.* 24, 534-536, 1986.

8. Chen, C. J., Guthowski, R.M. & Puckett, J. A. Plate bending analysis of unequally spaced splines. *Thin-walled Struct.,* 11,409-430, 1991.

9. Cheung, M.S. & Li, W. A modified finite strip method for geometrically non-linear analysis of plates. *Computers and Structures*, 33, 1031-1035, 1989.

10. Cheung, Y. K. & Fan, S. C. Static analysis of right box girder bridges by spline finite strip method. Proc. Instn. *Civ. Engng.*, 75, 311-323, 1983.

11. Cheung, Y.K. & Cheung, M.S. Flexible vibration of rectangular and other polygonal plates. *ASCE J. Engng. Mech. Div.*, 97, 391-411,1971.

12. Cheung, Y.K. & Li, W.Y. Spline finite strip Analysis of general Plates. *J. Engng. Mech.*, 112, 43-54, 1986.

13. Cheung, Y.K., Li, W.Y&Tham, L.G. Free vibration analysis of singly curved shell by spline finite strip method. *Journal of Sound and Vibration*, 128, 411-422, 1989.

14. Cheung,Y.K. *Finite strip method in structural analysis.* Pergamon press, Oxford, 1976.

15. Cheung, M.S. & Li, W. Finite strip method combined with other numerical methods for the analysis of plates. *Computers ans Structures*, 45, 1-7, 1992.

16. Cheung, Y.K. & Kong, J. The application of a new finite strip to the free vibration of rectangular plates of varying complexity, *J. Sound & Vib.* ,181, 341-353, 1995.

17. Clint, M. & Jennings, A. The evaluation of eigenvalues by simultaneous iterations. *Computer Journal*, 13, 76-80, 1970.

18. Corr, R. B. & Jennings, A. A simultaneous iteration algorithm for symmetric eigenvalue problem, *Int. J. Numer. Methods Engng.*, 10, 647-663, 1976.

19. Craig, T.J. & Dawe, D.J. Vibration of shear-deformable laminated plates structures using the finite strip method. *Computers and Structures,* 27, 61-72, 1987.

20. Dawe, D.J. & Tan, D. Buckling and vibration analysis of composite laminated plates and shells using general spline function. *Composite structures*, 40,25-42, 1997.

21. Dawe, D. J. Finite strip models for vibration of Mindlin plates, *J. Sound Vibration,* 59 , 441-452, 1978.

22. Dawe, D. J. & Tan, D. Finite strip buckling and free vibration analysis of stepped rectangular composite plates. *Int. J. Num. Method in Engg.*, 46, 1313-1334, 1999.

23. Dawe, D. J. & Wang, S. Vibration of shear deformable rectangular plates using a spline-function Rayleigh-Ritz approach. *Int. J. Num. Methods Engng.*, 36, 595-611, 1993.

24. Dawe, D.J. & Peshkam,V. Buckling and vibration of finite length composite prismatic plates structures with diaphragm ends, part 1: Finite strip formulation. *Compu. Meth. Appl. Mech. Engng.*, 77, 1-30, 1989.

25. Dawe, D. J. & Peshkam, V. Buckling and vibration of finite length composite prismatic plates structures with diaphragm ends, part 1: Finite strip formulation. *Compu. Meth. Appl. Mech. Engng.*, 77, 227-252, 1989.

26. Dawe, D. J. & Tan, D., Finite strip buckling & free vibration analysis of stepped rectangular composite laminated plates. *Int. J. Numer. Meth. Engng.* 46, 1313-1334. 1999.

27. Dawe, D.J., Lam, S.S.E. & Azizian, Z.G. Non-linear analysis of rectangular laminates under end shortening using shear deformation plate theory. *Int. J. Num. Method in Engg.* , 36, 1045-1064, 1993.

28. Donaldson, S.L. The effect of inter-laminar fracture properties on the delamination buckling of composite laminates.*Composites Science & Technology*, 28,33-44, 1987.

29. El-Zafrany, A. M. *Finite element methods. MSc lecture notes,* Cranfield University. 2000.

30. El-Zafrany, A.M. & Cookson, R.A. An explicit formula for the generalized Hermitian problem, *Communications in Applied Numerical Methods*, 1, 85-91, 1985.

31. Grenestedt, J. L. A study on the effect of bending-twisting coupling on buckling strength. *Composite Structures*, 12, 271-290, 1989.

32. Hegaze, M.M.E. *Finite element analysis of fatigue damage of composite laminated structures.* PhD Thesis, Cranfield university, 2002.

33. Hrudey, T.M. & Hrabok, M.M. Singularity finite elements for plate bending. J.

Engng. Mech. 112, 666-681, 1986.

34. Hui, D. Shear buckling of anti-symmetric cross-ply rectangular plates. *Fibre Science and Technology*, 21, 327-340, 1984.

35. Hu, X. Free vibration analysis of symmetrical cylindrical honeycomb panels by using the finite strip method. *J. Vib. & Con.*, 3, 19-32, 1997.

36. Irons, B. M. A frontal solution program for finite element analysis. *Int. J.Numer. Methods Engng.*, 2 5-32, 1970.

37. Jones, R. M. *Mechanics of composite materials*. McGraw-Hill, New York, 1975.

38. Khong, P.W. Improvement to the higher order finite strip method. *Proceedings of the thirteenth Canadian congress os applied mechanics*, 07-39, 1991a.

39. Khong, P.W. Improvement to the higher order finite strip method. *Proceedings of the thirteenth Canadian congress of applied mechanics*, 616-621, 1991b.

40. Kopal, Z. *Numerical analysis*. 2nd edition, Chapman & Hall, London, 1961.

41. Lam, S.S.E. & Zou, G.P. Finite strip analysis of laminated plates under in-plane loads. *International conference on advances in structural engineering and mechanics, Korea*, 1267-1272, 1999.

42. Loughlan, J. A finite strip analysis of the buckling characteristics of some composite stiffened shear panels. *Compos. Struc.*, 27, 283-294, 1993.

43. Loughlan, J. & Delaunoy, J. M. The buckling of composite stiffened plates with some emphasis on the effects of fibre orientation and on loading configuration. Compos. Struc., 25, 485-494, 1993.

44. Loughlan, J. The buckling and vibrational behaviour of some stiffened panels subjected to in-pane shear loading. *Applied Solid Mechanics-4, Edited by A. R. S. Ponter &A. C. F. Cocks, Elsevier Applied Science, London*, 275-302, 1991.

45. Lu, H., Xi, X. & Ma, L. Structural dynamic analysis of engine case and supporting system. *J. Aerospace power*, 9, 151-155, 1994.

46. Madasamy, C. M. *Analysis of plated structures with rectangular cutouts and internal supports*, Department of Civil Engineering, Madras, India, 1993.

47. Michael, O. & Averashi, J. A combined boundary element and finite strip solution. *Sixteeneth boundary element method conference, U.K.* , 593-600, 1994.

48. Minguet, P.J., Dugundji, J.& Lagace, P. Post-buckling behaviour of laminated plates using a direct energy-minimisation technique. *AIAA Journal*,27, 87-92, 1989.

49. Morris, I.R. & Dawe, D. J. Free vibration of curved-plate assemblies with diaphragm ends. *J. Solids Vibration*, 73, 1-17, 1980.

50. Nemeth, M.P. Importance of an-isotropy buckling on buckling compression-loaded symmetric composite plates. *AIAA journal*, 24, 1831-1855, 1986.

51. Plank, R. J. & Wittrick, W.H. Buckling under combined loading of thin, flat-

walled structures by a complex finite strip method. *Int. J. Num. Meth. Engng.*, 8, 323-339, 1974.

52. Plank, R.J. & Williams, F. W. Critical buckling of some stiffened panels in compression, shear and bending. *Aeronautical Quarterly*, 165-179. 1974.

53. Plank, R. J. & Wittrick, W. H. Buckling under combined loading of thin, flat-walled structures by a complex finite method. *Int,. J. Numer. Methods Engng.*, 8, 323-339, 1974.

54. Peshkam, V. & Dawe, D.J. Buckling and vibration analysis of composite prismatic plate. *Composite structures 5. Proceedings of fifth international conference Scotland*, A91-17376, 05-39, 1989.

55. Sharma,S., Iyengar, N.G.R. & Murtha, P.N. Buckling of anti-symmetric cross- and angle-ply laminated plates. *Int. J. Mech. Scien.*, 22, 607-620, 1980.

56. Sheinman, I., Frostig,Y. & Segal, A. Bifuration buckling analysis of stiffened laminated composite panels. *In Buckling of Structures: Theory and experiment. Elsevier Applied Science, London*, 355-380, 1988.

57. Sheikh, Abdul Hamid. Large amplitude free flexural vibration of stiffened plates. *AIAA J. on Disc*, 2, 1-7, 1997.

58. Snell,M.B. & Greeves, L.J. Buckling and strength characteristics of some CFRP stiffened curved panels. *In Aerospace Structures, ed. J. Loughlan. Elsevier, London*, 149-176, 1990.

59. Srinivasan, R.S. & Chellapandi, P. Dynamic stability of rectangular laminated composite plates. *Computers & Structures*, 24, 233-238, 1986.

60. Starnes, L.H., Knight, N.F. & Rouse, M. Post-buckling behaviour of selected flat stiffened graphite-epoxy panels loaded in compression. *AIAA J.*, 23, 1236-46, 1985.

61. Tarn, J. Sa, & D. A hybrid finite strip analysis of multilayer laminated plates. *Chinese Institute of engineers. Journal*, 10, 647-656, 1987.

62. Tham, L.J. Application of spline finite strip Method in the Analysis of Space Structures. *Thin-walled Struct.*, 10, 235-246, 1990.

63. Tham, L.G. & Szeto, H.Y. Buckling analysis of arbitrarily shaped plates by spline strip method. *Computers and Structures*, 36, 726-735, 1990.

64. Turvey, G.J. & Wittrick, W.H. The influence of orthotropy on the stability of some multi-plate structures in compression. *Aeronaut.*, 24, 1-8, 1973.

65. Whitney, J. M. *Structural Analysis of Laminated Anisotropic plates*. Technomic, PA, 1987.

66. Wang, S. & Dawe, D. J. Spline finite strip analysis of the buckling and vibration of composite prismatic plate structures. *Int. J. Mech. Sci.*,39, 1161-1180, 1997.

67. Zienkiewicz, O. C. & Taylor, R. L. *The finite element method.* 5*th* edn, Butterworth & Heinemann, Oxford, 2000.

Tables

Tables

Table 9.1 Material properties of Carbon/Epoxy and Glass/Epoxy plates

Parameter	Carbon/Epoxy [C/E]	Glass/Epoxy [E/G]
Longitudinal Modulus E_{11} [GPa]	134.75	45.37
Transverse Modulus E_{22} [GPa]	8.24	15.2
Shear Modulus in x-y plane μ_{12} [GPa]	7.0	6.0
Shear Modulus in y-z plane μ_{23} [GPa]	7.0	6.0
Shear Modulus in z-x plane μ_{31} [GPa]	7.0	6.0
Major Poisson's Ratio ν_{12}	0.325	0.289
Number of Layers	12	12
Thickness of each layer [mm]	2.5	2.5
Stacking Sequence	$[-45,0,45]_{2s}$	$[-45,0,45]_{2s}$

Table 9.2 Material properties of the square plate

Parameter	value
Longitudinal Modulus E_{11} [MPa]	40.0
Transverse Modulus E_{22} [MPa]	1.0
Shear Modulus in x-y plane μ_{12} [MPa]	0.6
Shear Modulus in y-z plane μ_{23} [MPa]	0.6
Shear Modulus in z-x plane μ_{31} [MPa]	0.6
Major Poisson's Ratio ν_{12}	0.25
Number of Layers	8
Thickness of each layer [mm]	2.5
Stacking Sequence	$[0,45,-45,90]_s$

Table 9.3 Non-dimensional central deflection for the square plate

L/(2h)		Mindlin-Type Element	Kirchhoff-Type Element	Reissner-Type Element	Spline-type Kirchhoff	Spline-type Reissner
25.0	2-noded	0.514	0.501	0.528	0.522	0.540
	3-noded	0.515	0.501	0.528	0.522	0.540
	FEM	0.559				
12.5	2-noded	0.539	0.501	0.580	0.522	0.581
	3-noded	0.540	0.501	0.580	0.522	0.581
	FEM	0.583				
10.0	2-noded	0.559	0.501	0.611	0.522	0.608
	3-noded	0.559	0.501	0.611	0.522	0.608
	FEM	0.602				
6.25	2-noded	0.642	0.501	0.718	0.522	0.719
	3-noded	0.643	0.501	0.718	0.522	0.722
	FEM	0.681				
5.0	2-noded	0.718	0.501	0.806	0.522	0.819
	3-noded	0.718	0.501	0.806	0.522	0.819
	FEM	0.754				
4.0	2-noded	0.836	0.501	0.935	0.522	0.971
	3-noded	0.837	0.501	0.935	0.522	0.971
	FEM	0.869				
2.5	2-noded	1.346	0.501	1.456	0.522	1.612
	3-noded	1.347	0.501	1.456	0.522	1.612
	FEM	1.369				

Table 9.4 Material properties of Cranfield Carbon/Epoxy and Glass/Epoxy plates

Parameter	Carbon/Epoxy [C/E]	Glass/Epoxy [E/G]
Longitudinal Modulus E_{11} [GPa]	128.0	35.0
Transverse Modulus E_{22} [GPa]	11.0	8.22
Shear Modulus in x-y plane μ_{12} [GPa]	4.48	4.1
Shear Modulus in y-z plane μ_{23} [GPa]	4.48	4.1
Shear Modulus in z-x plane μ_{31} [GPa]	4.48	4.1
Major Poisson's Ratio ν_{12}	0.25	0.26
Number of Layers	13	12
Thickness of each layer [mm]	0.25	0.15
Density ρ [kg/m^3]	1500	2000
Stacking Sequence [Degrees]	[0/ 90/ 45/ 0/ -45/90/ 0/90/-45/0/45/90/0]	$[0/90/45/0/-45/90]_s$

Table 9.5 Natural frequencies for
Carbon-Epoxy plate (in hz)

		1st Natural Frequency	2nd Natural Frequency	3rd Natural Frequency
Mindlin-Type Element	2-noded	1.141	5.224	7.173
	3-noded	1.139	6.142	7.156
	4-noded	1.139	6.006	7.146
Kirchhoff -Type Element	2-noded	1.143	6.402	7.226
	3-noded	1.141	6.122	7.152
	4-noded	1.142	6.088	8.852
Reissner-Type Element	2-noded	1.130	6.926	7.036
	3-noded	1.132	5.989	6.946
	4-noded	1.134	5.995	6.923
Spline-Type Kirchhoff	2-noded	1.144	6.064	7.203
	3-noded	1.147	6.099	7.207
	4-noded	1.141	6.071	7.214
Spline-Type Reissner	2-noded	1.140	5.978	7.134
	3-noded	1.141	6.010	7.138
	4-noded	1.132	5.980	7.049
FEM	9-noded	1.135	6.372	7.124

Table 9.6 Natural frequencies for
Glass-Epoxy plate (in hz)

		1st Natural Frequency	2nd Natural Frequency	3rd Natural Frequency
Mindlin-Type Element	2-noded	0.299	1.561	1.944
	3-noded	0.3055	1.911	2.135
	4-noded	0.304	1.910	2.131
Kirchhoff-Type Element	2-noded	0.308	1.928	2.124
	3-noded	0.308	1.927	2.013
	4-noded	0.308	1.928	2.001
Reissner-Type Element	2-noded	0.305	1.908	2.036
	3-noded	0.305	1.909	2.002
	4-noded	0.306	1.915	2.001
Spline-Type Kirchhoff	2-noded	0.309	1.920	2.014
	3-noded	0.309	1.921	2.026
	4-noded	0.309	1.923	2.016
Spline-Type Reissner	2-noded	0.309	1.918	2.009
	3-noded	0.309	1.918	2.021
	4-noded	0.306	1.913	2.011
FEM	9-noded	0.306	1.913	2.171

Table 9.7 Buckling eigenvalues for
Carbon-Epoxy plate

		First Eigenvalue	Second Eigenvalue
Mindlin-Type Element	2-noded	1.610	12.725
	3-noded	1.611	14.391
	4-noded	1.615	14.410
Kirchhoff-Type Element	2-noded	1.623	14.591
	3-noded	1.621	14.572
	4-noded	1.621	14.572
Reissner-Type Element	2-noded	1.589	14.165
	3-noded	1.593	14.193
	4-noded	1.600	14.249
Spline-Type Kirchhoff	2-noded	1.624	14.595
	3-noded	1.633	14.602
	4-noded	1.620	14.571
Spline-Type Reissner	2-noded	1.617	14.391
	3-noded	1.618	14.406
	4-noded	1.595	14.432
FEM	9-noded	1.599	14.292

Table 9.8 Buckling eigenvalues for
Glass-Epoxy plate

		First Eigenvalue	Second Eigenvalue
Mindlin-Type Element	2-noded	0.0852	0.785
	3-noded	0.0866	0.779
	4-noded	0.0849	0.782
Kirchhoff-Type Element	2-noded	0.0875	0.787
	3-noded	0.0872	0.784
	4-noded	0.0875	0.787
Reissner-Type Element	2-noded	0.0853	0.767
	3-noded	0.0854	0.769
	4-noded	0.0864	0.776
Spline-Type Kirchhoff	2-noded	0.0875	0.787
	3-noded	0.0881	0.788
	4-noded	0.0875	0.786
Spline-Type Reissner	2-noded	0.0875	0.786
	3-noded	0.0876	0.786
	4-noded	0.0859	0.789
FEM	9-noded	0.0857	0.772

Table 9.9 Natural frequencies for C/E trapezoidal panel (in hz)

Type of Element	Number of Nodes	1st Natural Frequency	2nd Natural Frequency	3rd Natural Frequency
Mindlin	2-noded	1.313	7.522	11.482
	3-noded	1.327	7.027	7.685
Kirchhoff	2-noded	1.740	7.642	8.247
	3-noded	1.670	6.710	8.071
Reissner	2-noded	1.676	7.912	8.025
	3-noded	1.648	7.938	8.414
Spline Kirchhoff	2-noded	1.309	6.333	7.542
	3-noded	1.339	6.477	7.556
Spline Reissner	2-noded	1.305	6.239	7.466
	3-noded	1.330	6.373	7.482
FEM	9-noded	1.297	7.121	8.284

Table 9.10 Natural frequencies for E/G trapezoidal panel (in hz)

Type of Element	Number of Nodes	1st Natural Frequency	2nd Natural Frequency	3rd Natural Frequency
Mindlin	2-noded	0.355	1.642	2.038
	3-noded	0.358	1.985	2.018
Kirchhoff	2-noded	0.471	2.210	2.527
	3-noded	0.451	2.175	2.191
Reissner	2-noded	0.353	1.704	2.264
	3-noded	0.446	1.910	2.157
Spline Kirchhoff	2-noded	0.354	2.011	2.089
	3-noded	0.362	2.020	2.129
Spline Reissner	2-noded	0.353	2.008	2.084
	3-noded	0.360	2.016	2.119
FEM	9-noded	0.352	1.981	2.708

Table 9.11 Buckling eigenvalues for C/E trapezoidal panel

Type of Element	Number of Nodes	First Eigenvalue	Second Eigenvalue
Mindlin	2-noded	1.737	15.550
	3-noded	1.756	14.340
Kirchhoff	2-noded	2.522	15.352
	3-noded	2.375	15.154
Reissner	2-noded	1.877	15.110
	3-noded	2.329	14.797
Spline Kirchhoff	2-noded	1.739	14.661
	3-noded	1.786	14.555
Spline Reissner	2-noded	1.732	14.442
	3-noded	1.764	14.351
FEM	9-noded	1.684	13.475

Table 9.12 Buckling eigenvalues for E/G trapezoidal panel

Type of Element	Number of Nodes	First Eigenvalue	Second Eigenvalue
Mindlin	2-noded	0.0933	0.783
	3-noded	0.0944	0.777
Kirchhoff	2-noded	0.136	0.829
	3-noded	0.128	0.817
Reissner	2-noded	0.120	0.988
	3-noded	0.125	0.801
Spline Kiechhoff	2-noded	0.0938	0.792
	3-noded	0.0964	0.785
Spline Reissner	2-noded	0.0937	0.790
	3-noded	0.0956	0.783
FEM	9-noded	0.0916	0.743

Figures

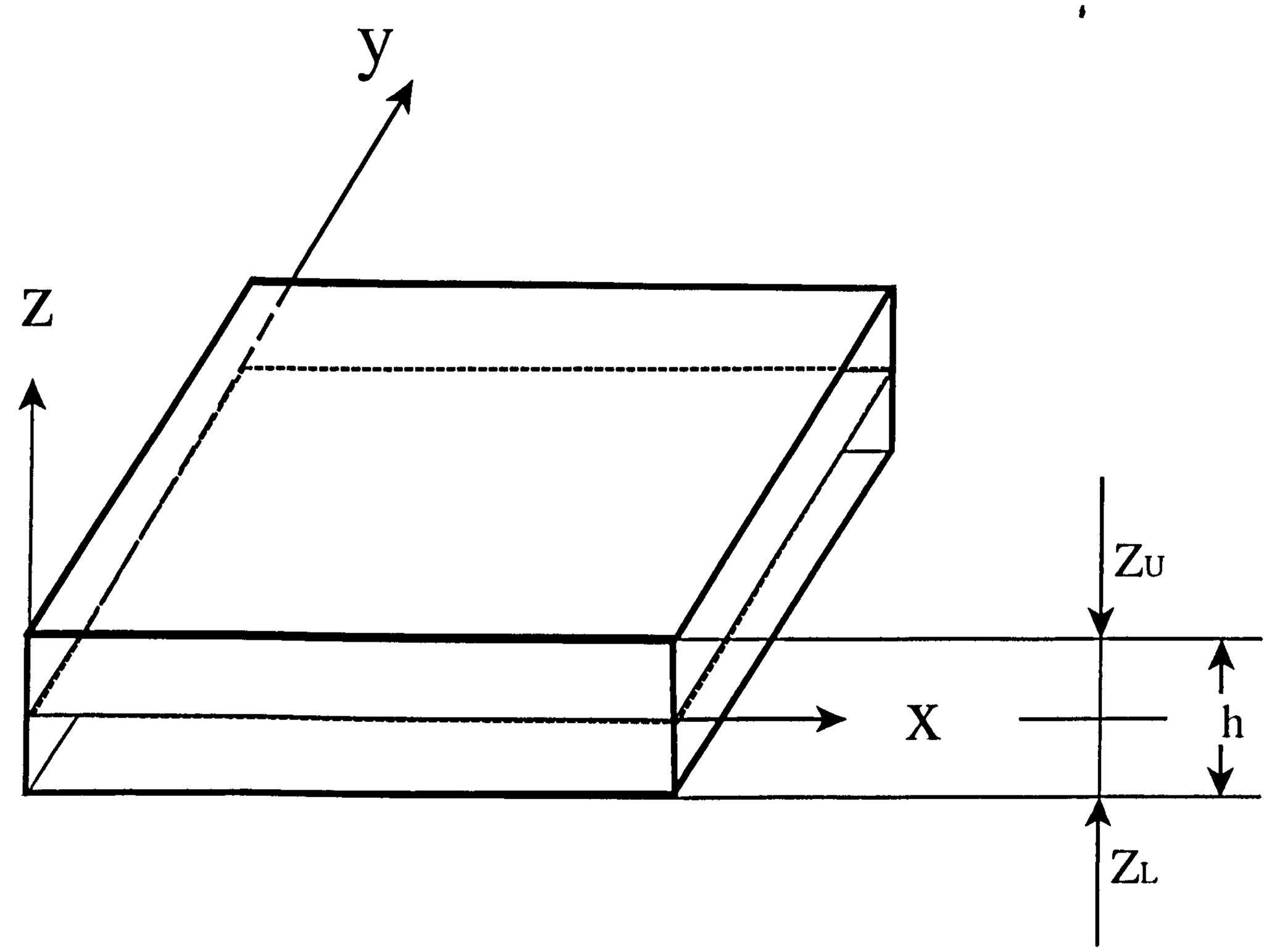

Figure 3.1 Plate axes and midplane

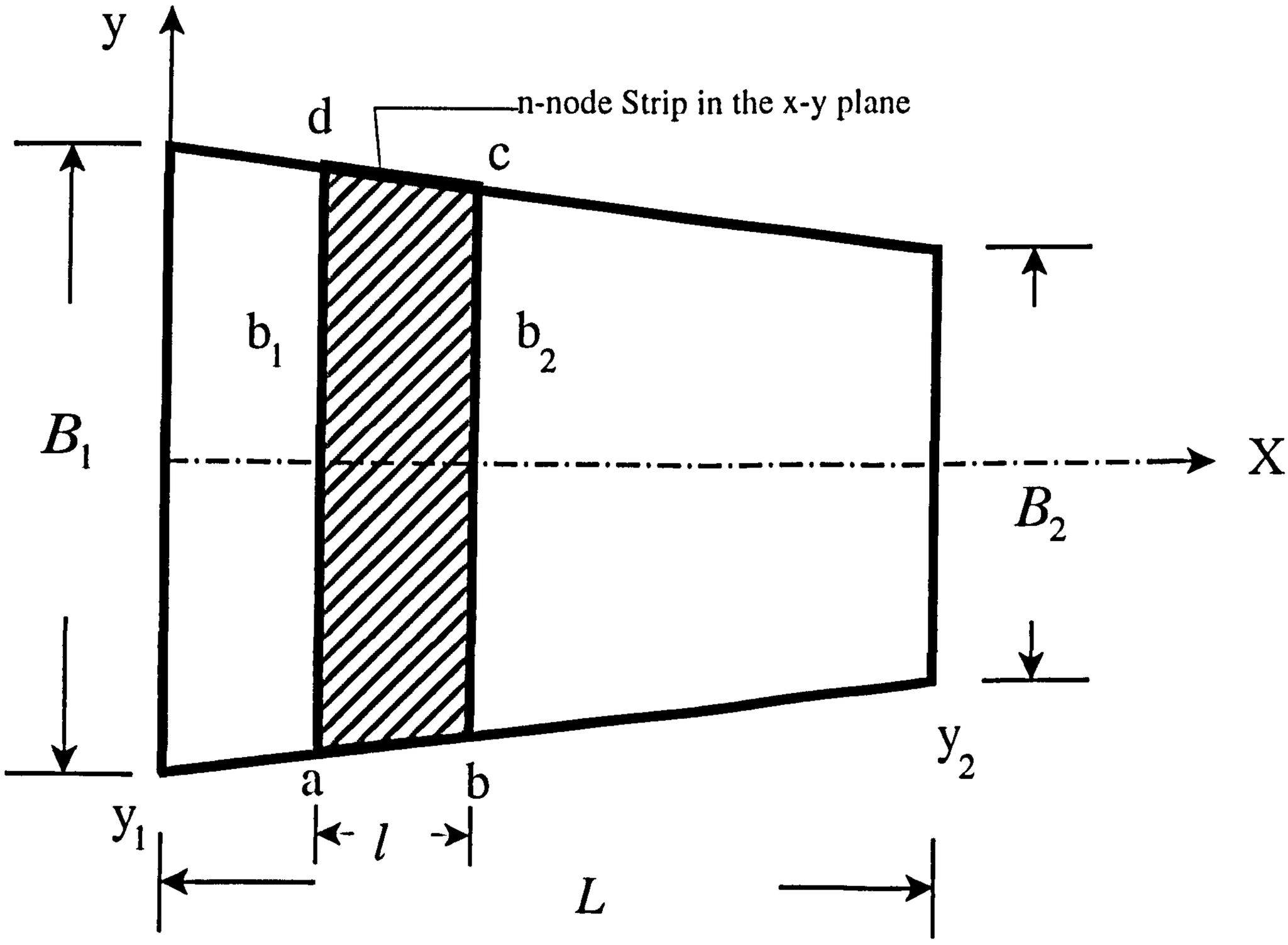

Figure 3.2 A finite strip in a trapezoidal panel

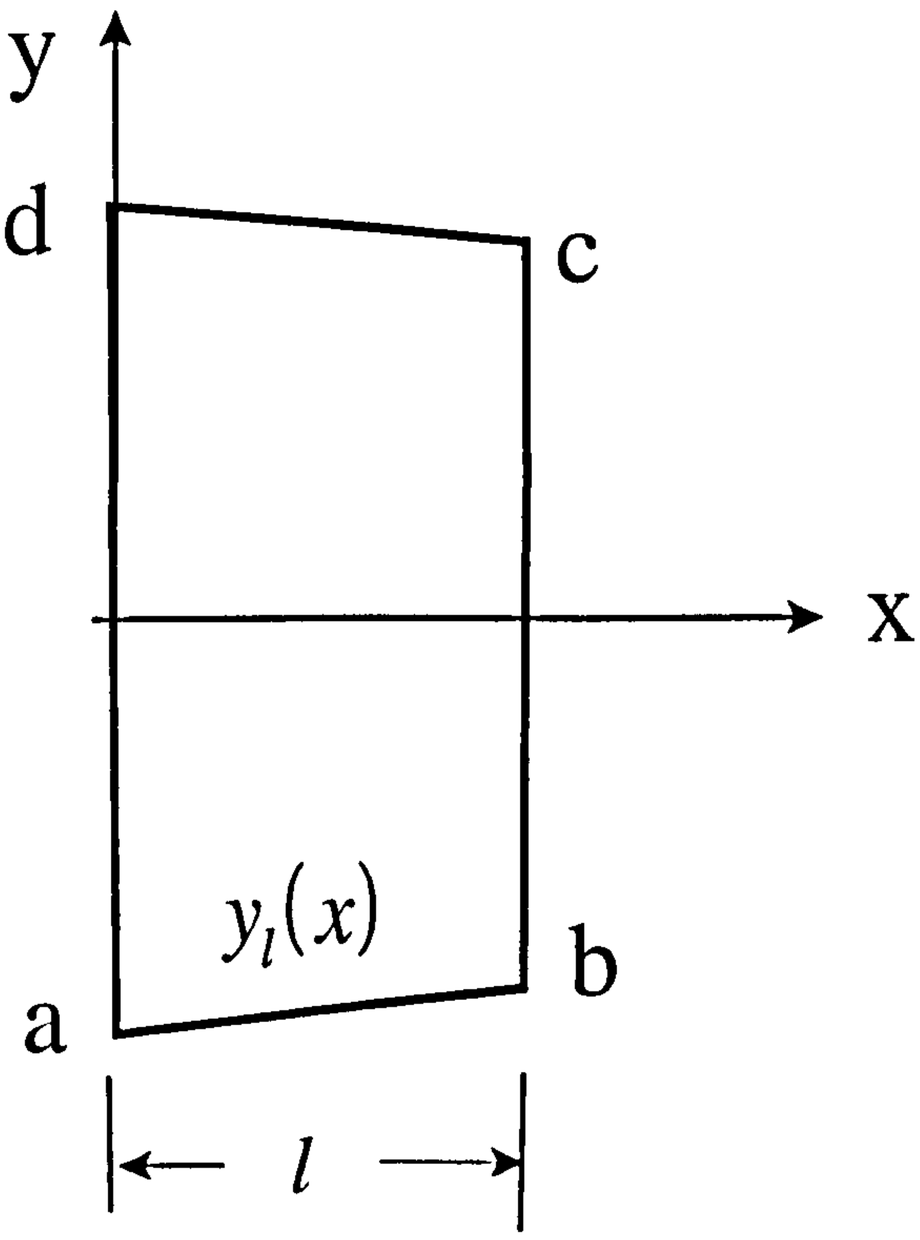

(a) Strip in local plane

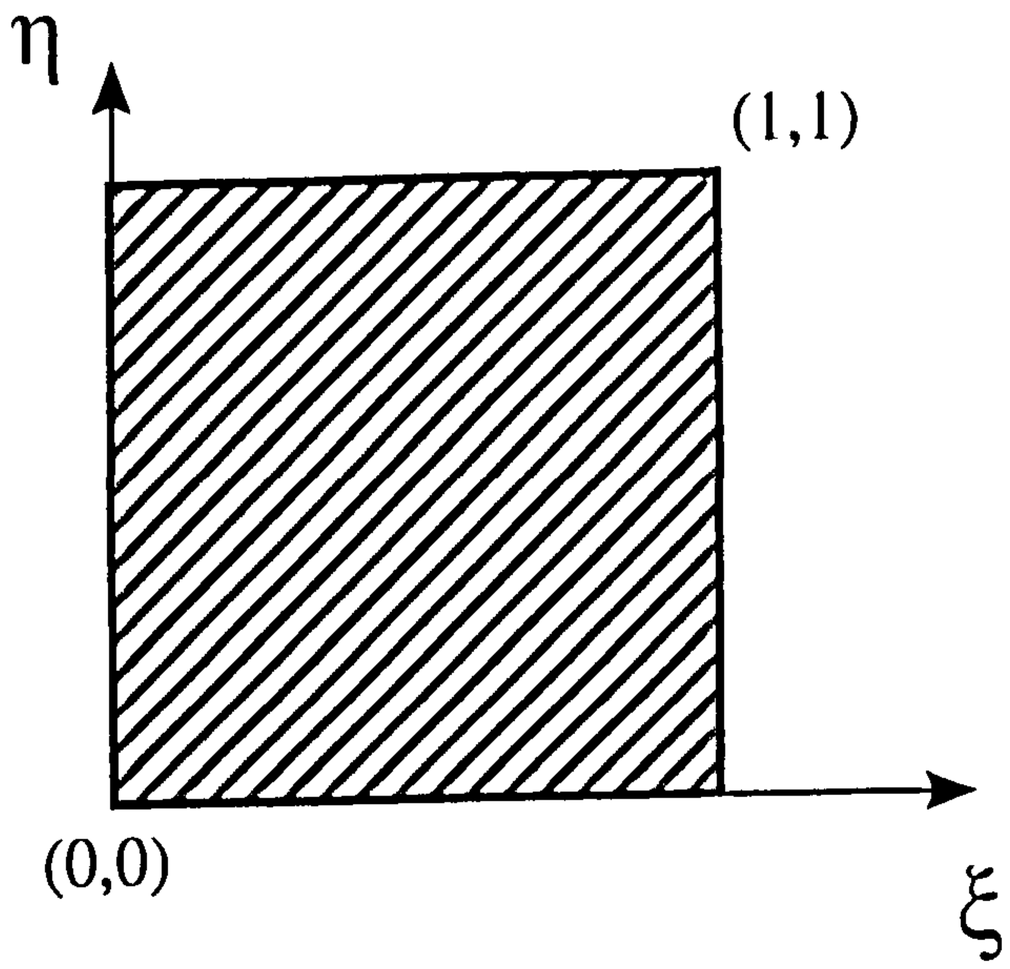

(b) Strip in intrinsic plane

Figure 3.3 Strip local and intrinsic axes

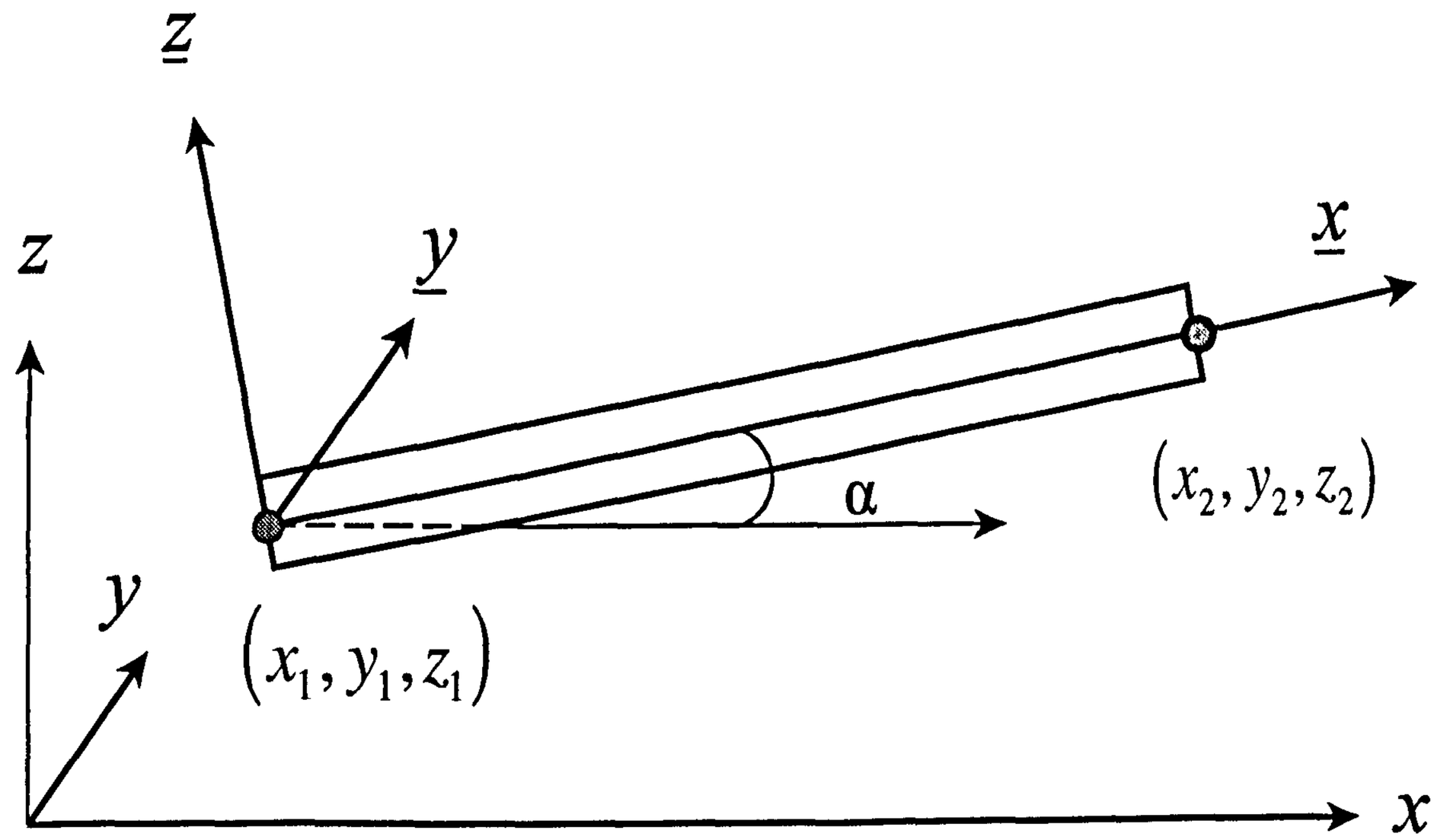

Figure 7.1 Plate local and global axes

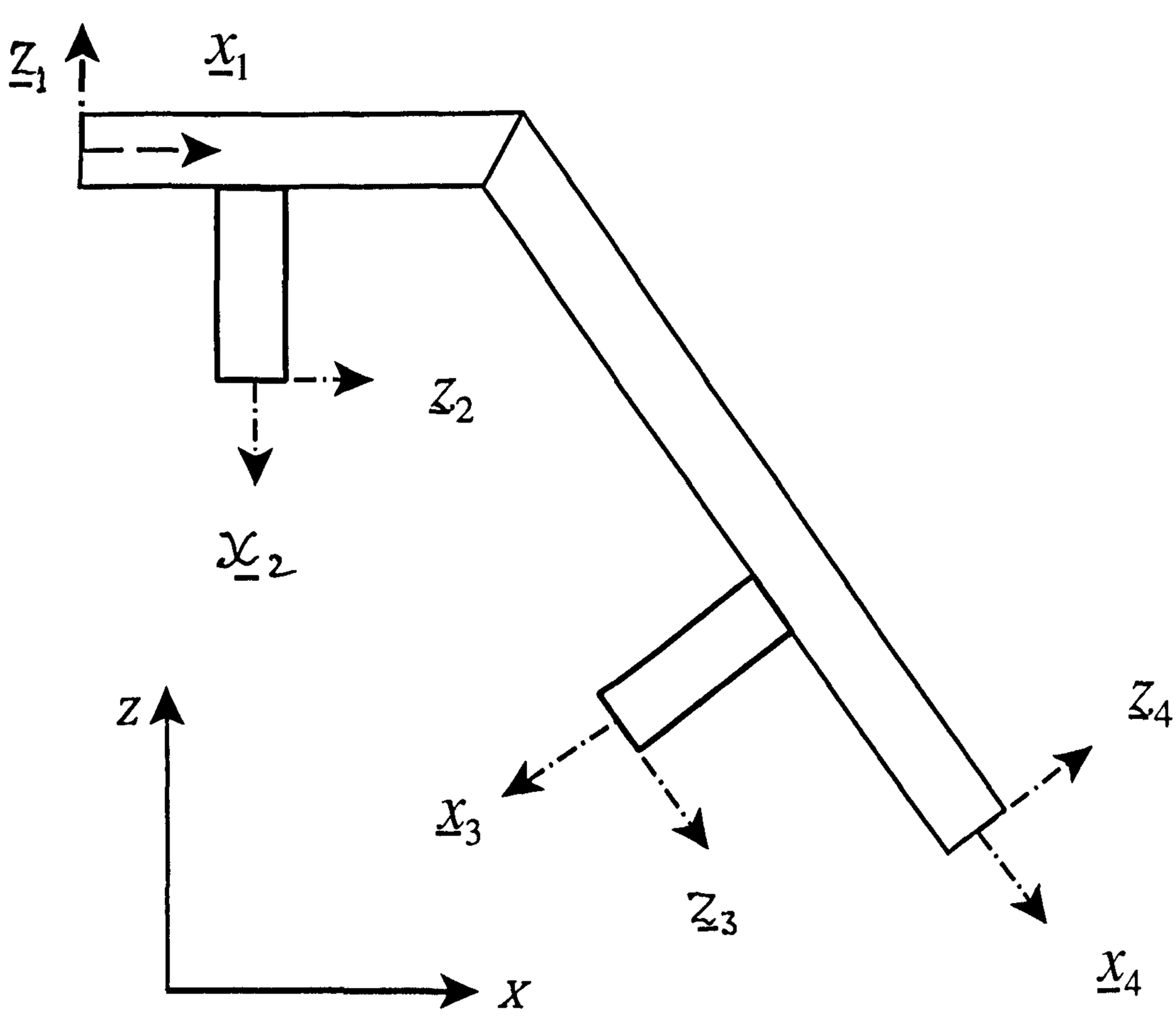

Figure 7.2 Local and global axes for a folded plate

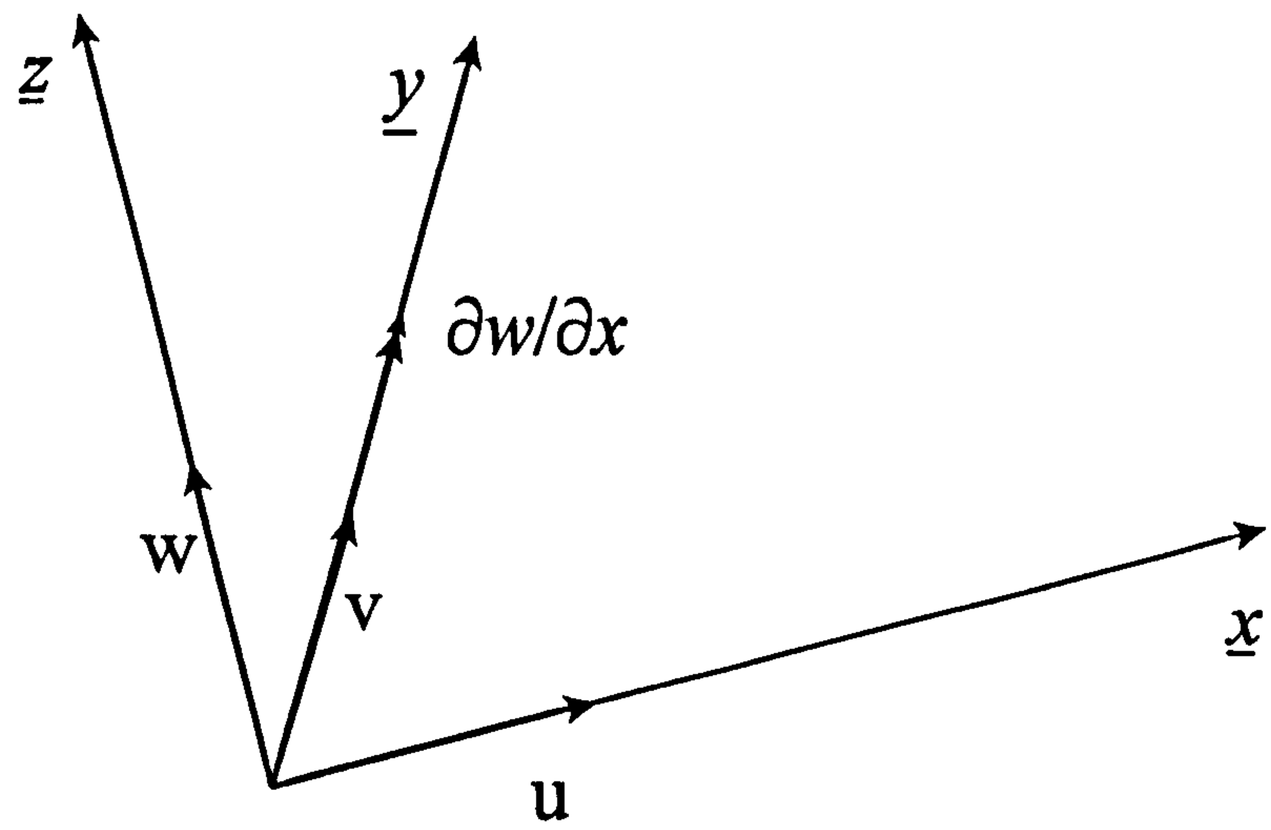

Figure 7.3 Degrees of freedom for Kirchhoff-type finite strip element

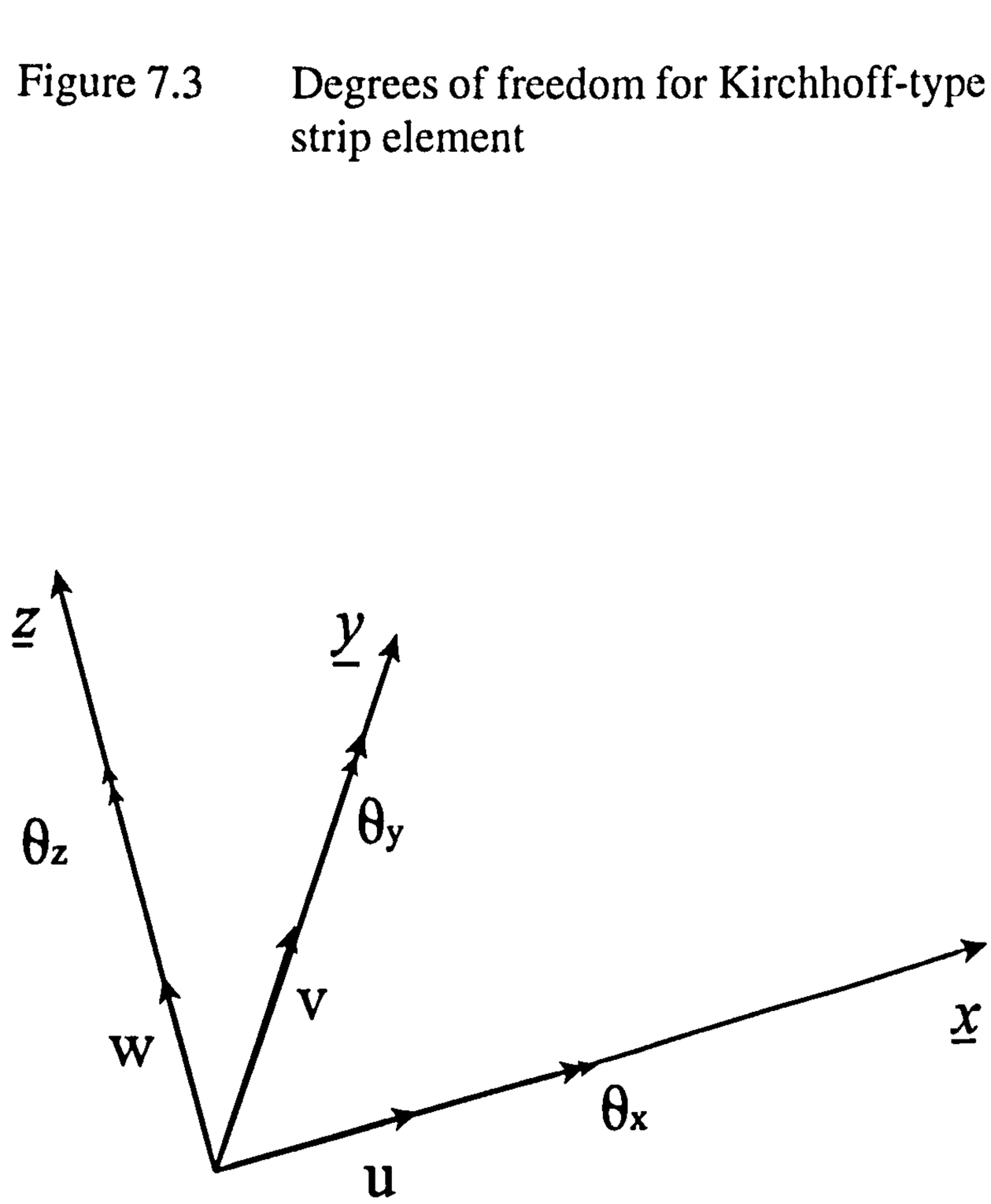

Figure 7.4 Degrees of freedom for Mindlin-type finite strip element

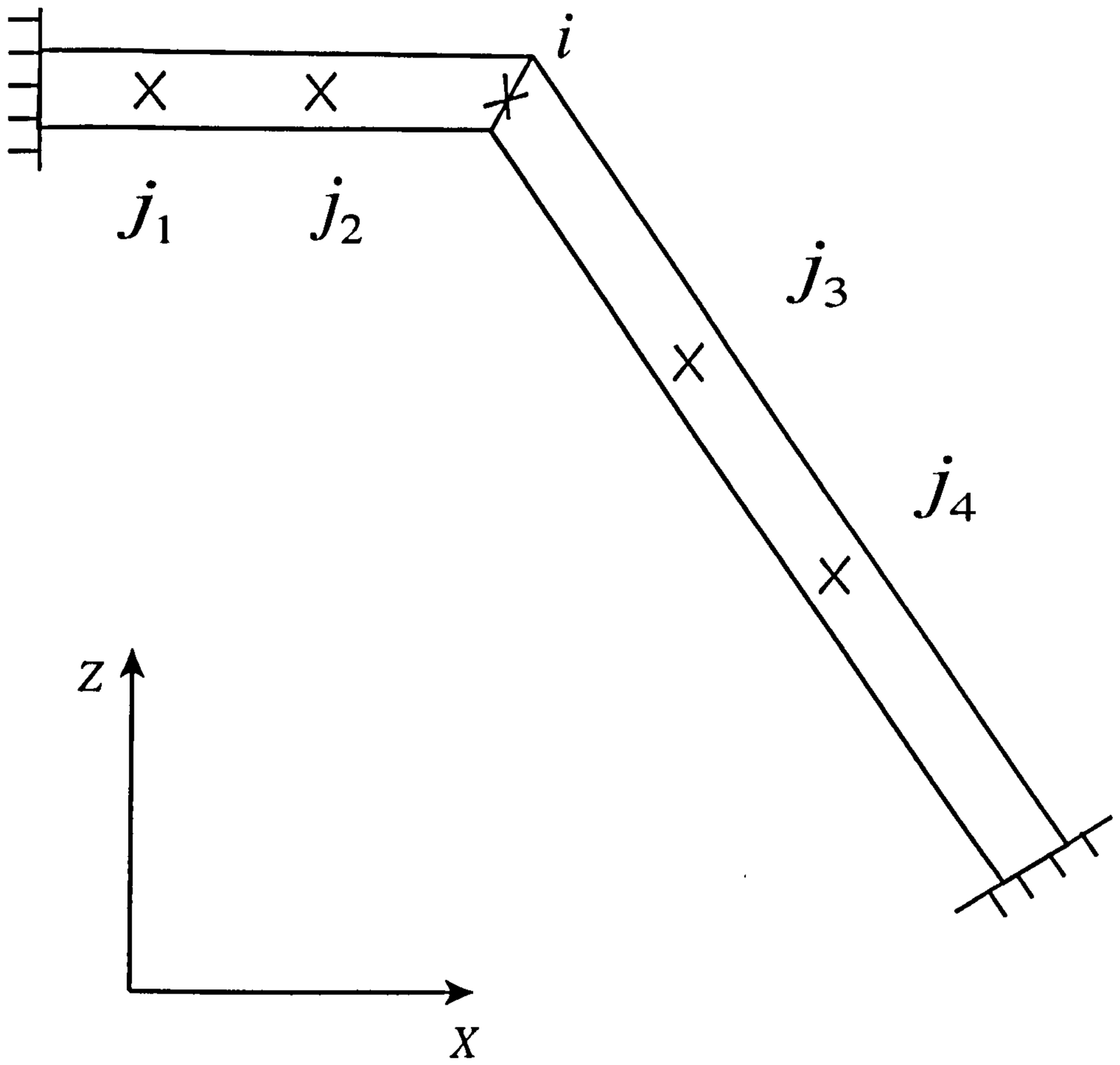

Figure 7.5 Co-planar and non-coplanar nodes

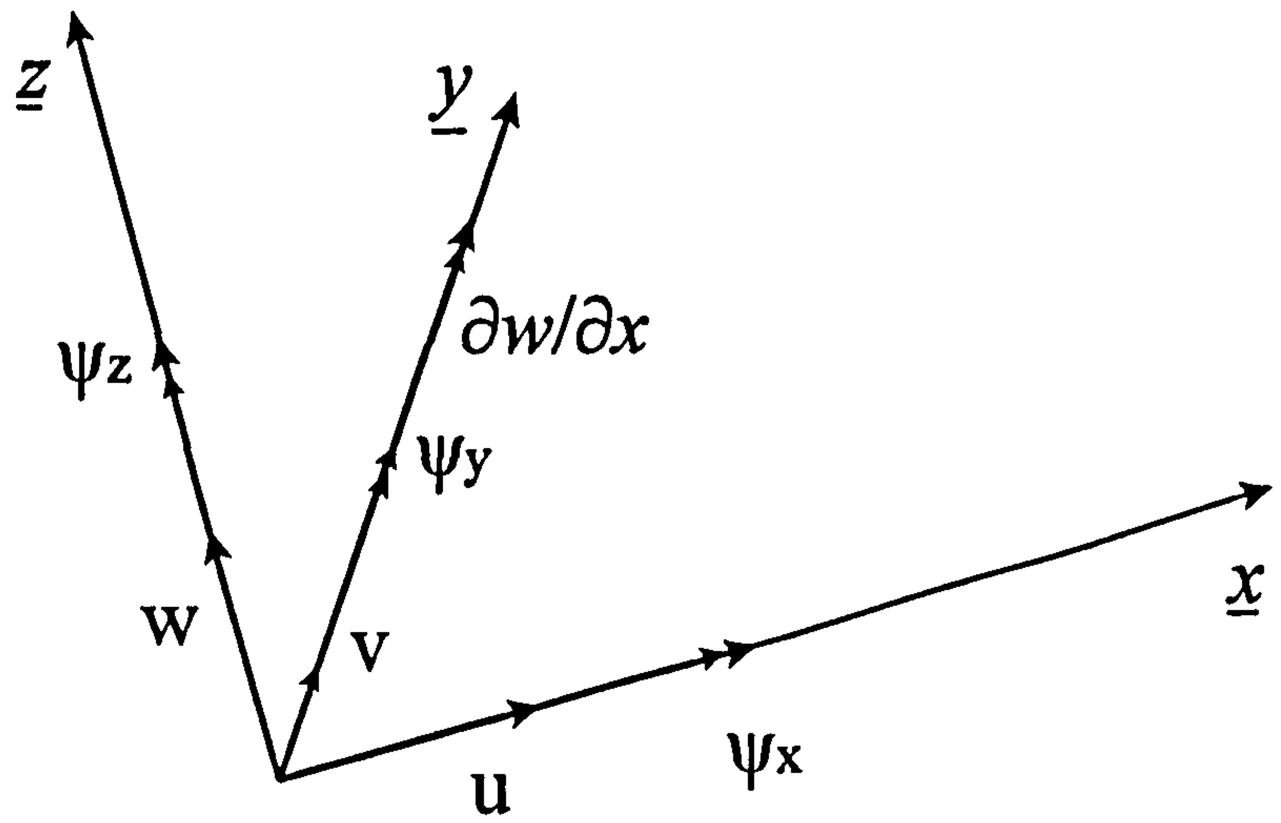

Figure 7.6 Degrees of freedom for Reissner-type finite strip element

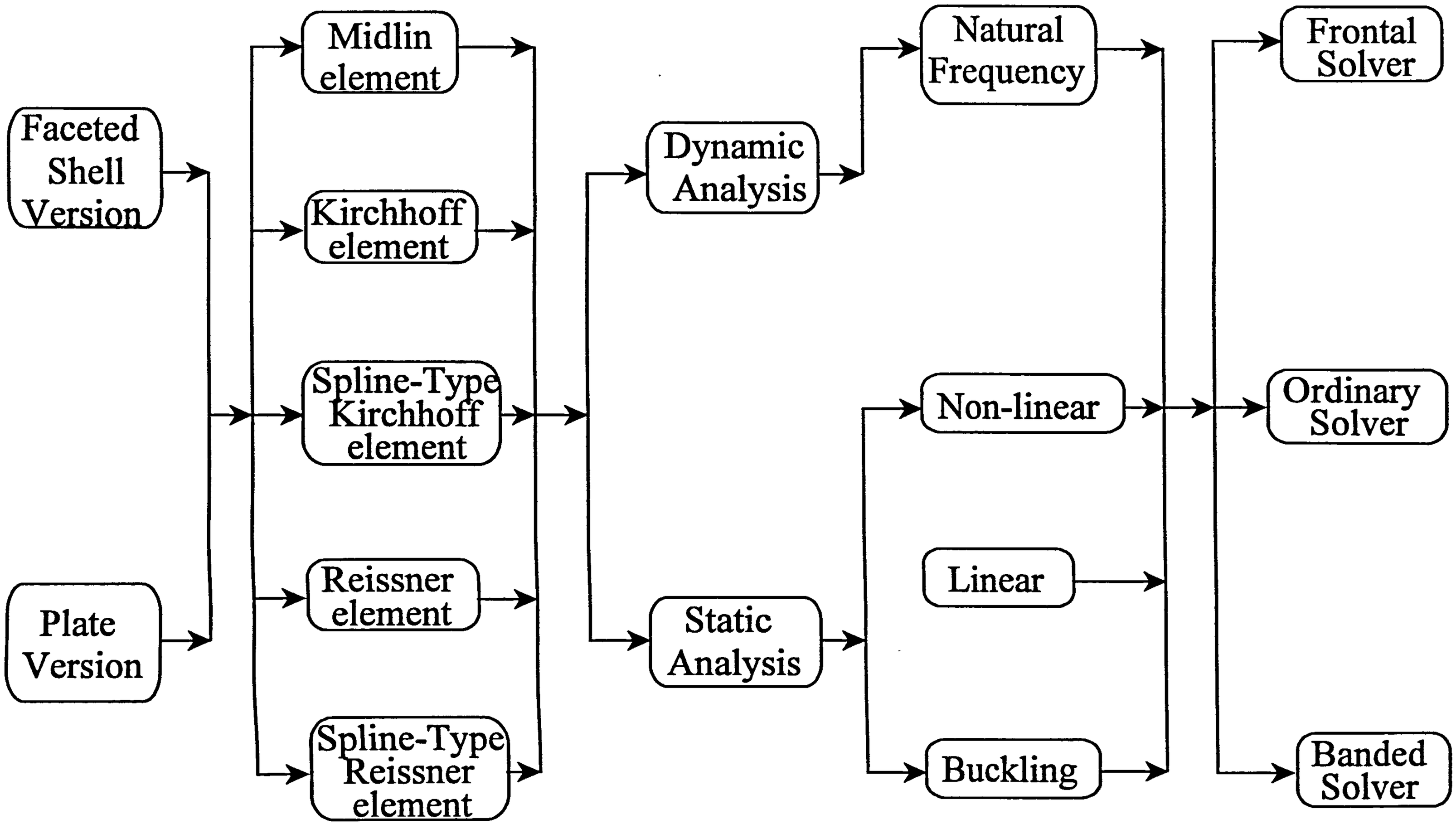

Figure 8.1 Basic layout of the programming package

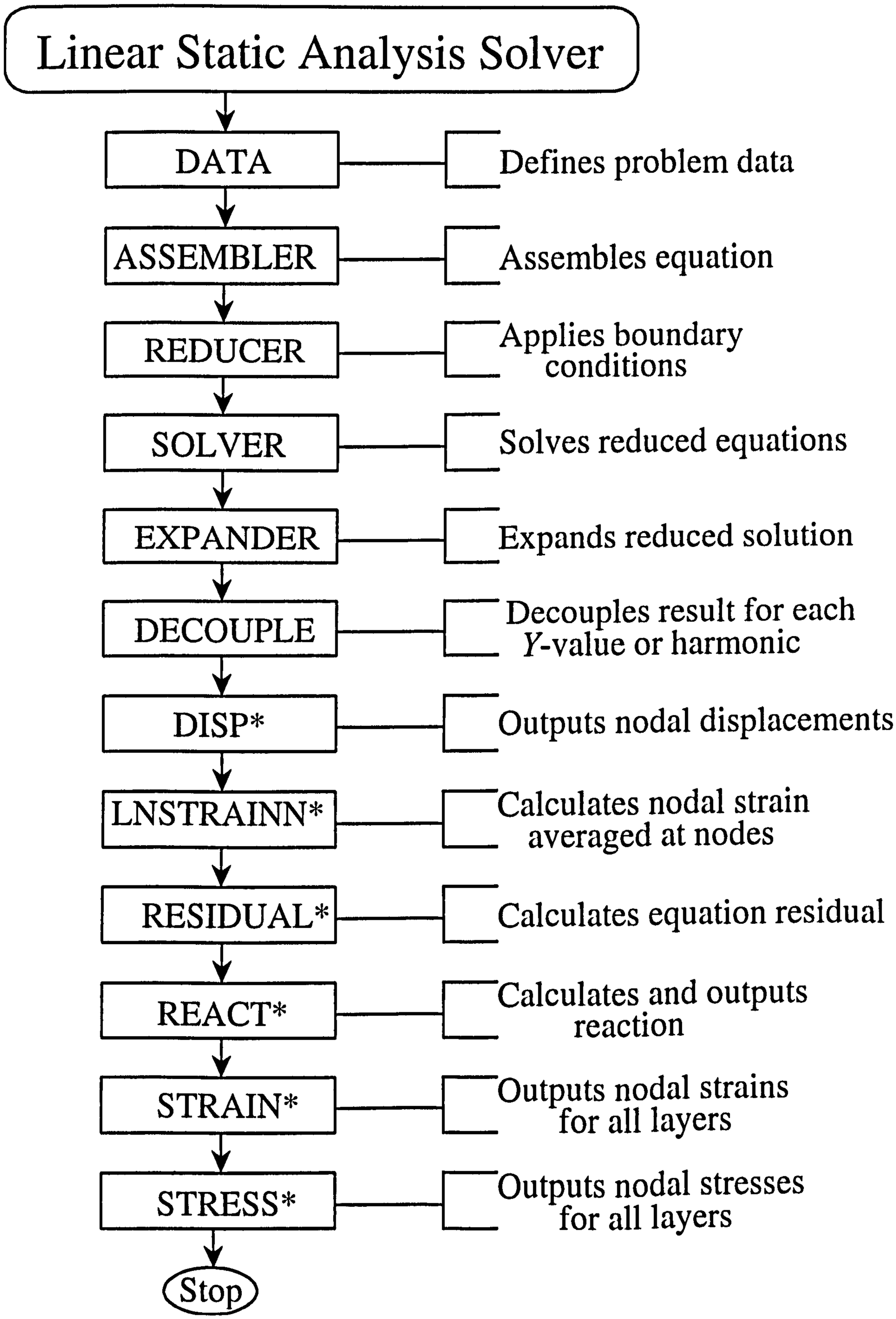

(*) These subroutines are in -LNS file

Figure 8.2 Linear static analysis solver

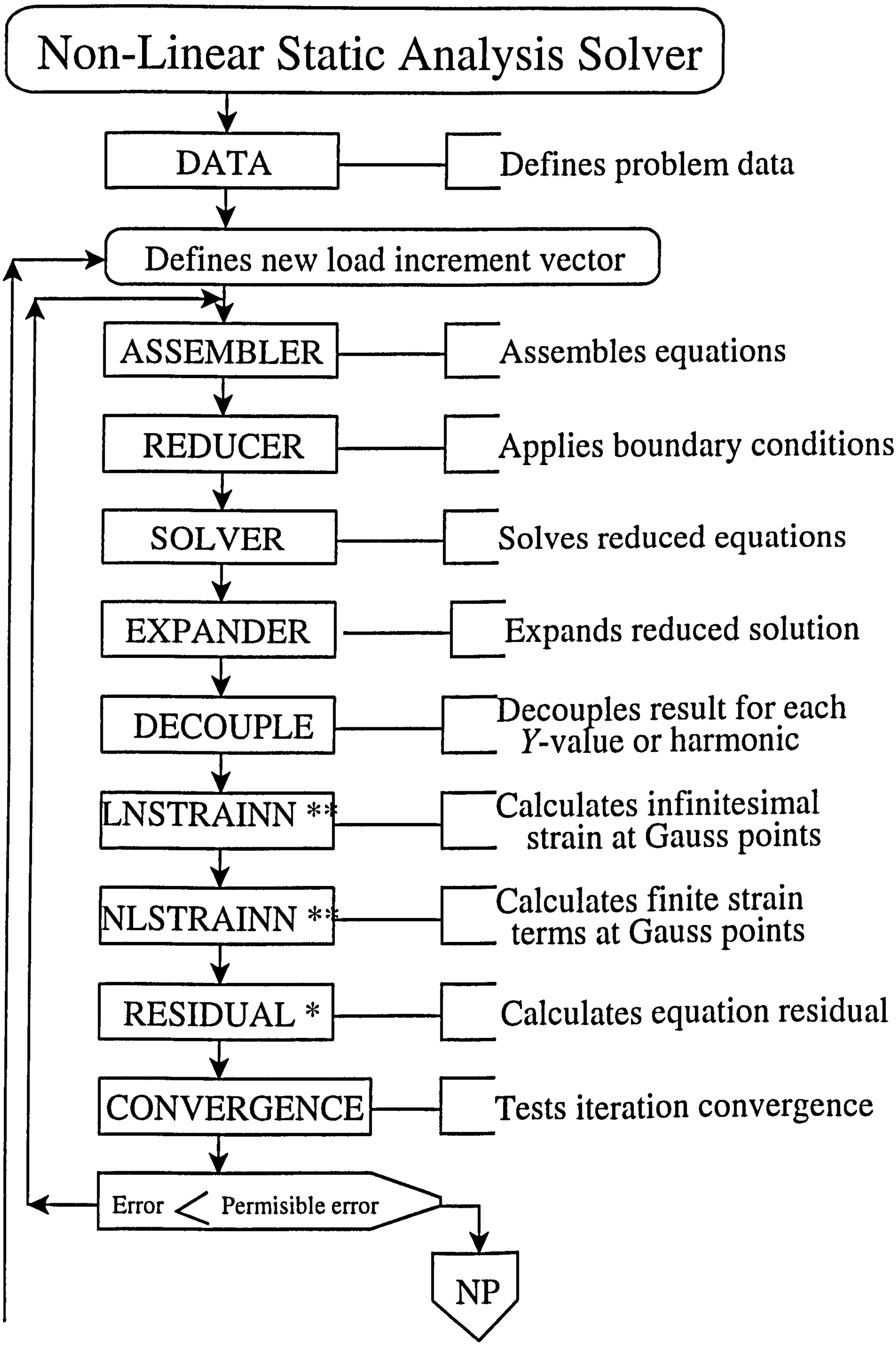

Figure 8.3 (Continued next page)

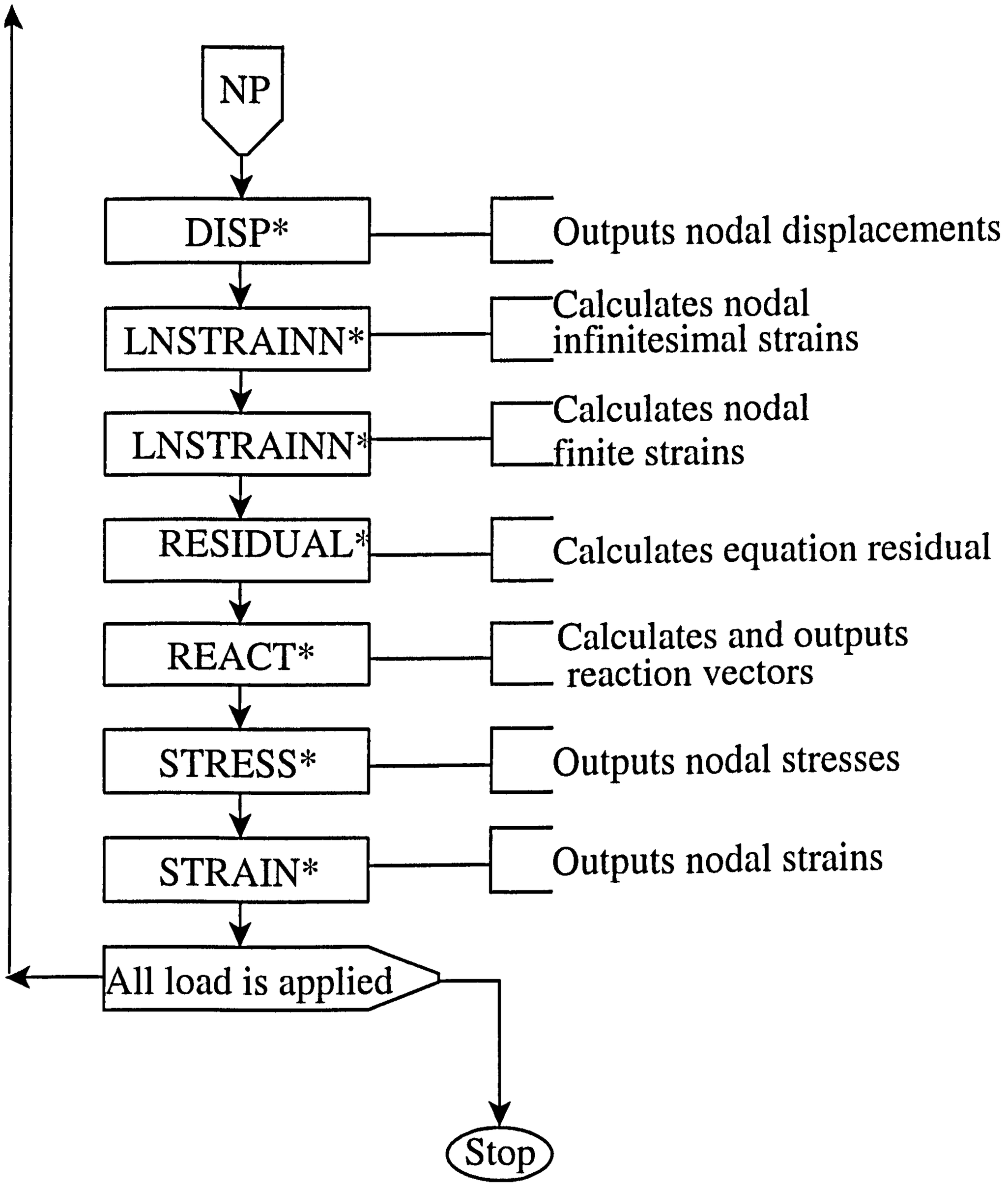

(*) These subroutines are in -LNS file
(**) These subroutines are in -NLS file

Figure 8.3 Non-linear static analysis solver

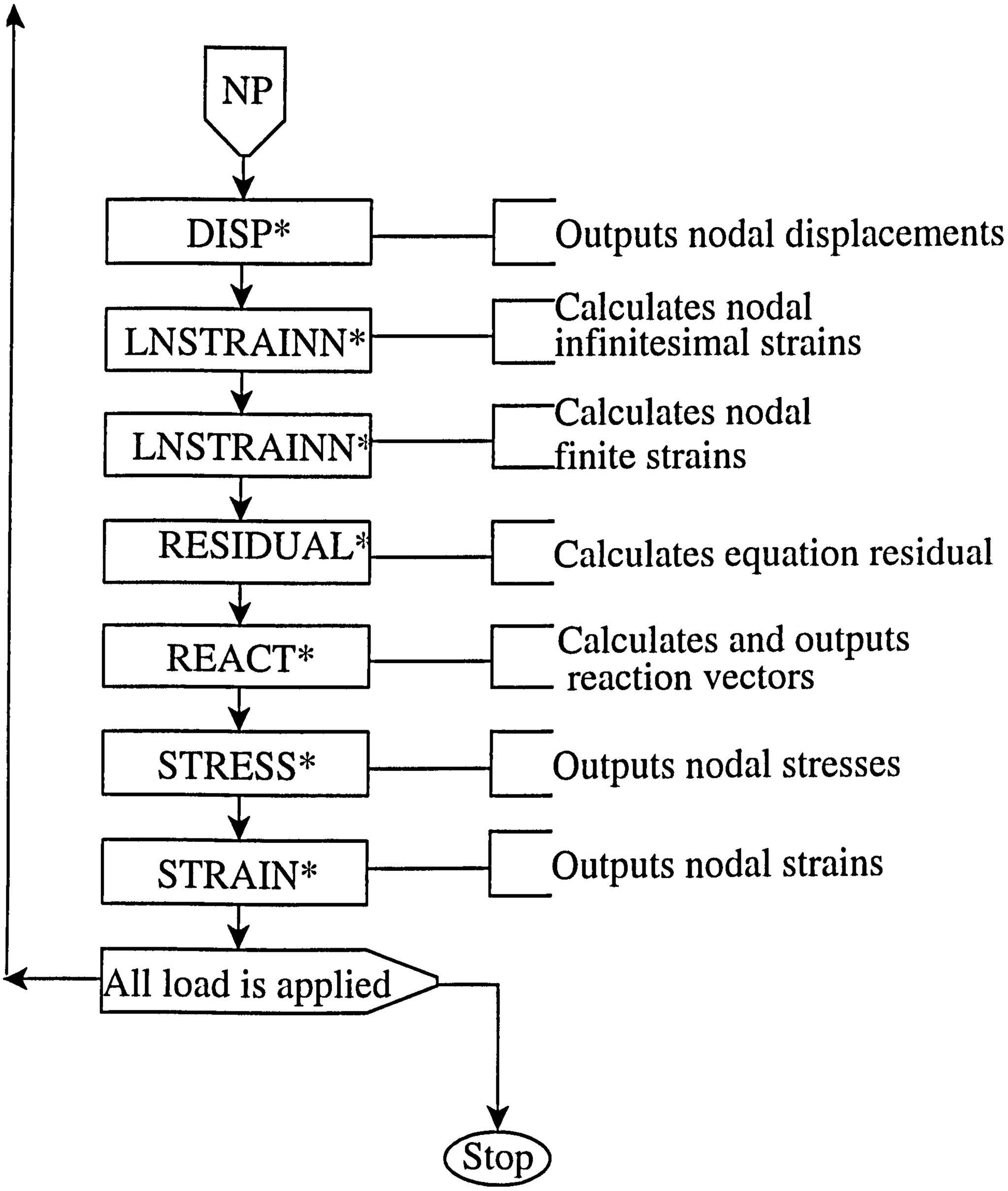

(*) These subroutines are in -LNS file
(**) These subroutines are in -NLS file

Figure 8.3 Non-linear static analysis solver

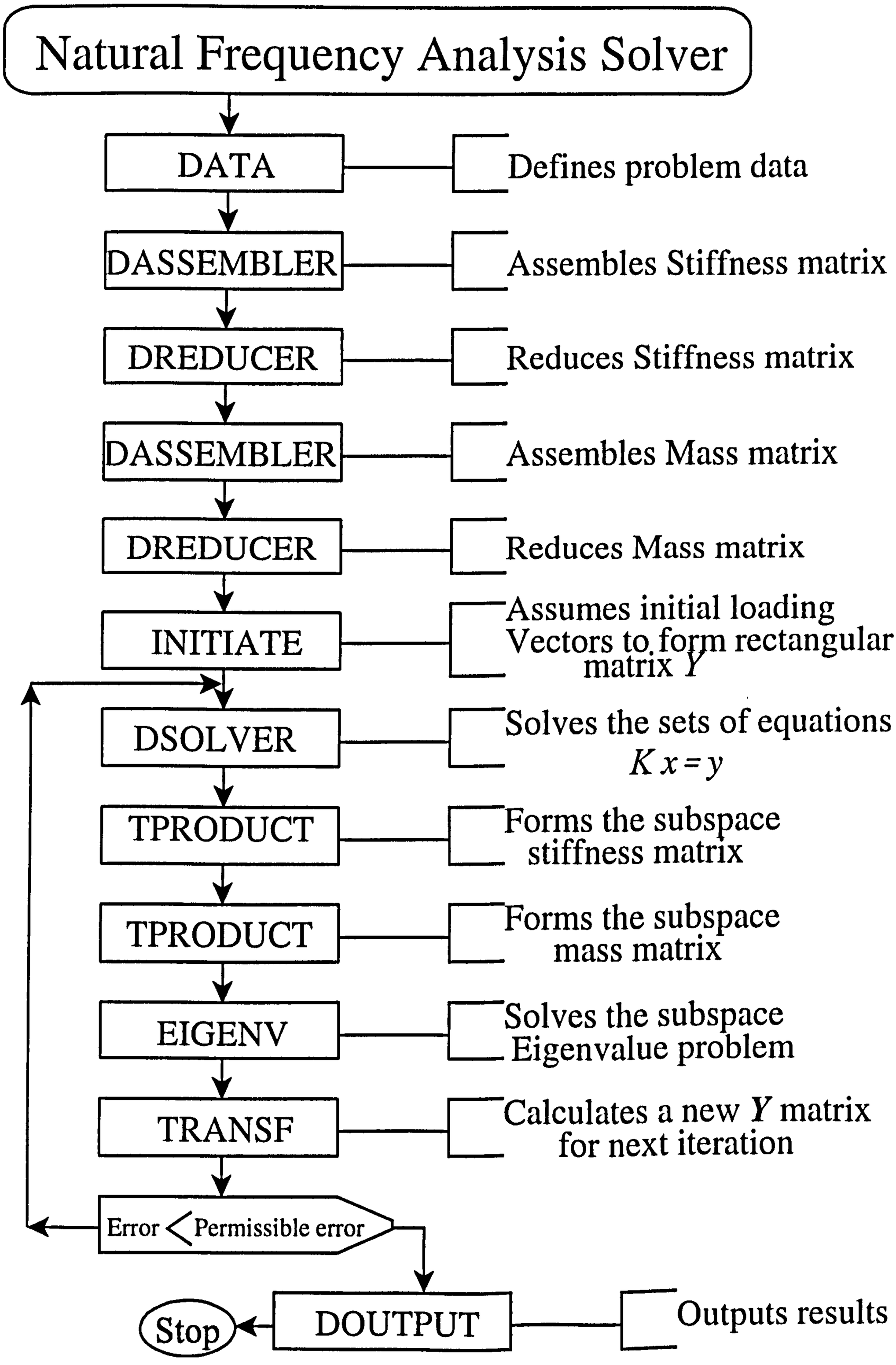

Figure 8.4 Natural frequency analysis solver

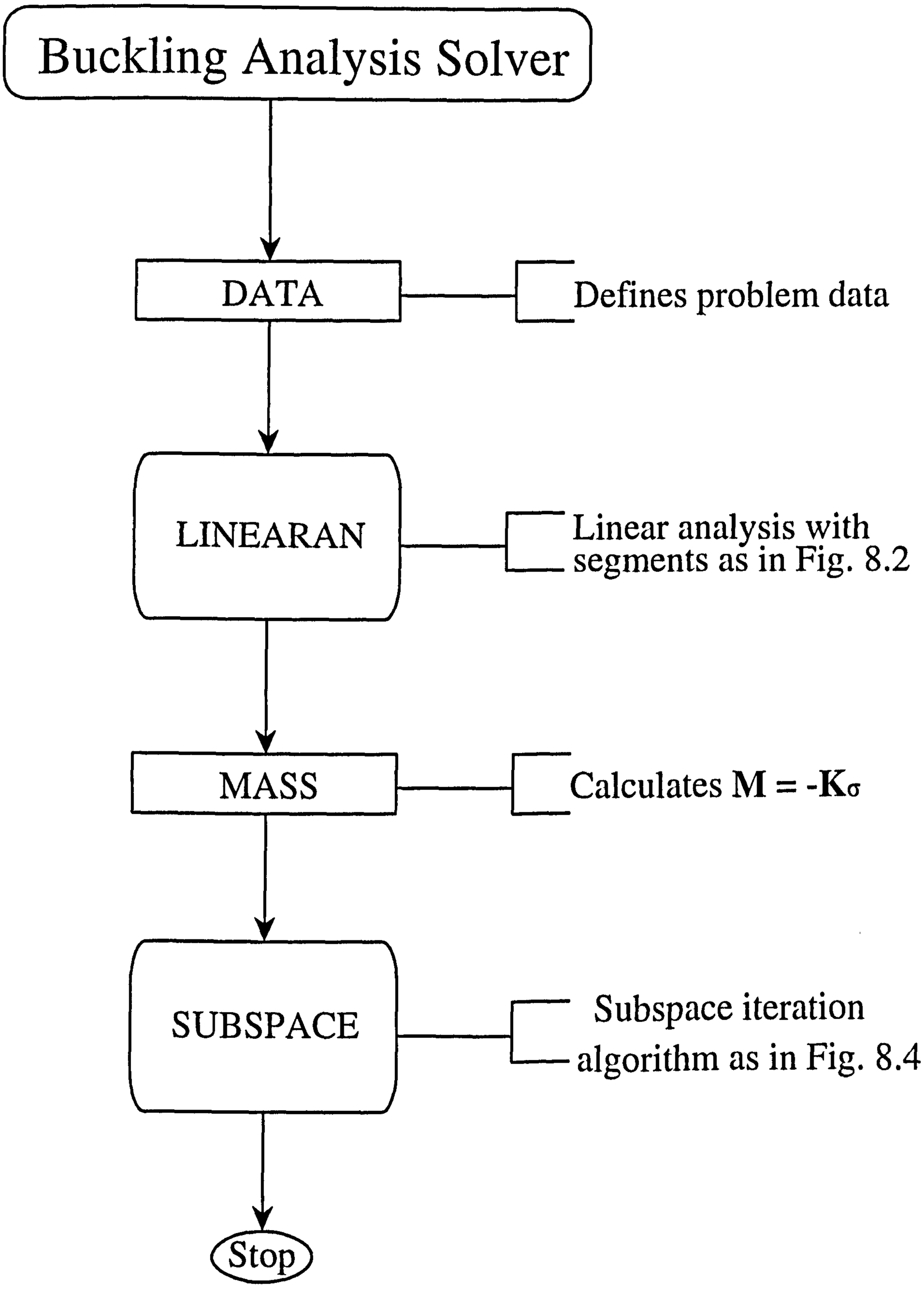

Figure 8.5 Buckling analysis solver

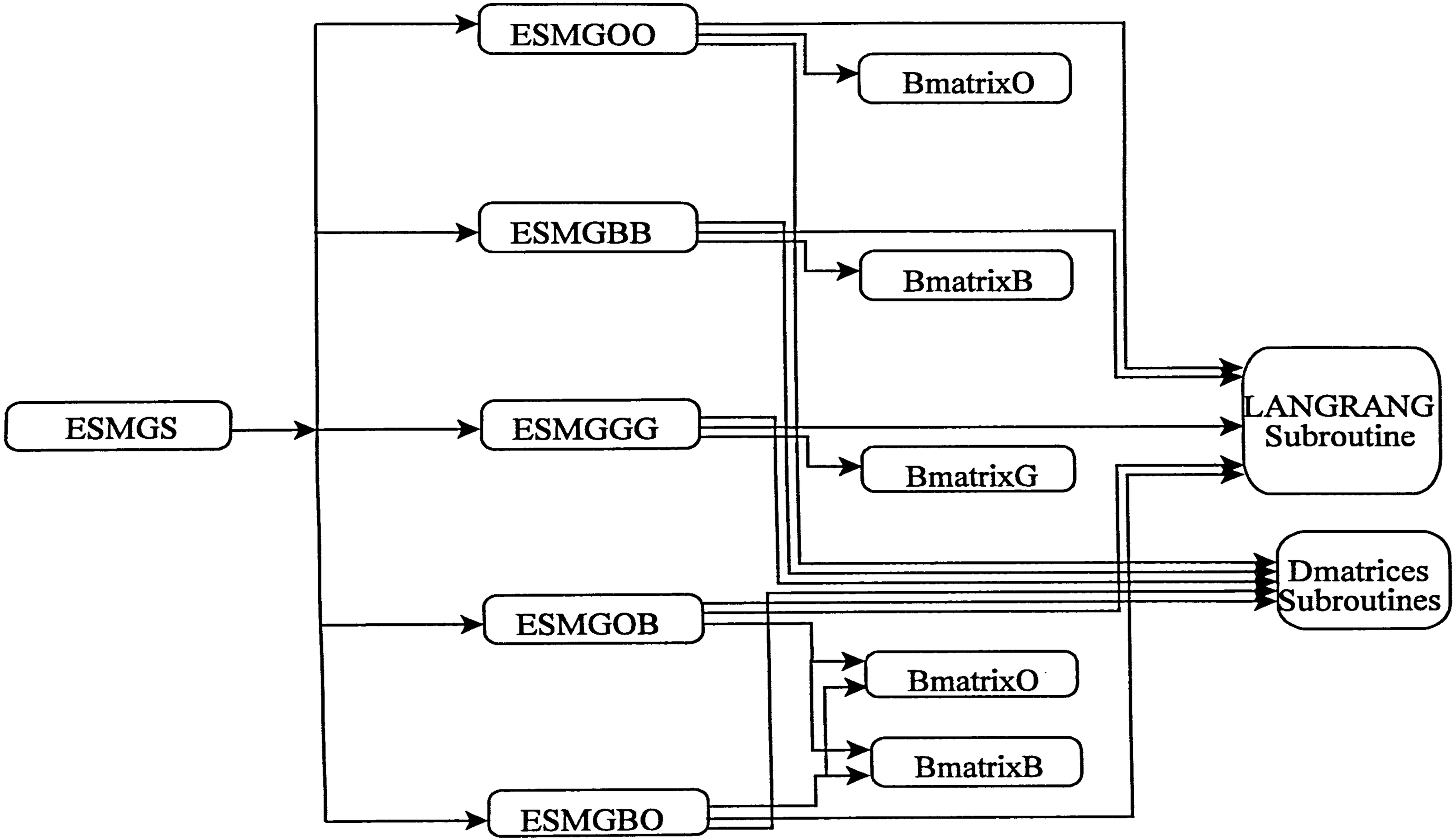

Figure 8.6 Element stiffness matrix generator for Mindlin-type elements

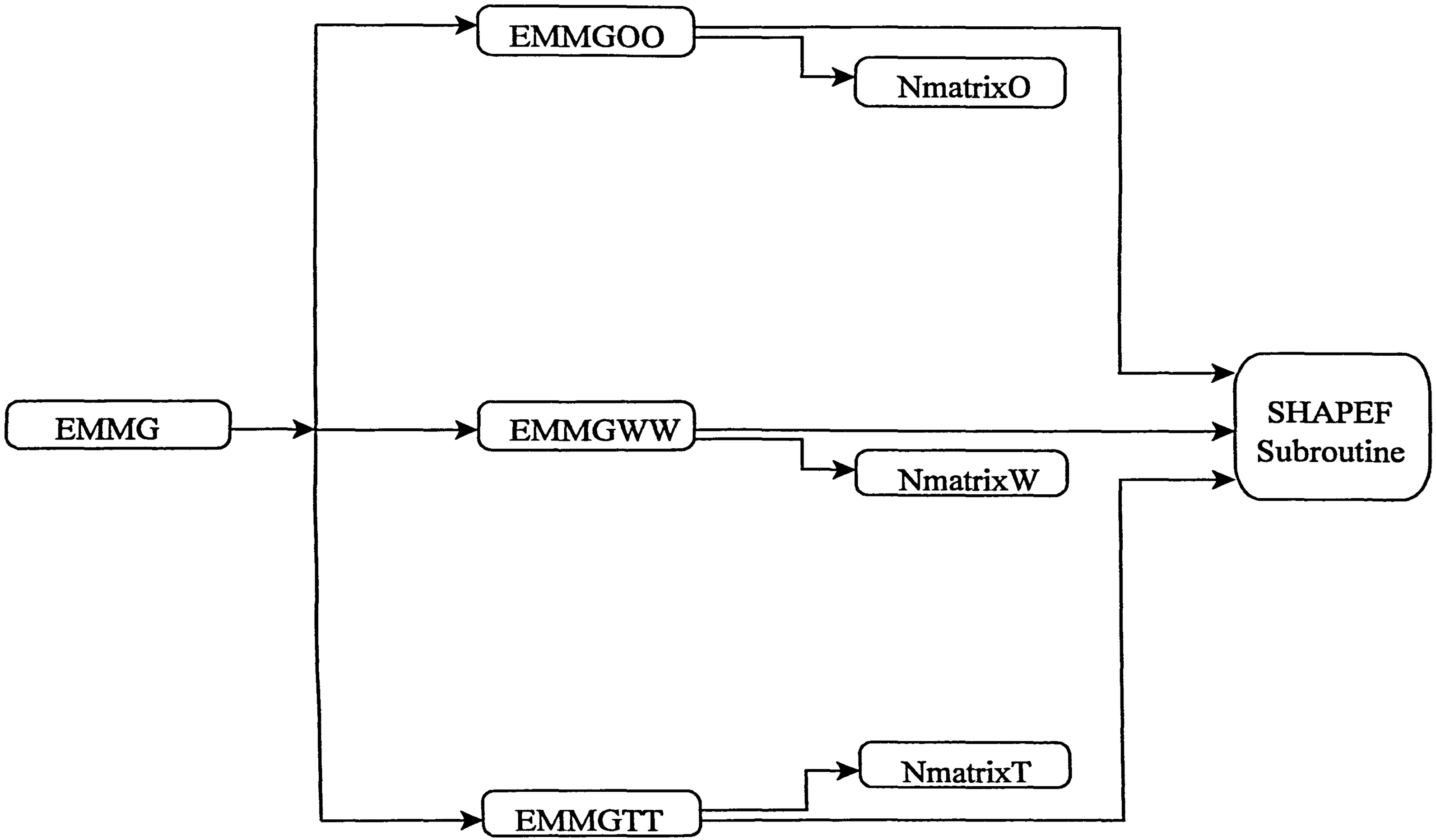

Figure 8.7 Element mass matrix generator for Mindlin-type elements

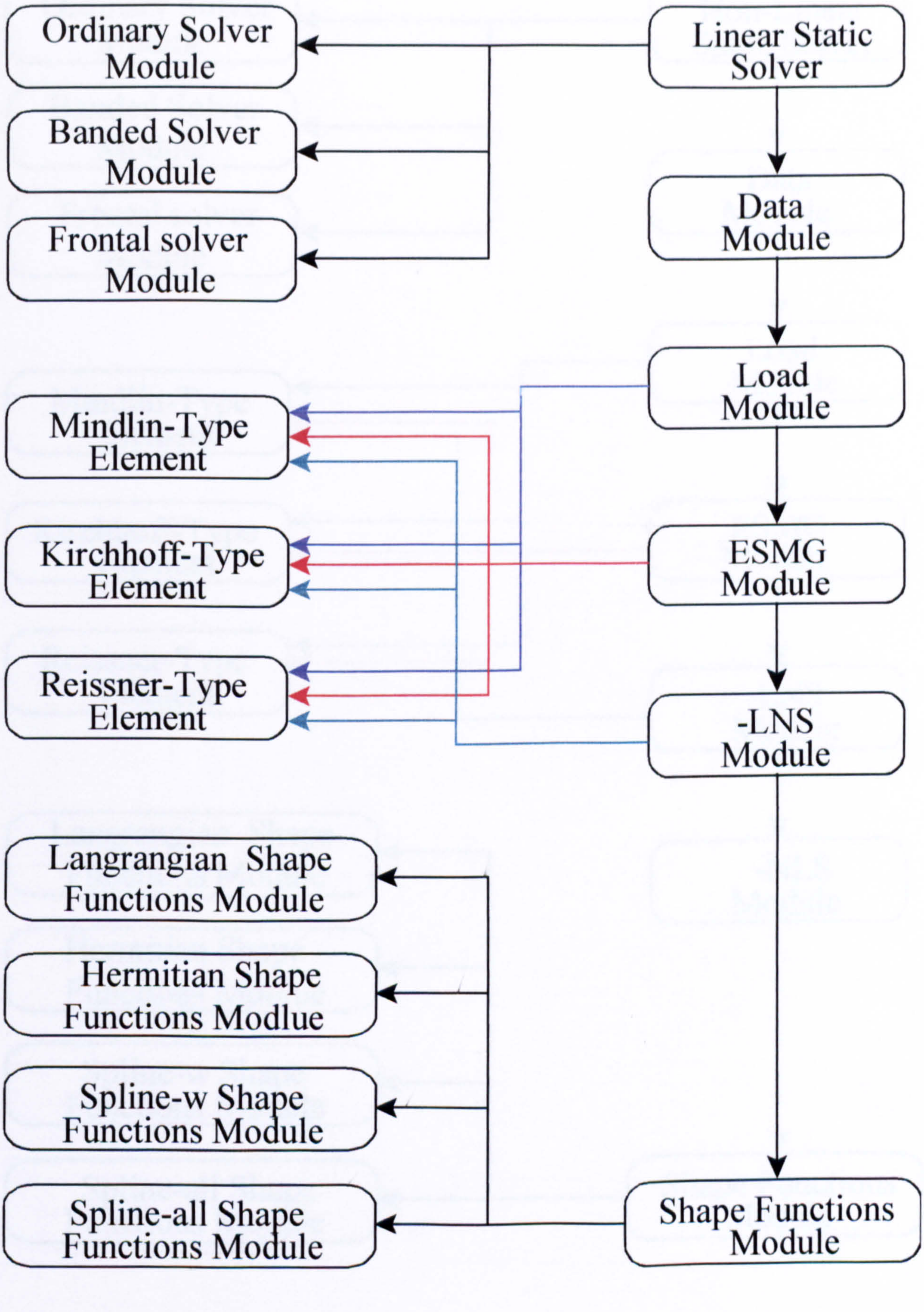

Figure 8.8 Linear static analysis modules

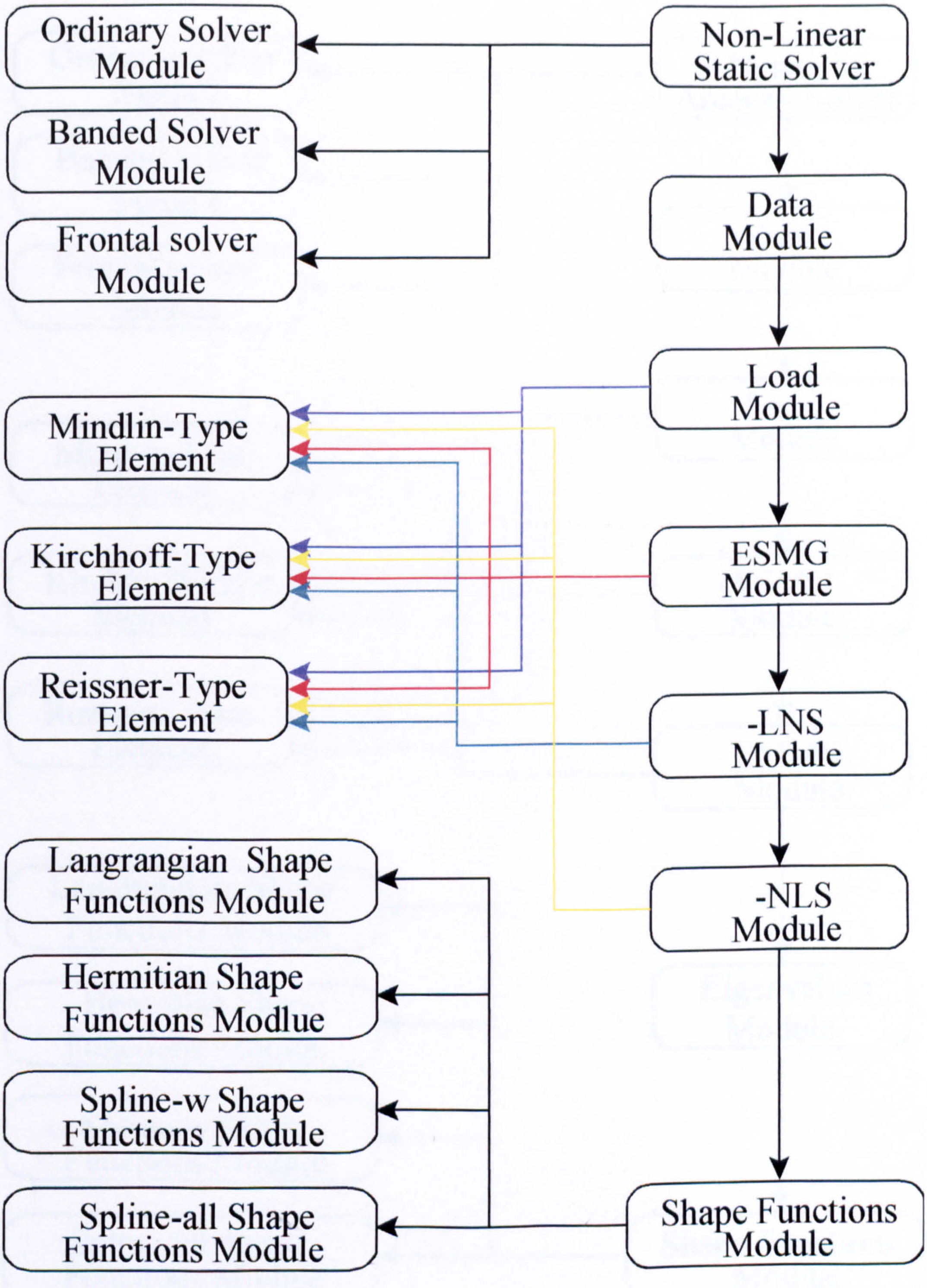

Figure 8.9 Non-linear static analysis modules

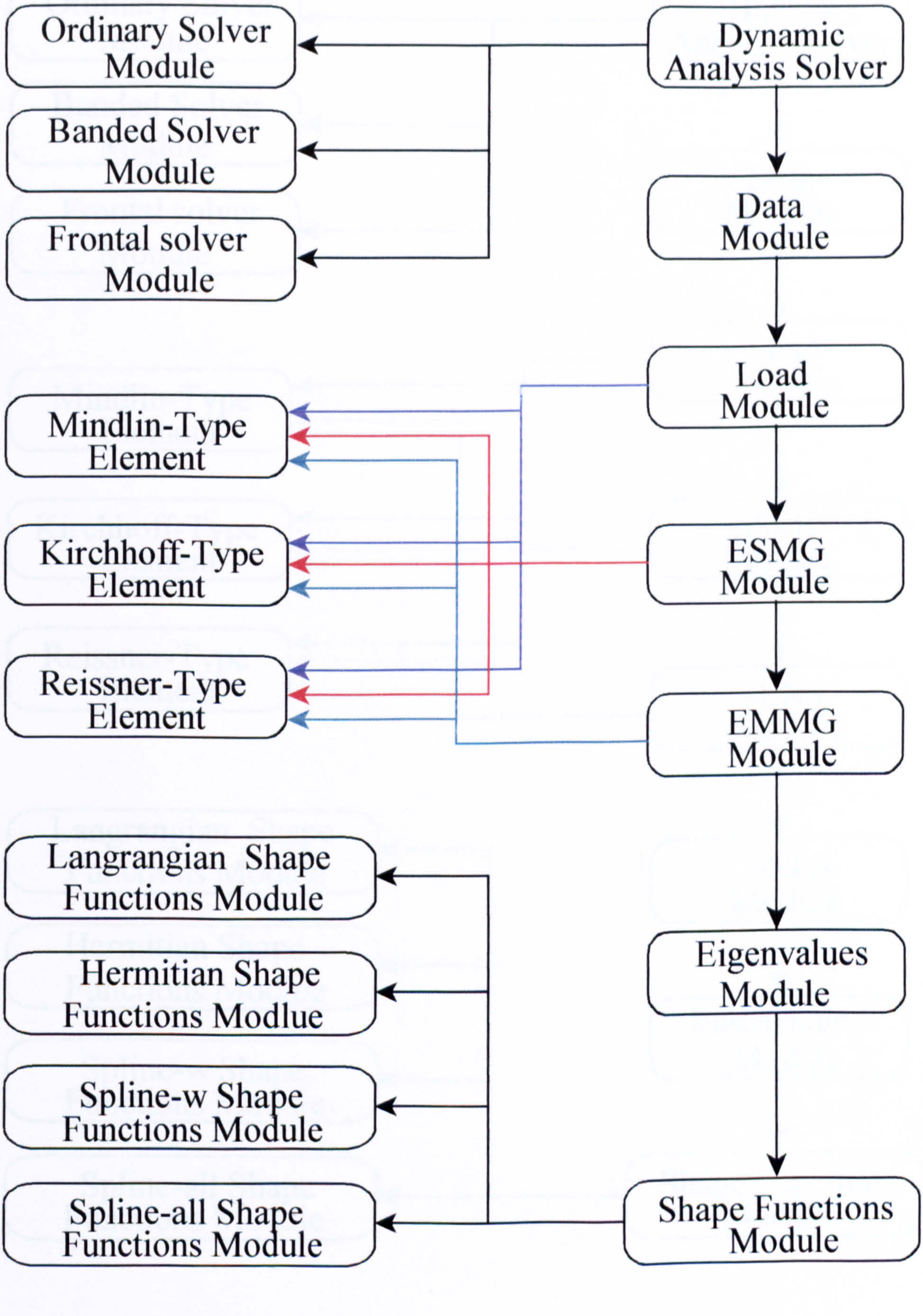

Figure 8.10 Natural frequency analysis modules

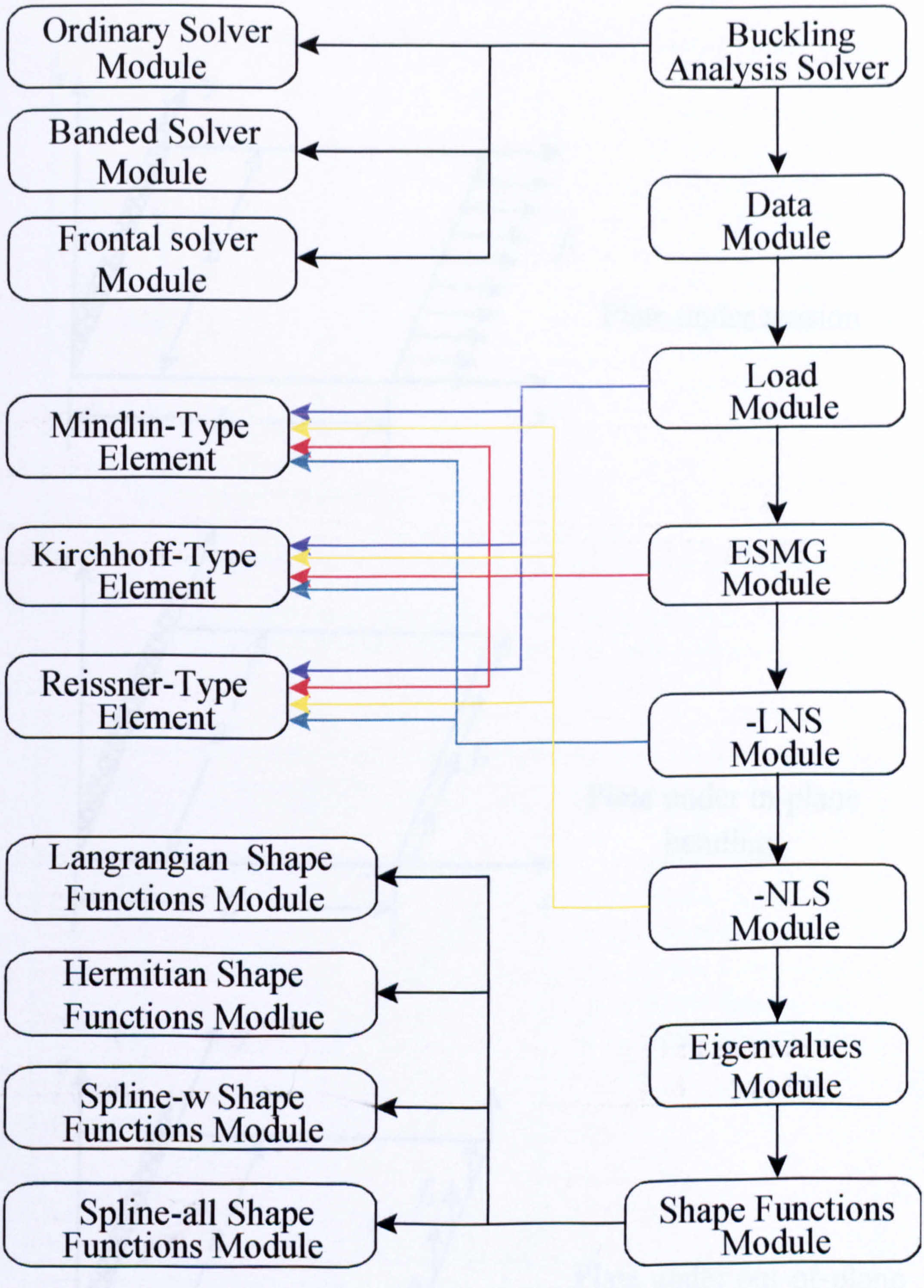

Figure 8.11 Buckling analysis modules

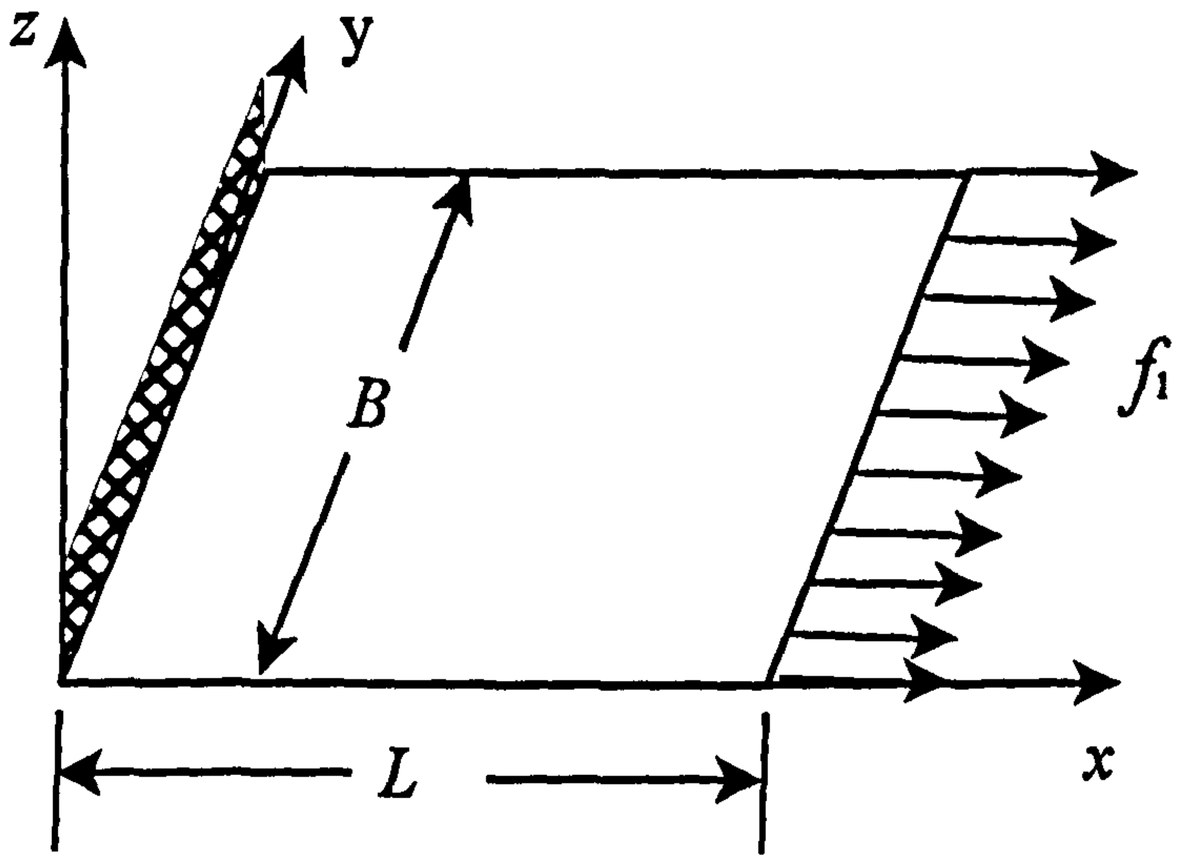

Plate under tension

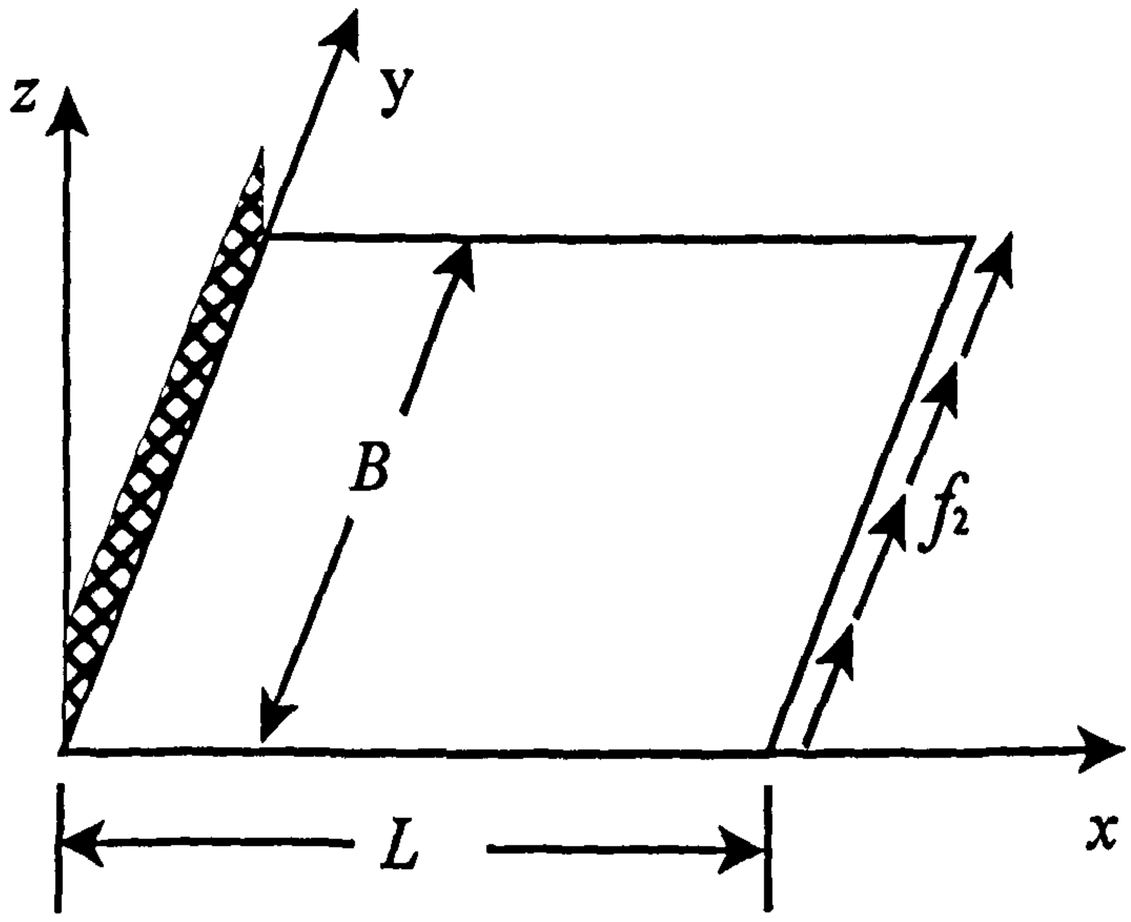

Plate under in-plane bending

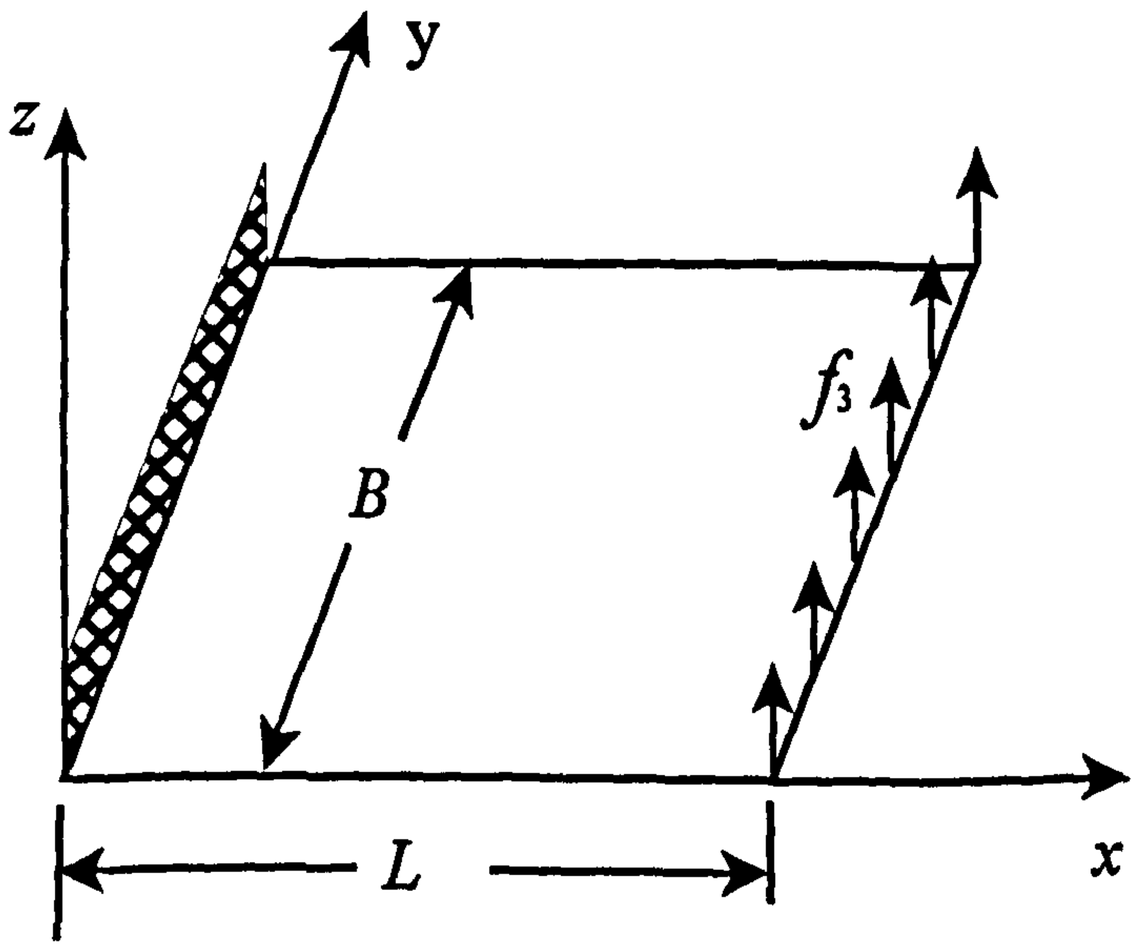

Plate under out-of-plane bending

Figure 9.1 Cantilever plate cases

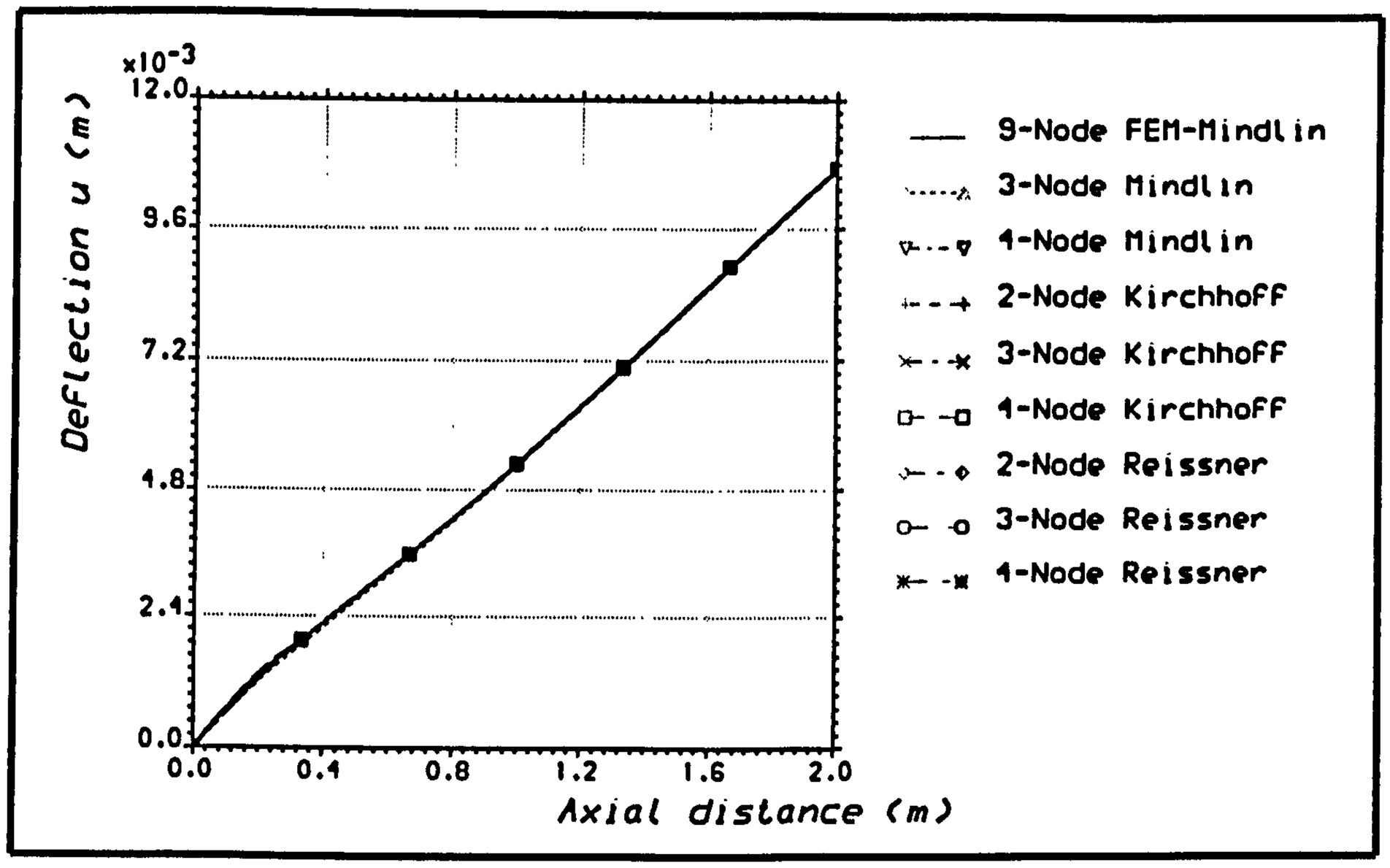

Figure 9.2 Axial displacement distribution for C/E cantilever plate under tension using polynomial finite strip elements, and linear analysis.

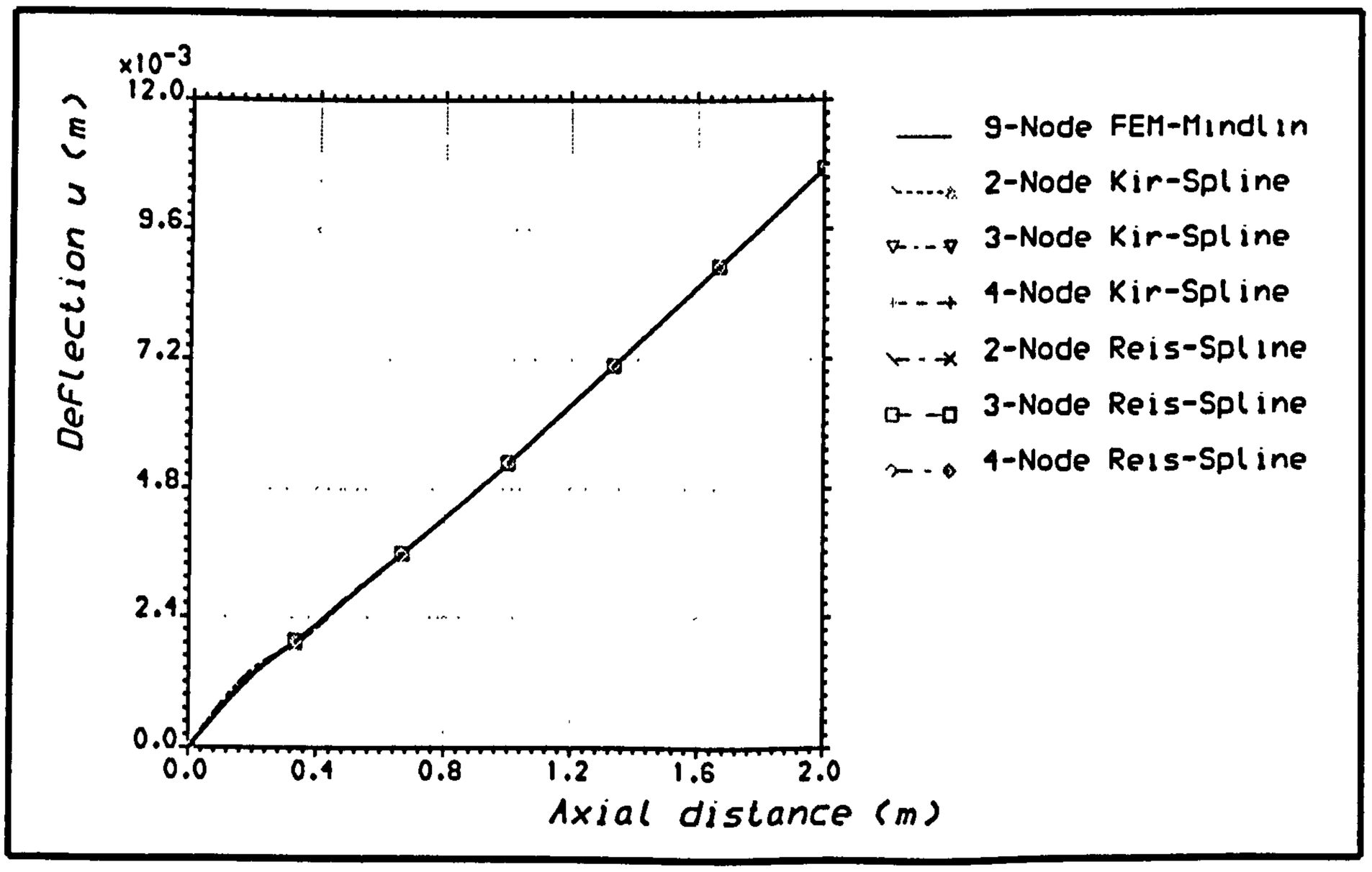

Figure 9.3 Axial displacement distribution for C/E cantilever plate under tension using spline-type finite strip elements, and linear analysis.

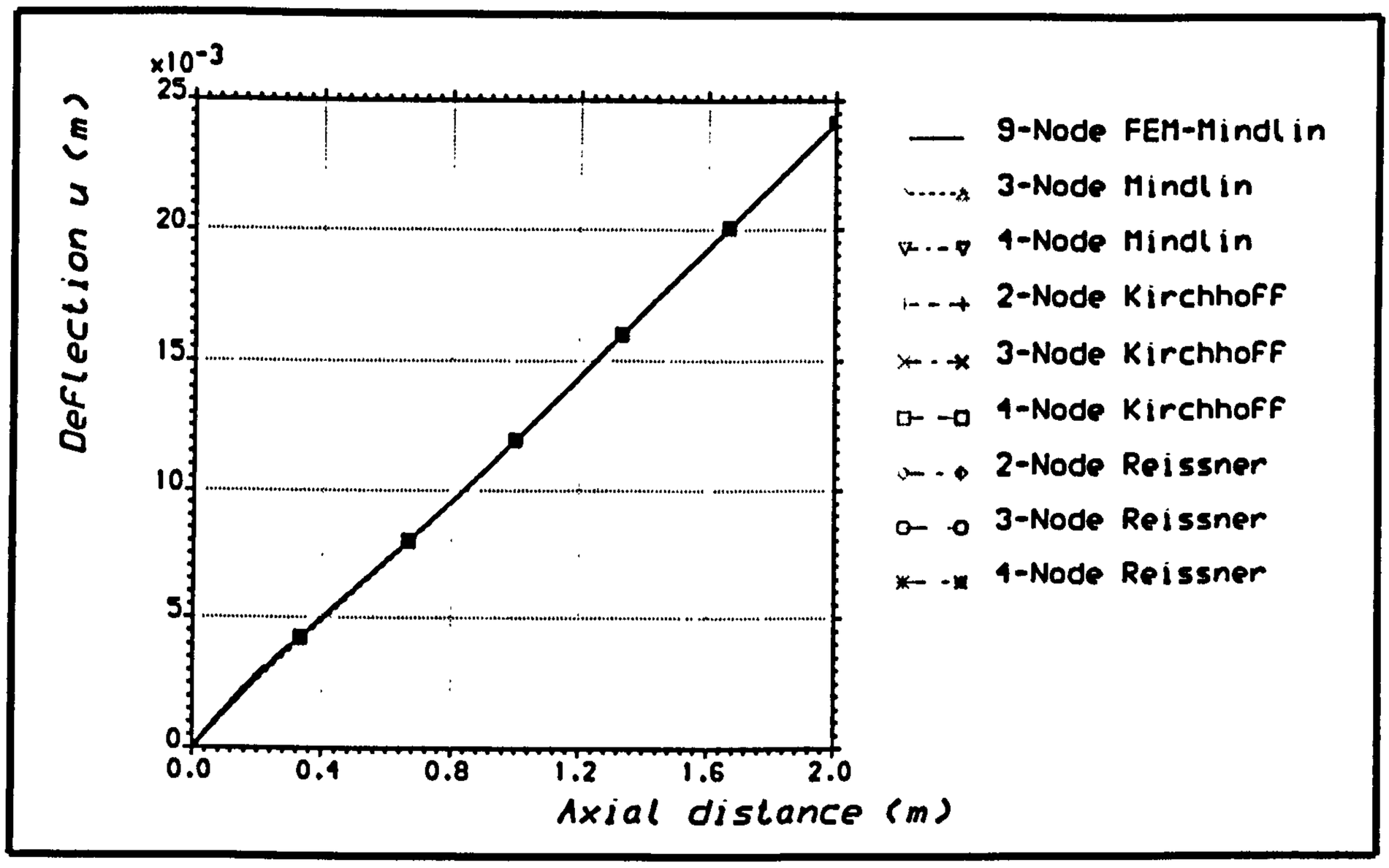

Figure 9.4 Axial displacement distribution for E/G cantilever plate under tension using polynomial finite strip elements, and linear analysis.

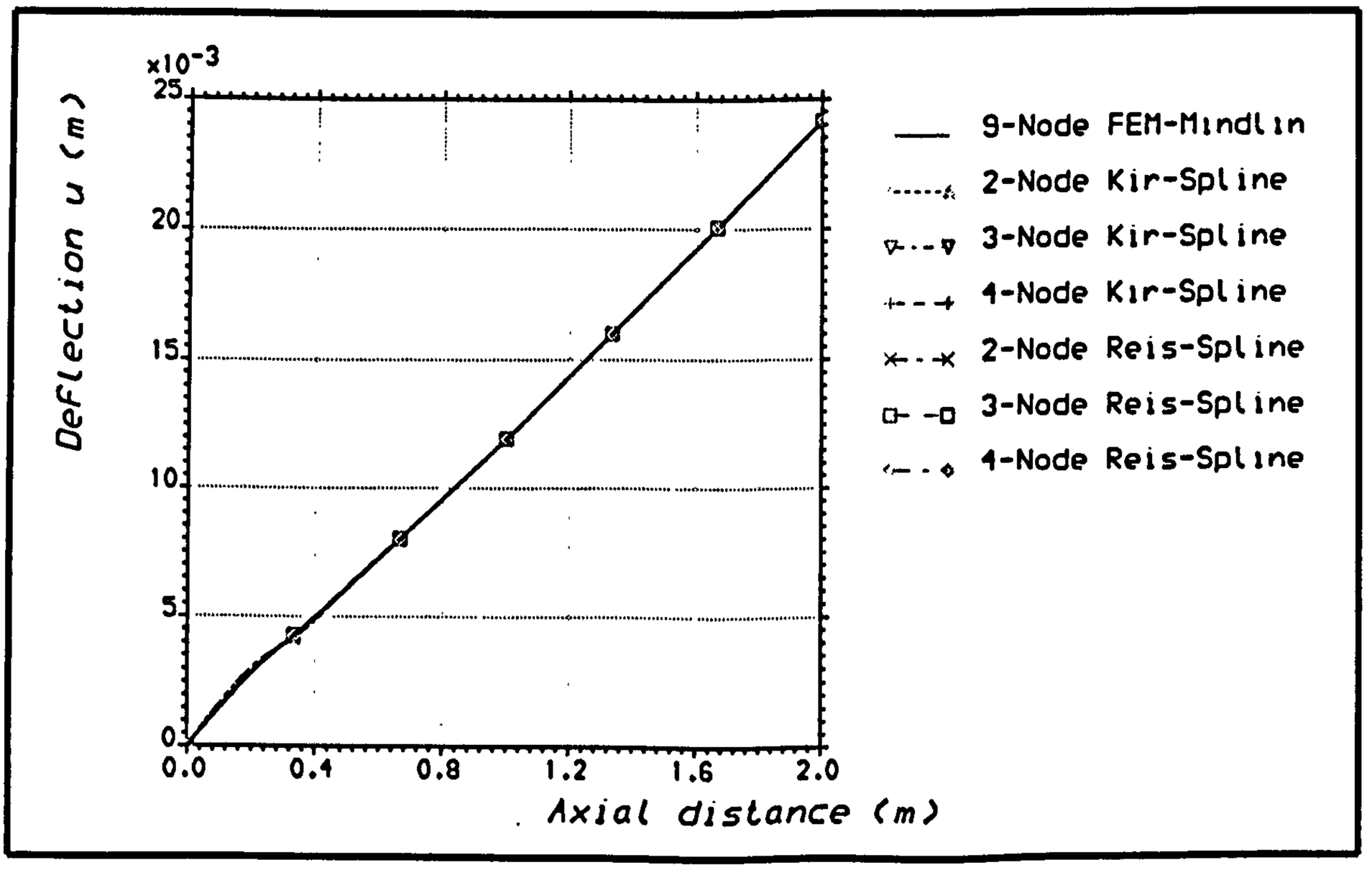

Figure 9.5 Axial displacement distribution for E/G cantilever plate under tension using spline-type finite strip elements, and linear analysis.

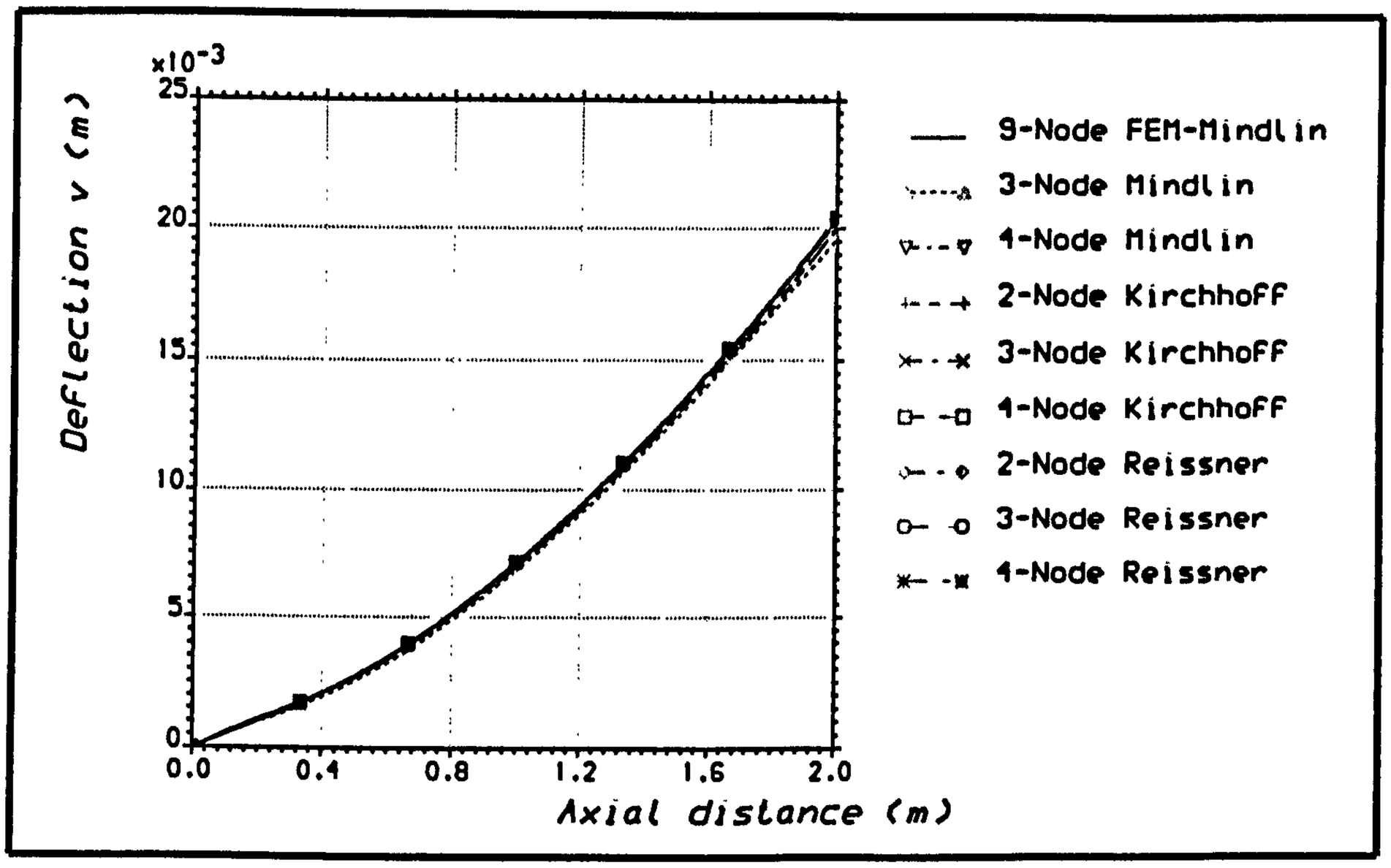

Figure 9.6 Transverse displacement distribution for C/E cantilever plate under in-plane bending, using polynomial strip elements, and linear analysis.

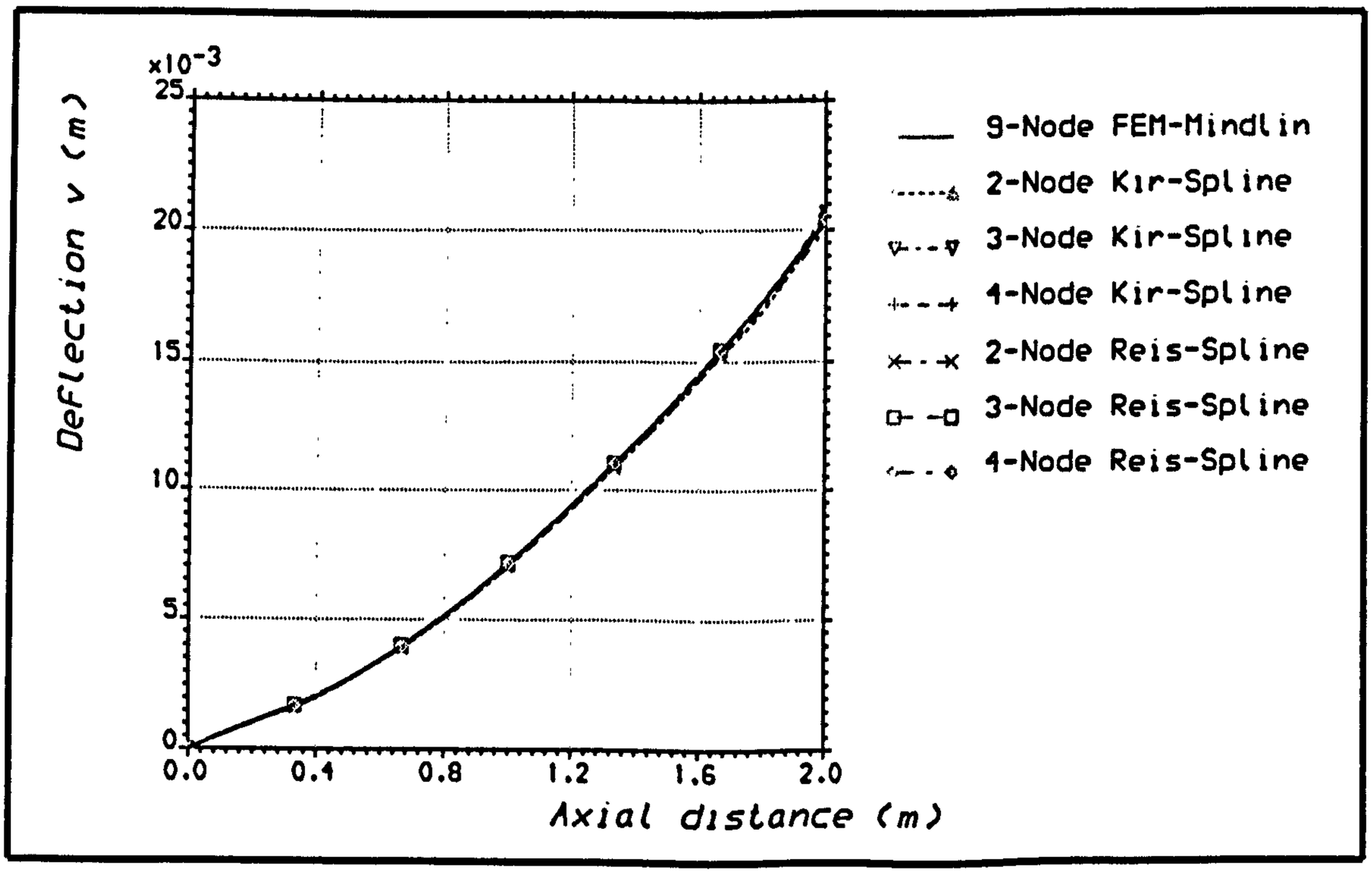

Figure 9.7 Transverse displacement distribution for C/E cantilever plate under in-plane bending, using spline-type strip elements, and linear analysis.

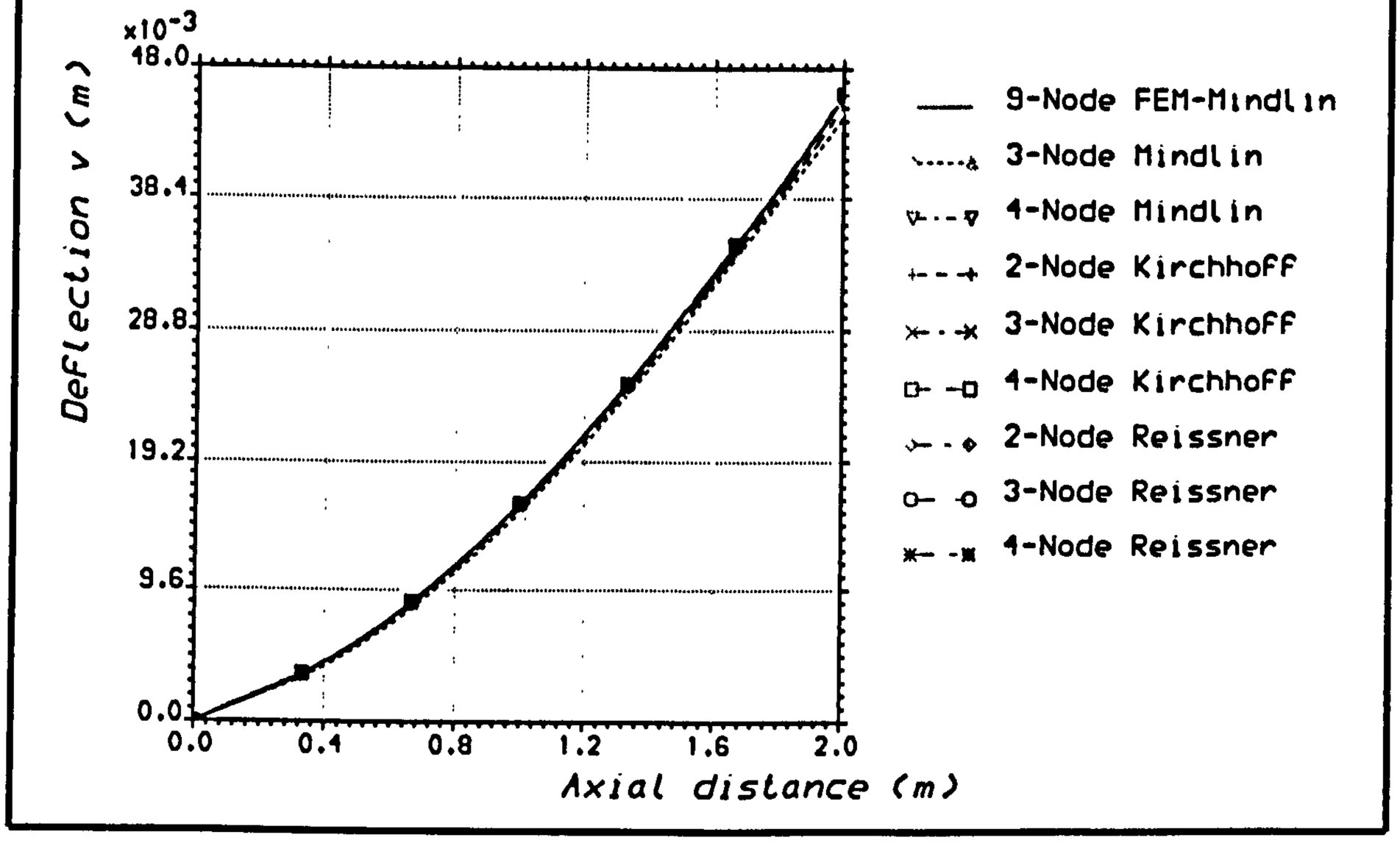

Figure 9.8 Transverse displacement distribution for E/G cantilever plate under in-plane bending, using polynomial strip elements, and linear analysis.

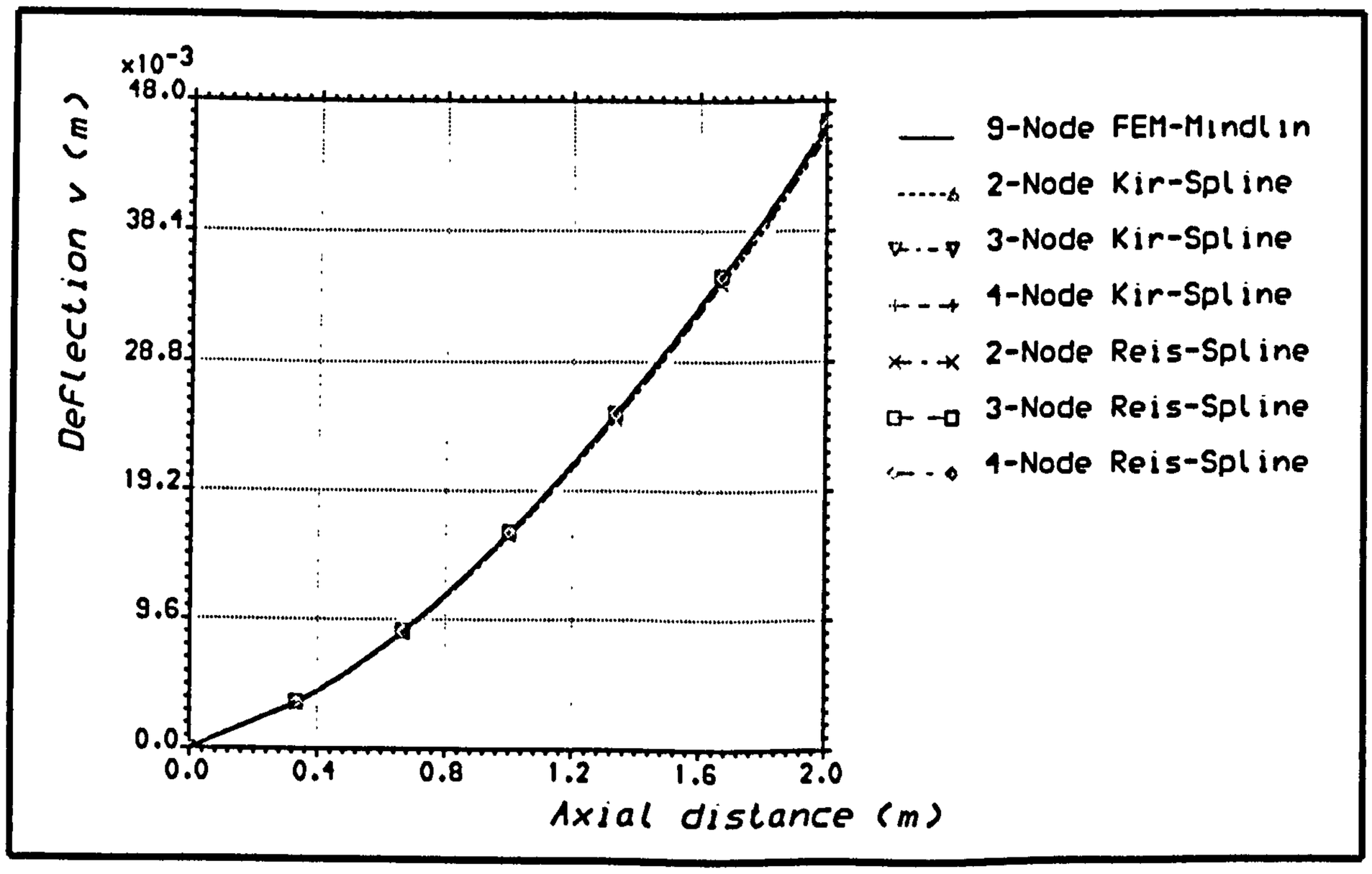

Figure 9.9 Transverse displacement distribution for E/G cantilever plate under in-plane bending, using spline-type strip elements, and linear analysis.

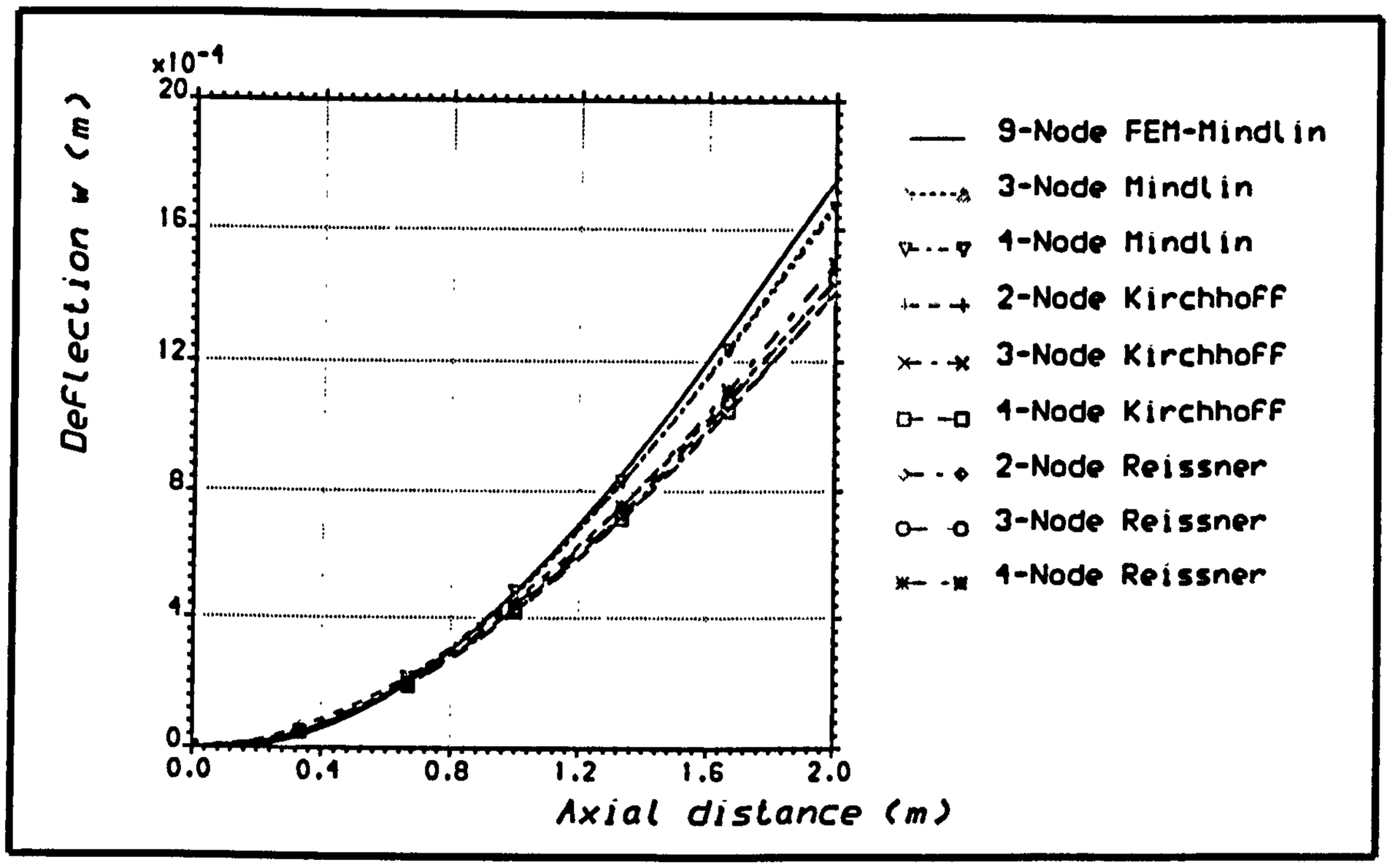

Figure 9.10 Lateral displacement distribution for C/E cantilever plate under out-of-plane bending, using polynomial strip elements, and linear analysis.

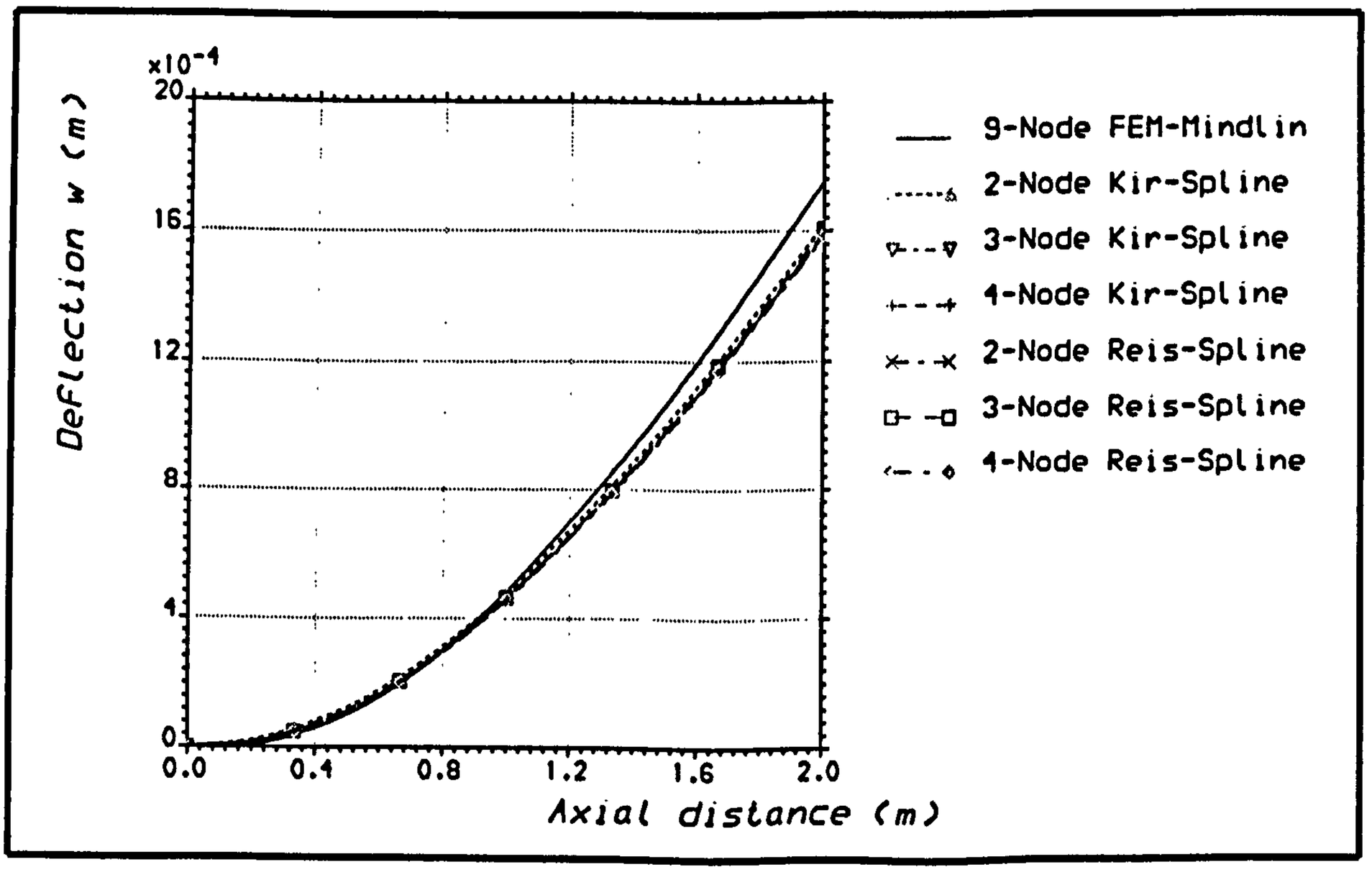

Figure 9.11 Lateral displacement distribution for C/E cantilever plate under out-of-plane bending, using spline-type strip elements, and linear analysis.

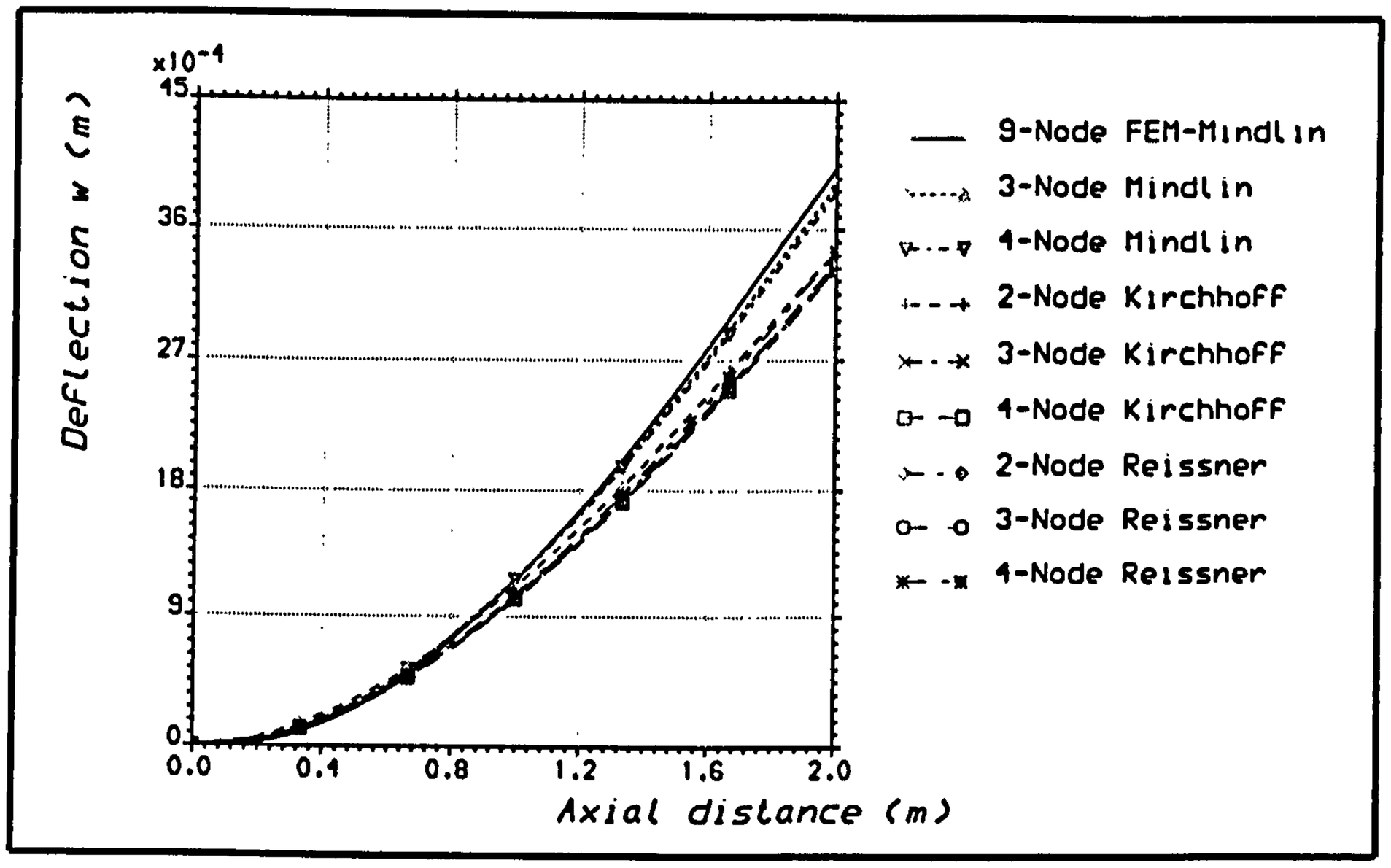

Figure 9.12 Lateral displacement distribution for E/G cantilever plate under out-of-plane bending, using polynomial strip elements, and linear analysis.

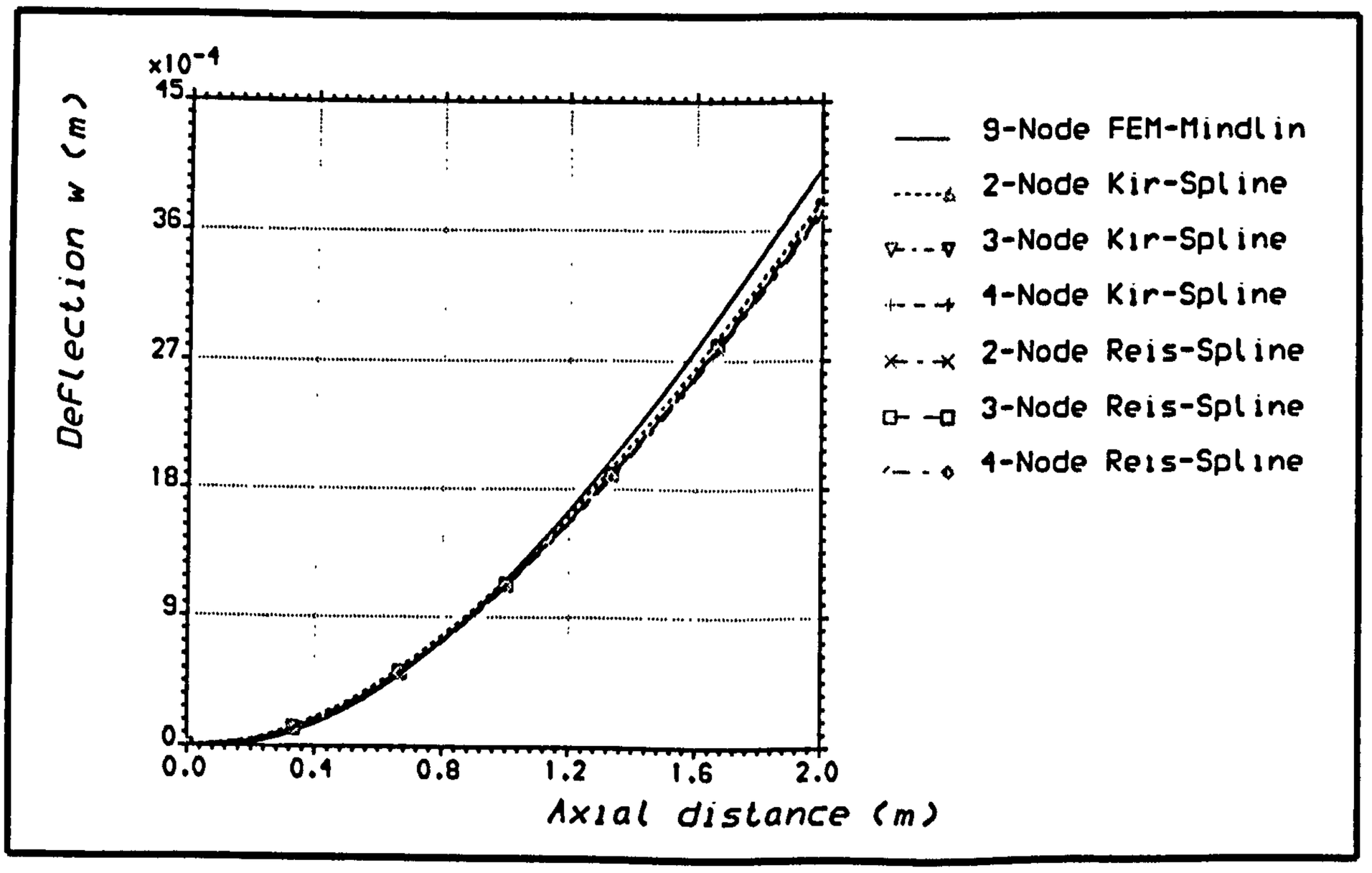

Figure 9.13 Lateral displacement distribution for E/G cantilever plate under out-of-plane bending, using spline-type strip elements, and linear analysis.

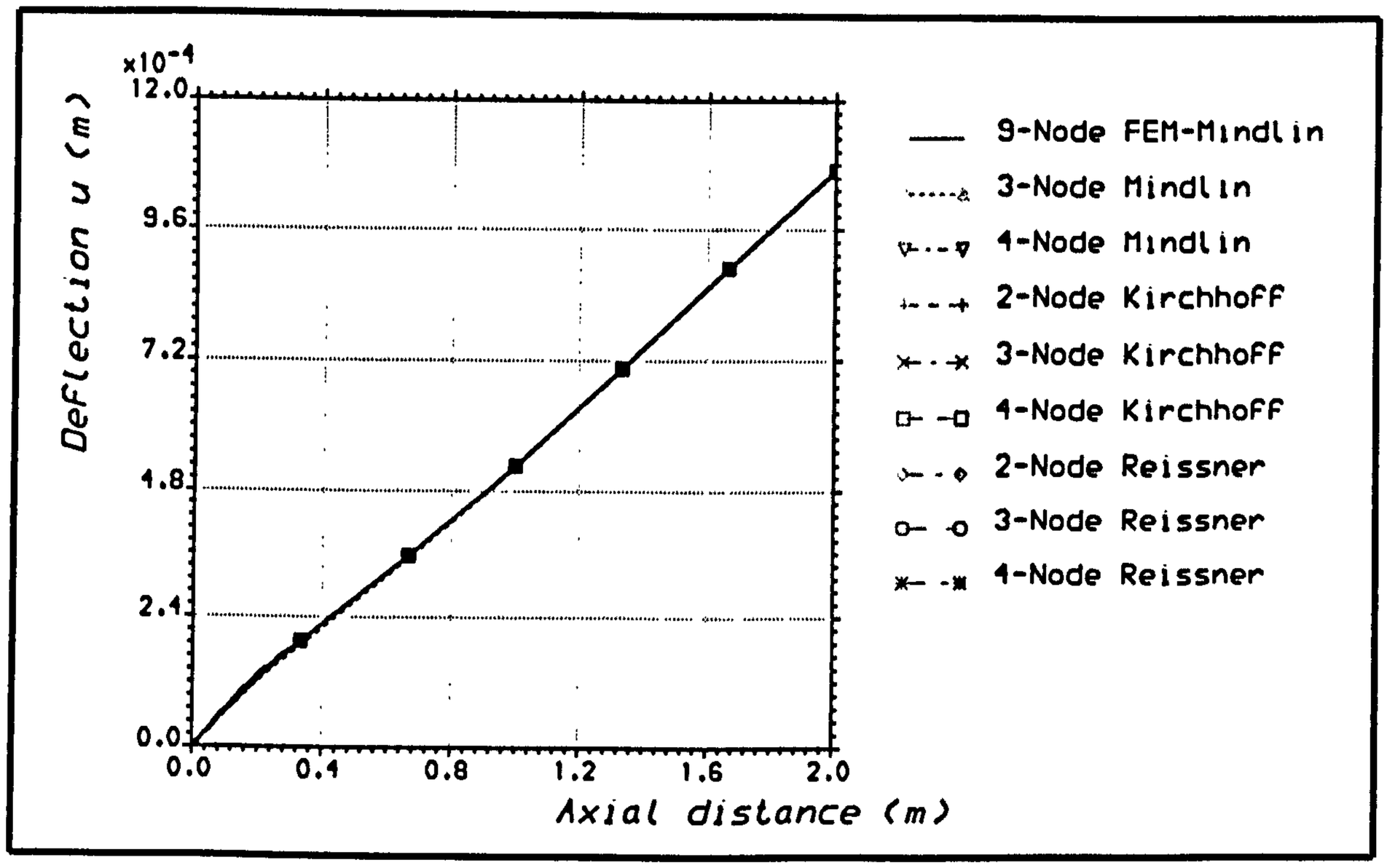

Figure 9.14 Axial displacement distribution for C/E cantilever plate under tension using polynomial finite strip elements, and non-linear analysis.

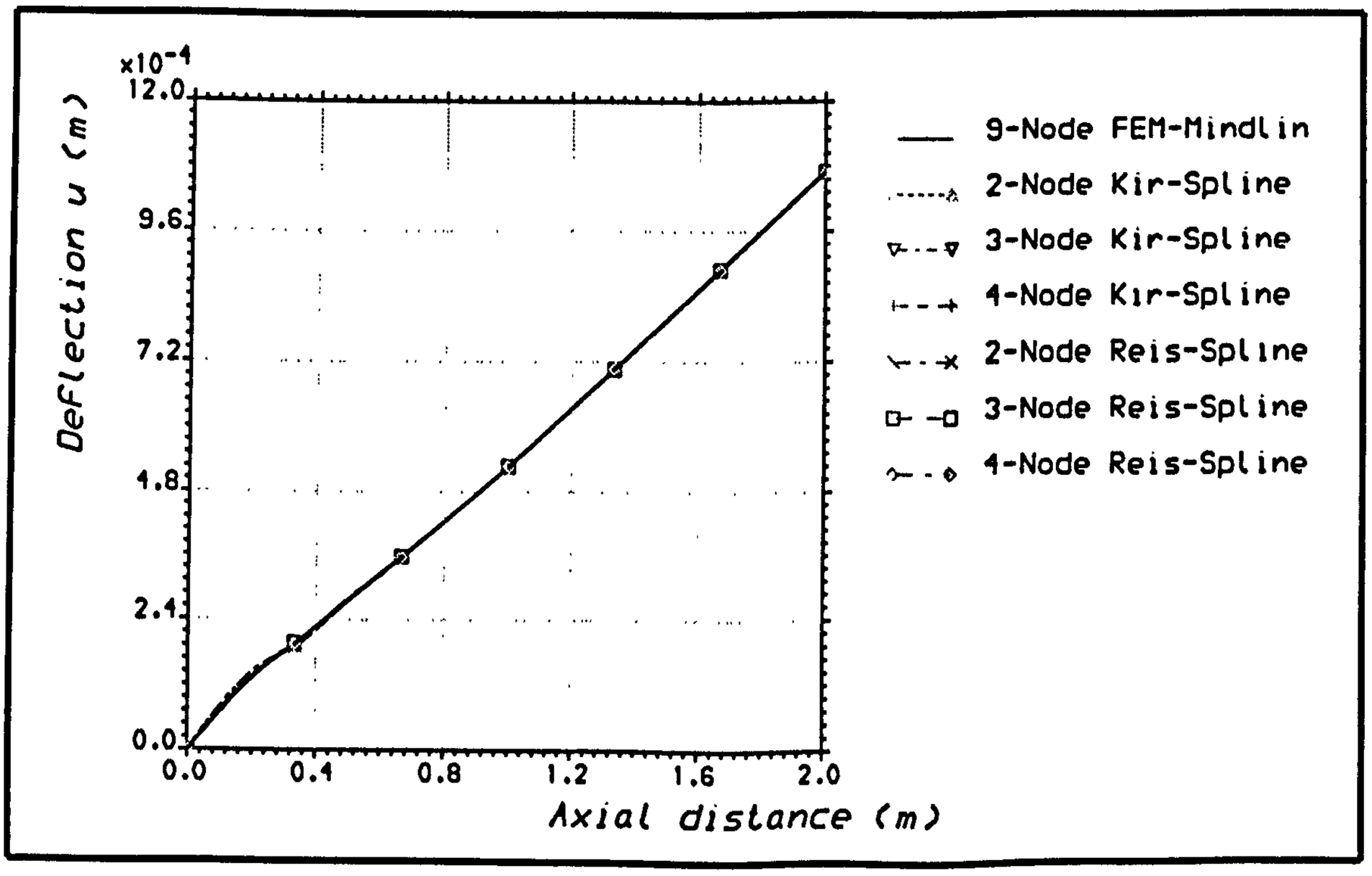

Figure 9.15 Axial displacement distribution for C/E cantilever plate under tension using spline-type finite strip elements, and non-linear analysis.

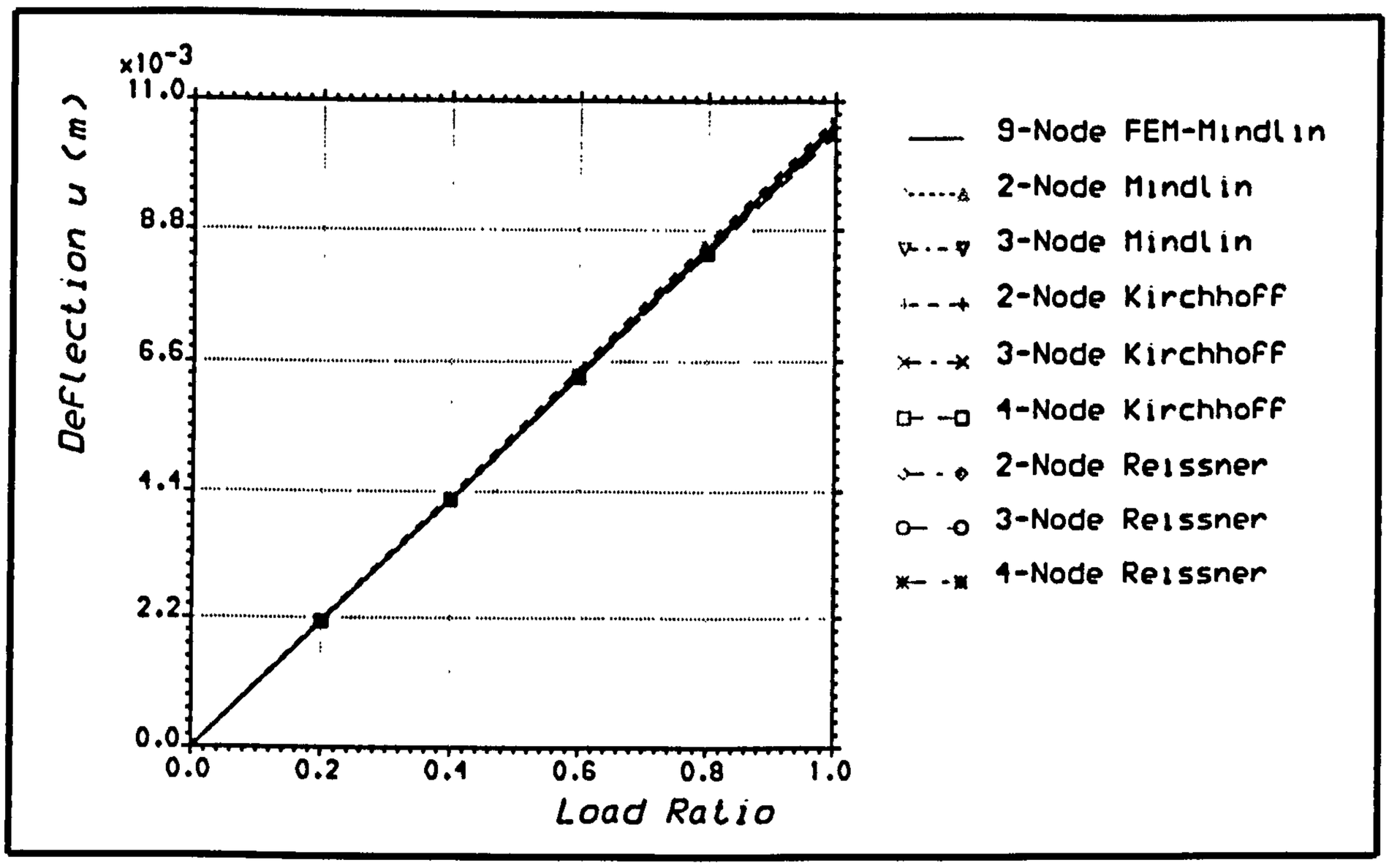

Figure 9.16 Axial displacement versus load for C/E cantilever plate under tension using polynomial finite strip elements, and non-linear analysis.

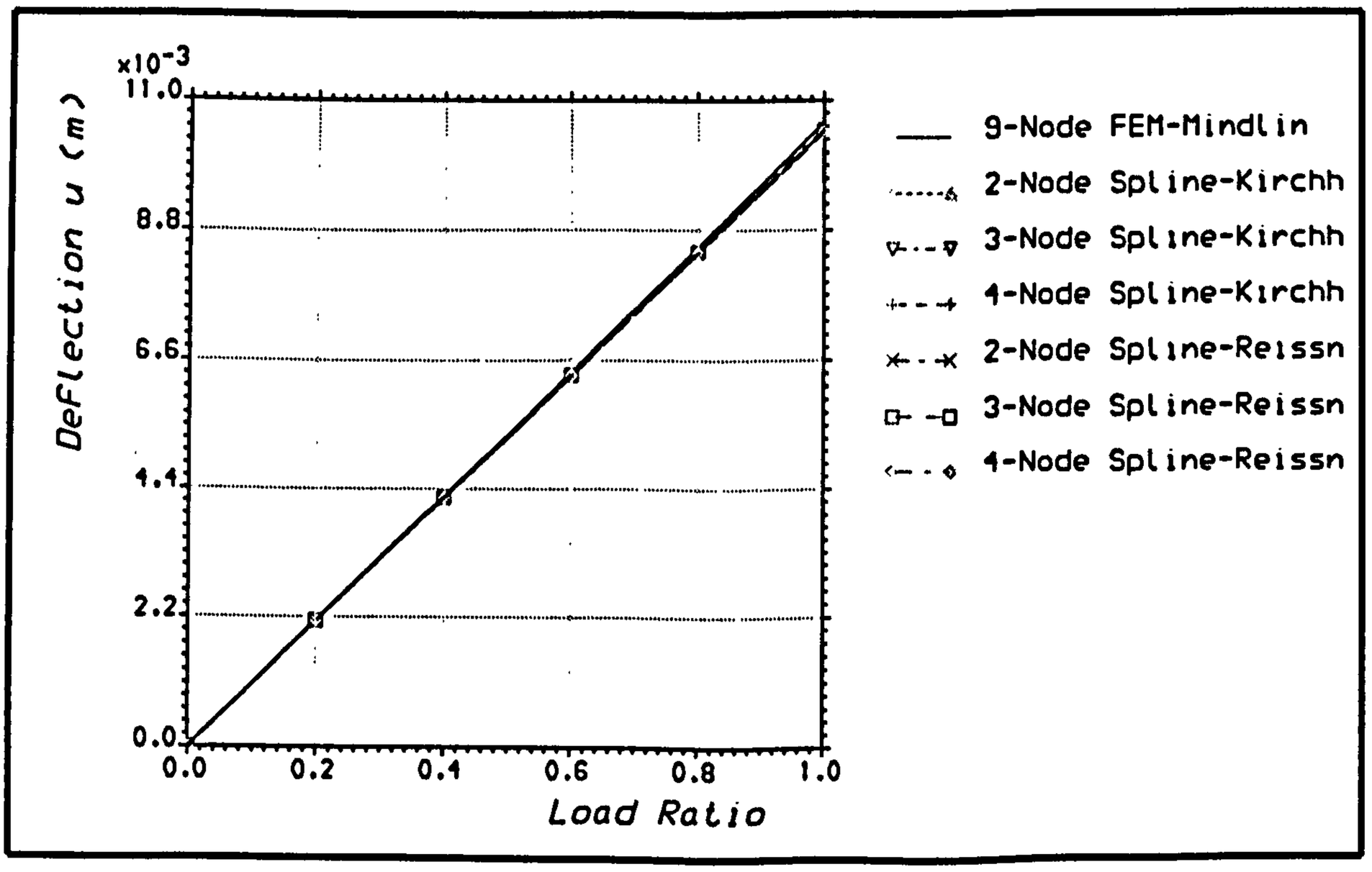

Figure 9.17 Axial displacement versus load for C/E cantilever plate under tension using spline-type finite strip elements, and non-linear analysis.

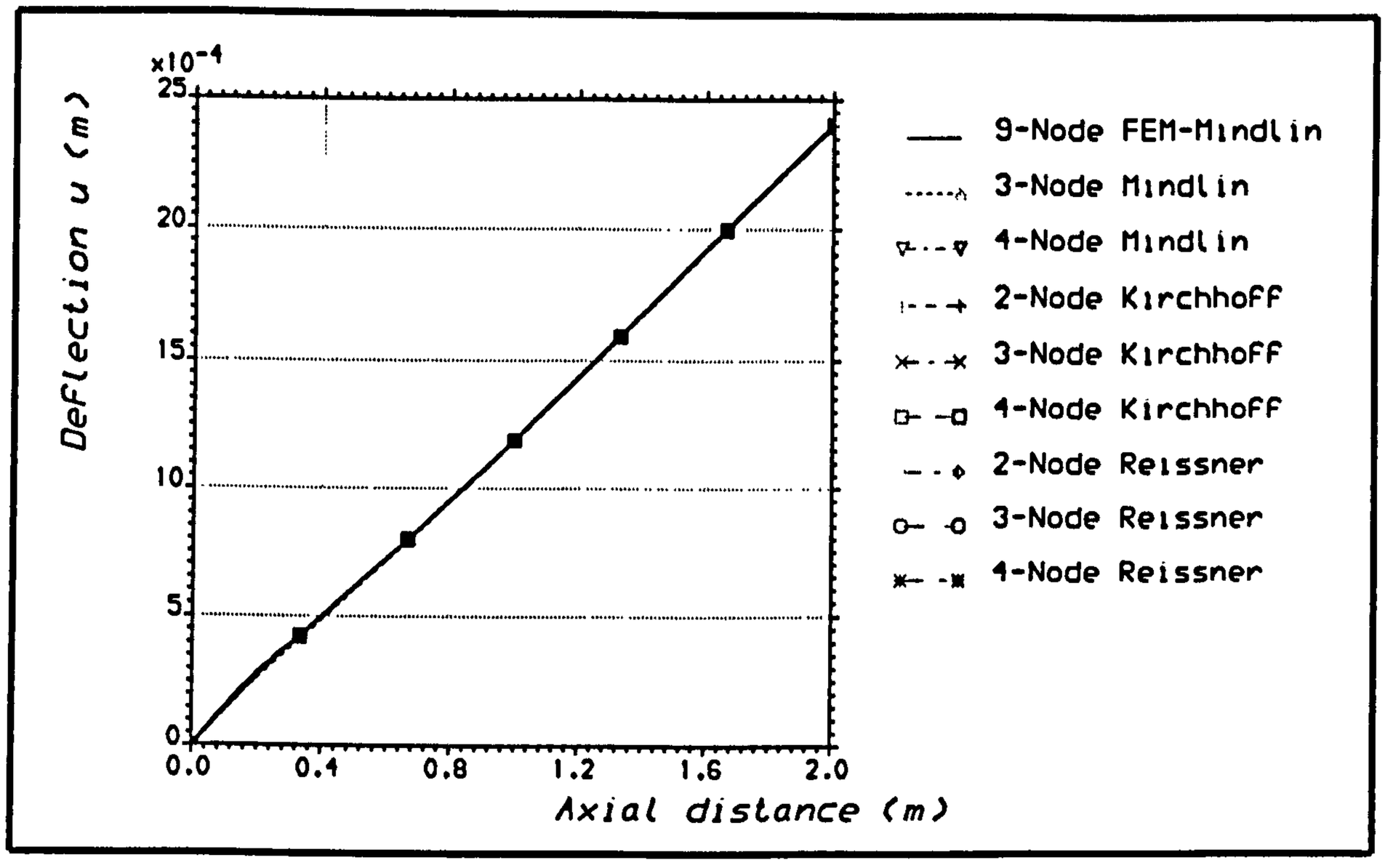

Figure 9.18 Axial displacement distribution for E/G cantilever plate under tension, using polynomial strip elements, and non-linear analysis.

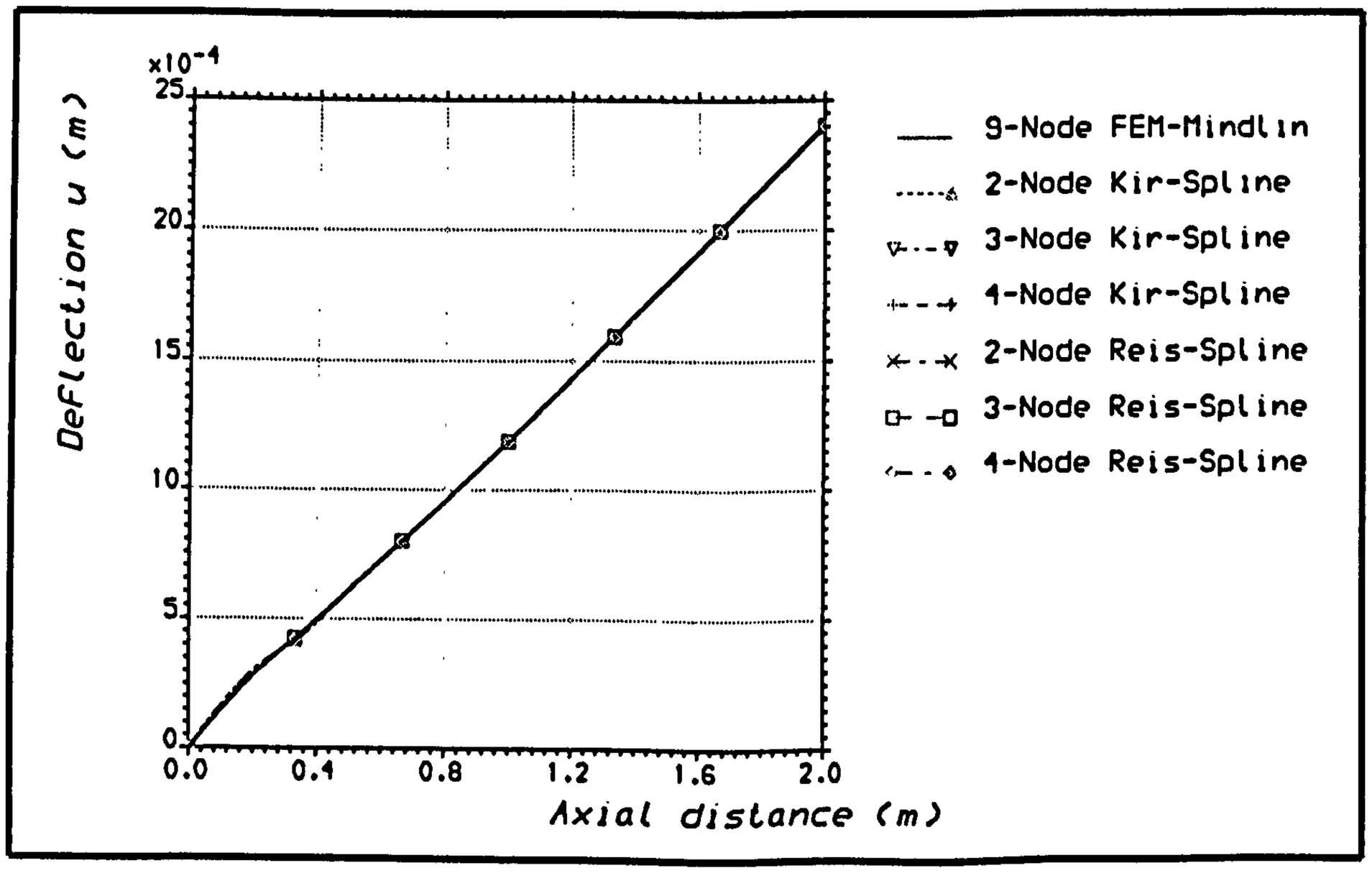

Figure 9.19 Axial displacement distribution for E/G cantilever plate under tension, using spline-type strip elements, and non-linear analysis.

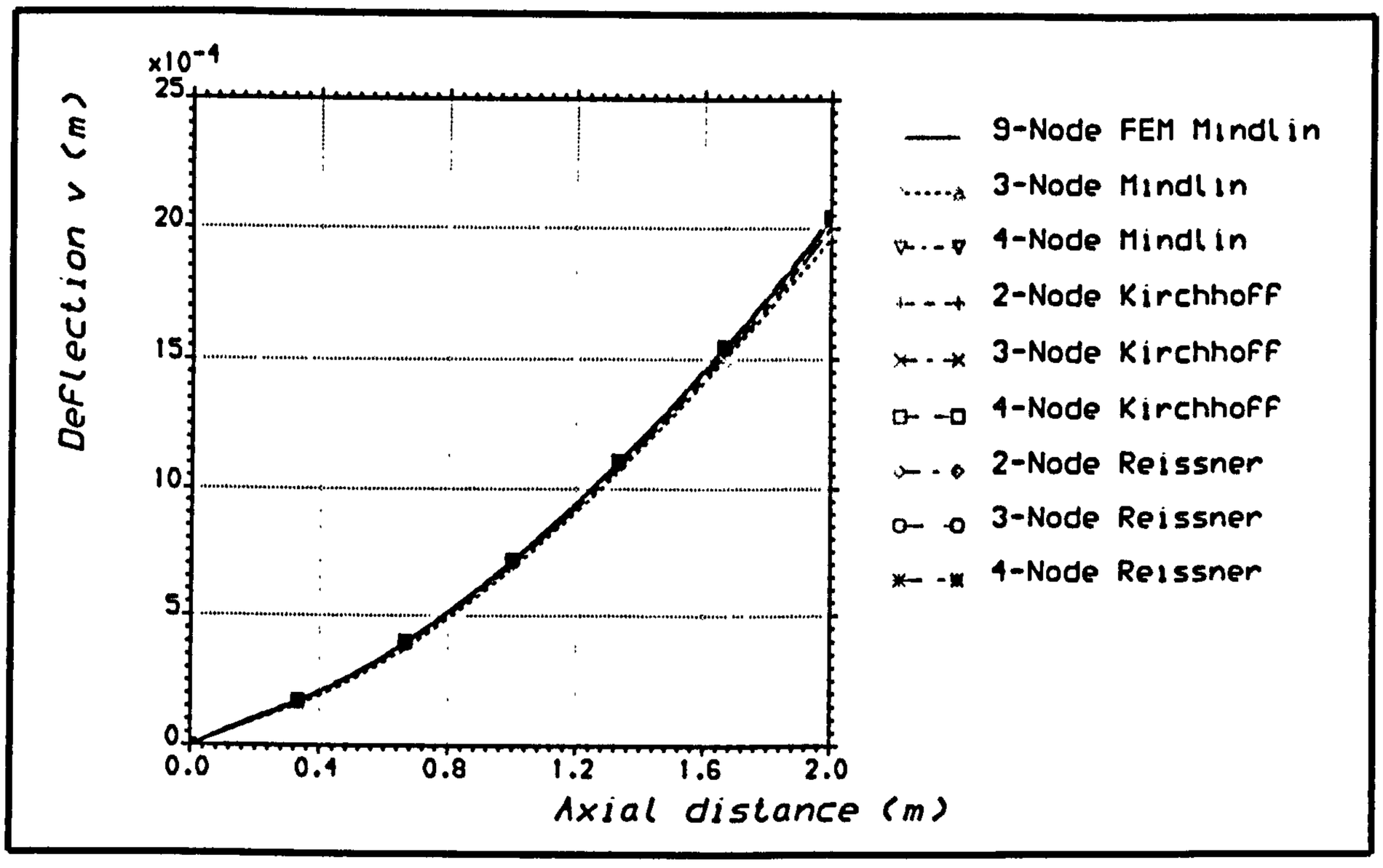

Figure 9.20 Transverse displacement distribution for C/E cantilever plate under in-plane bending, using polynomial strip elements, and non-linear analysis.

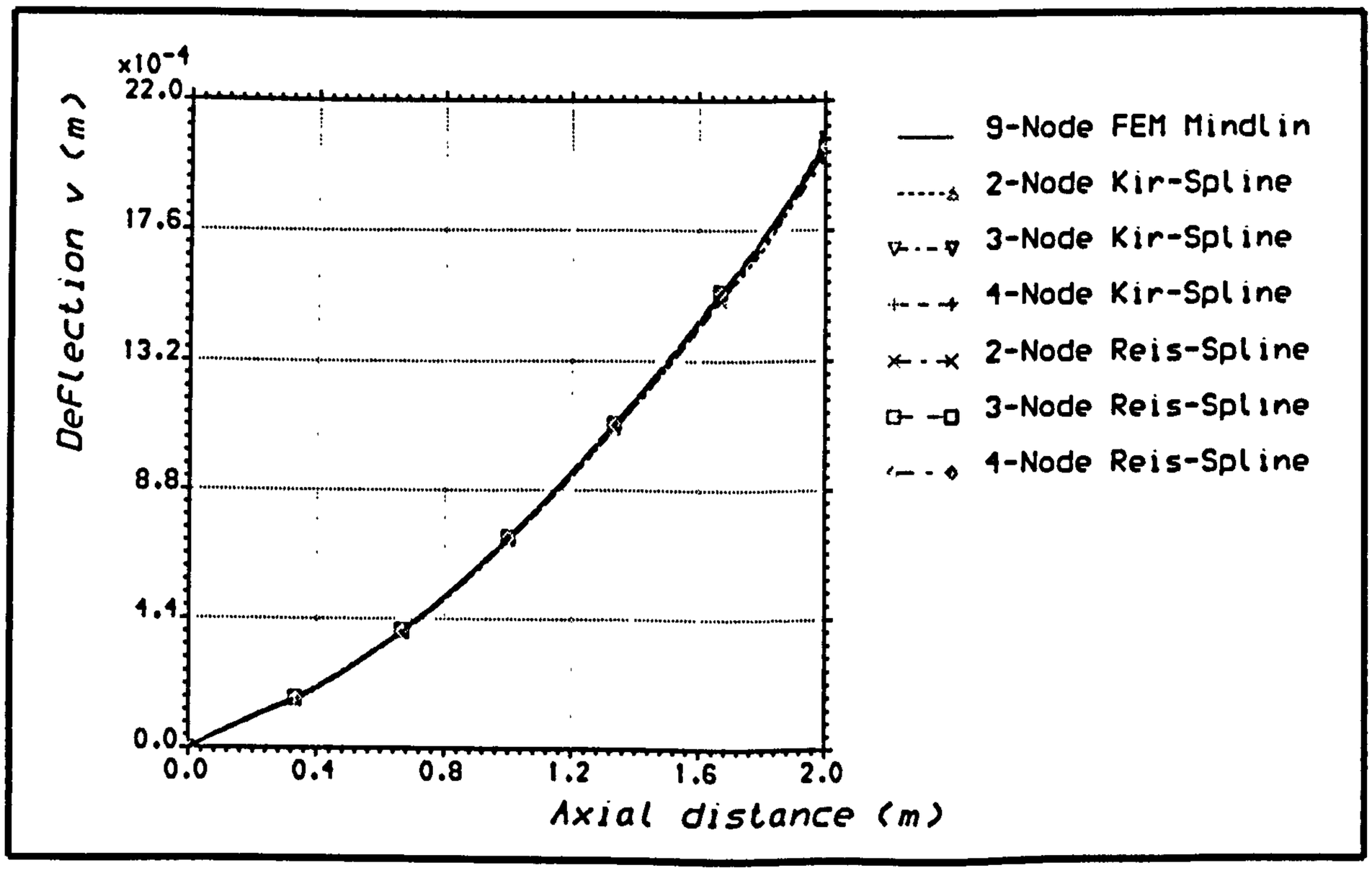

Figure 9.21 Transverse displacement distribution for C/E cantilever plate under in-plane bending, using spline-type strip elements, and non-linear analysis.

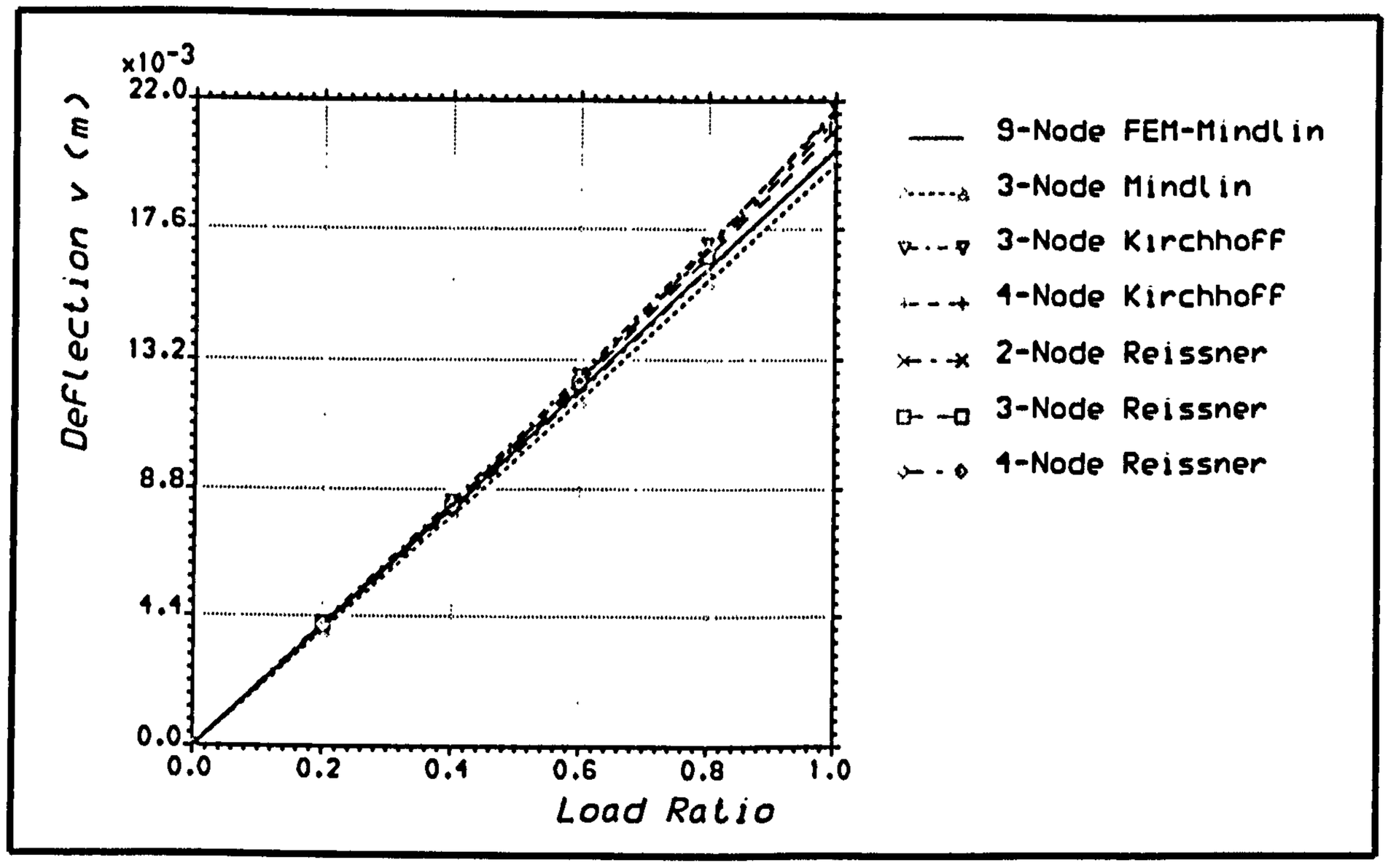

Figure 9.22 Transverse displacement versus load for C/E cantilever plate under in-plane bending, using polynomial strip elements, and non-linear analysis.

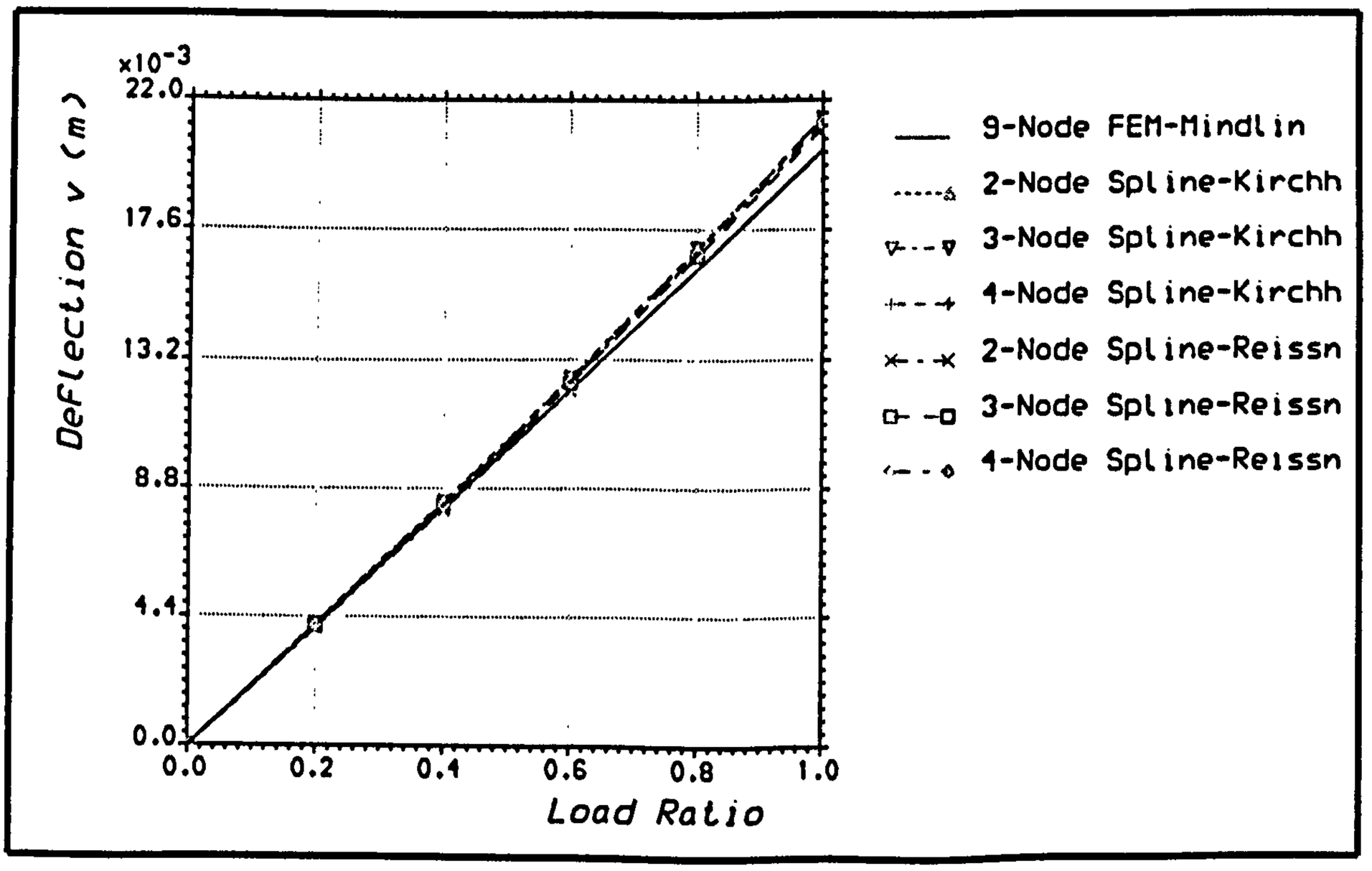

Figure 9.23 Transverse displacement versus load for C/E cantilever plate under in-plane bending, using spline-type strip elements, and non-linear analysis.

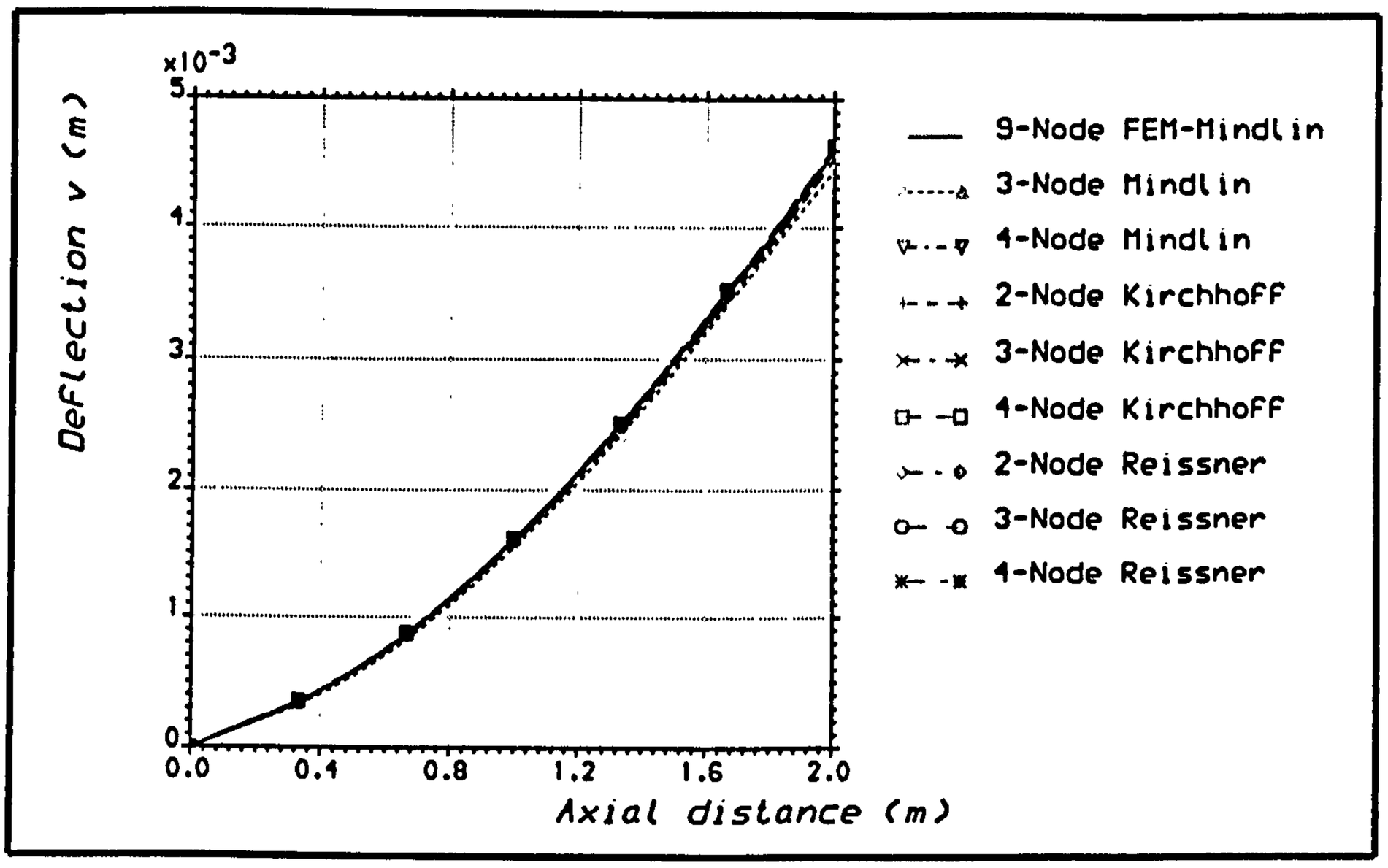

Figure 9.24 Transverse displacement distribution for E/G cantilever plate under in-plane bending, using polynomial strip elements, and non-linear analysis.

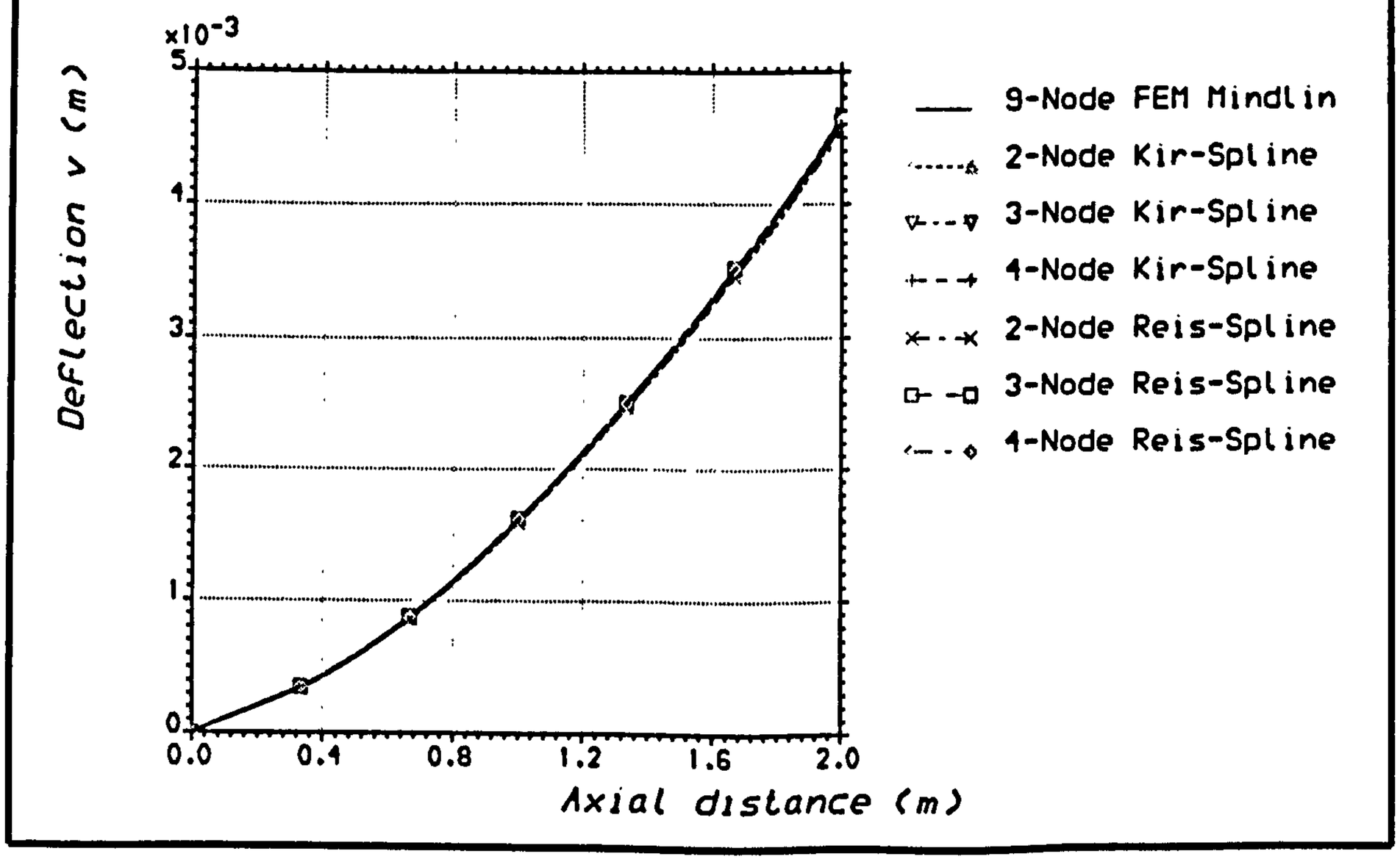

Figure 9.25 Transverse displacement distribution for E/G cantilever plate under in-plane bending, using spline-type strip elements, and non-linear analysis.

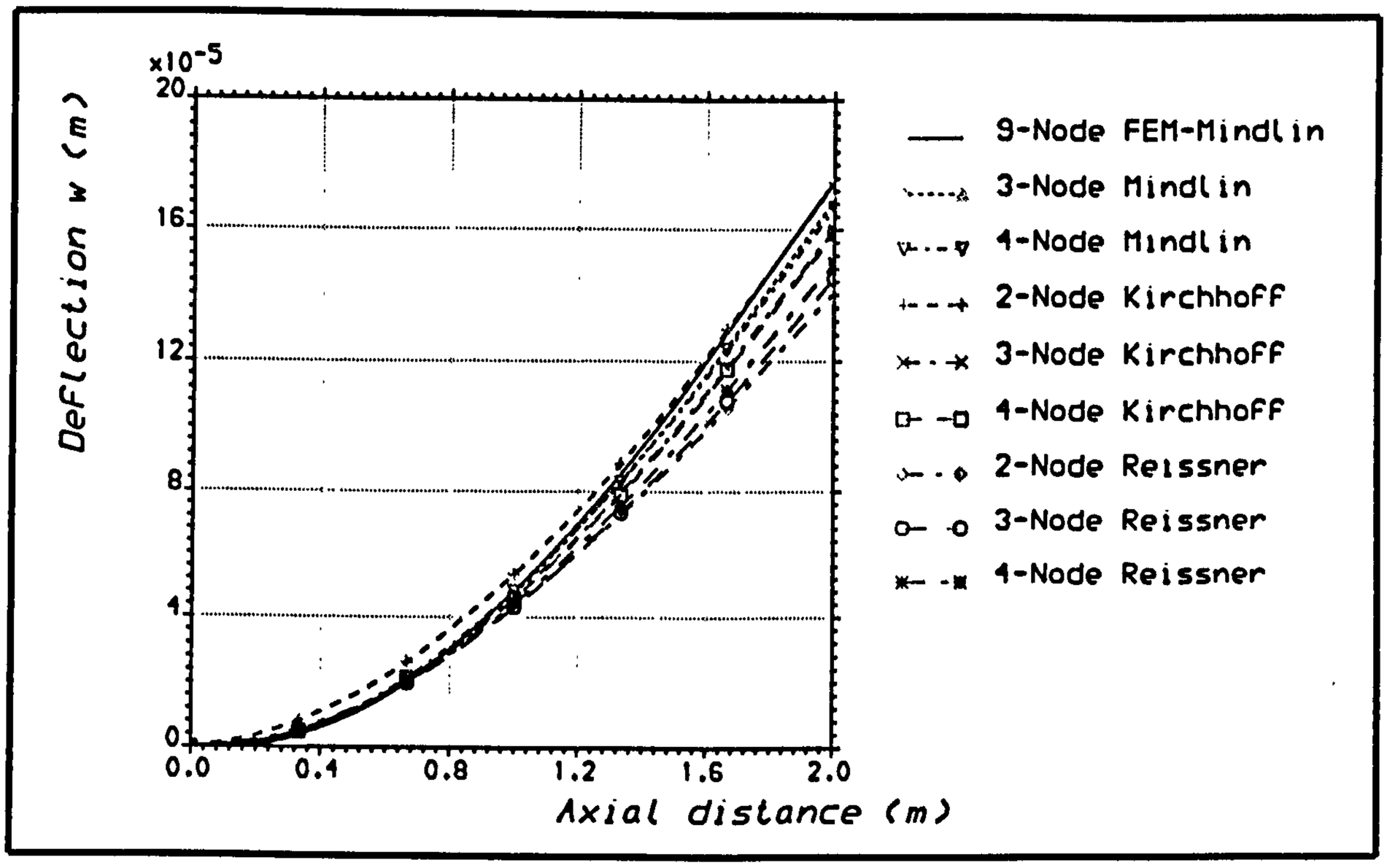

Figure 9.26 Lateral displacement distribution for C/E cantilever plate under out-of-plane bending, using polynomial strip elements, and non-linear analysis.

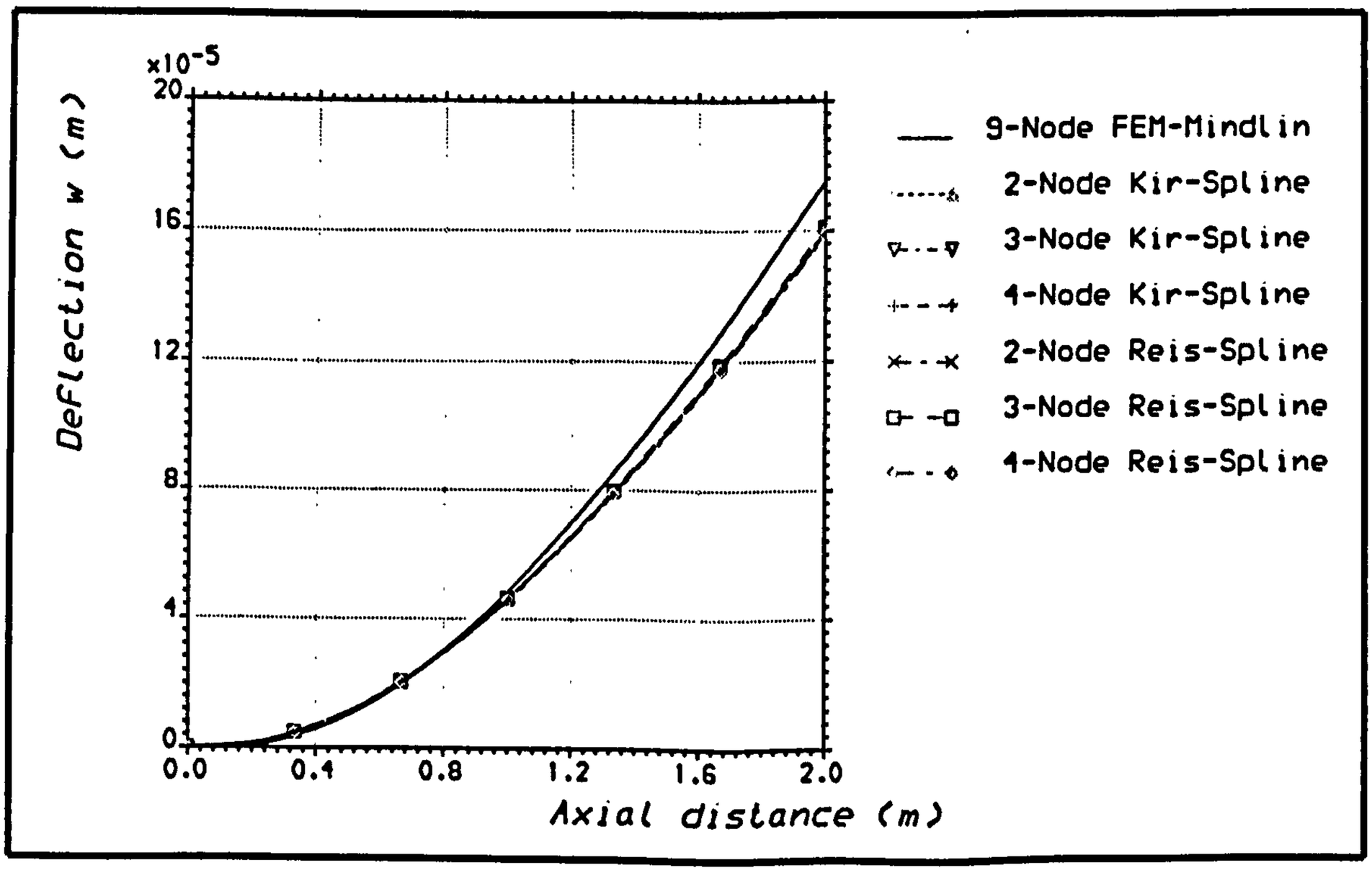

Figure 9.27 Lateral displacement distribution for C/E cantilever plate under out-of-plane bending, using spline-type strip elements, and non-linear analysis.

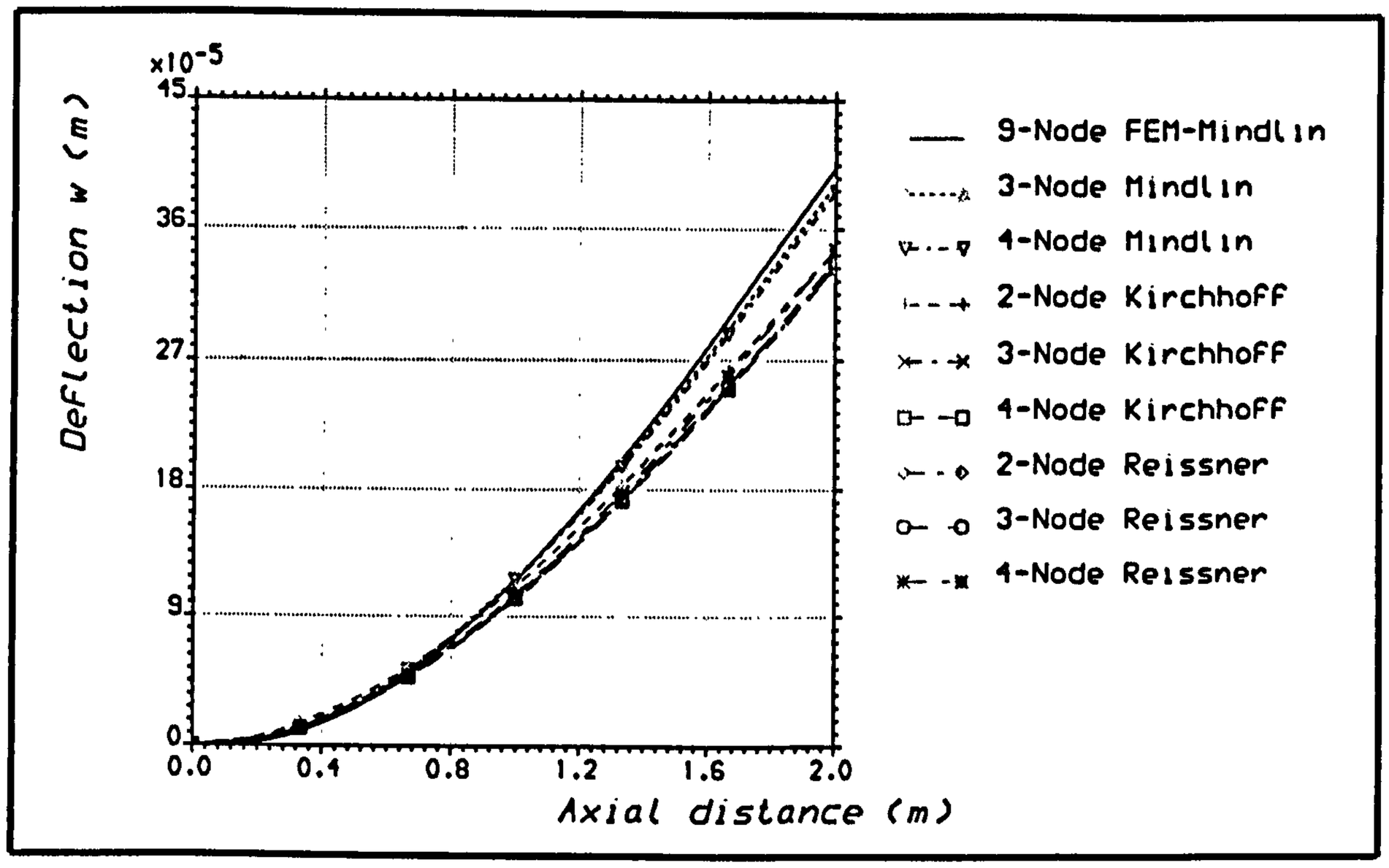

Figure 9.28 Lateral displacement distribution for E/G cantilever plate under out-of-plane bending, using polynomial strip elements, and non-linear analysis.

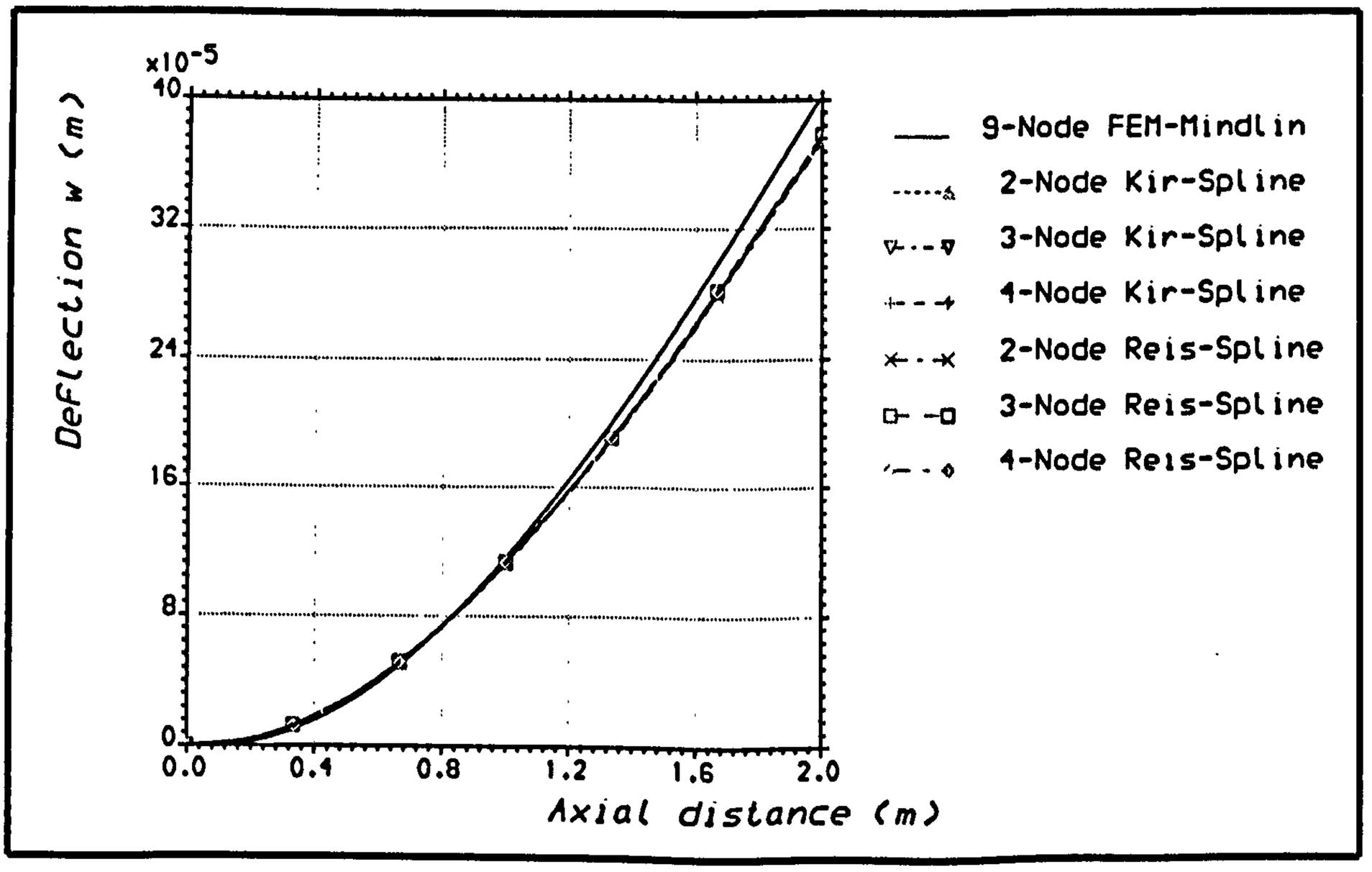

Figure 9.29 Lateral displacement distribution for E/G cantilever plate under out-of-plane bending, using spline-type strip elements, and non-linear analysis.

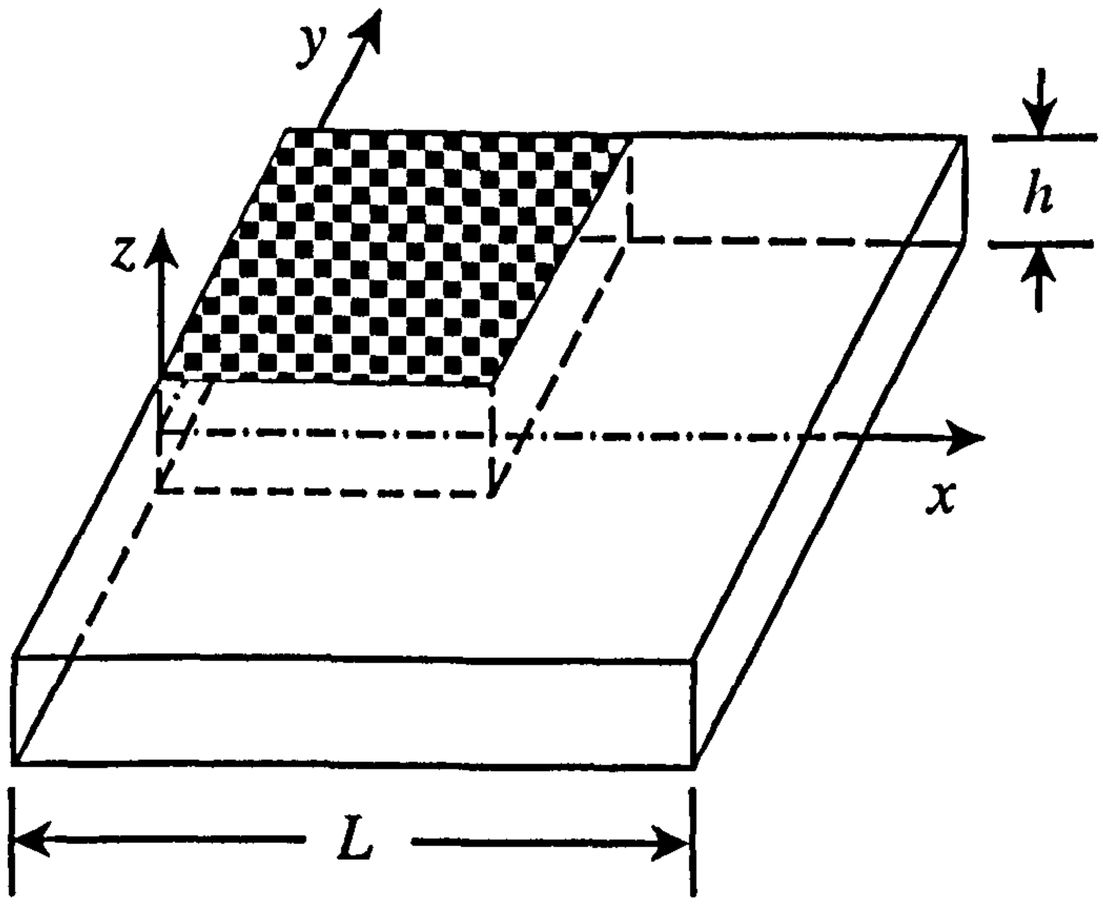

Full plate

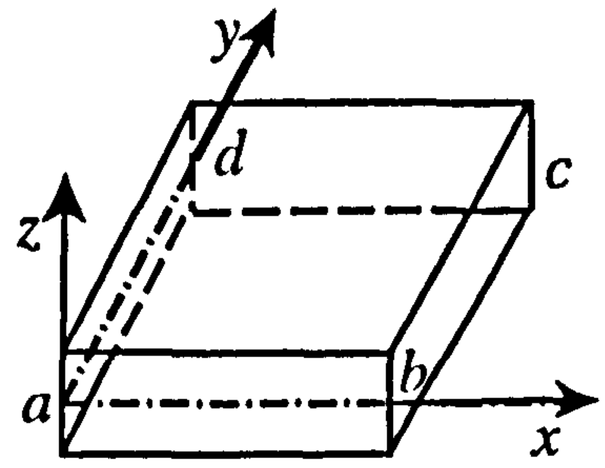

One quarter
of the plate

Figure 9.30 Square plate case

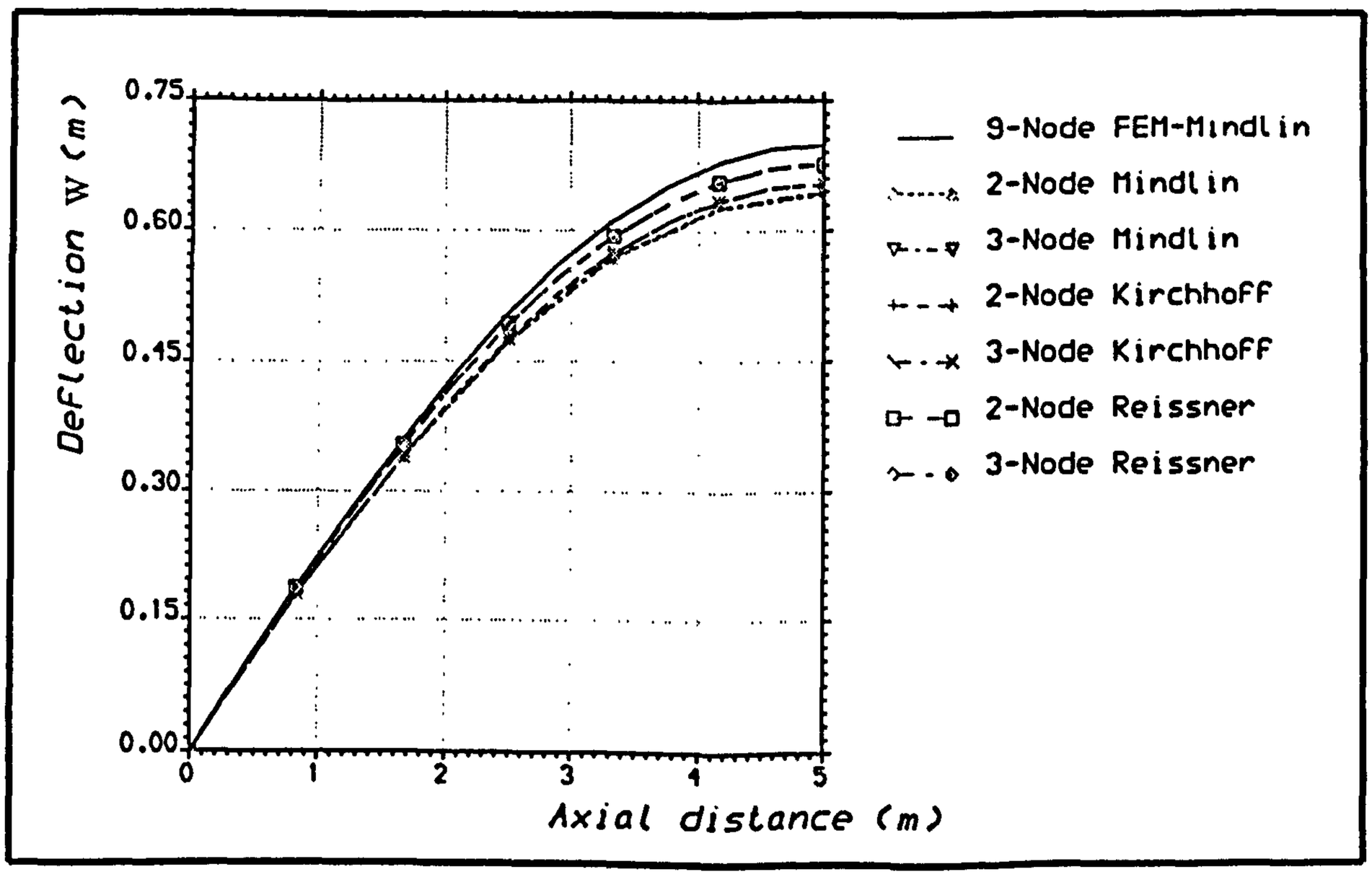

Figure 9.31 Lateral displacement distribution for thin square plate using polynomial finite strip elements.

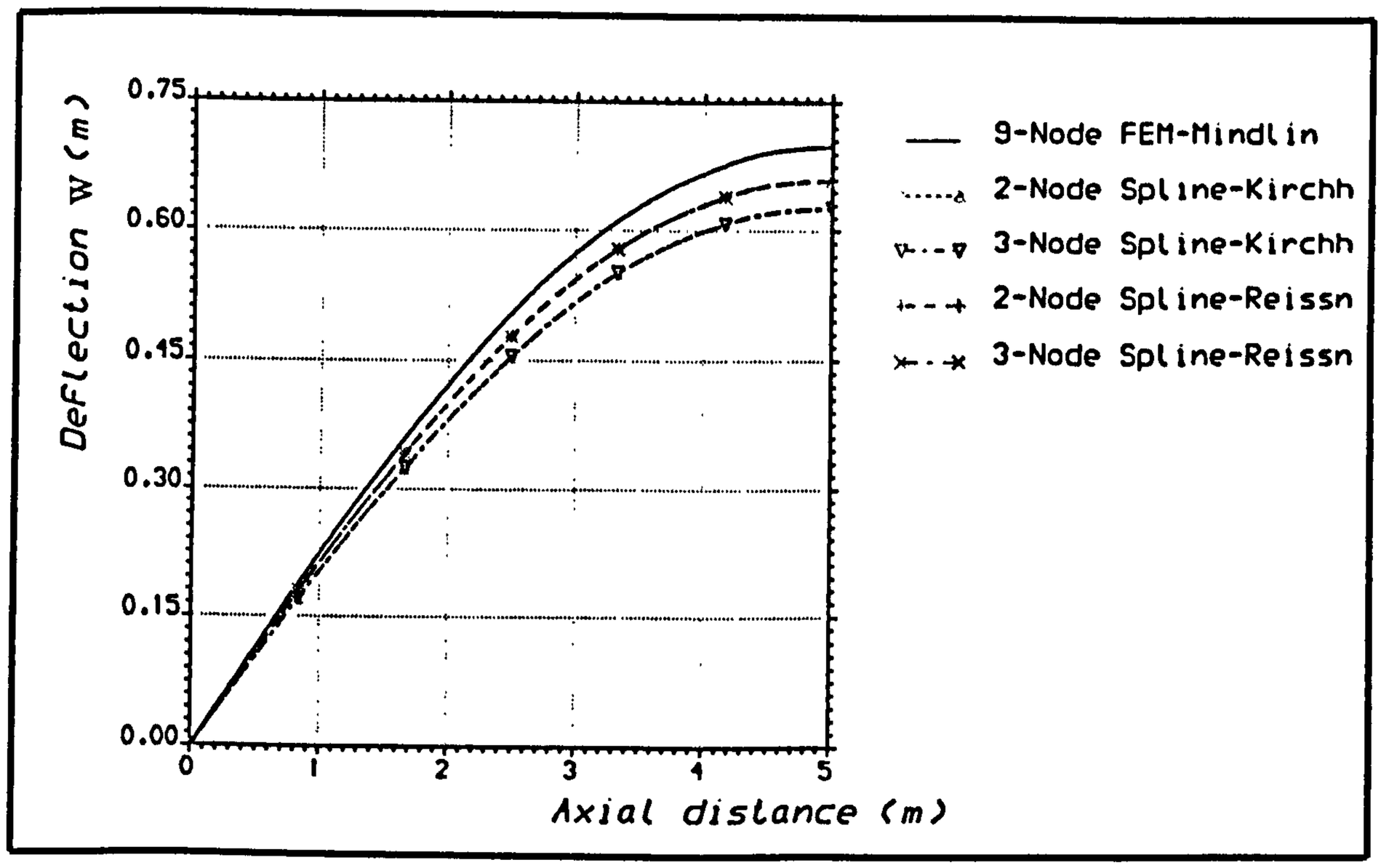

Figure 9.32 Lateral displacement distribution for thin square plate using spline-type finite strip elements.

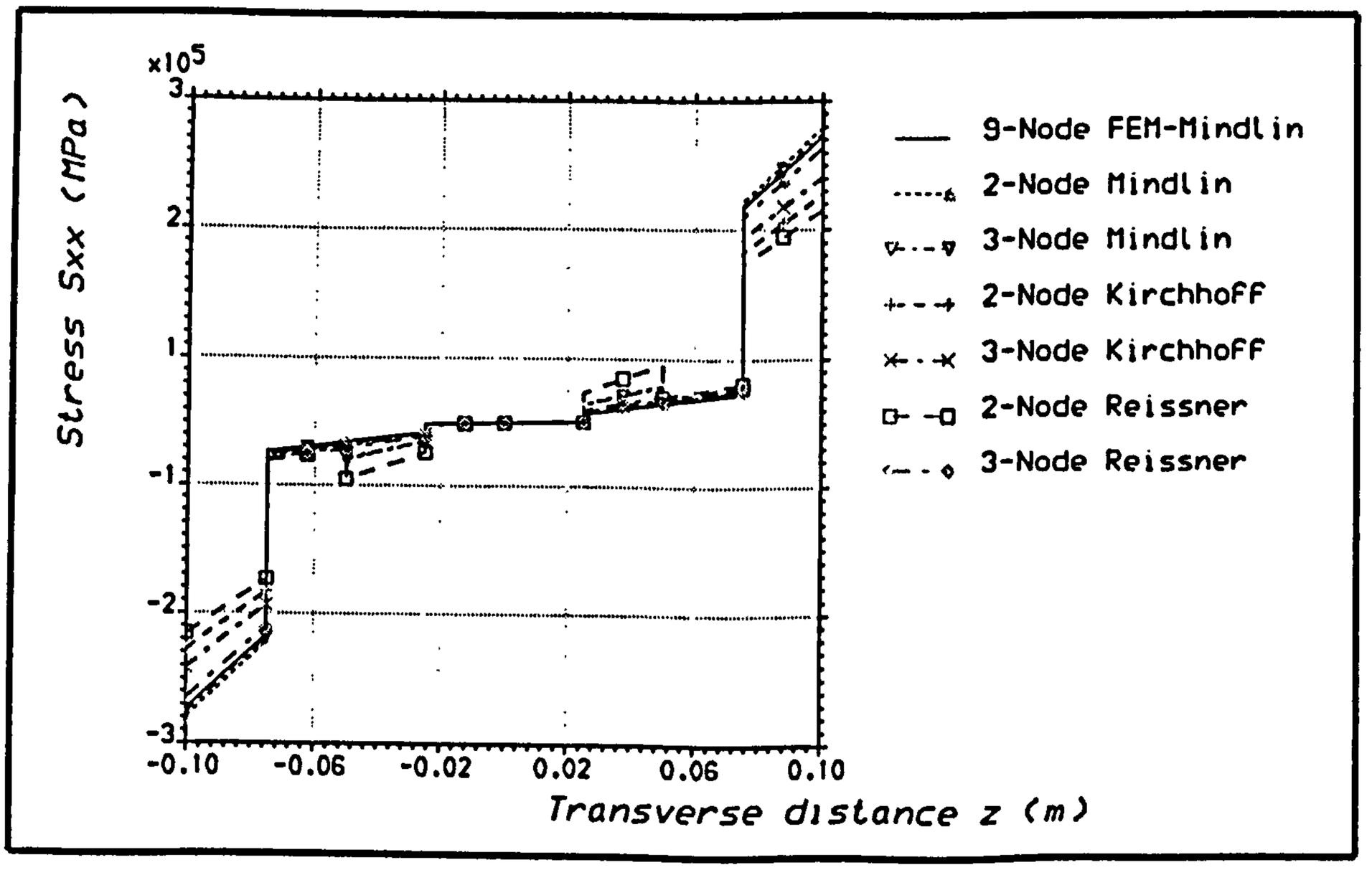

Figure 9.33 Axial stress distribution for thin square plate using polynomial finite strip elements.

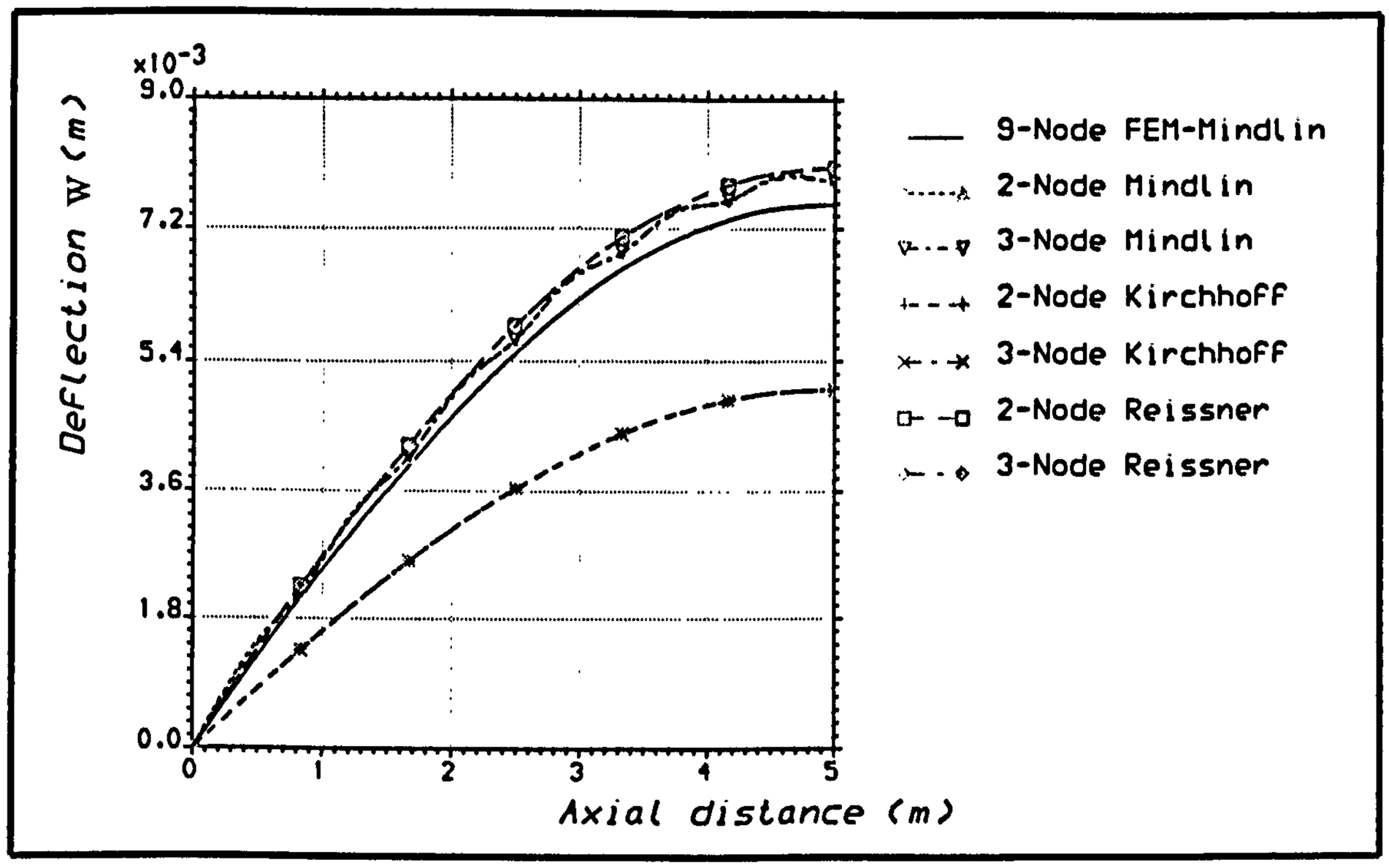

Figure 9.34 Lateral displacement distribution thick square plate using polynomial strip elements.

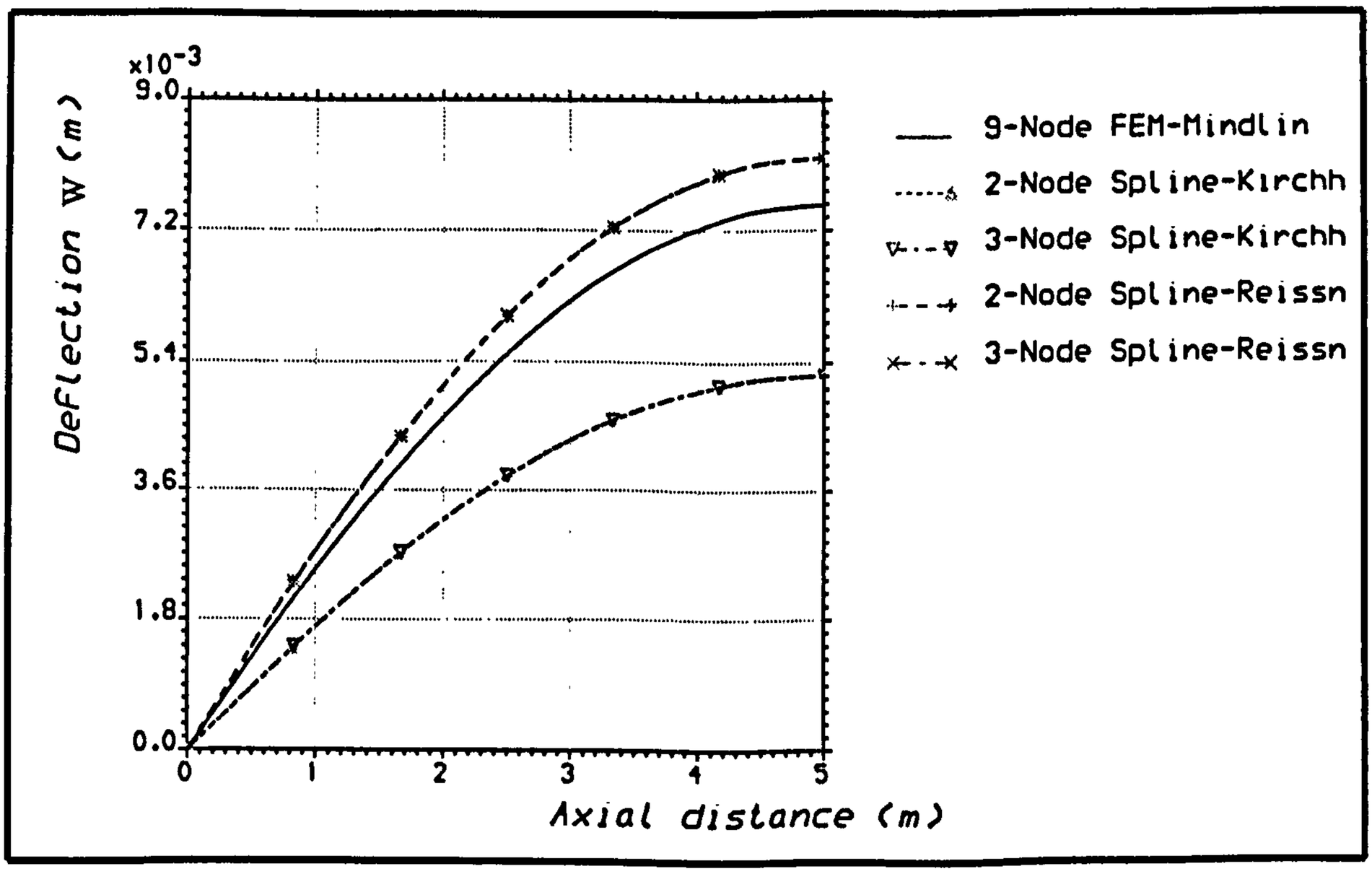

Figure 9.35 Lateral displacement distribution for thick square plate using spline-type strip elements.

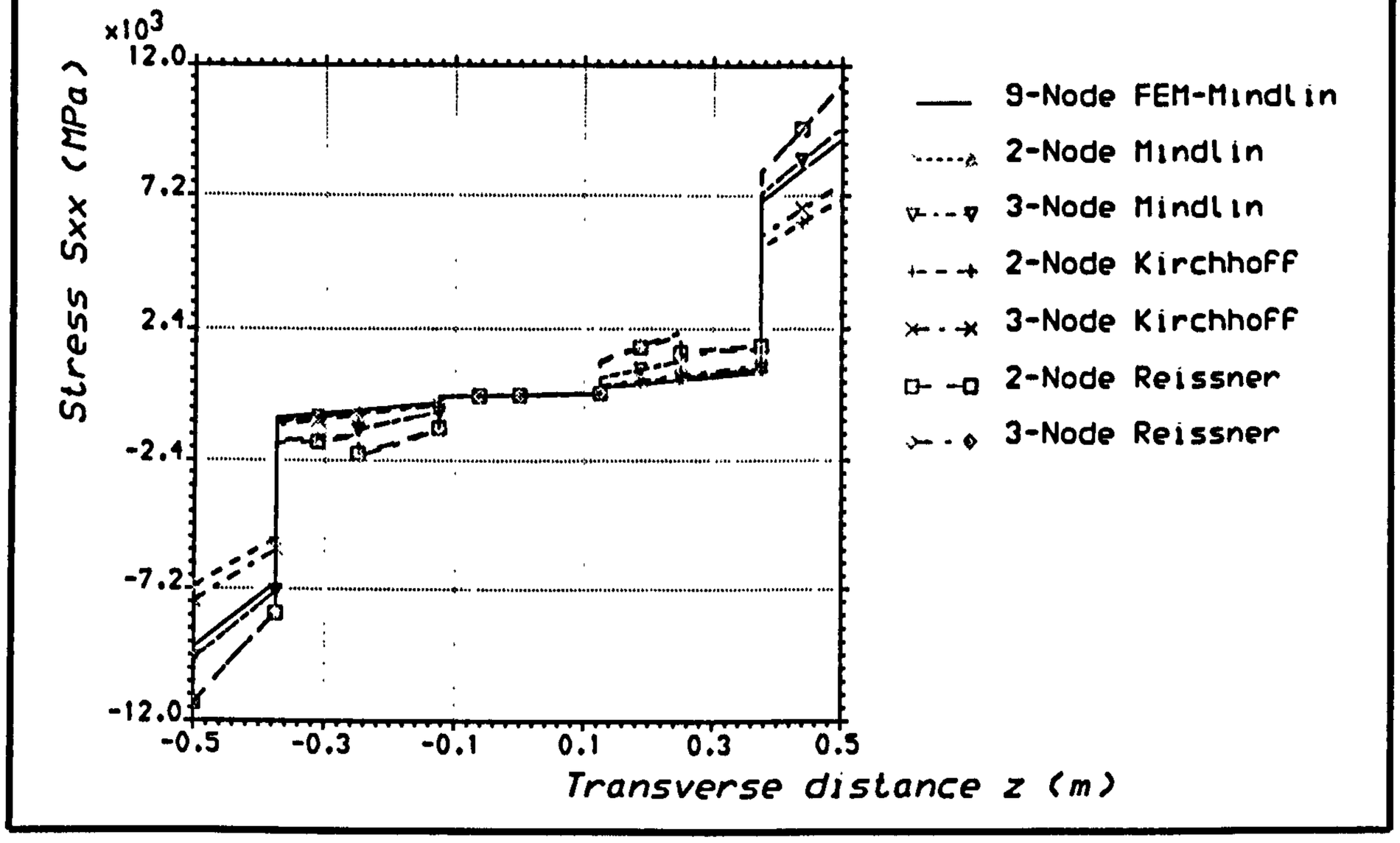

Figure 9.36 Axial stress distribution for thick square plate using polynomial strip elements.

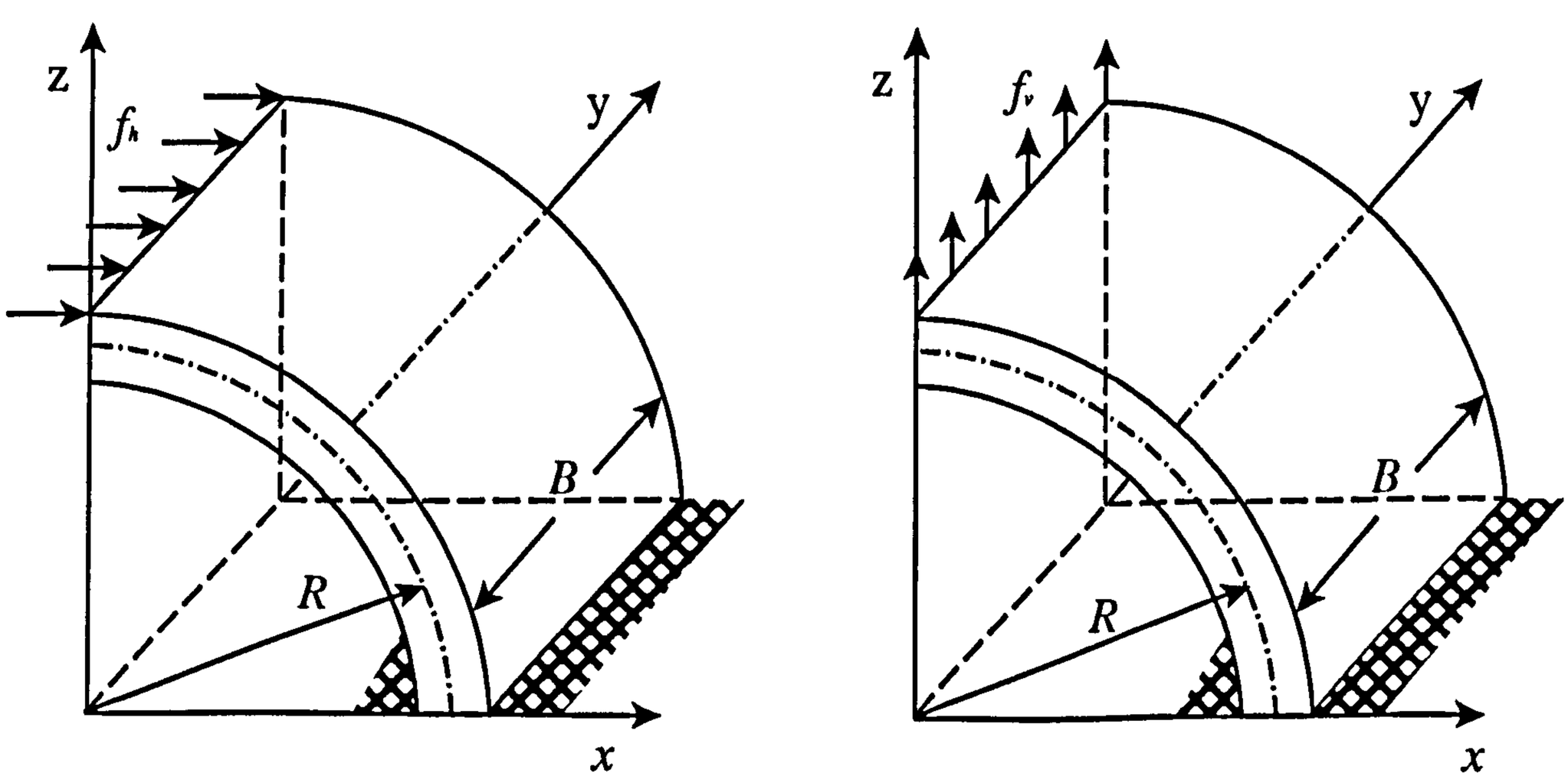

Figure 9.37 Curved shell case

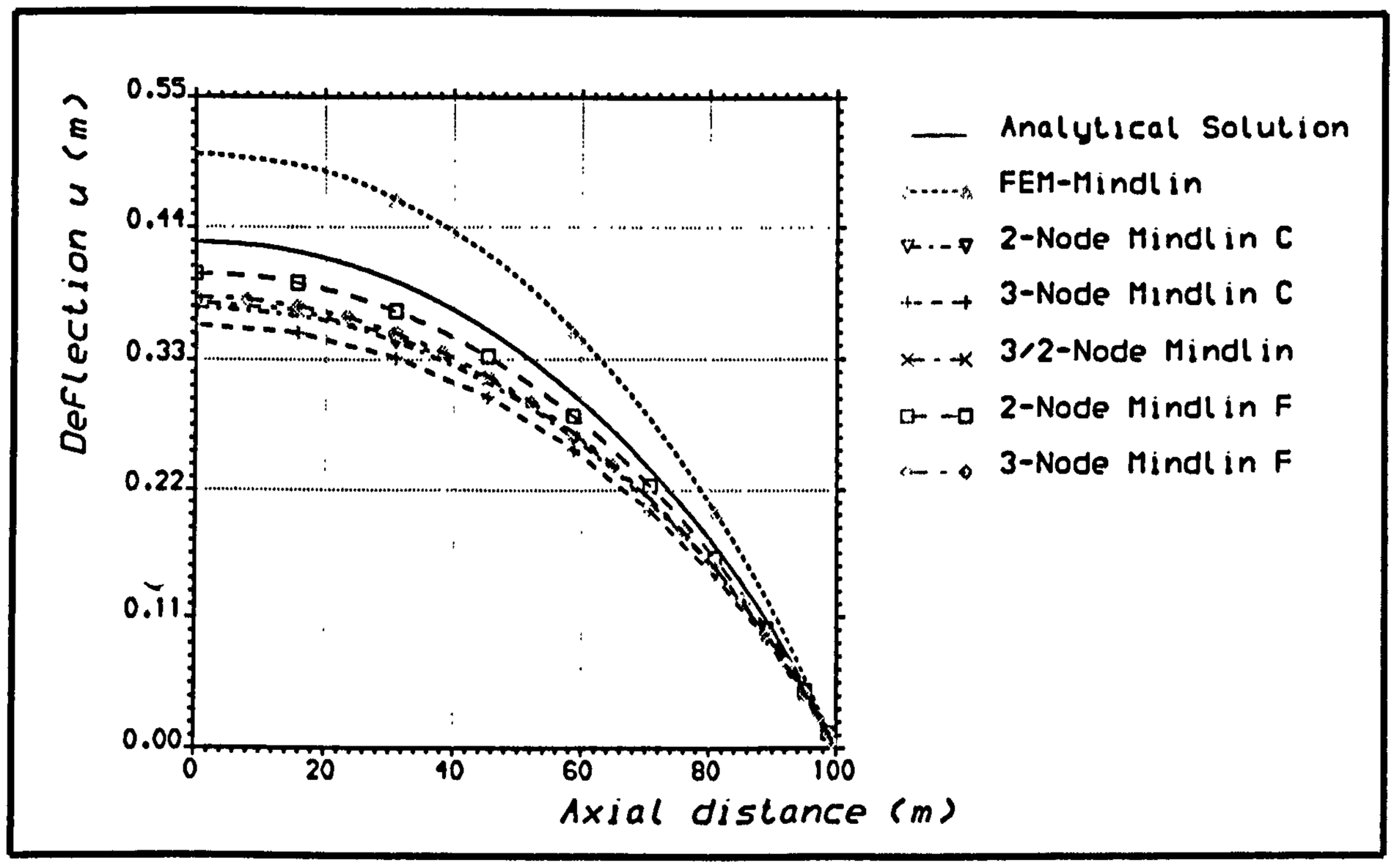

Figure 9.38 Horizontal displacement distribution for a curved shell under horizontal loading.

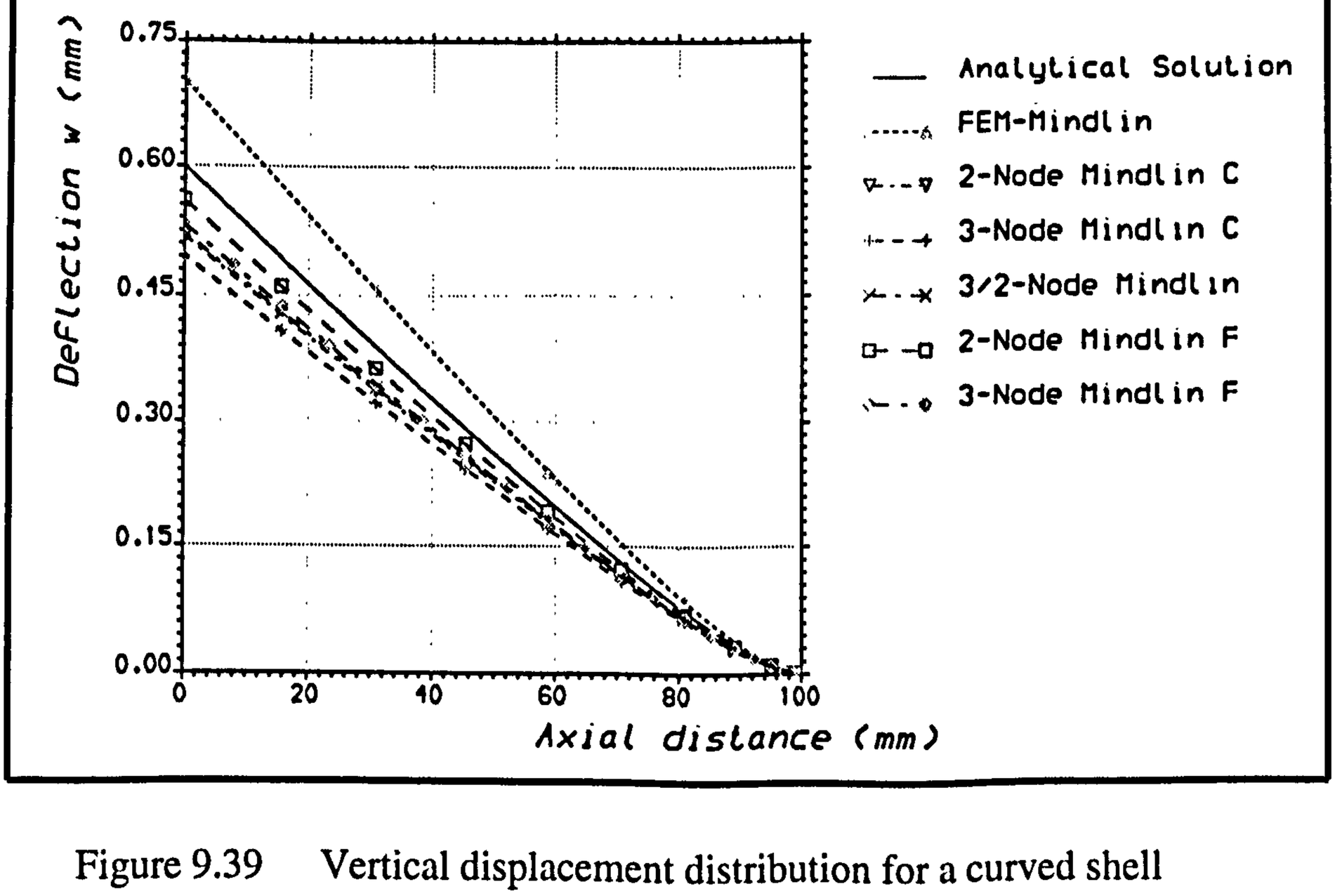

Figure 9.39 Vertical displacement distribution for a curved shell under horizontal loading.

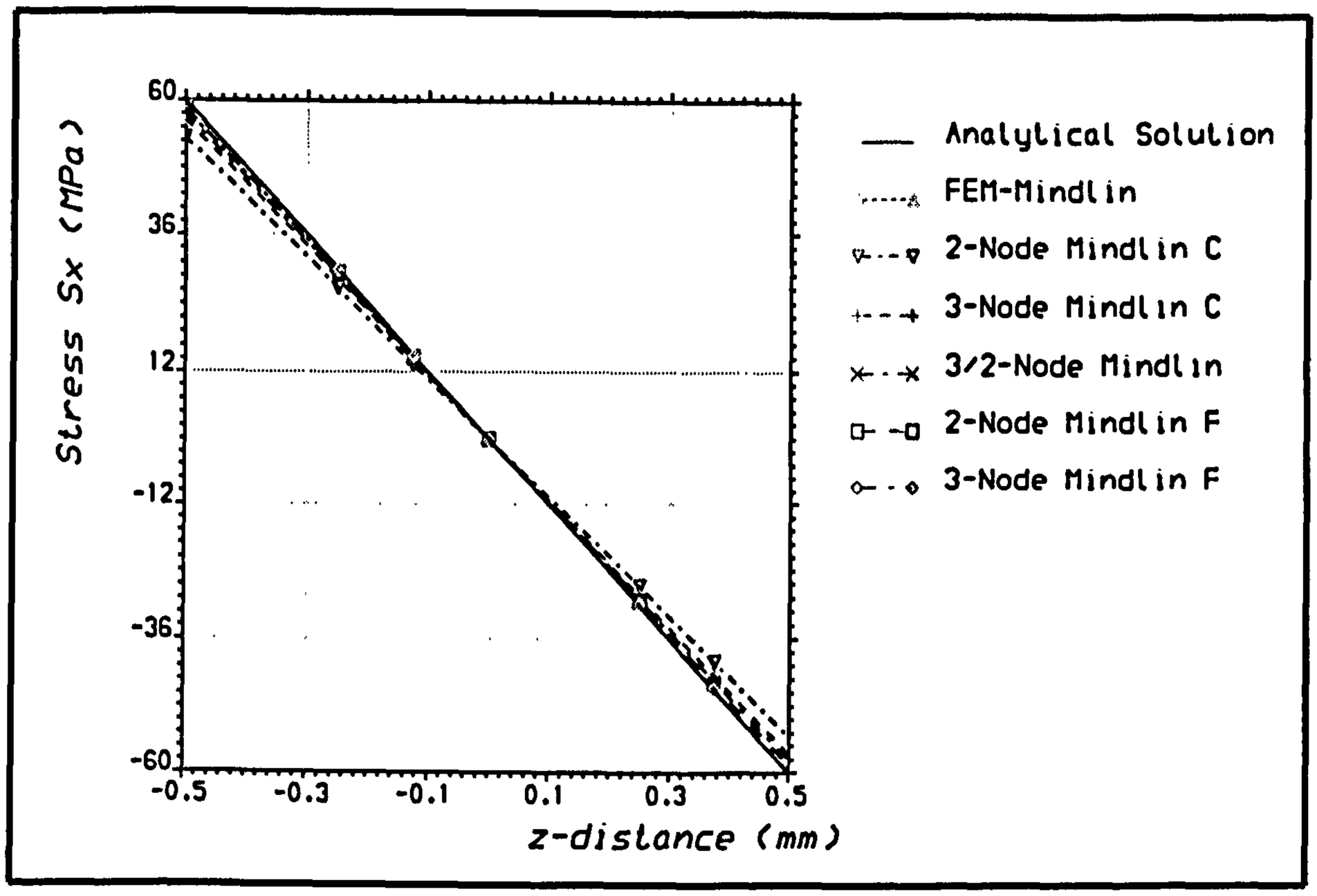

Figure 9.40 Axial stress distribution for a curved shell under horizontal loading.

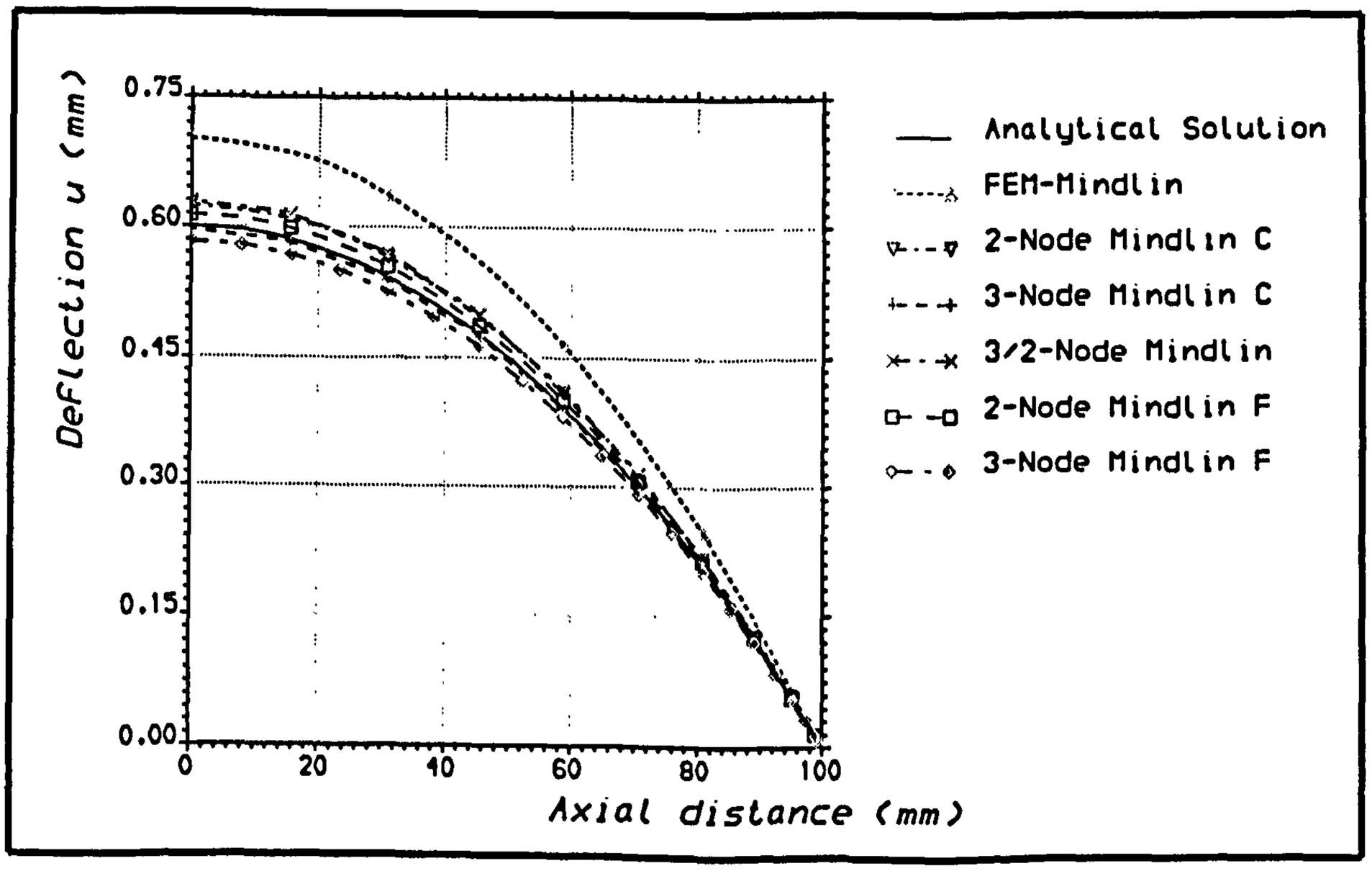

Figure 9.41 Horizontal displacement distribution for a curved shell under vertical loading.

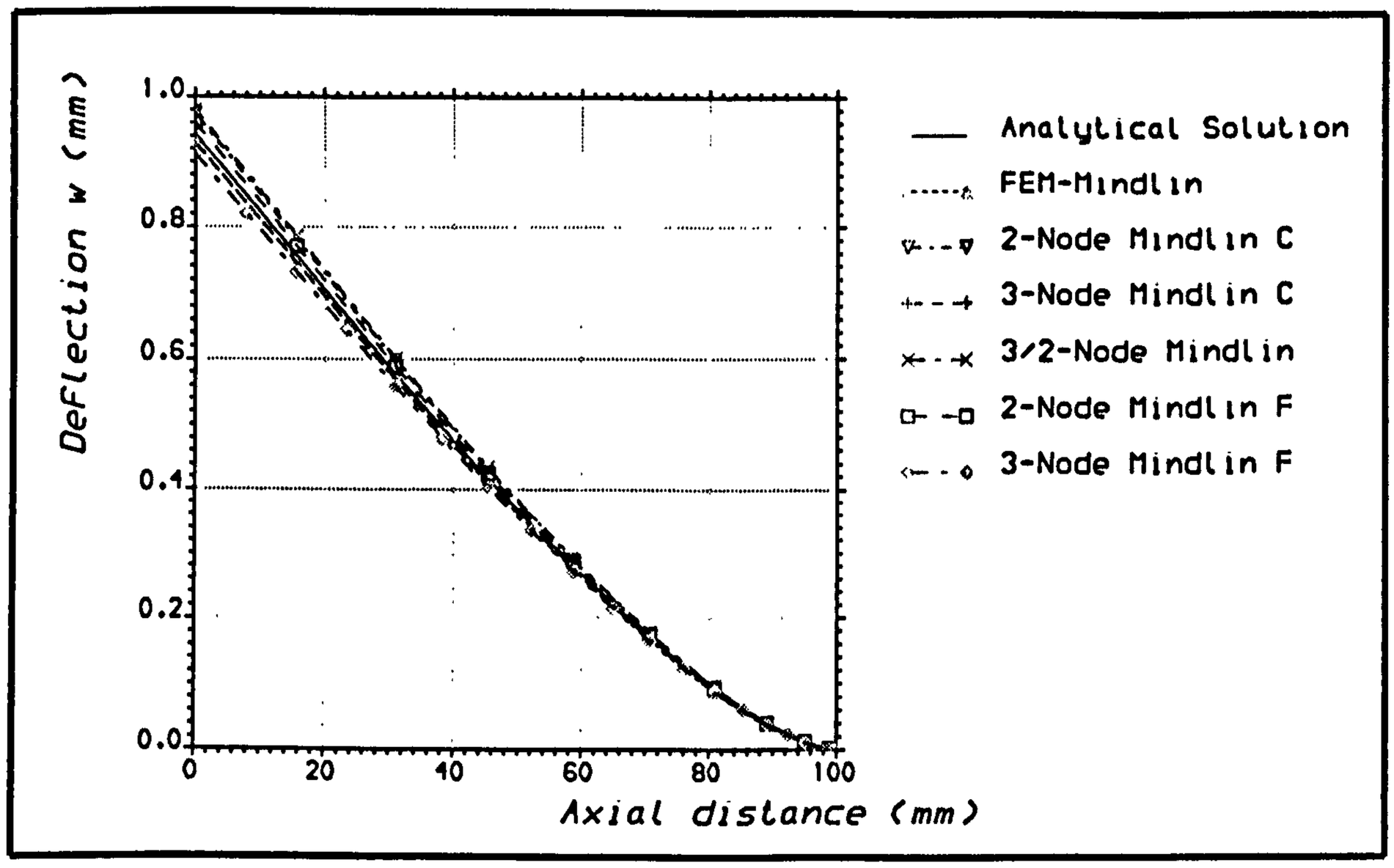

Figure 9.42 Vertical displacement distribution for a curved shell under vertical loading.

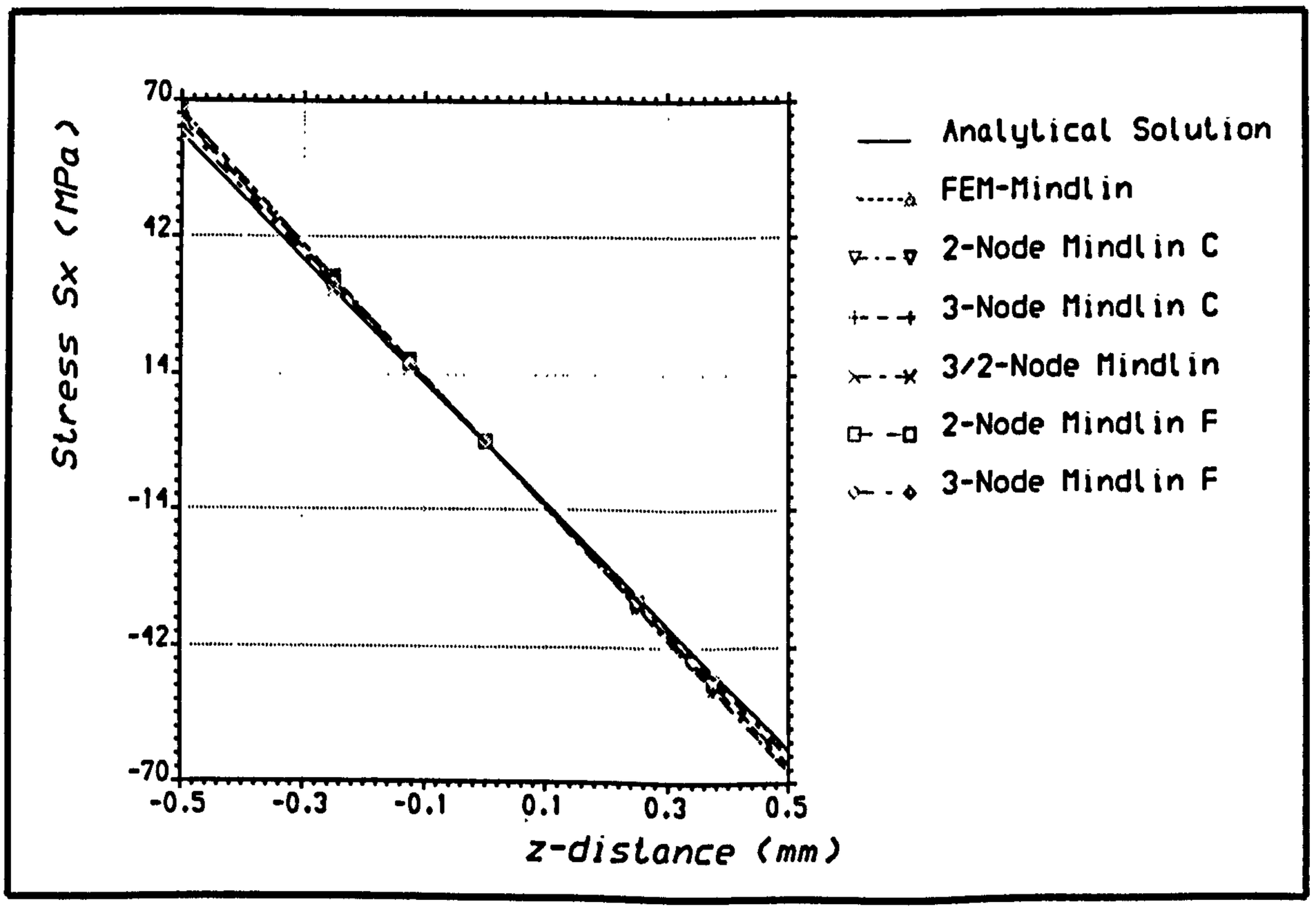

Figure 9.43 Axial stress distribution for a curved shell under vertical loading.

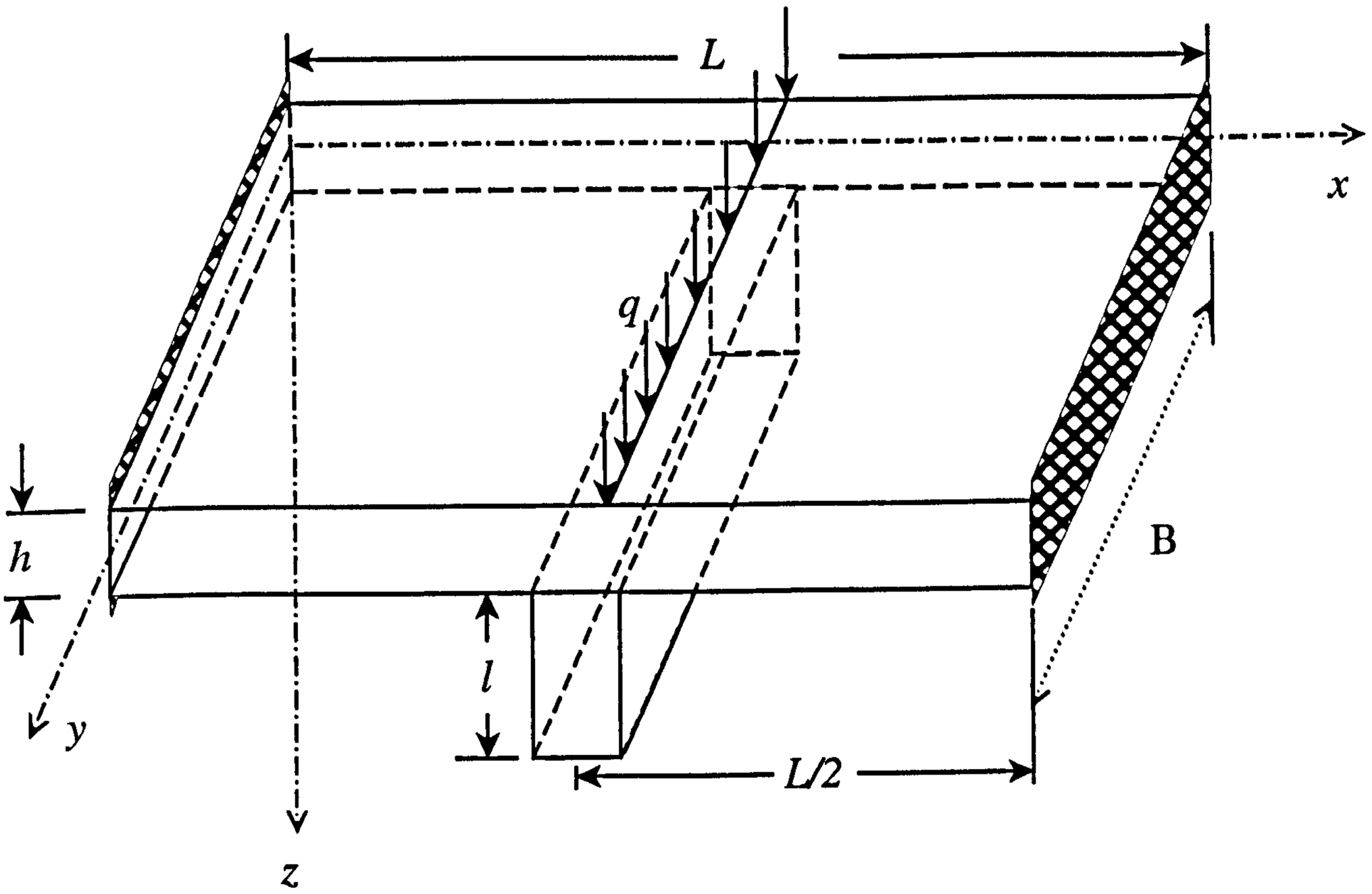

Figure 9.44 Stiffened plate case

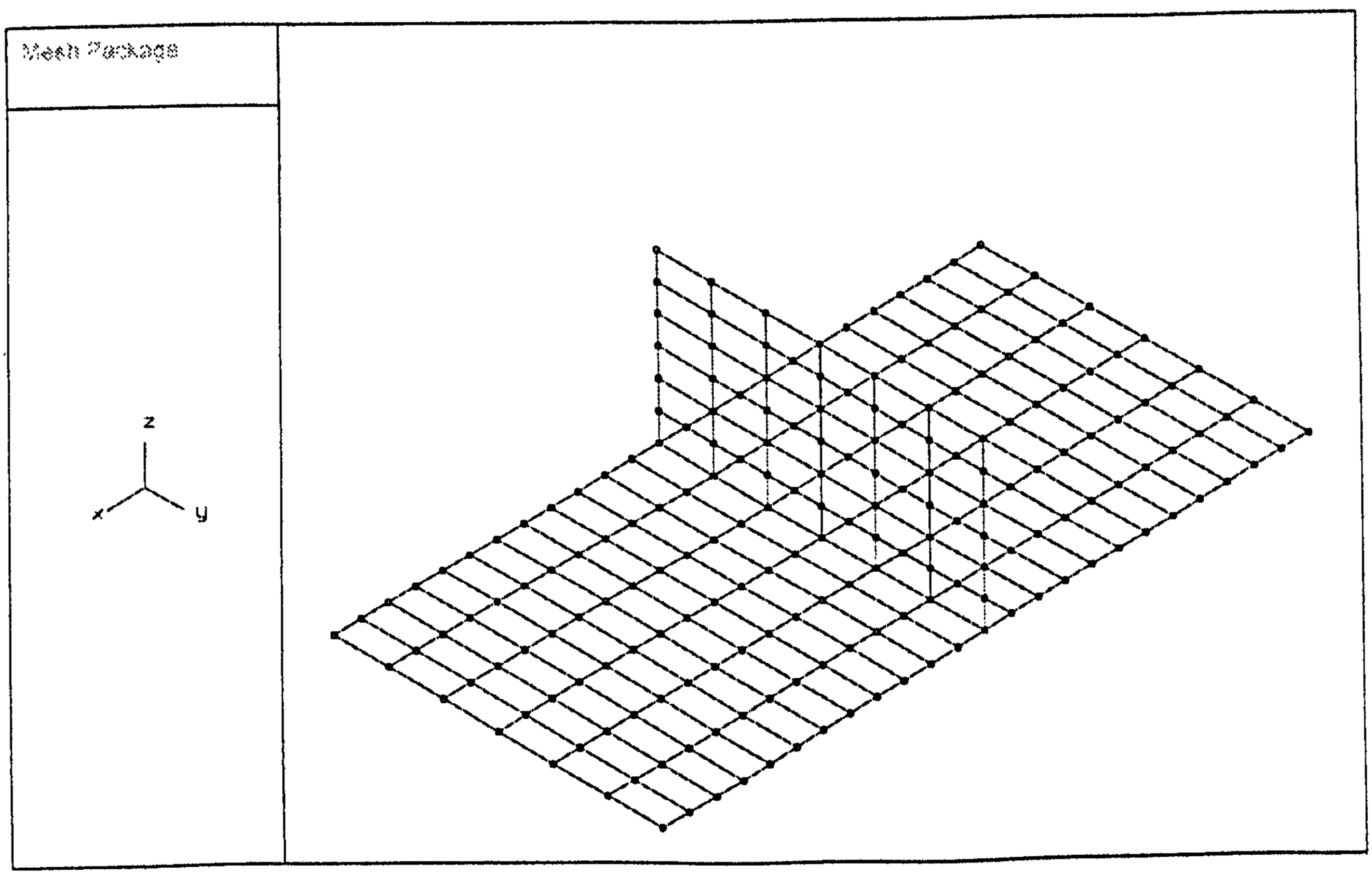

Figure 9.45 Four-node finite element mesh for the stiffened plate case.

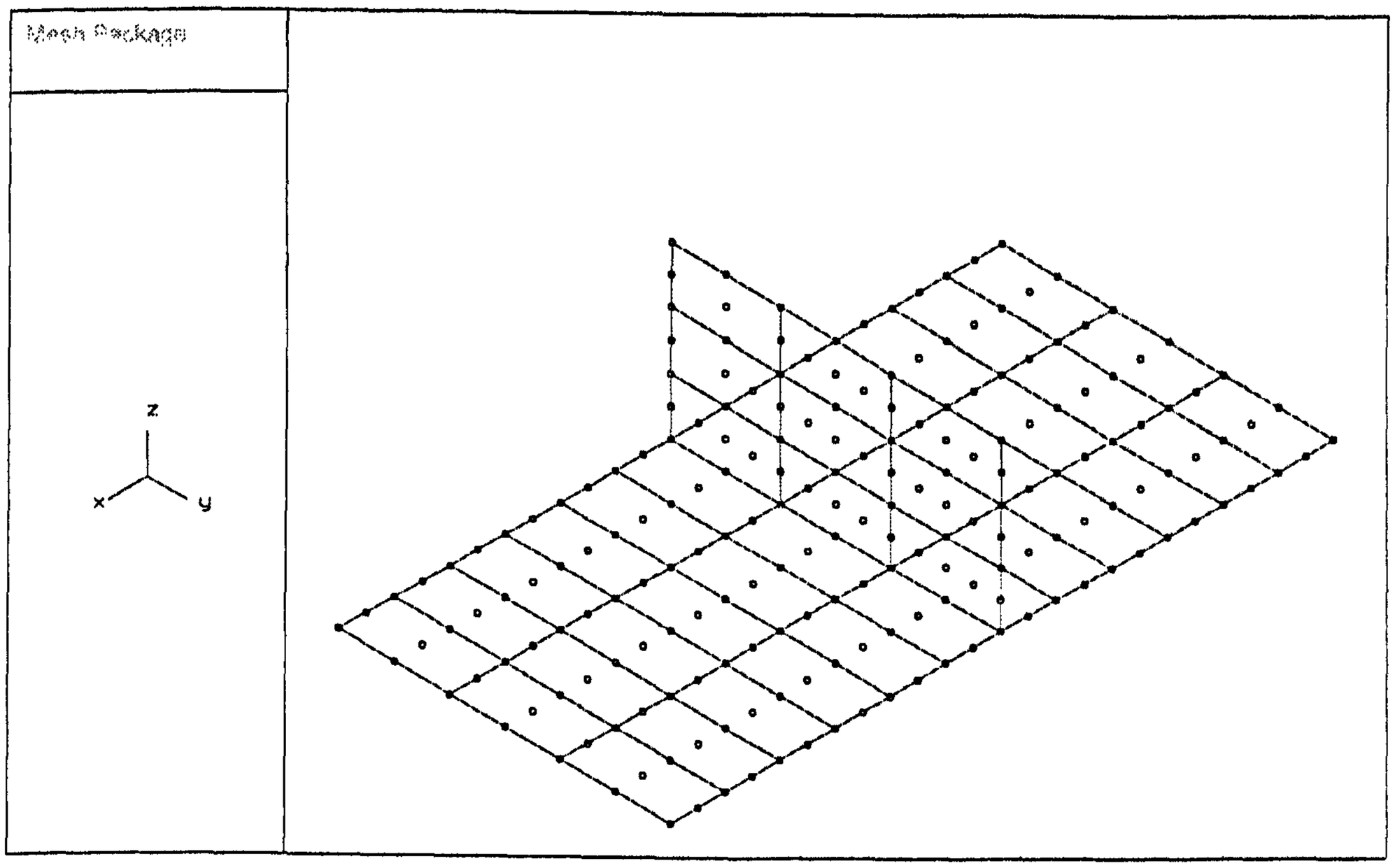

Figure 9.46 Nine-node finite element mesh for the stiffened plate case

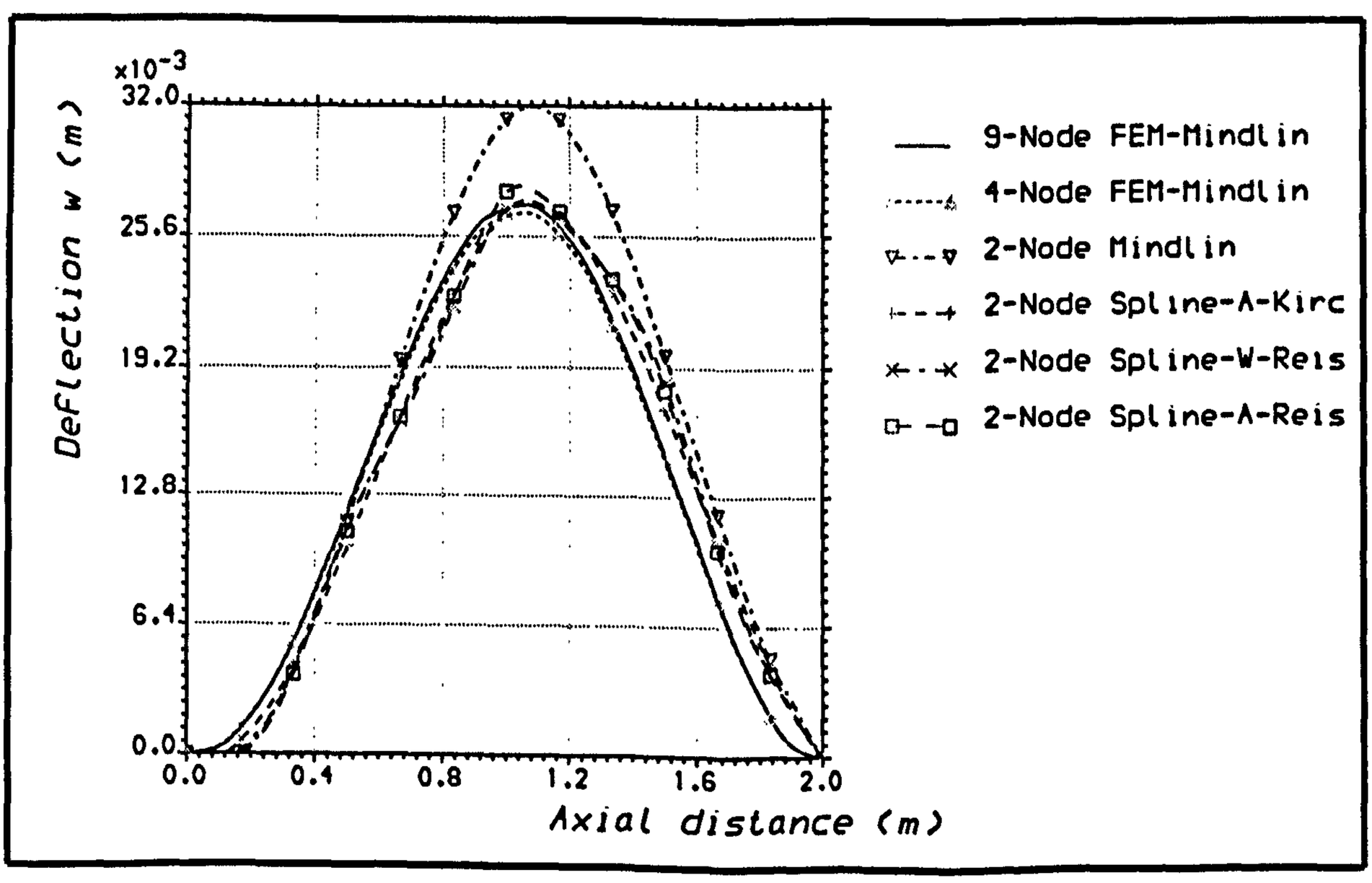

Figure 9.47 Lateral displacement distribution for thin stiffened plate under line loading, using two-node finite strip elements.

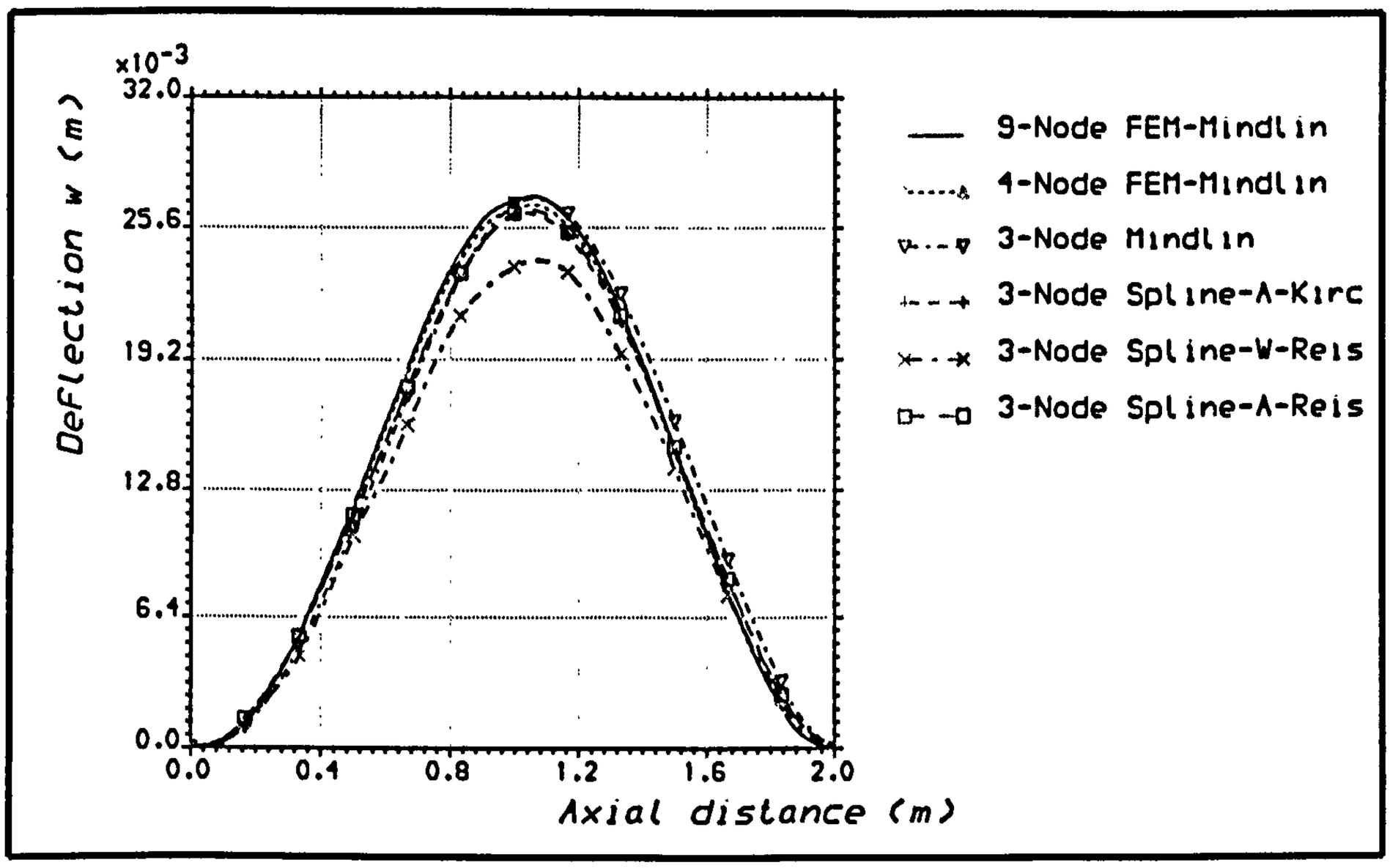

Figure 9.48 Lateral displacement distribution for thin stiffened plate under line loading, using three-node finite strip elements.

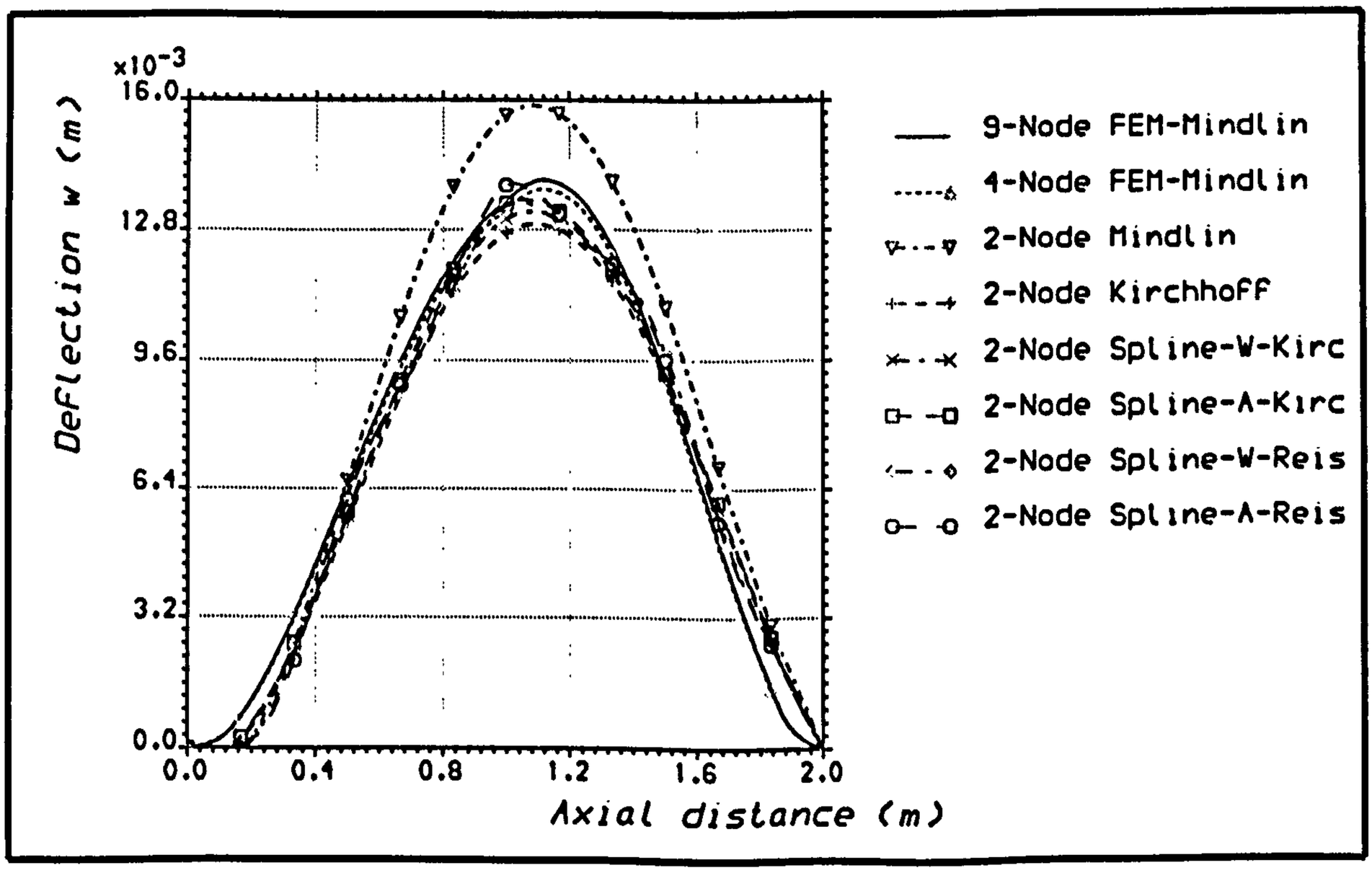

Figure 9.49 Lateral displacement distribution for thin stiffened plate under uniform distributed loading, using two-node finite strip elements.

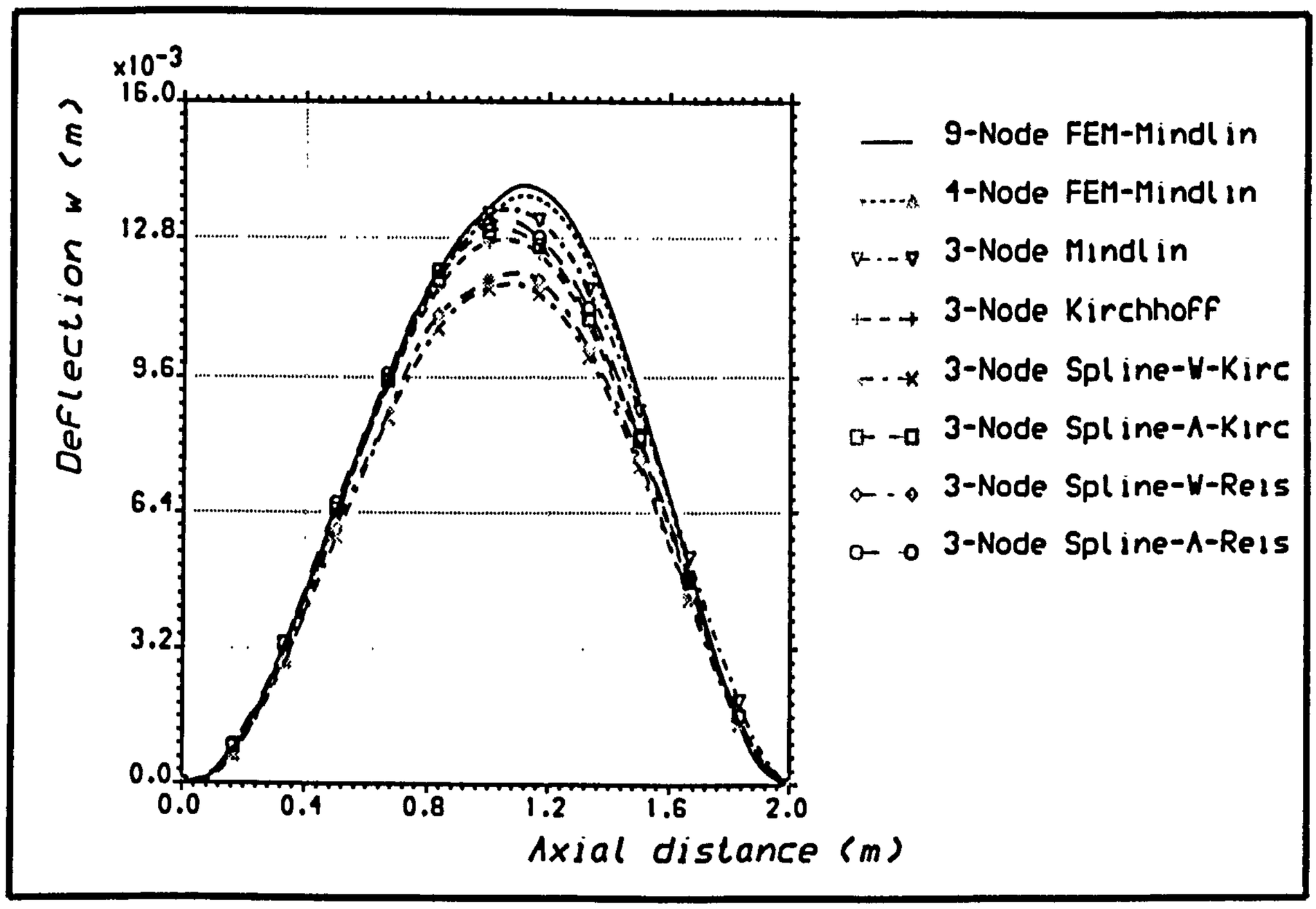

Figure 9.50 Lateral displacement distribution for thin stiffened plate under uniform distributed loading, using three-node finite strip elements.

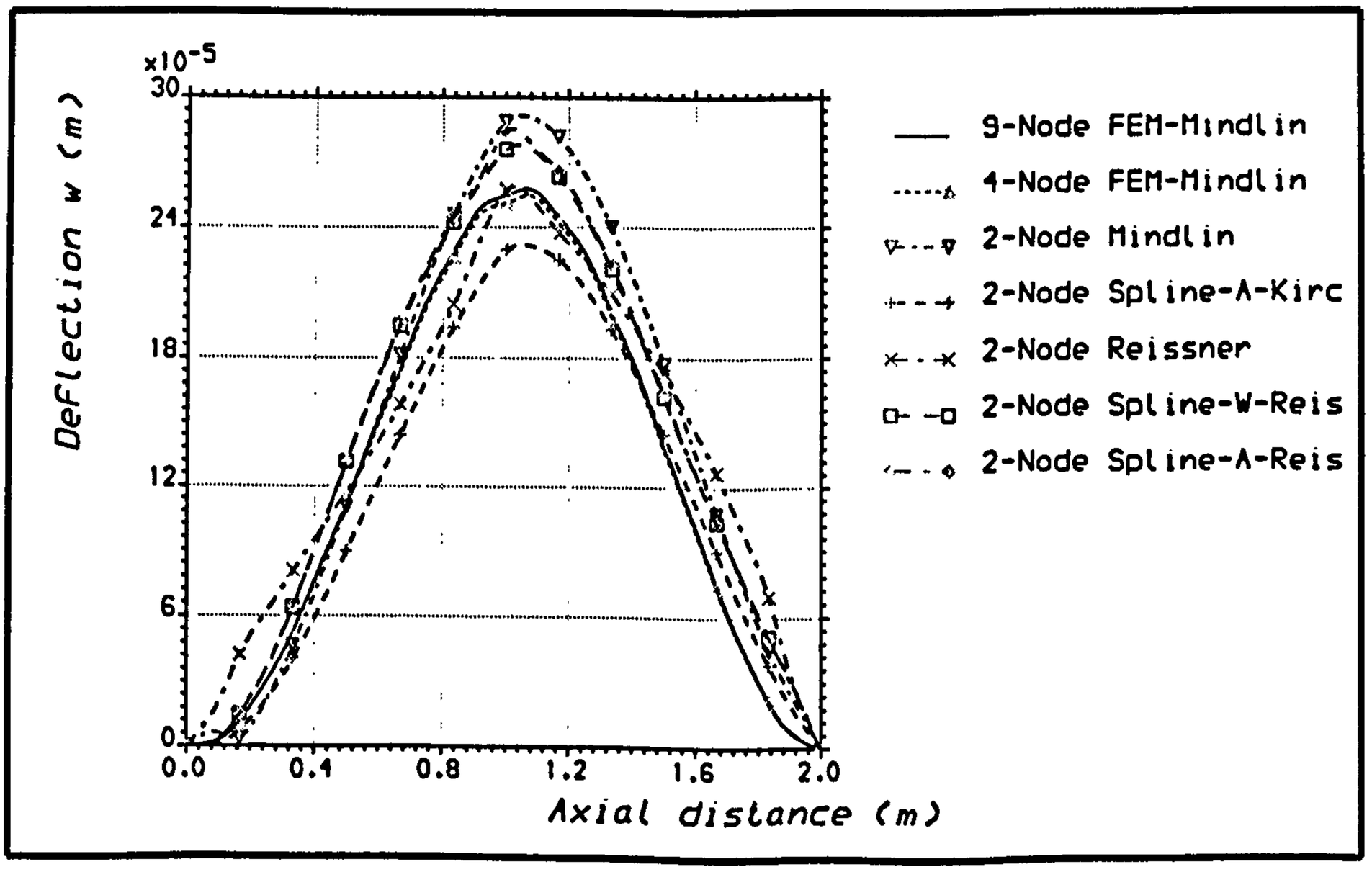

Figure 9.51 Lateral displacement distribution for thick stiffened plate under line loading, using two-node finite strip elements.

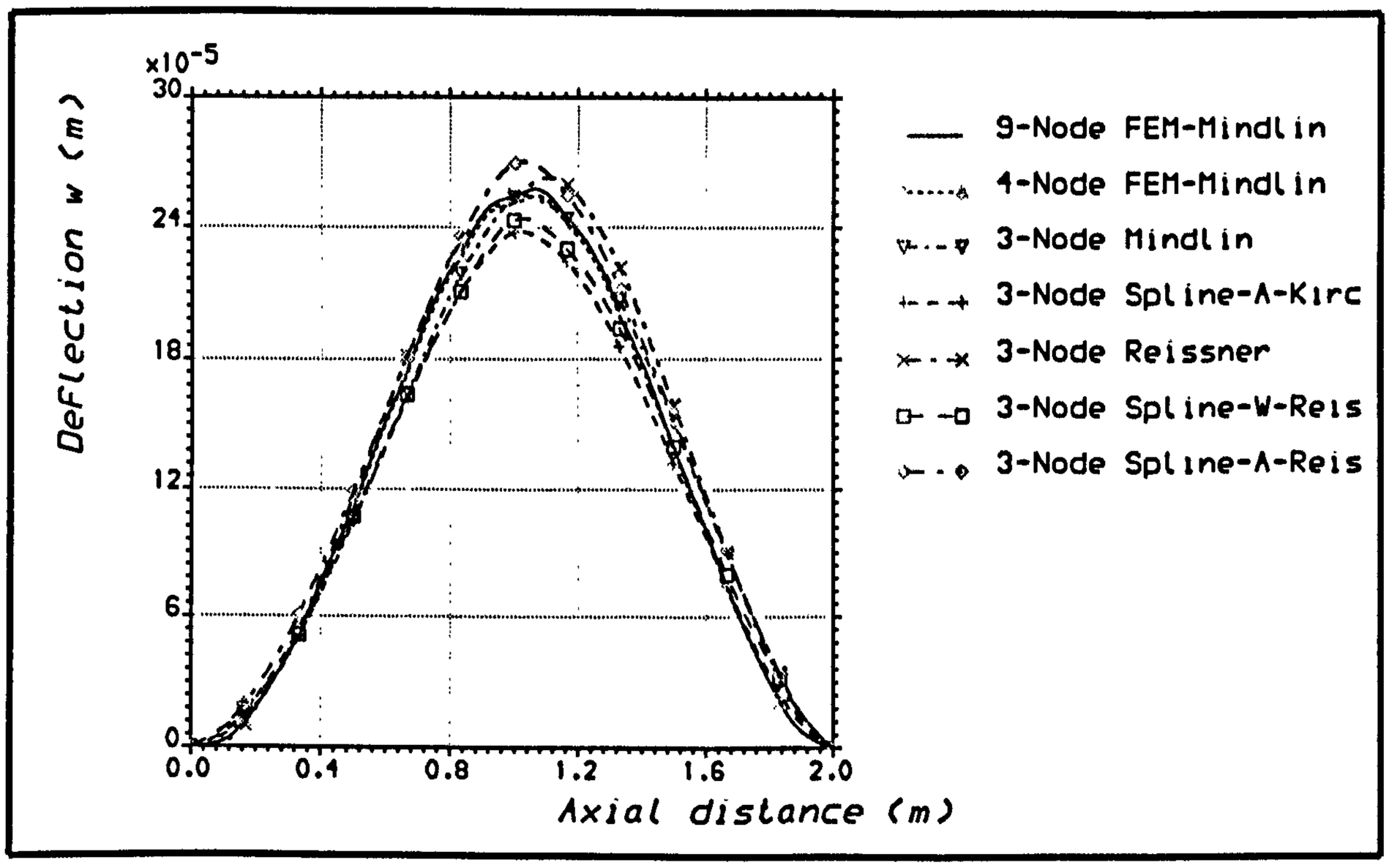

Figure 9.52 Lateral displacement distribution for thick stiffened plate under line loading, using three-node finite strip elements.

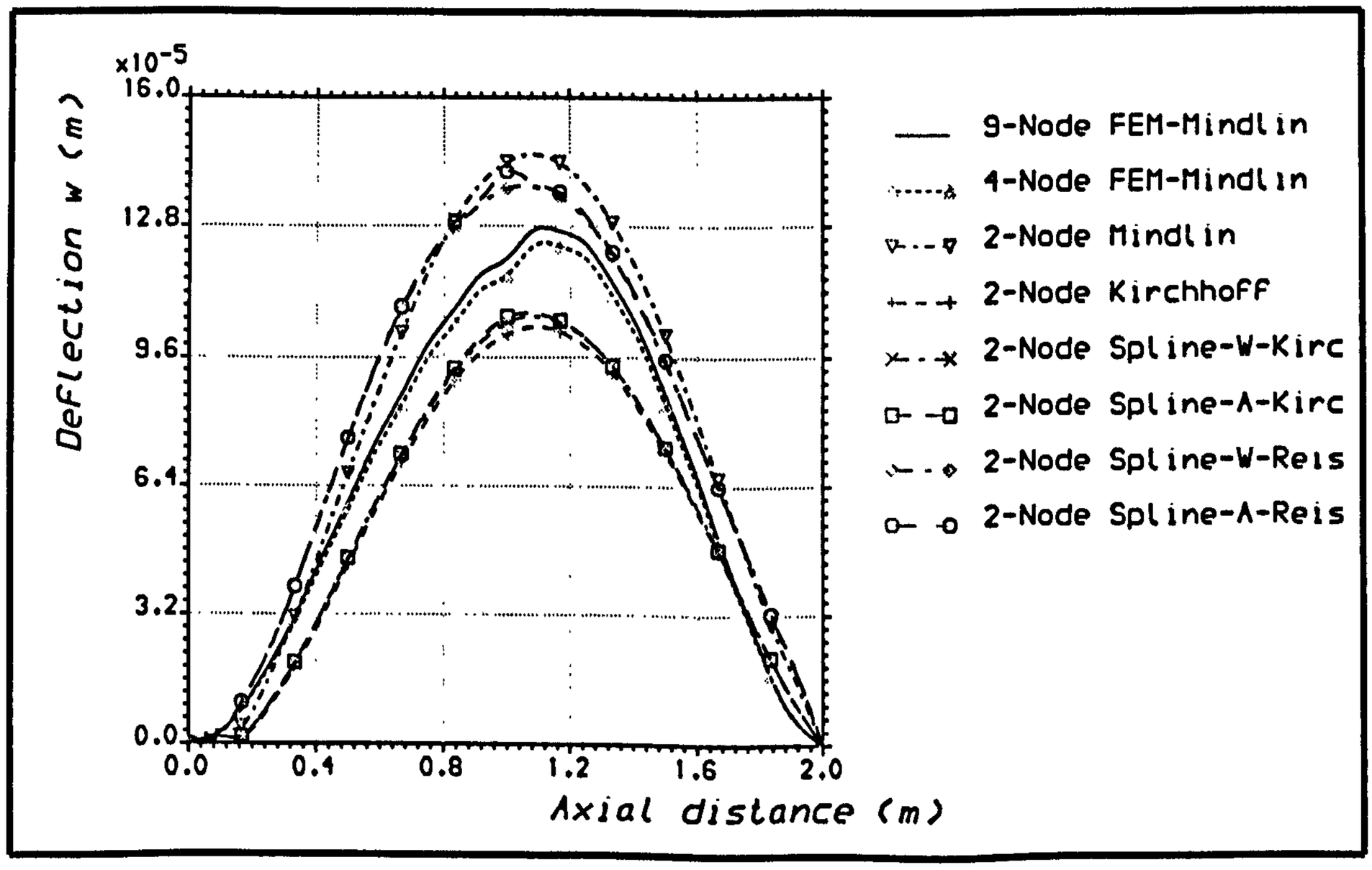

Figure 9.53 Lateral displacement distribution for thick stiffened plate under uniform distributed loading, using two-node finite strip elements.

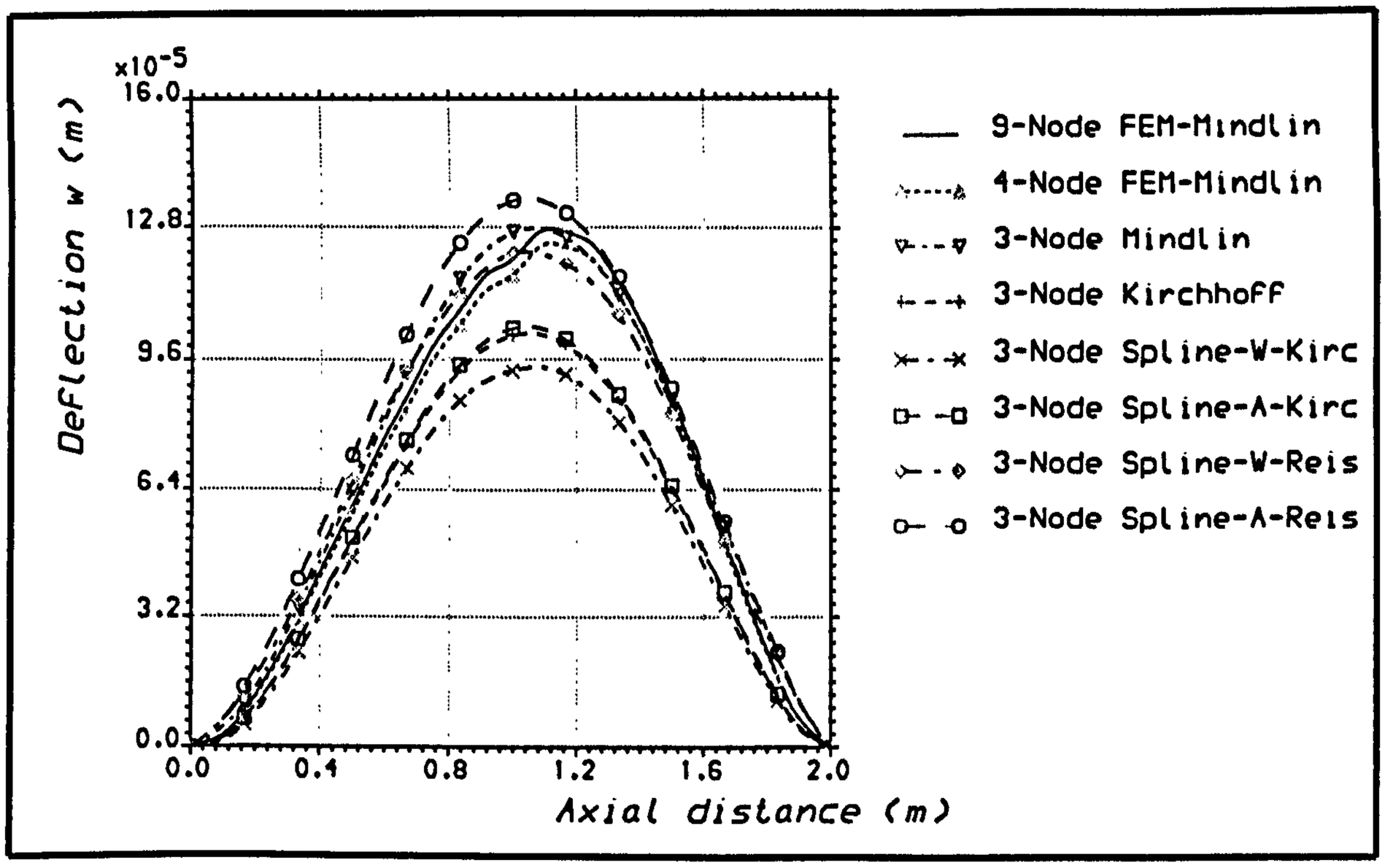

Figure 9.54 Lateral displacement distribution for thick stiffened plate under uniform distributed loading, using three-node finite strip elements.

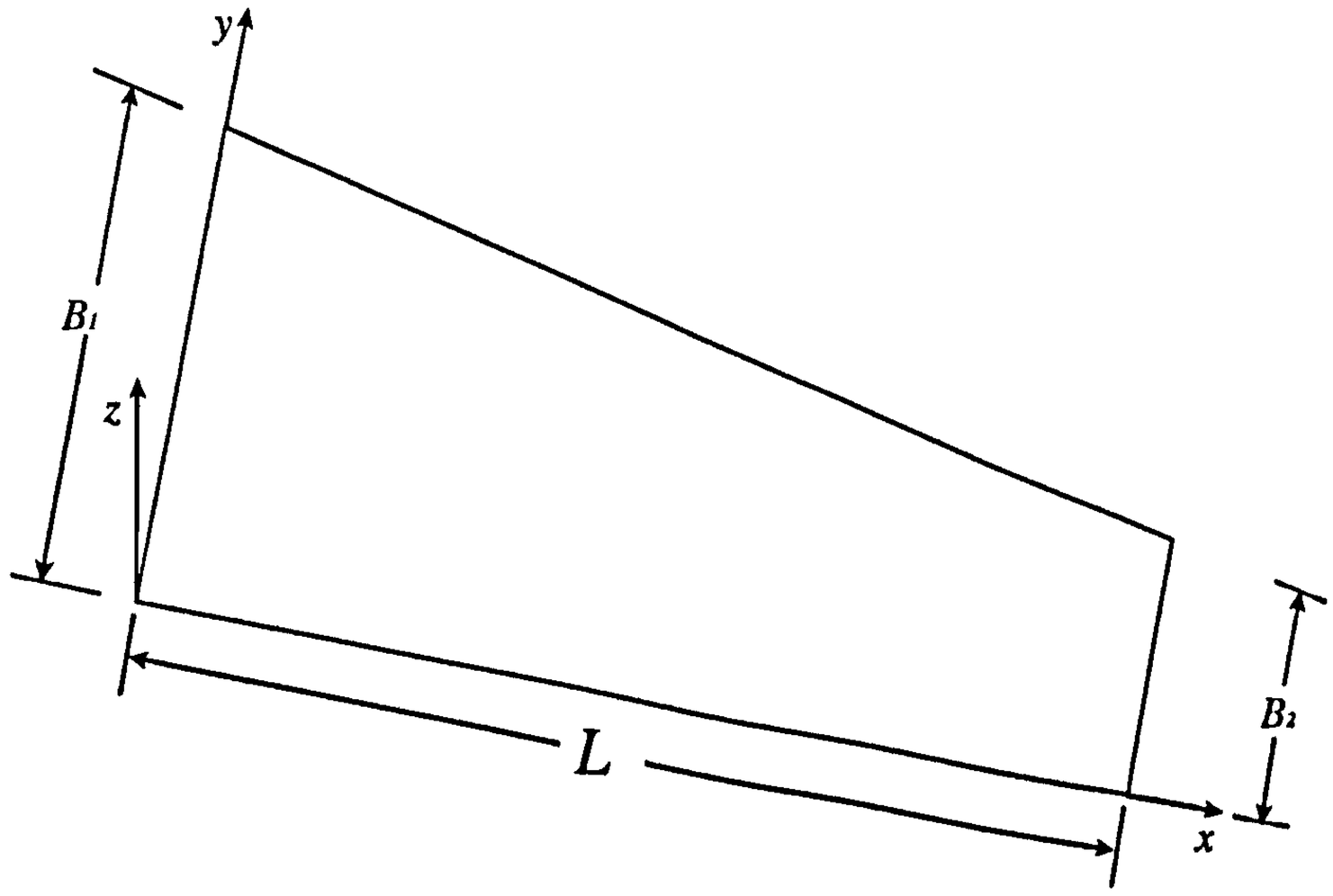

Figure 9.55 Trapezoidal panel

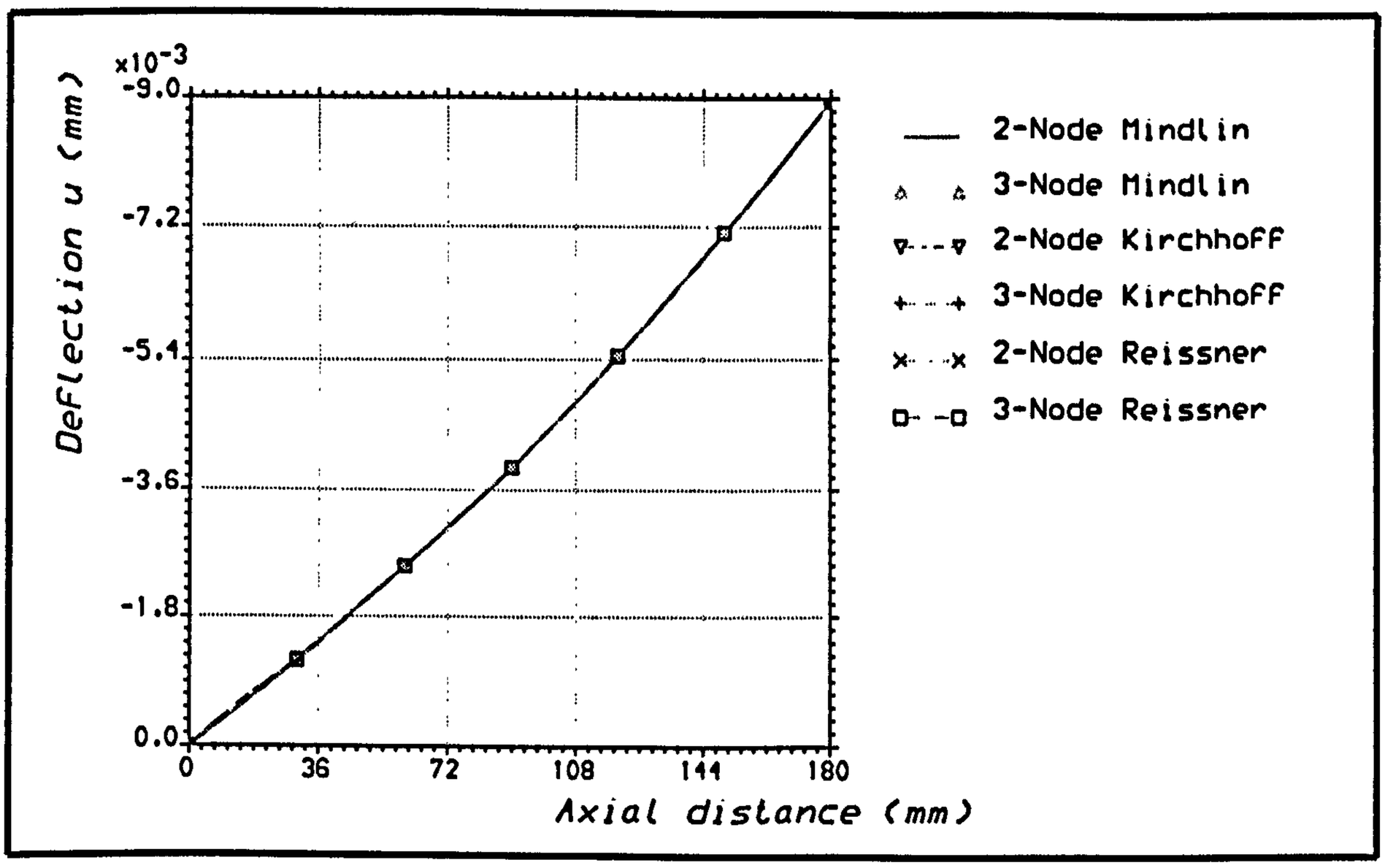

Figure 9.56 Axial displacement distribution for C/E trapezoidal panel under compression, using polynomial finite strip elements.

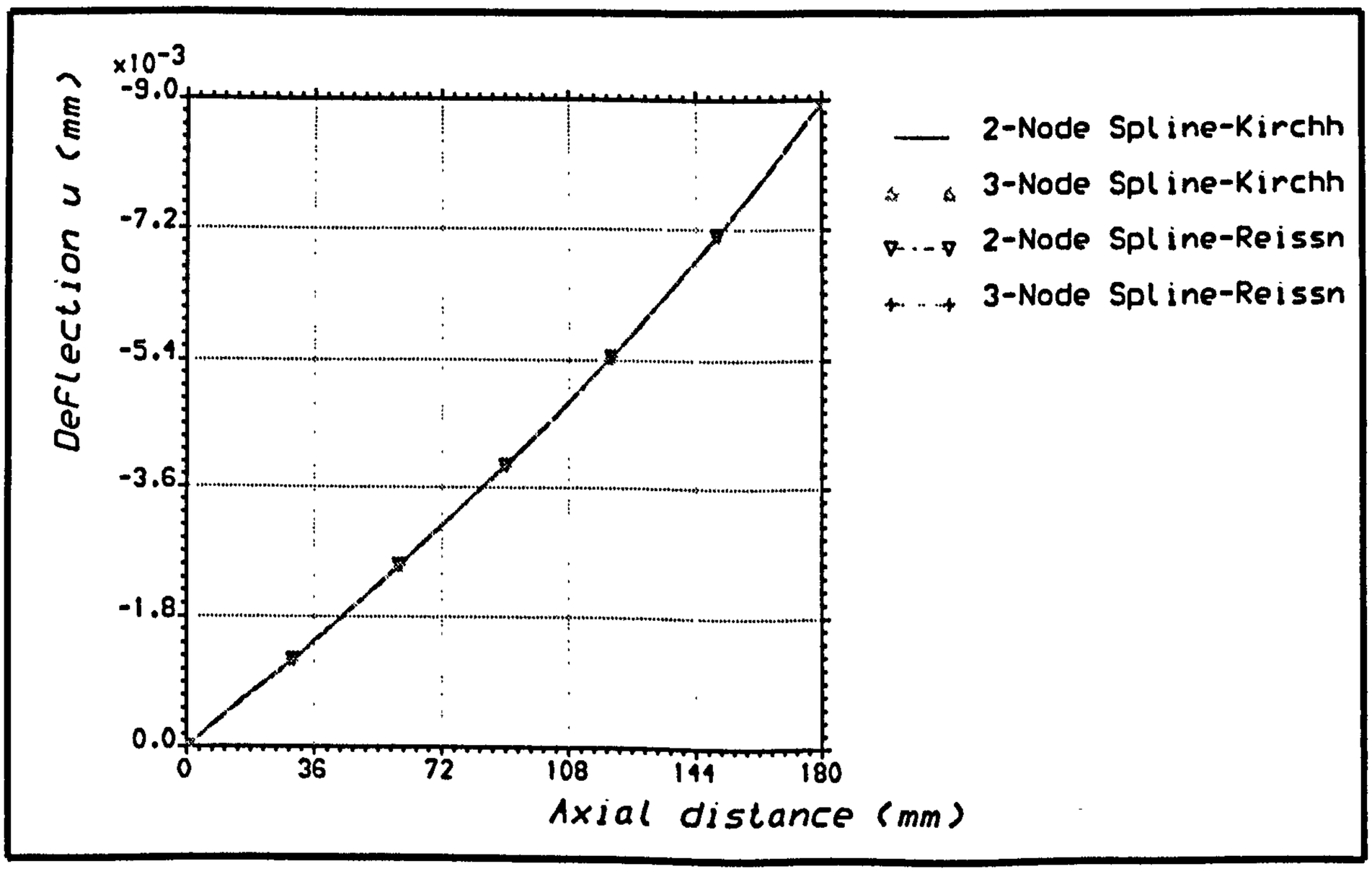

Figure 9.57 Axial displacement distribution for C/E trapezoidal panel under compression, using spline-type finite strip elements.

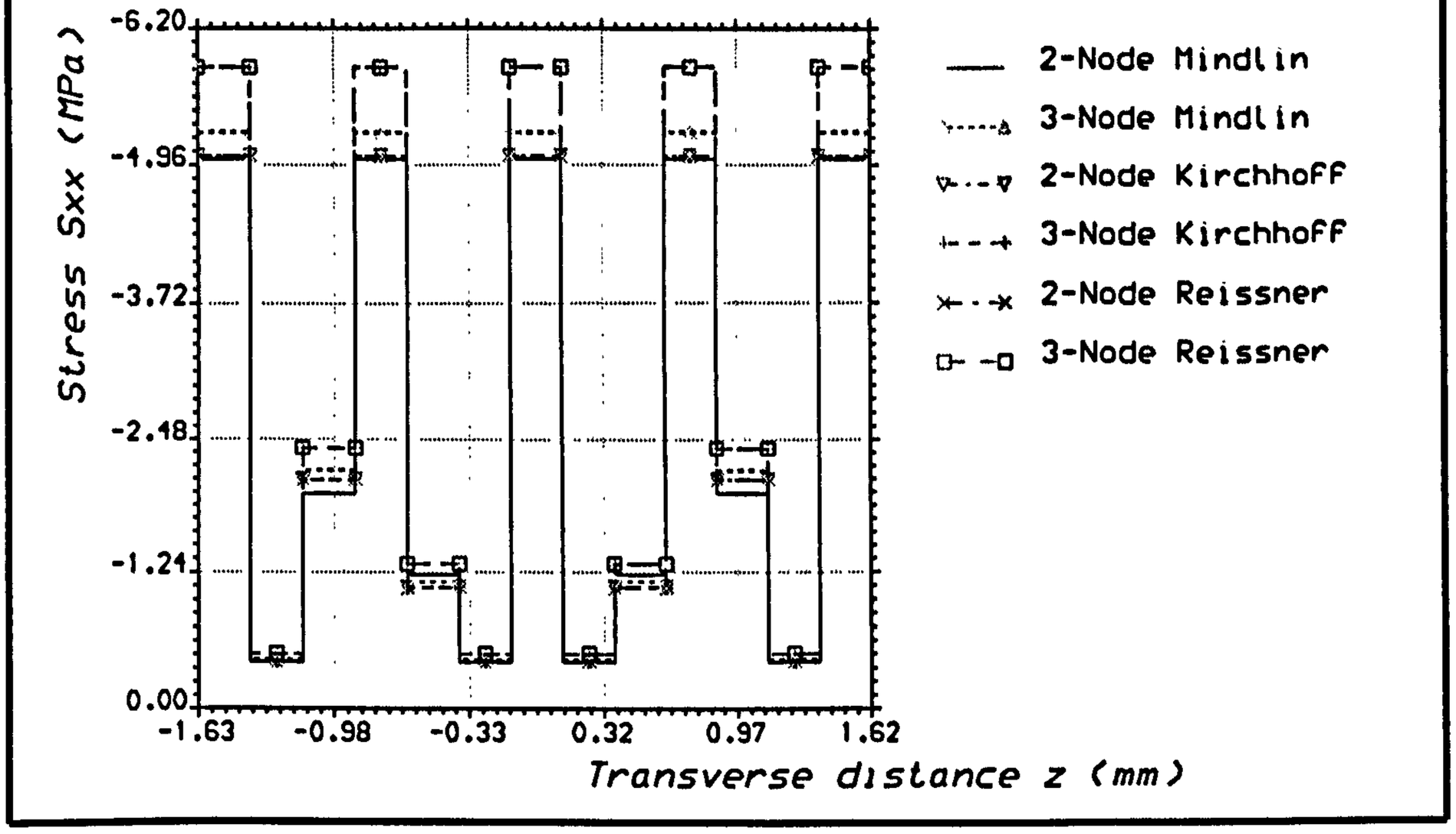

Figure 9.58 Axial stress distribution for C/E trapezoidal panel under Compression, using polynomial strip elements.

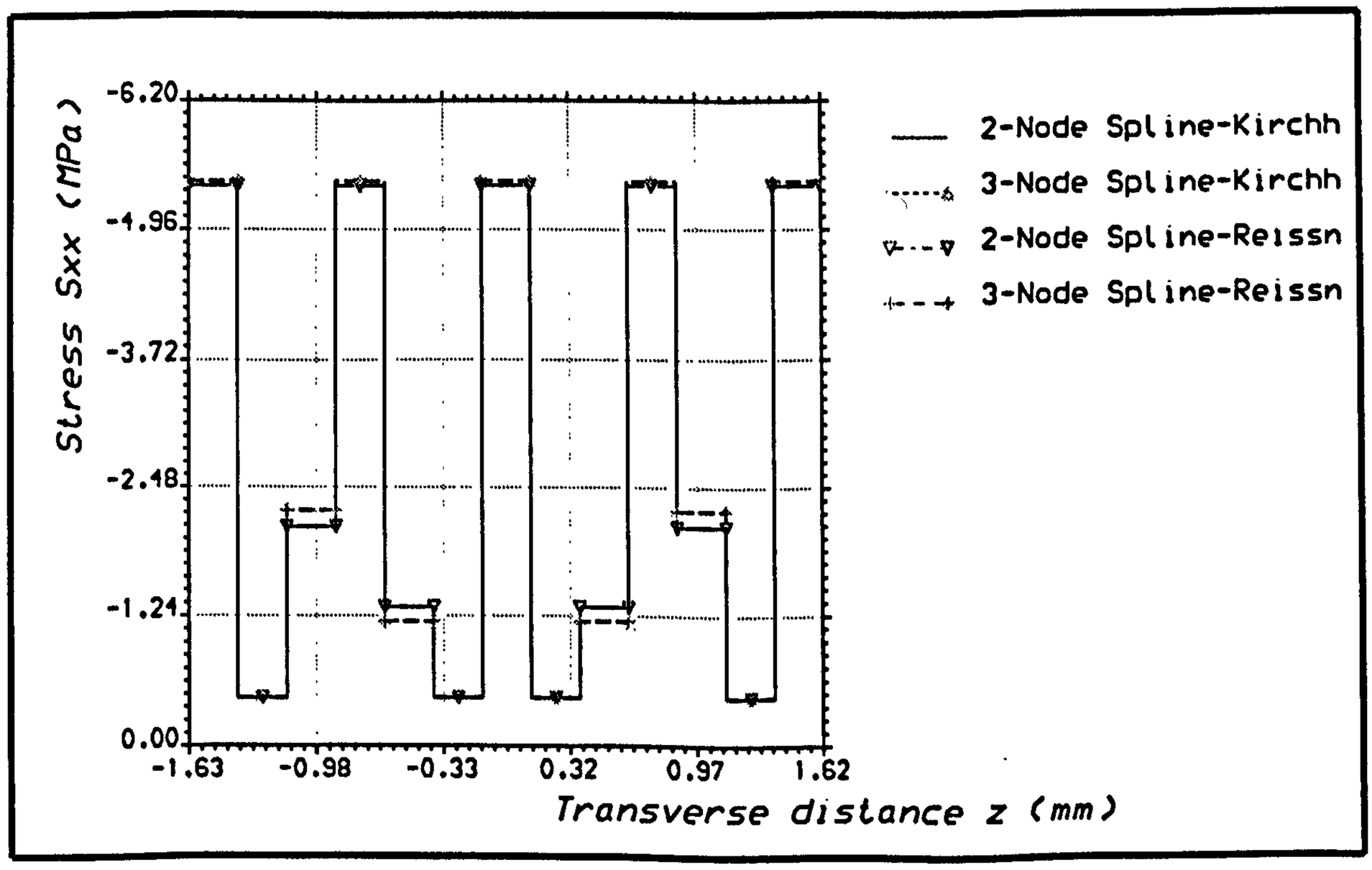

Figure 9.59 Axial stress distribution for C/E trapezoidal panel under Compression, using spline-type strip elements.

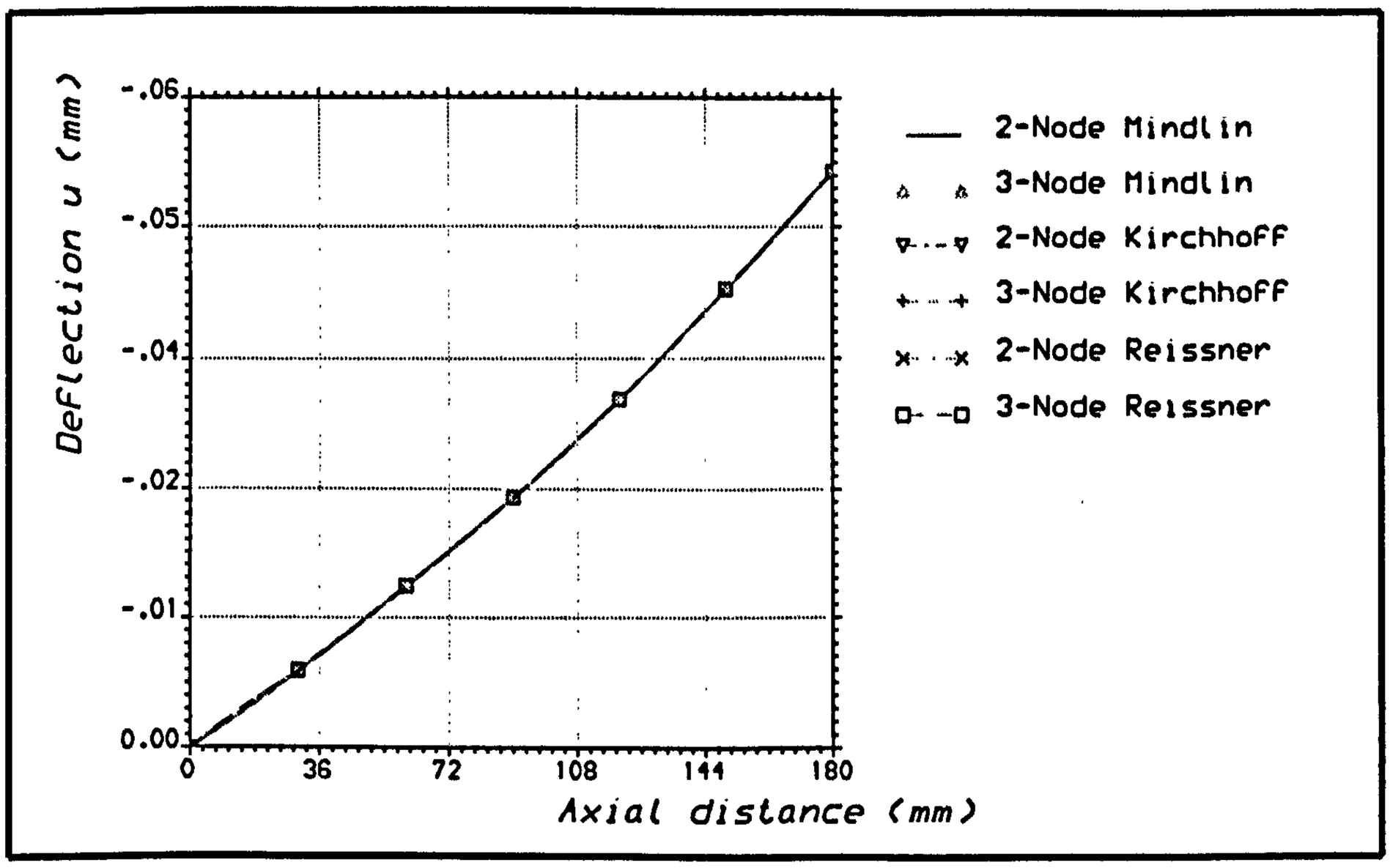

Figure 9.60 Axial displacement distribution for E/G trapezoidal panel under compression, using polynomial strip elements.

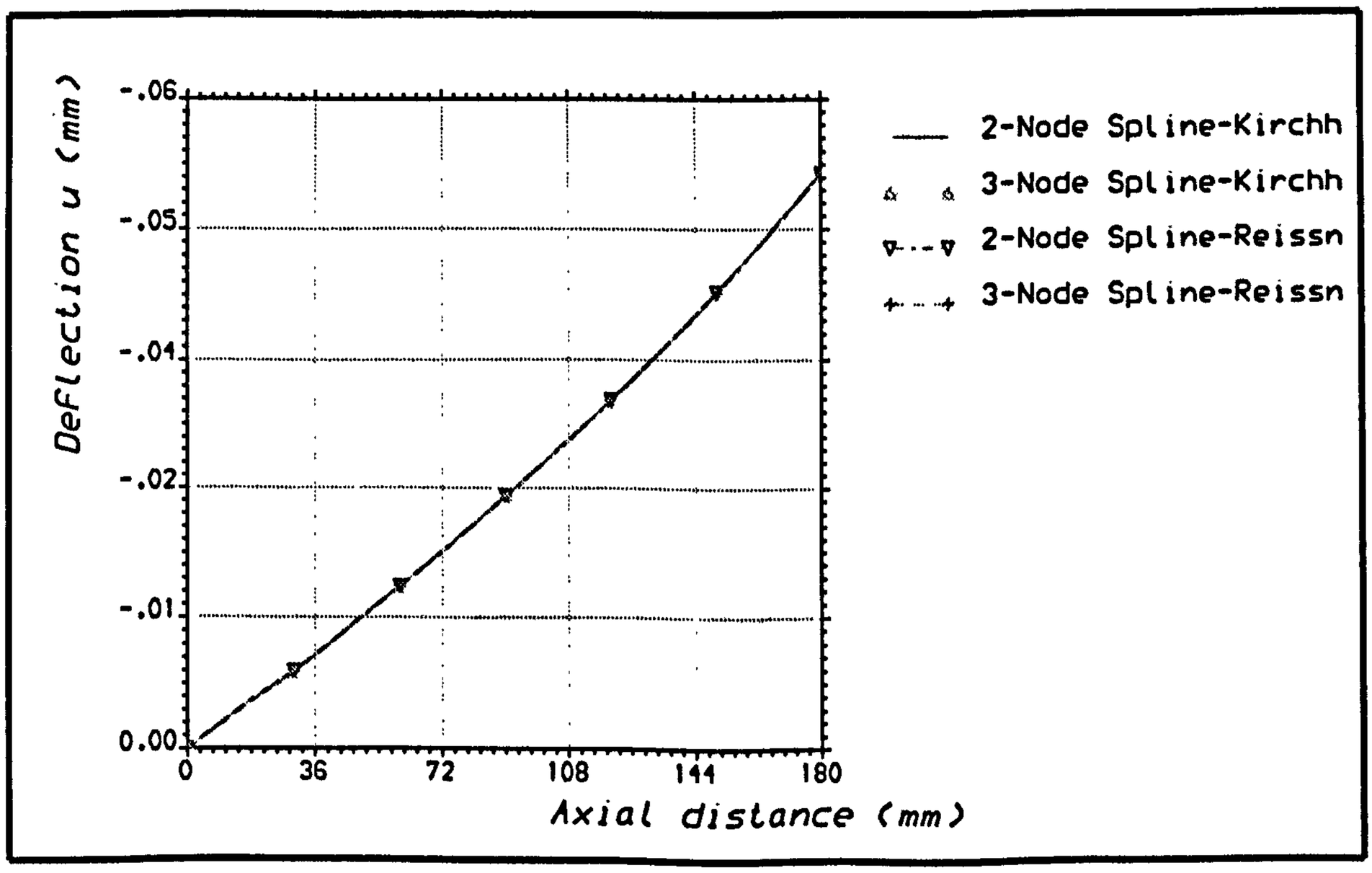

Figure 9.61 Axial displacement distribution for E/G trapezoidal panel under compression, using spline-type strip elements.

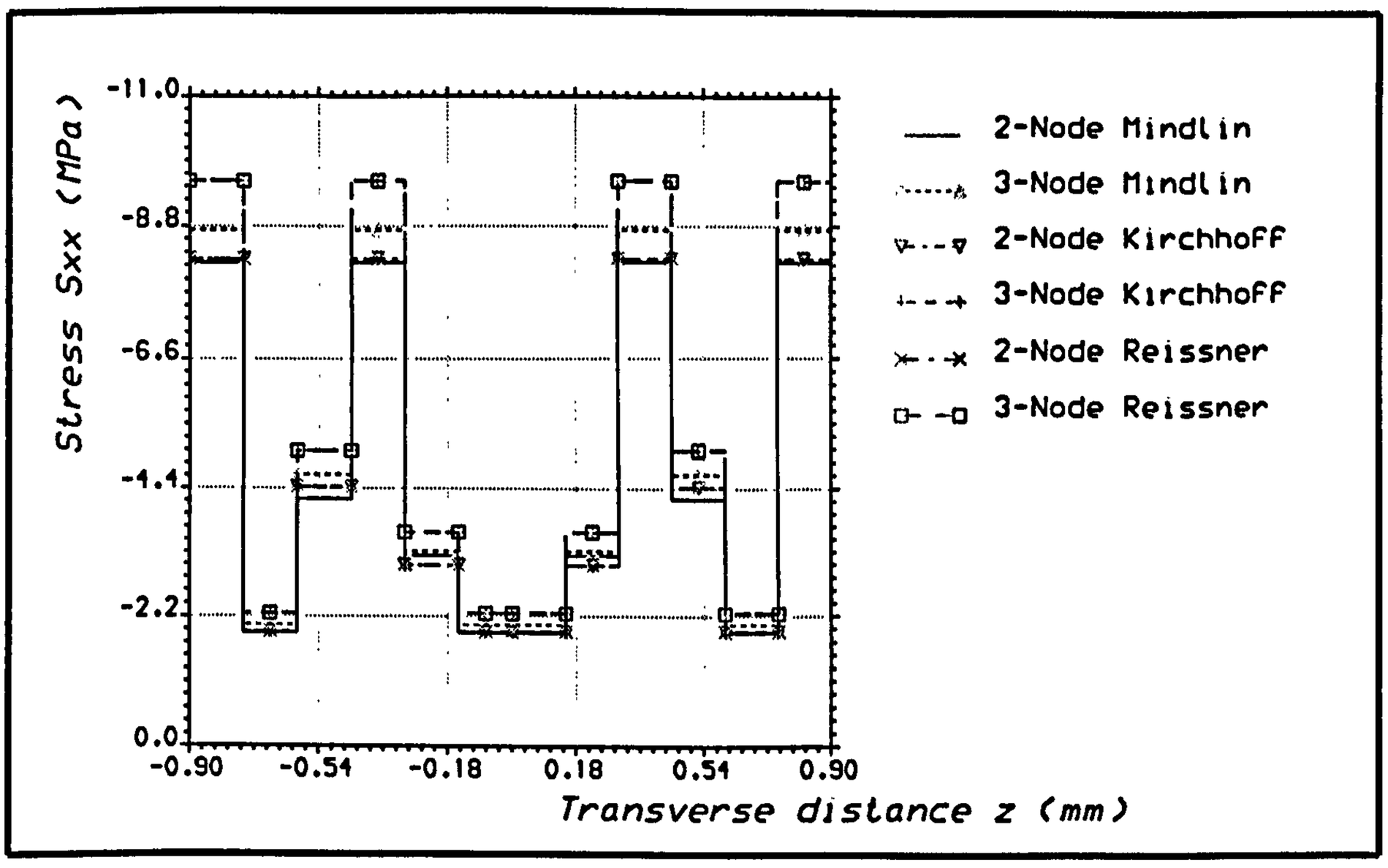

Figure 9.62 Axial stress distribution for E/G trapezoidal panel under compression, using polynomial strip elements.

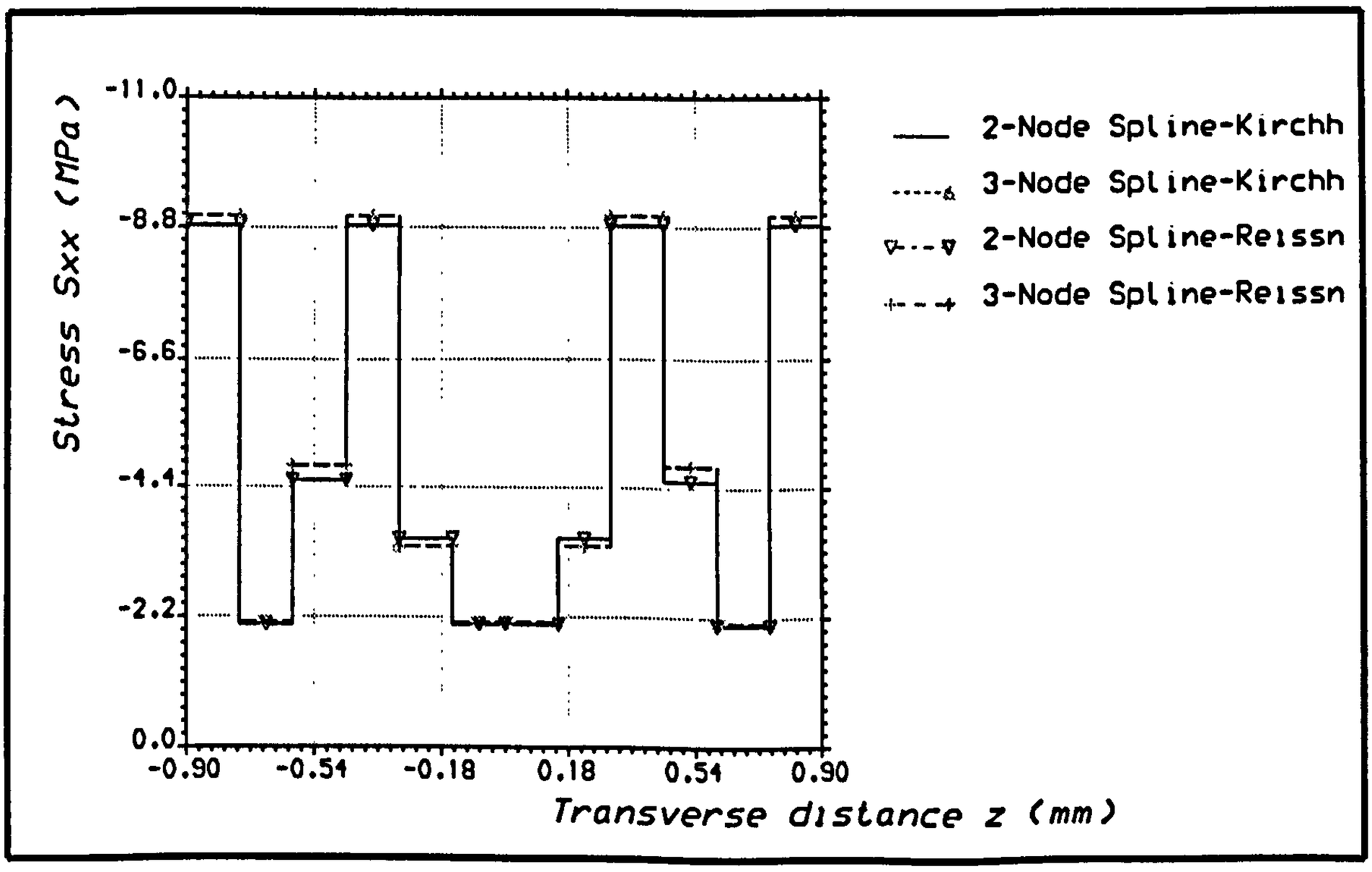

Figure 9.63 Axial stress distribution for E/G trapezoidal panel under compression, using spline-type strip elements.

Appendices

Appendix A Linking Instructions

A.1 LINEAR STATIC ANALYSIS

Files to be linked to form the executable programs are listed as follows:

A.1.1 Mindlin Elements

(a) Plate version

LST-FS-O (or LST-FS-B or LST-FS-F)+STRN-DATA+STRN-ESM + STRN-LNS +STRN-LOAD+ NEWL-SHF.

(b) Faceted shell version

LST-FF-O (or LST-FF-B or LST-FF-F)+FACM-DATA+FACM-ESM +FACM-LNS + FACM-LOAD+ NEWL-SHF.

A.1.2 Hermitian Kirchhoff Elements

(a) Plate version

LST-FS-O (or LST-FS-B or LST-FS-F)+STRK-DATA+STRK-ESM + STRK-LNS +STRK-LOAD+ HERM-W.

(b) Faceted shell version

LST-FF-O (or LST-FF-B or LST-FF-F)+FACK-DATA+FACK-ESM +FACK-LNS + FACK-LOAD+ HERM-W.

A.1.3 Hermitian Reissner Elements

(a) Plate version

LST-FS-O (or LST-FS-B or LST-FS-F)+STRH-DATA+STRH-ESM + STRH-LNS +STRH-LOAD+ HERM-W.

(b) Faceted shell version

LST-FF-O (or LST-FF-B or LST-FF-F)+FACR-DATA+FACR-ESM +FACR-LNS + FACR-LOAD+ HERM-W.

A.1.4 Spline-type Kirchhoff Elements

(a) Plate version

LST-FS-O (or LST-FS-B or LST-FS-F)+STKS-DATA+STKS-ESM + STKS-LNS +STKS-LOAD+ SPLINE-W (or SPLINE-ALL)

(b) Faceted shell version

LST-FF-O (or LST-FF-B or LST-FF-F)+FCKS-DATA+FCKS-ESM +FCKS-LNS + FCKS-LOAD+SPLINE-W (or SPLINE-ALL)

A.1.5 Spline-type Rissner Elements

(a) Plate version

LST-FS-O (or LST-FS-B or LST-FS-F)+STRS-DATA+STRS-ESM +STRS-LNS +STRS-LOAD+ SPLINE-W (or SPLINE-ALL)

(b) Faceted shell version

LST-FF-O (or LST-FF-B or LST-FF-F)+FCHS-DATA+FCHS-ESM +FCHS-LNS + FCHS-LOAD+SPLINE-W (or SPLINE-ALL)

A.2 NON-LINEAR STATIC ANALYSIS

Files to be linked to form the executable programs are as follows:

A.2.1 Mindlin Elements

(a) Plate version

NST-FS-O (or NST-FS-B or NST-FS-F)+STRN-DATA+STRN-ESM +DTRN-LNS + STRN-NLS + STRN-LOAD+ NEWL-SHF.

(b) Faceted shell version

LST-FF-O (or LST-FF-B or LST-FF-F)+FACM-DATA+FACM-ESM +FACM-LNS + FACM-NLS + FACM-LOAD+ NEWL-SHF.

A.2.2 Hermitian Kirchhoff Elements

(a) Plate version

NST-FS-O (or NST-FS-B or NST-FS-F)+STRK-DATA+STRK-ESM+STRK-LNS + STRK-NLS +STRK-LOAD+ HERM-W

(b) Faceted shell version

NST-FF-O (or NST-FF-B or NST-FF-F)+FACK-DATA+FACK-ESM +FACK-LNS + FACK-NLS+ FACK-LOAD+ HERM-W.

A.2.3 Hermitian Reissner Elements

(a) Plate version

NST-FS-O (or NST-FS-B or NST-FS-F)+STRH-DATA+STRH-ESM + STRH-LNS + STRH-NLS+ STRH-LOAD+ HERM-W.

(b) Faceted shell version

NST-FF-O (or NST-FF-B or NST-FF-F)+FACR-DATA+FACR-ESM +FACR-LNS + FACR-NLS+FACR-LOAD+ HERM-W.

A.2.4 Spline-type Kirchhoff Elements

(a) Plate version

NST-FS-O (or NST-FS-B or NST-FS-F)+STKS-DATA+STKS-ESM + STKS-LNS + STKS-NLS+STKS-LOAD+ SPLINE-W (or SPLINE-ALL)

(b) Faceted shell version

NST-FF-O (or NST-FF-B or NST-FF-F)+FCKS-DATA+FCKS-ESM +FCKS-LNS + FCKS-NLS+ FCKS-LOAD+SPLINE-W (or SPLINE-ALL)

A.2.5 Spline-type Rissner Elements

(a) Plate version

NST-FS-O (or NST-FS-B or NST-FS-F)+STRS-DATA+STRS-ESM +STRS-LNS + STRS-NLS+ STRS-LOAD+ SPLINE-W (or SPLINE-ALL)

(b) Faceted shell version

NST-FF-O (or NST-FF-B or NST-FF-F)+FCHS-DATA+FCHS-ESM +FCHS-LNS + FCHS-NLS+ FCHS-LOAD+SPLINE-W (or SPLINE-ALL)

A.3 NATURAL FREQUENCY ANALYSIS

Files to be linked to form the executable programs are as follows:

A.3.1 Mindlin Elements

(a) Plate version

DYN-FS-O (or DYN-FS-B or DYN-FS-F) + EIGENV1 + STRN-DATA + STRN-ESM +STRN-EMM + STRN-LOAD+ NEWL-SHF.

(b) Faceted shell version

DYN-FF-O (or DYN-FF-B or DYN-FF-F) + EIGENV1 +FACM-DATA + FACM-ESM+FACM-LOAD+ NEWL-SHF.

A.3.2 Hermitian Kirchhoff Elements

(a) Plate version

DYN-FS-O (or DYN-FS-B or DYN-FS-F) + EIGENV1+STRH-DATA+STRH-ESM + STRH-EMM +STRH-LOAD+ HERM-W.

(b) Faceted shell version

DYN-FF-O (or DYN-FF-B or DYN-FF-F) + EIGENV1+FACR-DATA+FACR-ESM +FACR-EMM + FACR-LOAD+ HERM-W.

A.3.3 Hermitian Reissner Elements

(a) Plate version

DYN-FS-O (or DYN-FS-B or DYN-FS-F) + EIGENV1+STRH-DATA+STRH-ESM + STRH-EMM +STRH-LOAD+ HERM-W.

(b) Faceted shell version

DYN-FF-O (or DYN-FF-B or DYN-FF-F) + EIGENV1+FACR-DATA+FACR-ESM +FACR-EMM + FACR-LOAD+ HERM-W.

A.3.4 Spline-type Kirchhoff Elements

(a) Plate version

DYN-FS-O (or DYN-FS-B or DYN-FS-F) + EIGENV1+STKS-DATA+STKS-ESM + STKS-EMM +STKS-LOAD+ SPLINE-W (or SPLINE-ALL)

(b) Faceted shell version

DYN-FF-O (or DYN-FF-B or DYN-FF-F) + EIGENV1+FCKS-DATA+FCKS-ESM +FCKS-EMM + FCKS-LOAD+SPLINE-W (or SPLINE-ALL)

A.3.5 Spline-type Rissner Elements

(a) Plate version

DYN-FS-O (or DYN-FS-B or DYN-FS-F) + EIGENV1+STRS-DATA+STRS-ESM +STRS-EMM +STRS-LOAD+ SPLINE-W (or SPLINE-ALL)

(b) Faceted shell version

DYN-FF-O (or DYN-FF-B or DYN-FF-F) + EIGENV1+FCHS-DATA+FCHS-ESM +FCHS-EMM + FCHS-LOAD+SPLINE-W (or SPLINE-ALL)

A.4 BUCKLING ANALYSIS

Files to be linked to form the executable programs are as follows:

A.4.1 Mindlin Elements

(a) Plate version

BUC-FS-O (or BUC-FS-B or BUC-FS-F) + EIGENV2 + STRN-DATA+STRN-ESM + STRN-LNS + STRN-NLS + STRN-LOAD+ NEWL-SHF.

(b) Faceted shell version

BUC-FF-O (or BUC-FF-B or BUC-FF-F) + EIGENV2 +FACM-DATA+FACM-ESM + FACM-LNS + FACM-NLS + FACM-LOAD + NEWL-SHF.

A.4.2 Hermitian Kirchhoff Elements

(a) Plate version

BUC-FS-O (or BUC-FS-B or BUC-FS-F) + EIGENV2 +STRK-DATA+STRK-ESM+STRK-LNS + STRK-NLS +STRK-LOAD+ HERM-W

(b) Faceted shell version

BUC-FF-O (or BUC-FF-B or BUC-FF-F) + EIGENV2 +FACK-DATA+FACK-ESM +FACK-LNS + FACK-NLS+ FACK-LOAD+ HERM-W.

A.4.3 Hermitian Reissner Elements

(a) Plate version

BUC-FS-O (or BUC-FS-B or BUC-FS-F) + EIGENV2 +STRH-DATA+STRH-ESM + STRH-LNS + STRH-NLS+ STRH-LOAD+ HERM-W.

(b) Faceted shell version

BUC-FF-O (or BUC-FF-B or BUC-FF-F) + EIGENV2 +FACR-DATA+FACR-ESM +FACR-LNS + FACR-NLS+FACR-LOAD+ HERM-W.

A.4.4 Spline-type Kirchhoff Elements

(a) Plate version

BUC-FS-O (or BUC-FS-B or BUC-FS-F) + EIGENV2 +STKS-DATA+STKS-ESM + STKS-LNS + STKS-NLS+STKS-LOAD+ SPLINE-W (or SPLINE-ALL)

(b) Faceted shell version

BUC-FF-O (or BUC-FF-B or BUC-FF-F) + EIGENV2 +FCKS-DATA+FCKS-ESM +FCKS-LNS + FCKS-NLS+ FCKS-LOAD+SPLINE-W (or SPLINE-ALL)

A.4.5 Spline-type Rissner Elements

(a) Plate version

BUC-FS-O (or BUC-FS-B or BUC-FS-F) + EIGENV2 +STRS-DATA+STRS-ESM +STRS-LNS + STRS-NLS+ STRS-LOAD+ SPLINE-W (or SPLINE-ALL)

(b) Faceted shell version

BUC-FF-O (or BUC-FF-B or BUC-FF-F) + EIGENV2 +FCHS-DATA+FCHS-ESM +FCHS-LNS + FCHS-NLS+ FCHS-LOAD+SPLINE-W (or SPLINE-ALL)

Appendix B Samples of input data files

Examples of the data files for the stiffened plate and trapezoidal panel cases are listed in this section.

B.1 STIFFENED PLATE

B.1.1 Two-node Mindlin element data file

```
** Carbon/Epoxy Composite Stiffened Plate
** Using Mindlin Finite Strip 2-node Element
** Linear static analysis under out-ofplane loading

Harmonics: NHAR,IHAR
2,2

Strips: NBN,NBL,NODE/I,XB(I),ZB(I)
4,3,2
1,0.0,0.0
2,1.0,0.0
3,2.0,0.0
4,1.0,0.5
1,1.0,1.0,1,1,2,12
2,1.0,1.0,1,2,3,12
3,1.0,1.0,1,2,4,6


COMPOSITE MODULE
1
134.75E9,8.24E9,0.325,7.0E9,7.0E9,7.0E9,800
12
1,-45,2.5E-3
2,  0,2.5E-3
3, 45,2.5E-3
4,-45,2.5E-3
5,  0,2.5E-3
6, 45,2.5E-3
7, 45,2.5E-3
8,  0,2.5E-3
9,-45,2.5E-3
10,45,2.5E-3
11, 0,2.5E-3
12,-45,2.5E-3

Boundary Conditions
1
0,2,1,3
0,0


Loads: NLINC,NLN,NLX,NLY,NDL
0,0,1,0,0
1,-13,1,0.0,0.0,1.0E5, 0.0, 0.0
```

```
STATIC MODULE
1

OUTPUT MODULE
0
0,0
3,13,1,25

Gauss Quadrature Data (Reduced)
2,1,2
```

B.1.2 Two-node Kirchoff element data file

```
** Carbon/Epoxy Composite Stiffened Plate
** Using Kirchhoff Finite Strip 2-node Element
** Linear static analysis under out-ofplane loading

Harmonics: NHAR,IHAR
4,2

Strips: NBN,NBL,NODE/I,XB(I),ZB(I)
4,3,2
1,0.0,0.0
2,1.0,0.0
3,2.0,0.0
4,1.0,0.5
1,1.0,1.0,1,1,2,12
2,1.0,1.0,1,2,3,12
3,1.0,1.0,1,2,4,6

COMPOSITE MODULE
1
134.75E9,8.24E9,0.325,7.0E9,7.0E9,7.0E9,800
12
1,-45,2.5E-3
2,  0,2.5E-3
3, 45,2.5E-3
4,-45,2.5E-3
5,  0,2.5E-3
6, 45,2.5E-3
7, 45,2.5E-3
8,  0,2.5E-3
9,-45,2.5E-3
10,45,2.5E-3
11, 0,2.5E-3
12,-45,2.5E-3

Boundary Conditions
1
0,2,1,3
0,0
0

Loads: NLINC,NLN,NLX,NLY,NDL
```

```
0,0,1,0,0
1,-13,1,0.0,0.0,1.0E5, 0.0, 0.0


STATIC MODULE
1

OUTPUT MODULE
0
0,0
3,13,1,25

Gauss Quadrature Data (Reduced)
2,1,2
```

B.2 TRAPEZOIDAL PANEL BUCKLING DATA

B.2.1 Three-node Mindlin element data file

```
** Carbon/Epoxy Composite
** Using Mindlin Finite Strip 3-node Element
** Buckling analysis

Harmonics: NHAR,IHAR
3,3

Strips: NBN,NBL,NODE/I,XB(I),ZB(I)
2,1,3
1,0.0,0.0
2,180.0,0.0
1,50.0,30.0,1,1,2,6

COMPOSITE MODULE
1
128.0E3,11.0E3,0.25,4.48E3,4.48E3,4.48E3,1500
13
1,  0,0.25
2, 90,0.25
3, 45,0.25
4,  0,0.25
5,-45,0.25
6, 90,0.25
7,  0,0.25
8, 90,0.25
9,-45,0.25
10, 0,0.25
11,45,0.25
12,90,0.25
13, 0,0.25

Boundary Conditions
1
0,1,1
0,0


Loads: NLINC,NLN,NLX,NLY,QO
```

```
0,0,1,0,0.0
1,-13,1,-13.33333333, 0.0, 0.0, 0.0, 0.0


DYNAMIC MODULE
-1,8,100,0.1E-8,0.1


OUTPUT MODULE
0
0,0
0

Gauss Quadrature Data (Reduced)
3,2,3
```

B2.2 Three-node Spline-type Reissner data file

```
** E-Glass Composite
** Using Reissner Finite Strip 3-node Element
** Buckling analysis

Harmonics: NHAR,IHAR
6,4

Strips: NBN,NBL,NODE/I,XB(I),ZB(I)
2,1,3
1,0.0,0.0
2,180.0,0.0
1,50.0,30.0,1,1,2,6

COMPOSITE MODULE
1
35.0E3,8.22E3,0.26,4.1E3,4.1E3,4.1E3,2000
12
1,   0,0.15
2,  90,0.15
3,  45,0.15
4,   0,0.15
5,-45,0.15
6,  90,0.15
7,  90,0.15
8,-45,0.15
9,   0,0.15
10,45,0.15
11,90,0.15
12,  0,0.15

Boundary Conditions
1
0,1,1
0,0


Loads: NLINC,NLN,NLX,NLY,QO
0,0,1,0,0.0
1,-13,1,-13.33333333, 0.0, 0.0, 0.0, 0.0
```

```
DYNAMIC MODULE
-1,8,100,0.1E-8,0.1


OUTPUT MODULE
0
0,0
0

Gauss Quadrature Data (Reduced)
3,2,3
```